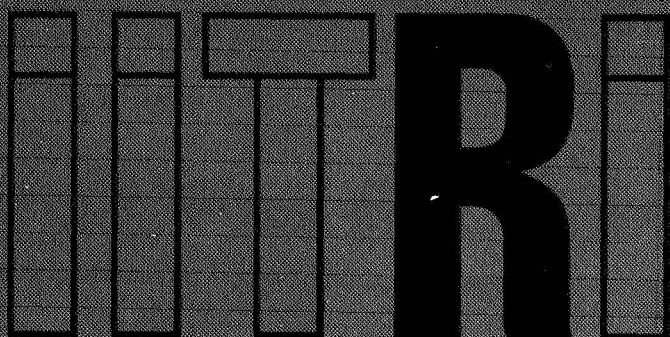


Mook

N69-37456



CASE FILE  
COPY

Report No. IITRI-U6061-17  
(Interim Summary Report)

STUDY OF IN SITU DEGRADATION OF  
THERMAL CONTROL SURFACES

National Aeronautics & Space Administration  
George C. Marshall Space Flight Center  
Huntsville, Alabama

Report No. IITRI-U6061-17  
(Interim Summary Report)

STUDY OF IN SITU DEGRADATION OF  
THERMAL CONTROL SURFACES

National Aeronautics & Space Administration  
George C. Marshall Space Flight Center  
Huntsville, Alabama

IIT RESEARCH INSTITUTE

Report No. IITRI-U6061-17  
(Interim Summary Report)

STUDY OF IN SITU DEGRADATION OF  
THERMAL CONTROL SURFACES

March 7, 1967 to September 7, 1968

NASA Contract NAS8-21074  
IITRI Project U6061

Prepared by

G.A. Zerlaut  
and  
J.E. Gilligan

of

IIT RESEARCH INSTITUTE  
Technology Center  
Chicago, Illinois 60616

for

National Aeronautics & Space Administration  
George C. Marshall Space Flight Center  
Huntsville, Alabama

March 7, 1969

IIT RESEARCH INSTITUTE





## FOREWORD

This is Report No. IITRI-U6061-17 (Interim Summary Report) on IITRI Project U6061, Contract No. NAS8-21074, entitled "Study of In Situ Degradation of Thermal-Control Surfaces." This report covers the period from March 7, 1967 to September 7, 1968.

Major contributors to the program during this period include Gene A. Zerlaut, project leader, and alphabetically: William C. Courtney, consultation on vacuum problems; Henry DeYoung, gas-adsorbate testing; John E. Gilligan, general consultation and theoretical considerations; George Kimura, space-simulation and gas-adsorbate tests; Frederick O. Rogers, specimen preparation; and Samuel Shelfo, space-simulation tests. The work reported herein was performed under the technical direction of the Space Sciences Laboratory of the George C. Marshall Space Flight Center. Mr. Edgar R. Miller was the Contracting Officer's Technical Representative.


The authors wish to acknowledge the cooperation of the following persons for their help in furnishing and/or securing samples: Mr. E.R. Miller of NASA-MSFC, Mr. Robert Jewell of NASA-Langley, Mr. John Millard of NASA-Ames, Mr. Paul M. Blair of Hughes Aircraft Corp., and Dr. Merle Seibert of Lockheed Missiles and Space Company.

Respectfully submitted,

IIT RESEARCH INSTITUTE

APPROVED:

  
M.J. Klein  
Director  
Chemistry Research

  
Gene A. Zerlaut  
Manager  
Polymer Chemistry Research

GAZ:jss

IIT RESEARCH INSTITUTE

## ABSTRACT

This research program was planned to provide the technical background that is necessary for the proper evaluation of the space-environment-induced damage that has been sustained by Pegasus III spacecraft test coupons and to evaluate the mechanisms of space ultraviolet damage employing gas adsorbate techniques. Twenty-eight different samples of thermal-control surfaces were irradiated in one or both IRIF-I and IRIF-II space-simulation facilities. The in situ behavior of these surfaces were determined and on the basis of their in situ behavior, gaseous adsorbate tests were planned. These studies have suggested that surface sites may be expeditiously investigated by adsorbate studies. A number of problems inherent in space simulation testing were elucidated and recommendations are advanced on the basis of their interpretation. The role of coating constituents, i.e., curing agents, solvents and even binders, as contaminants, is discussed. The adsorption of gases and foreign species on the surface of pigments is experimentally evaluated.

## TABLE OF CONTENTS

	<u>Page</u>
FOREWORD	iii
ABSTRACT	iv
LIST OF TABLES	vi
LIST OF FIGURES	vii
I. INTRODUCTION	1
II. SPECIMEN SELECTION AND PROCUREMENT	3
III. EXPERIMENTAL PROCEDURES	8
A. The IRIF-I Space-Simulation Facility	8
B. The IRIF-II Space-Simulation Facility	10
C. Computation of Solar Adsorptance	10
D. Ultraviolet Sources Employed	13
E. Gas Adsorbate Apparatus	17
F. Major Problems Encountered	22
IV. SPACE SIMULATION SCREENING TESTS	26
A. Introduction	26
B. IRIF-I Test No. 10	26
C. IRIF-I Test No. 13	54
D. IRIF-I Test No. 15	66
E. IRIF-I Test No. 16	78
F. Discussion	85
V. GAS ADSORBATE TESTS	93
A. Introduction	93
B. IRIF-II Test 2-2 (Oxygen Bleaching)	93
C. IRIF-II Test 2-3 (Oxygen Bleaching)	103
D. IRIF-II Test 2-4 (Nitrogen Bleaching)	117
E. IRIF-II Test 2-8 (Carbon Dioxide Bleaching)	123
F. Discussion	133
VI. SUMMARY AND CONCLUSIONS	137
REFERENCES	147
APPENDIX A - GAS ADSORBATE PROCEDURES	

IIT RESEARCH INSTITUTE

## LIST OF TABLES

<u>Number</u>		<u>Page</u>
1	INORGANIC SURFACES (NONPAINTS) CONSIDERED FOR SCREENING AND ADSORBATE TESTS	4
2	INORGANIC PIGMENTED COATINGS (PAINTS) CONSIDERED FOR SCREENING AND ADSORBATE TESTS	5
3	ORGANIC AND SILICONE PIGMENTED COATINGS (PAINTS) CONSIDERED FOR SCREENING AND ADSORBATE TESTS	6
4	ANALYSIS OF RESEARCH GASES	23
5	EFFECT OF 800 ESH ULTRAVIOLET IRRADIATION IN THE IRIF ON PEGASUS COUPONS (Solar Intensity, 5X; Sample Temperature 8°C)	28
6	EFFECT OF ULTRAVIOLET IRRADIATION IN THE IRIF ON SELECTED THERMAL-CONTROL SURFACE COATINGS (IRIF Test 13; Solar Intensity = 6X)	56
7	EFFECT OF ULTRAVIOLET IRRADIATION IN THE IRIF ON SELECTED THERMAL-CONTROL SURFACE COATINGS (IRIF Test 15; Solar Intensity, 6X; Substrate Temperature 85°C)	67
8	CHANGE IN SPECTRAL ABSORPTANCE (%) OF SEVERAL PEGASUS COUPONS ON IRRADIATION FOR 800 ESH (Test 15)	66
9	EFFECT OF ULTRAVIOLET IRRADIATION IN THE IRIF ON SELECTED THERMAL-CONTROL SURFACE COATINGS (IRIF Test 16; Solar Intensity 6X)	79
10	BEHAVIOR OF A NUMBER OF SPECIMENS IN THE GASEOUS ADSORBATE TEST (OXYGEN)	94
11	EFFECT OF OXYGEN PRESSURE ON S-13	101
12	BEHAVIOR OF A NUMBER OF SPECIMENS IN THE GASEOUS ADSORBATE TEST (OXYGEN)	104
13	BEHAVIOR OF A NUMBER OF SPECIMENS IN THE GASEOUS ADSORBATE TEST (NITROGEN)	118

## LIST OF FIGURES

<u>Figure No.</u>		<u>Page</u>
1	THE IRIF MATED TO THE BECKMAN DK-2A SPECTRO-REFLECTOMETER	9
2	IRIF-II SPACE SIMULATION FACILITY	11
3	IRIF-II COMBINED RADIATION ENVIRONMENT FACILITY (CREF)	12
4a	RADIATION DISPLAYED (EPPLEY THERMOPILE) FOR AN AVERAGE A-H6 LAMP	14
4b	SOLAR FACTOR AT SAMPLE SURFACE AS A FUNCTION OF TOTAL ENERGY RECEIVED	16
5	CONTROLLED LEAK ASSEMBLY	18
6	GRANVILLE-PHILLIPS CONTROLLED LEAK	19
7	BAGGED IRIF-II: PUMP ADAPTOR COLUMN AND VALVE SOURCE ASSEMBLY	20
8	BAGGED IRIF-II: ALPHATRON GAUGE	21
9	GRID CURRENT AS A FUNCTION OF GRID VOLTAGE	25
10	ABSOLUTE REFLECTANCE OF ETCHED ALUMINUM SUBSTRATE AS A FUNCTION OF UV IRRADIATION IN IRIF TEST 10 (Not shown in Table 1)	29
11	ABSOLUTE REFLECTANCE OF ETCHED ALUMINUM SUBSTRATE AS A FUNCTION OF UV IRRADIATION IN IRIF TEST 10 (Not shown in Table 1)	30
12	ABSOLUTE REFLECTANCE OF TABOR MANGANESE BLACK SPECIMEN (#2) AS A FUNCTION OF UV IRRADIATION IN IRIF TEST 10	31
13	ABSOLUTE REFLECTANCE OF TABOR MANGANESE BLACK SPECIMEN (#2) AS A FUNCTION OF UV IRRADIATION IN IRIF TEST 10	32
14	ABSOLUTE REFLECTANCE OF MTL-3 CONVERSION COATING (#5) AS A FUNCTION OF UV IRRADIATION IN IRIF TEST 10	33

IIT RESEARCH INSTITUTE



<u>Figure No.</u>		<u>Page</u>
15	ABSOLUTE REFLECTANCE OF MTL-3 CONVERSION COATING (#5) AS A FUNCTION OF UV IRRADIATION IN IRIF TEST 10	34
16	ABSOLUTE REFLECTANCE OF SCHELD AHL 1275 ALODINED ALUMINIZED MYLAR (#7) AS A FUNCTION OF UV IRRADIATION IN IRIF TEST 10	35
17	ABSOLUTE REFLECTANCE OF SCHELD AHL 1275 ALODINED ALUMINIZED MYLAR (#7) AS A FUNCTION OF UV IRRADIATION IN IRIF TEST 10	36
18	ABSOLUTE REFLECTANCE OF SCHELD AHL GT-1015 ALUMINA COATED ALUMINUM (#8) AS A FUNCTION OF UV IRRADIATION IN IRIF TEST 10	37
19	ABSOLUTE REFLECTANCE OF SCHELD AHL GT-1015 ALUMINA COATED ALUMINUM (#8) AS A FUNCTION OF UV IRRADIATION IN IRIF TEST 10	38
20	ABSOLUTE REFLECTANCE OF Z93 (#16) AS A FUNCTION OF UV IRRADIATION IN IRIF TEST 10	39
21	ABSOLUTE REFLECTANCE OF Z93 (#16) AS A FUNCTION OF UV IRRADIATION IN IRIF TEST 10	40
22	ABSOLUTE REFLECTANCE OF TANTALA-PIGMENTED POTASSIUM SILICATE PAINT (#17) AS A FUNCTION OF UV IRRADIATION IN IRIF TEST 10	41
23	ABSOLUTE REFLECTANCE OF TANTALA-PIGMENTED POTASSIUM SILICATE PAINT (#17) AS A FUNCTION OF UV IRRADIATION IN IRIF TEST 10	42
24	ABSOLUTE REFLECTANCE OF LITHIUM FLUORIDE-PIGMENTED POTASSIUM SILICATE PAINT (#19) AS A FUNCTION OF UV IRRADIATION IN IRIF TEST 10	43
25	ABSOLUTE REFLECTANCE OF LITHIUM FLUORIDE-PIGMENTED POTASSIUM SILICATE PAINT (#19) AS A FUNCTION OF UV IRRADIATION IN IRIF TEST 10	44
26	ABSOLUTE REFLECTANCE OF ZIRCONIA-PIGMENTED POTASSIUM SILICATE PAINT (#23) AS A FUNCTION OF UV IRRADIATION IN IRIF TEST 10	45
27	ABSOLUTE REFLECTANCE OF ZIRCONIA-PIGMENTED POTASSIUM SILICATE PAINT (#23) AS A FUNCTION OF UV IRRADIATION IN IRIF TEST 10	46

<u>Figure No.</u>		<u>Page</u>
28	ABSOLUTE REFLECTANCE OF CLEANED S-13 (#30) AS A FUNCTION OF UV IRRADIATION IN IRIF TEST 10	47
29	ABSOLUTE REFLECTANCE OF CLEANED S-13 (#30) AS A FUNCTION OF UV IRRADIATION IN IRIF TEST 10	48
30	ABSOLUTE REFLECTANCE OF S-13 (UNCLEANED) (#34) AS A FUNCTION OF UV IRRADIATION IN IRIF TEST 10	49
31	ABSOLUTE REFLECTANCE OF S-13 (UNCLEANED) (#34) AS A FUNCTION OF UV IRRADIATION IN IRIF TEST 10	50
32	ABSOLUTE REFLECTANCE OF S-13G (BATCH A-295) (#35) AS A FUNCTION OF UV IRRADIATION IN IRIF TEST 10	51
33	ABSOLUTE REFLECTANCE OF S-13G (BATCH A-295) (#35) AS A FUNCTION OF UV IRRADIATION IN IRIF TEST 10	52
34	DEGRADATION RATES OF SEVERAL SURFACES EVALUATED IN IRIF-I TEST 13	58
35	DEGRADATION RATES OF SEVERAL SURFACES EVALUATED IN IRIF-I TEST 13	59
36	DEGRADATION RATES OF SEVERAL SURFACES EVALUATED IN IRIF-I TEST 13	60
37	ABSOLUTE REFLECTANCE OF PLASMOCLAY/ $K_2O \cdot SiO_2$ (#20) AS A FUNCTION OF UV IRRADIATION IN IRIF TEST 13	62
38	ABSOLUTE REFLECTANCE OF LITHAFRAX (#10) AS A FUNCTION OF UV IRRADIATION IN IRIF TEST 13	63
39	ABSOLUTE REFLECTANCE OF FEP TEFLON MIRROR AS A FUNCTION OF UV IRRADIATION IN IRIF TEST 13	64
40	ABSOLUTE REFLECTANCE OF RUTILE-OPACIFIED-POR- CELAIN ENAMEL (#25) AS A FUNCTION OF UV IRRADIATION IN IRIF TEST 13	65
41	ABSOLUTE REFLECTANCE OF AN OPTICAL SOLAR REFLECTOR (#2) AS A FUNCTION OF UV IRRADIATION IN IRIF TEST 15	68
42	ABSOLUTE REFLECTANCE OF LITHAFRAX (#11) AS A FUNCTION OF UV IRRADIATION IN IRIF TEST 15	69

<u>Figure No.</u>		<u>Page</u>
43	ABSOLUTE REFLECTANCE OF RUTILE-PIGMENTED LMSC-3 (#27) AS A FUNCTION OF UV IRRADIATION IN IRIF TEST 15	70
44	ABSOLUTE REFLECTANCE OF ZINC SULFIDE/O-I 650 (#36) AS A FUNCTION OF UV IRRADIATION IN IRIF TEST 15	71
45	ABSOLUTE REFLECTANCE OF ALUMINA/K-Sil (#26) AS A FUNCTION OF UV IRRADIATION IN IRIF TEST 15	72
46	ABSOLUTE REFLECTANCE OF WHITE KEMACRYL (#37) AS A FUNCTION OF UV IRRADIATION IN IRIF TEST 15	73
47	ABSOLUTE REFLECTANCE OF CAT-A-LAC BLACK (#38) AS A FUNCTION OF UV IRRADIATION IN IRIF TEST 15	74
48	ABSOLUTE REFLECTANCE OF CLEANED PEGASUS S-13 (#30) AS A FUNCTION OF UV IRRADIATION IN IRIF TEST 15	75
49	ABSOLUTE REFLECTANCE OF ZIRCONIA/K-Sil (#23) AS A FUNCTION OF UV IRRADIATION IN IRIF TEST 15	76
50	DEGRADATION RATES OF SEVERAL SURFACES EVALUATED IN IRIF TEST 16	80
51	DEGRADATION RATES OF SEVERAL SURFACES EVALUATED IN IRIF TEST 16	81
52	DEGRADATION OF SEVERAL SURFACES EVALUATED IN IRIF TEST 16	82
53	ABSOLUTE REFLECTANCE OF ZINC SULFIDE/O-I 650 (#36) AS A FUNCTION OF UV IRRADIATION IN IRIF TEST 16	83
54	ABSOLUTE REFLECTANCE OF TIN OXIDE/K-Sil (#22) AS A FUNCTION OF UV IRRADIATION IN IRIF TEST 16	84
55	DETAILED SPECTRA OF SCHJELDAHL GT-1015 (UV AND VISIBLE)	87
56	DETAILED SPECTRA OF SCHJELDAHL GT-1015 (INFRARED)	88
57	COMPARISON OF RATE DATA FROM IRIF-I TESTS FOR THE PEGASUS S-13 SPECIMENS (#30)	90

<u>Figure No.</u>		<u>Page</u>
58	COMPARISON OF RATE DATA FROM IRIF-I TESTS FOR THE ZIRCONIA/K-Sil SPECIMENS (#23)	91
59	EFFECT OF PARTIAL PRESSURES OF O <sub>2</sub> ON IRRADIATED RF-1 TiO <sub>2</sub> /O-I 650 (#39) TEST 2-2 <sup>2</sup>	95
60	EFFECT OF PARTIAL PRESSURES OF O <sub>2</sub> ON IRRADIATED PLASMOCLAY/K <sub>2</sub> O·SiO <sub>2</sub> (#20) TEST 2-2 <sup>2</sup>	96
61	EFFECT OF PARTIAL PRESSURES OF O <sub>2</sub> ON IRRADIATED PEGASUS S-13 (#30) TEST 2-2	97
62	EFFECT OF PARTIAL PRESSURES OF O <sub>2</sub> ON IRRADIATED RUTILE-PIGMENTED LMSC-3 (#27) TEST 2-2	98
63	EFFECT OF PARTIAL PRESSURES OF O <sub>2</sub> ON IRRADIATED LITHAFRAX (#11) TEST 2-2	99
64	EFFECT OF PARTIAL PRESSURES OF O <sub>2</sub> ON IRRADIATED ZINC SULFIDE/O-I 650 (#36) TEST 2-2	100
65	OXYGEN BLEACHING S-13 at 2.05μ	102
66	EFFECT OF 500 ESH Hg-Xe IRRADIATION AND BLEACHING WITH 760 TORR AMBIENT AIR ON A ZINC ORTHOTITANATE/O-I 650 PAINT - TEST 2-3	106
67	EFFECT OF 500 ESH Hg-Xe IRRADIATION AND BLEACHING WITH 760 TORR AMBIENT AIR ON IITRI'S BATCH A-574 S-13G - TEST 2-3	107
68	EFFECT OF 500 ESH Hg-Xe IRRADIATION AND BLEACHING WITH 760 TORR AMBIENT AIR ON RF-1 TiO <sub>2</sub> /O-I 650 (#39) - TEST 2-3	108
69	EFFECT OF 500 ESH Hg-Xe IRRADIATION AND BLEACHING WITH 760 TORR AMBIENT AIR ON TIN OXIDE/K-Sil (#22) - TEST 2-3	109
70	EFFECT OF 500 ESH Hg-Xe IRRADIATION AND BLEACHING WITH 760 TORR AMBIENT AIR ON ALUMINA/K-Sil (#26) - TEST 2-3	110
71	EFFECT OF 500 ESH Hg-Xe IRRADIATION AND BLEACHING WITH 760 TORR AMBIENT AIR ON ZIRCONIA/K-Sil (#23) - TEST 2-3	111

<u>Figure No.</u>		<u>Page</u>
72	EFFECT OF 500 ESH Hg-Xe IRRADIATION AND BLEACH- ING WITH 760 TORR AMBIENT AIR ON ZINC SULFIDE/ O-I 650 (#36) - TEST 2-3	112
73	BLEACHING BEHAVIOR TO OXYGEN OF S-13 AT 2050-nm WAVELENGTH (TEST 2-3)	114
74	OXYGEN BLEACHING OF S-13 THERMAL COATING AT 2.05 MICRONS	115
75	OXYGEN BLEACHING RATES OF S-13 AT 2.05 MICRONS	116
76	EFFECT OF 740 ESH Hg-Xe IRRADIATION AND BLEACH- ING WITH N <sub>2</sub> OF ZIRCONIA/K-Sil (#23) - TEST 2-4	119
77	EFFECT OF 740 ESH Hg-Xe IRRADIATION AND BLEACH- ING WITH N <sub>2</sub> OF A ZINC ORTHOTITANATE/O-I 650 PAINT - TEST 2-4	120
78	EFFECT OF 740 ESH Hg-Xe IRRADIATION AND BLEACH- ING WITH N <sub>2</sub> OF PEGASUS S-13 (#30) - TEST 2-4	121
79	EFFECT OF 740 ESH Hg-Xe IRRADIATION AND BLEACH- ING WITH N <sub>2</sub> OF RUTILE-PIGMENTED LMSC-3 (#27) - TEST 2-4	122
80	NITROGEN BLEACHING OF S-13 AT 2.05 $\mu$	124
81	EFFECT OF 660 ESH Hg-Xe IRRADIATION AND BLEACH- ING WITH CO <sub>2</sub> OF PEGASUS S-13 (#30) - TEST 2-8	126
82	EFFECT OF 660 ESH Hg-Xe IRRADIATION AND BLEACH- ING WITH CO <sub>2</sub> OF DU PONT R900 RUTILE POWDER - TEST 2-8	127
83	EFFECT OF $\phi\phi$ ) ESH Hg-Xe IRRADIATION AND BLEACH- ING WITH CO <sub>2</sub> OF ZnO:Zn POWDER (SP500 ZnO) - TEST 2-8	128
84	EFFECT OF 660 ESH Hg-Xe IRRADIATION AND BLEACH- ING WITH CO <sub>2</sub> OF A ZINC SULFIDE/O-I 650 PAINT - TEST 2-8	129
85	EFFECT OF 660 ESH Hg-Xe IRRADIATION AND BLEACH- ING WITH CO <sub>2</sub> OF A ZINC ORTHOTITANATE/O-I 650 PAINT - TEST 2-8	130
86	REFLECTANCE OF S-13 AT 2050 nm AS A FUNCTION OF CARBON DIOXIDE PRESSURE	132



<u>Figure No.</u>		<u>Page</u>
87	A TYPICAL 100% LINE FOR THE IRIF-II FACILITY	138
88	SPECTRA OF UV IRRADIATED OSR (LMSC-1)	139

STUDY OF IN SITU DEGRADATION OF  
THERMAL CONTROL SURFACES

I. INTRODUCTION

The Pegasus III spacecraft, which was launched from Cape Kennedy on July 30, 1965, was used for an unique flight experiment to determine space-environment effects on a variety of thermal-control surfaces. A large number of "retrievable" coupons were coated with various thermal-control materials and were placed on the Pegasus III satellite with the intent that they would eventually be (1) measured "optically" in situ, and/or (2) returned to earth by a rendezvousing astronaut for evaluation. Although no mission to retrieve the coupons has been approved by NASA, it is hoped that a Pegasus rendezvous or a similar flight experiment can eventually be effected and that coupons of this type can be returned for study and evaluation.

This research program was planned to provide the technical background that is necessary for the proper evaluation of the space-environment-induced damage that has been sustained by the Pegasus coupons. The fact that many of the specimens will exhibit saturated damage in spectrally sensitive regions, coupled with the known sensitivity of many of the damaged specimens to even small partial pressures of oxygen, made the laboratory investigation of closely similar, if not identical, surface coatings necessary. A knowledge of the effects of very small partial pressures of oxygen and of "inert" gases such as argon are required in order to aid in the design of methods to retrieve the coupons. This information will also provide a basis for interpreting the effects of partial pressure of various gases at high vacuum that might result from the development of small leaks in transfer apparatus, as well as from any massive leaks that might

occur. Stated simply, it has been necessary to determine the extent to which all specimens are bleached by various partial pressures of a number of gases.

Although the primary reason for initiation of this study was to aid in the development of methods of handling and interpreting the damage to the flight-experiment coupons, it was believed that these studies would also help to advance our understanding of the mechanisms associated with space-radiation-induced damage. Indeed, this has been the case; for example, the gas-adsorbate studies have raised some very important questions concerning the role of the surface defect state in photolysis mechanisms. These studies have suggested that surface sites might be expeditiously investigated by gaseous adsorbate techniques. The effect of monomolecular and polymolecular layers of water ( $\text{OH}^-$ ) on photolysis reactions are suggested as an area to be more carefully assessed. A paint prepared from pigment that first possesses a low surface free energy, and secondly that has been fully desorbed of moisture (and for example carbon dioxide) might, if incorporated into the paint in this condition, exhibit considerably different optical properties compared to otherwise identical materials.

## II. SPECIMEN SELECTION AND PROCUREMENT

The thermal-control surfaces submitted to NASA's George C. Marshall Space Flight Center for inclusion on the Pegasus III experiment encompassed 50 major types of surfaces, 107 different systems, and 352 individual samples (ref. 1). These samples were submitted by six respondents and represented the efforts of 15 individual firms and organizations (ref. 1).

Our original objective was to select 20 different systems for initial screening. The selection was made on the basis that the greatest possible number of major types and pigment/binder combinations (in the case of pigment coatings) should be evaluated. Some of the factors that were considered in the selection of test specimens were:

- (1) Could identical, or exactly similar specimens be procured; i.e., were specimens still available?
- (2) Would evaluation of any given specimen have real significance in terms of either its potential as a thermal-control surface or its contribution to our understanding of environmental damage mechanisms?
- (3) Would evaluation of any of the specimens in the IRIF result in contamination of the facility?
- (4) Would any of the specimens be so severely damaged in short exposures (i.e., saturated) that their usefulness in the context of this program would be impaired?
- (5) Would the selection of specimens other than those flown on Pegasus III have utility within the context of this study?

A summary of the Pegasus samples that were considered for evaluation in this study is presented in Tables 1 through 3. Table 1 lists nine inorganic surfaces (nonpaints); of these, eight were included on Pegasus III. Table 2 lists 17 inorganic paints (i.e., they all employ inorganic binders as well as inorganic pigments), nine of which were flown on Pegasus III.

Table 1

## INORGANIC SURFACES (NONPAINTS) CONSIDERED FOR SCREENING AND ADSORBATE TESTS

Item	Specimen No. <sup>a</sup>	Description	Source (Manufacturer) <sup>b</sup>	Tested	IRIF Test No.		Comments
					Screening	Adsorbate	
1	LMSC-1	Optical solar reflector (OSR)	Lockheed MSC (OCLI)	Yes	15	2-2, 2-3	Specimens received on 11-1-67. Specimens used as control in adsorbate tests.
2	MN-1 (11)	Manganese black	Lockheed MSC (National Physical Institute, Israel) <sup>c</sup>	Yes	10	No	No response from Israel's NPI for additional specimens. Original prepared by Dr. Henry Taber; specimen furnished by NASA, Ames.
3	MSFC-10	SiO <sub>x</sub> + Al-Mylar	NASA, MSFC (?)	No	N/A	N/A	Specimen received on 5-1-67. Destroyed at IITRI during sample preparation. No others available.
4	MSFC-2	Anodized aluminum	NASA, MSFC	No	N/A	N/A	Specimen received on 5-1-67. Destroyed at IITRI during sample preparation.
5	MTL-3	Alodine (Pegasus I)	Fairchild Hiller	Yes	10, 19	No	Gas adsorbate studies were not performed. Specimen received on 5-1-67.
6	2	Al + SiO + Al	NASA, Ames (Hass, AERDL)	No	N/A	N/A	One specimen obtained; destroyed fabricating coupon. Unable to obtain additional specimens from AERDL (Al {opaque}+SiO(8/4 λ at 550 nm)+Al (~60 nm).
7	GT-1275	Alodine (Echo II) (Al-Mylar	NASA, Langley (Schjeldahl)	Yes	10, 13	No	Gas adsorbate studies were not performed. Specimens received on 8-26-67.
8	GT-1015	Al <sub>2</sub> O <sub>3</sub> +Al-Mylar	NASA, MSFC (Schjeldahl)	Yes	10, 13	No	Gas adsorbate studies were not performed. Specimens received on 5-1-67.
9	-	FEP Teflon second surface (aluminum)	JPL (?)	Yes	13	No	Although this material was not included on Pegasus III, it was flown on Mariner V and is included here. Gas adsorbate studies were not performed on the FEP mirror.

<sup>a</sup>Specimen numbers assigned to Pegasus III specimens by source.<sup>b</sup>Manufacturer given in parenthesis if different from source.<sup>c</sup>Although the Pegasus III specimen was furnished by Lockheed, the specimen irradiated in this test was furnished by NASA, Ames.



Table 2

## INORGANIC PIGMENTED COATINGS (PAINTS) CONSIDERED FOR SCREENING AND ADSORBATE TESTS

Item	Specimen No. <sup>a</sup>	Description	Source (Manufacturer) <sup>b</sup>	Tested	IRIF Test No. <sup>c</sup>		Comments
					Screening	Adsorbate <sup>d</sup>	
10	-	Lithafrax	IITRI (LMSC)	Yes	13	No	Different batch from that furnished Pegasus III. Specimen prepared by IITRI.
11	LMSC-2	Lithafrax (lithium aluminum silicate-pigmented Na <sub>2</sub> O·SiO <sub>2</sub> )	LMSC	Yes	15	2-2	Received from source on 11-1-67. Specimen prepared by LMSC.
12	D-9	Sb <sub>2</sub> O <sub>3</sub> /K-Sil	Fairchild Hiller	No	N/A	N/A	Specimens not requested due to known sensitivity to UV; probably saturated. (See Item 21).
13	1304	ZrO <sub>2</sub> /K-Sil	NASA, Ames	No	N/A	N/A	Decided to evaluate IITRI analog instead.
14	M76	r-TiO <sub>2</sub> /K-Sil	NASA, Goddard	No	N/A	N/A	Extra specimens not requested.
15	M86-94	Al <sub>2</sub> O <sub>3</sub> /K-Sil	NASA, Goddard	No	N/A	N/A	Extra specimens not requested in favor of IITRI preparation. (See Item 26).
16	E-1	Z93 (SP500 ZnO/PS7)	IITRI	Yes	10,13	No	Not tested in adsorbate experiments because of stability; i.e., no bleachable damage.
17	M	Ta <sub>2</sub> O <sub>5</sub> /K-Sil (PS7)	IITRI	Yes	10	No	Not tested in adsorbate experiments because of nonbleachability of excessive damage.
18	J	Y <sub>2</sub> O <sub>3</sub> /K-Sil (PS7)	IITRI	No	N/A	N/A	Additional specimens could not be prepared.
19	L	LiF/K-Sil (PS7)	IITRI	Yes	10	No	Not tested in adsorbate experiments because of nonbleachability of excessive damage.
20	-	Plasmoclay/K <sub>2</sub> O·SiO	Hughes AC	Yes	13	2-2,2-3,2-4	Surveyor coating received on 9-7-67.
21	-	Sb <sub>2</sub> O <sub>3</sub> /K-Sil (PS7)	IITRI	No	N/A	N/A	Not tested at all due to quick saturation of UV-induced damage.
22	-	SnO <sub>2</sub> /K-Sil (PS7) <sup>e</sup> (PBR=4.3)	IITRI	Yes	15,16	2-2,2-3,2-4	Simulated SNAP-10 radiator coatings.
23	-	ZrO <sub>2</sub> /K-Sil (PS7) (PBR=4.3)	IITRI	Yes	10,13,15,16	2-2,2-3,2-4	Prepared from TAM "CP".
24	-	Z93 (SP500 ZnO/PS7)	IITRI	Yes	13	No	This specimen of Z93 was 2-yr old when irradiated in Test 13.
25	-	Rutile-opacified procelain enamel <sup>f</sup>	IITRI (Chicago Vit.)	Yes	13	No	Not tested further due to high stability, i.e., no bleachable damage was sustained.
26	-	α-Al <sub>2</sub> O <sub>3</sub> /K-Sil (PS7) (PBR=4.3)	IITRI	Yes	15,16	2-2,2-3,2-4	Prepared from Alucer MC α-Al <sub>2</sub> O <sub>3</sub> .

<sup>a</sup>Specimen numbers assigned by source for Pegasus III specimens.<sup>b</sup>Manufacturer given in parenthesis if different from source.<sup>c</sup>IRIF I tests employing 1000 watt A-H6 source.<sup>d</sup>IRIF II tests employing 5000 watt Hg-Xe source.<sup>e</sup>Prepared according to instructions of J. Crosby, formerly with Atomics International.<sup>f</sup>Borosilicate glass frit.

Table 3

## ORGANIC AND SILICONE PIGMENTED COATINGS (PAINTS) CONSIDERED FOR SCREENING AND ADSORBATE TESTS

Item	Specimen No. <sup>a</sup>	Description	Source (Manufacturer) <sup>b</sup>	Tested	IRIF Test No.		Comments
					Screening <sup>c</sup>	Adsorbate <sup>d</sup>	
27	LMSC-3	r-TiO <sub>2</sub> /silicone elastomer	LMSC (Dow Corning)	Yes	15,16	2-2,2-3,2-4	Received on 11-1-67. Based on Dow Corning methyl silicone elastomer.
28	2-3	3-M black paint	NASA, Goddard (3M)	No	N/A	N/A	Not evaluated in favor of Cat-a-lac black. See Item 38.
29	2-7	Aluminum leafing paint	NASA, Goddard	No	N/A	N/A	Not requested.
30	MSFC-9	S-13 (Pegasus I) clean	NASA, MSFC (IITRI)	Yes	10,13,15,16	2-2,2-3,2-4	Specimens painted on 11-4-64 and removed (as control) from Pegasus I prior to launch.
31	EAL	r-TiO <sub>2</sub> (Cabot)/RTV-602	IITRI	No	N/A	N/A	Cabot's RF-1 flame process rutile used. Not evaluated in favor of Item 39 below.
32	51-62-24	ZnS/Q9-0108	IITRI	No	N/A	N/A	Not evaluated due to inability to procure identical Q9-0108. (See Item 36 below).
33	19	VMCH (0.3 mil)	NASA, Ames	No	N/A	N/A	Source could not prepare identical specimens and they were judged too sensitive to UV.
34	MSFC-9	S-13 (Pegasus I) uncleaned	NASA, MSFC (IITRI)	Yes	10		Specimen intentionally dirtied with sebum. (See Item 30 above).
35	-	S-13G (silicated SP500 ZnO/RTV-602)	IITRI	Yes	10,13	2-3	Early formulation employed. Batch A-295.
36	-	ZnS/Owens-Illinois (O-I) 650 (silicone enamel)	IITRI	Yes	15,16	2-2,2-3,2-4	XXXN ZnS employed at 30% PVC.
37	-	Kemacryl, white	IITRI (Sherwin Williams)	Yes	15,16	No	Not tested in IRIF II because of certainty of contamination of facility.
38	-	Cat-a-lac black	IITRI (Andrew Brown)	Yes	15,16	No	Not tested in IRIF II because of certainty of contamination of facility.
39	-	r-TiO <sub>2</sub> (Cabot)/O-I650	IITRI	Yes	No	2-2,2-3,2-4	Cabot's RF-1 flame process rutile employed at 30% PVC.
40	-	Zn <sub>2</sub> TiO <sub>4</sub> /O-I650 (silicone enamel)	IITRI	Yes	No	2-3,2-4	Zn <sub>2</sub> TiO <sub>4</sub> synthesized at IITRI. (PVC=30%).
41	-	CaWO <sub>4</sub> /O-I650 (silicone enamel)	IITRI	Yes	No	2-3,2-4	CaWO <sub>4</sub> purchased from Sylva. (PVC=30%).
42	-	Gd <sub>2</sub> O <sub>3</sub> /O-I650 (silicone enamel)	IITRI	Yes	No	2-4	Gd <sub>2</sub> O <sub>3</sub> purchased from American Potash (PVC=30%).

<sup>a</sup>Specimen numbers assigned by source for Pegasus III specimens.<sup>b</sup>Manufacturer given in parenthesis if different from source.<sup>c</sup>IRIF I tests employing 1000 watt A-H6 source.<sup>d</sup>IRIF II tests employing 5000 watt Hg-Xe source.<sup>e</sup>Prepared according to instructions of J. Crosby, formerly with Atomics International.

Table 3 lists 16 organic (and silicone-based) pigmented coatings; of these, eight were included on Pegasus III. In summary, 42 samples of thermal-control surfaces were considered for evaluation on this program; of this total 28 were irradiated in either or both IRIF-I and IRIF-II. Seventeen specimens that were not included on the Pegasus III coupons were considered for evaluation; of these, all but one were irradiated in this study.

The difficulties associated with sample procurement represented a major problem during the first ten months of the research program. For example, the initial sample procurement was not completed until November 1, 1967 - eight months after initiation of the research contract. In some instances, all specimens available were submitted for inclusion on Pegasus III; in other cases, specific coatings could be duplicated only with substitute ingredients; and in still other instances, the remaining specimens were too fragile for preparation of IRIF coupons.

It subsequently became both necessary and desirable to employ coatings prepared at IIT Research Institute that were not flown on Pegasus III. Such coatings were prepared for one or more of the following reasons:

- (1) The coatings were of technical interest because of their employment on other spacecraft (items 9, 20 and 22).
- (2) The coatings were easier to prepare at IITRI than to obtain from the original source (items 23, 26 and 39).
- (3) The coatings were of technical interest because of specific peculiarities of stability and/or degradation (items 25, 35-38 and 40-42).

### III. EXPERIMENTAL PROCEDURES

#### A. The IRIF-I Space-Simulation Facility

The IRIF-I space-simulation facility was employed in four specimen-screening tests - IRIF-I tests 10, 13, 15 and 16. The IRIF, an acronym for "In Situ Reflectometer/Irradiation Facility," is a multiple-sample, solar ultraviolet-simulation chamber that possesses the capability of performing in situ\* hemispherical-spectral-reflectance measurements. The integrating sphere is patterned after Edwards et al (ref. 2), modified for the Beckman DK-2A spectrophotometer. The facility is discussed in detail in a paper by Zerlaut and Courtney (ref. 3).

The major features of the facility include:

- (1) Operation as an easily detached module to the Beckman DK-2A spectrophotometer
- (2) Operation of the integrating sphere in vacuum at  $\sim 10^{-7}$  torr by pumping through a manifold (through which the incident light beams pass) and through the shuttered sample aperture between the sphere and the vacuum chamber
- (3) A 12-sample sample-exchange mechanism that maintains the specimens in contact with a temperature-controlled sample table and that permits the transfer of any one of the 12 samples to the integrating sphere for measurement and the subsequent return to the sample table for continued irradiation.

The IRIF-I, along with its 400 liter/sec Varian VacIon vacuum pump, rests on a heavy-duty dolly and is rolled from the A-H6 ultraviolet irradiation station to the Beckman DK-2A spectrophotometer. The facility is precision mounted to the spectrophotometer by turning down set screws into chocks that are mounted to the floor. Figure 1 shows the IRIF-I mated to the Beckman DK-2A spectrophotometer with the operator opening the shutter prior to transferring a sample into the integrating sphere.

---

\*In situ is taken to mean "measured without removal from vacuum" in the context of this discussion.

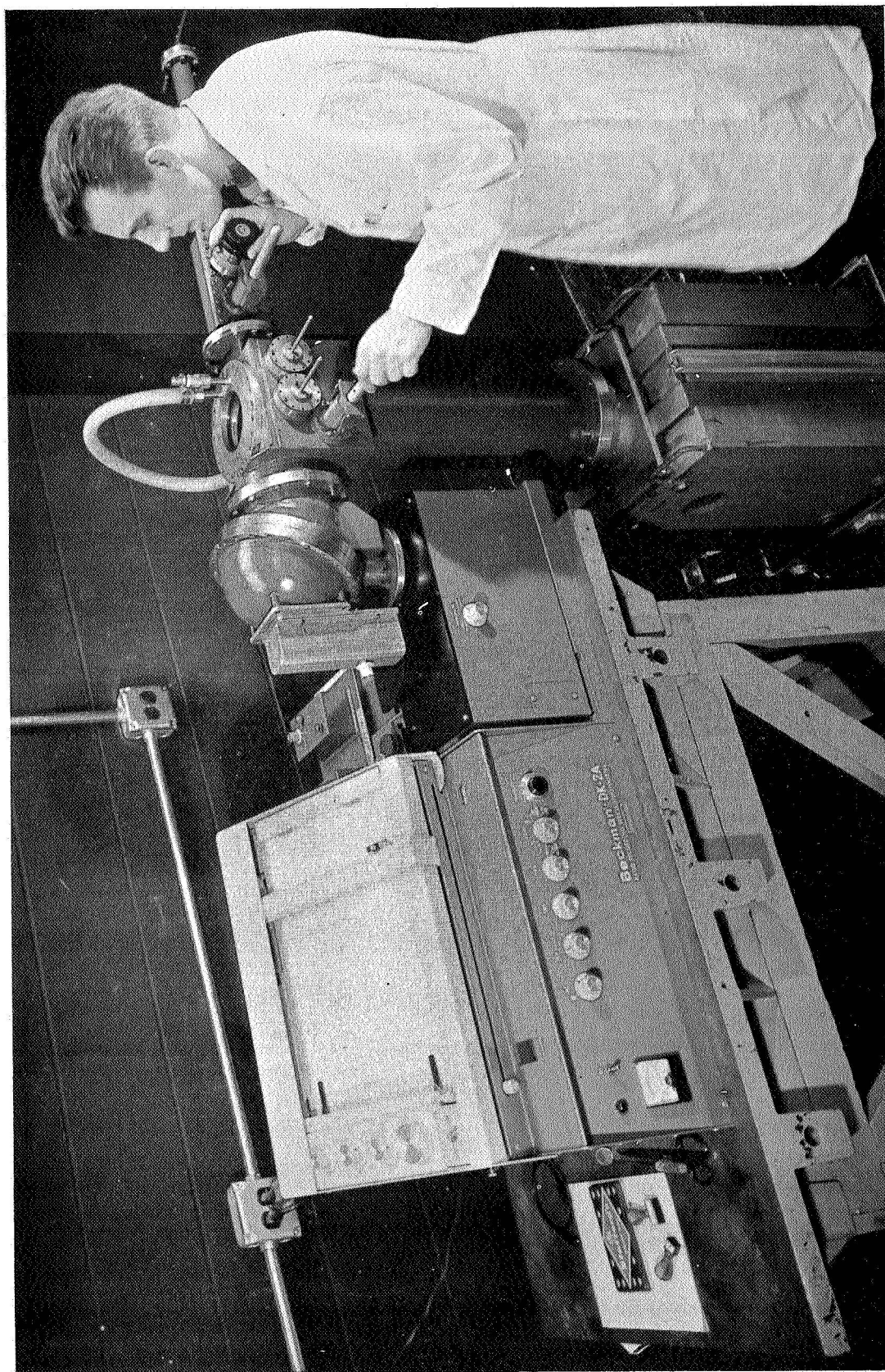


Figure 1: THE IRIF MATED TO THE BECKMAN DK-2A SPECTROREFLECTOMETER



## B. The IRIF-II Space-Simulation Facility

The IRIF-II space-simulation facility is similar to IRIF-I except that:

- (1) It possesses an improved sample-interchange mechanism.
- (2) It possesses an NRC Alphatron pressure gauge as an integral part of the facility.
- (3) It is permanently mated to a Beckman DK-1 spectrophotometer.
- (4) It possesses a multiple-source-housing adaptor that permits a solar-wind proton gun to be employed in conjunction with ultraviolet irradiation. (Solar-wind proton studies were not performed in this investigation.)

The IRIF-II is pumped with a 400 liter/sec Ultek ion pump and is rough-pumped with a pair of 'sorption pumps.

A 5-kw Hanovia mercury-xenon source is employed with IRIF-II. The facility with the ultraviolet source in place is shown in Figure 2. Figure 3 shows the IRIF-II with the proton gun (solar wind simulator) attached to the multiple-source adaptor.

## C. Computation of Solar Adsorptance

Solar absorptance is computed from the hemispherical spectral reflectance data by integration with the standard Johnson solar energy spectrum. The computation of solar reflectance is performed simply by the addition of the reflectances ( $\times 0.02$ ) of 50 equal-energy wavelengths. The reflectances are listed by employing a photo-positive overlay over the raw-data reflectance chart-paper: Two overlays (one for the 325- to 700-nm and one for the 700- to 2700-nm wavelength regions) are employed for the Beckman DK-2A data and one overlay is used in reducing the DK-1 data.

The data are divided into two solar-absorptance components,  $\alpha_1$  and  $\alpha_2$ ; these two components are chosen such that each encompasses one-half of the integrated energy in the Johnson

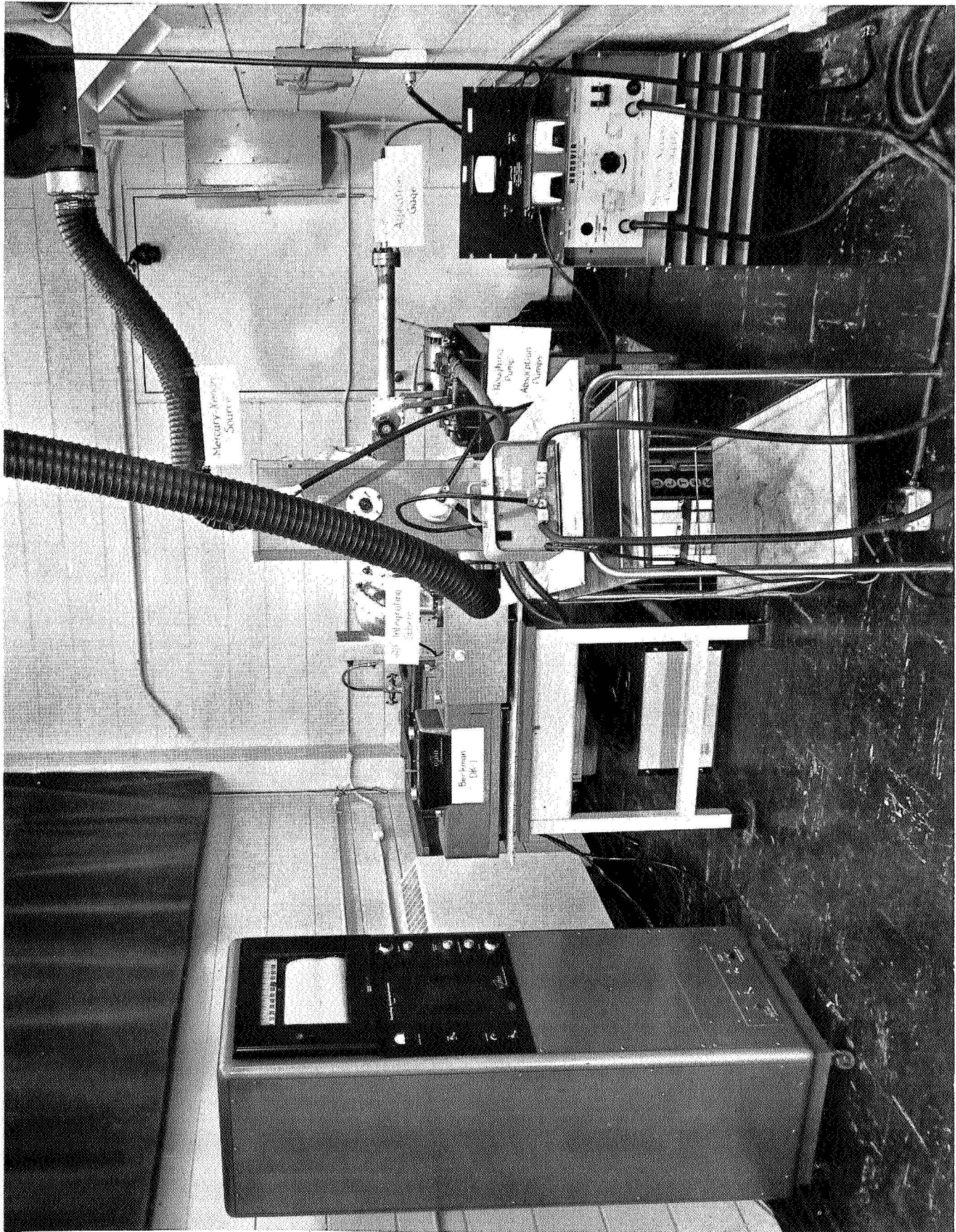


Figure 2: IRIF-II SPACE SIMULATION FACILITY



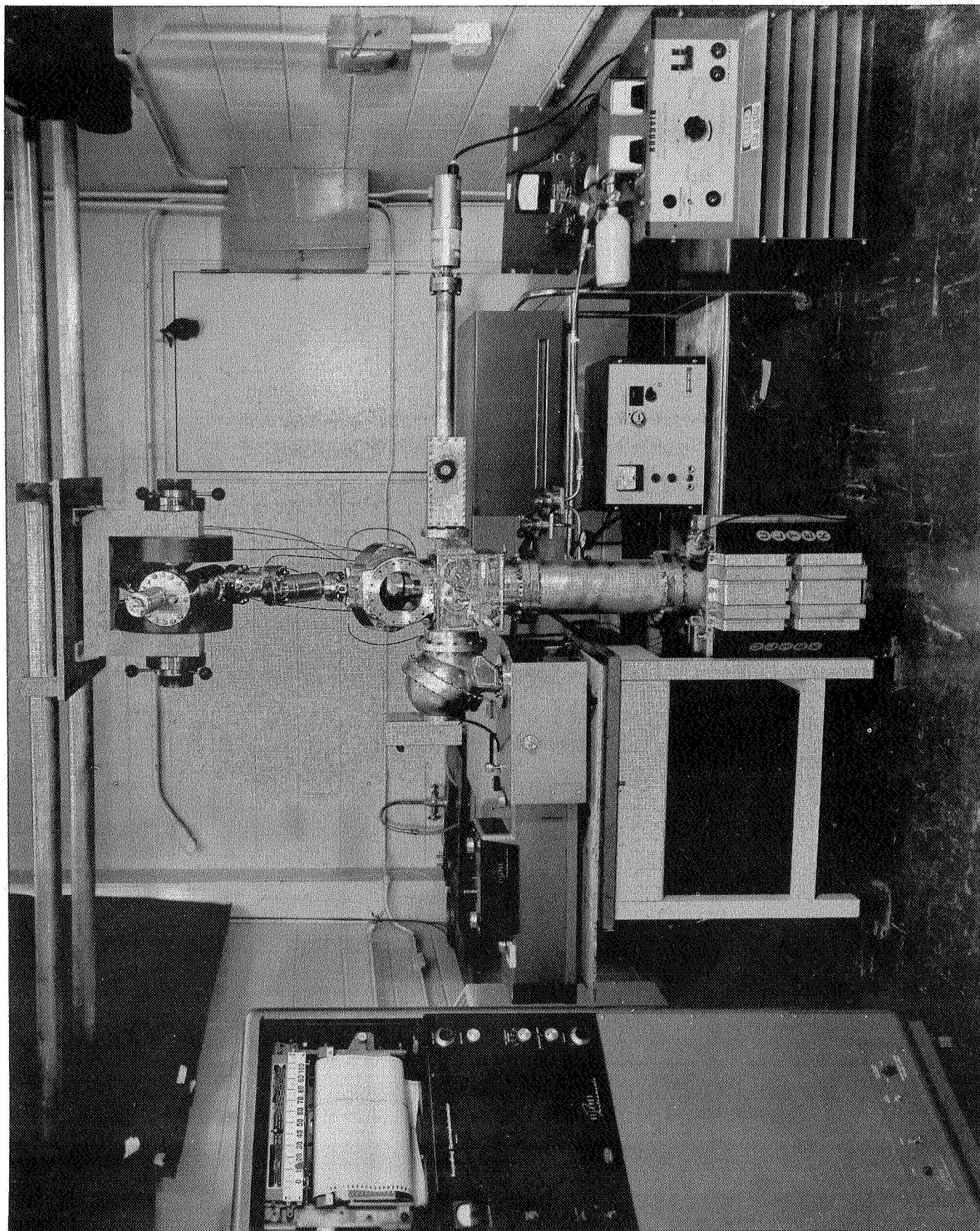


Figure 3: IRIF-II COMBINED RADIATION ENVIRONMENT FACILITY (CREF)

spectrum. Thus,  $\alpha_1$  represents all energy below about 700-nm and  $\alpha_2$  represents all energy of greater wavelength, such that the following identity can be made:

$$\alpha_1 + \alpha_2 = \alpha_s.$$

Computation and reporting of solar absorptance data in this manner permits quick and easy reference to that portion of the spectrum that undergoes the greatest amount of damage.

#### D. Ultraviolet Sources Employed

##### 1. The A-H6 Mercury Argon Source

Because of a number of factors, chief among which was economical operation, the General Electric 1000 watt A-H6 lamp was employed in all IRIF-I screening tests. Another factor that prompted its consideration is the high ratio of ultraviolet to visible (and infrared) energy. Accelerated ultraviolet testing at several equivalent solar factors (based on total ultraviolet only) is possible. Accelerations of 10 equivalent solar factors are easily achieved with an A-H6 lamp (compared to a maximum of about 4 for 5 kw mercury-xenon and about 1.5 for 5 kw xenon sources).

The principal problems associated with the use of A-H6 mercury-argon sources are twofold: (1) they possess a low order continuum with strong mercury emission lines superimposed, and (2) they exhibit short lifetimes and considerable instability of spectral distribution as a function of age and number of starts. For that reason, we change A-H6 lamps every 72 hr during tests of longer duration.

Lamp intensity (in equivalent solar factors) is determined by first comparing the lamp to be employed to the characteristics of an "average" lamp. The "average" lamp characteristics have been determined over a period of time by plotting the output in watts of a number of lamps as a function of lamp-to-detector distance. A linear plot (Figure 4a) was drawn as an "average"

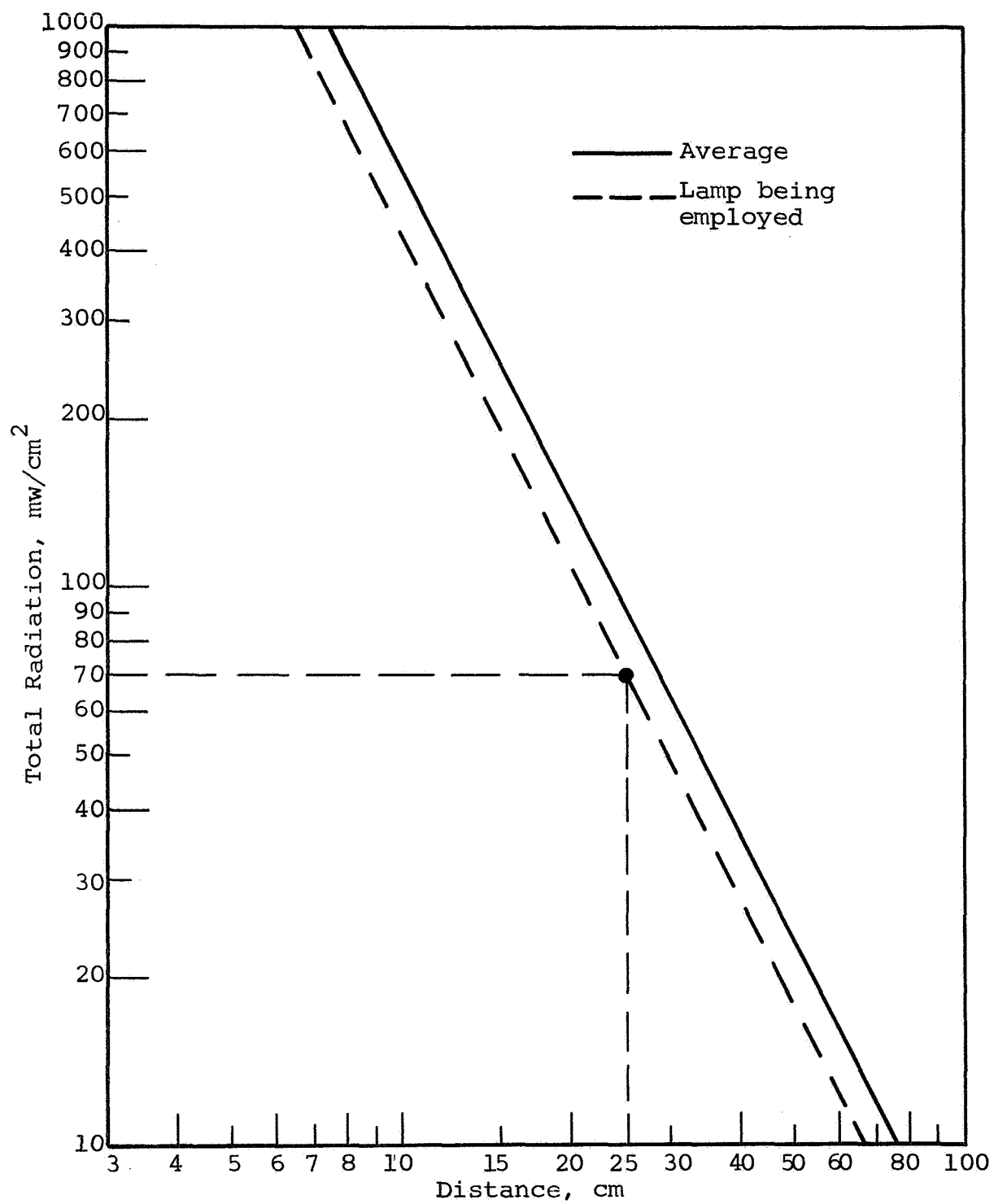


Figure 4a: RADIATION DISPLAYED (EPPLEY THERMOPILE) FOR AN AVERAGE A-H6 LAMP

to be used for calibrating A-H6 lamps. The detector employed is a Model S wide-angle temperature-compensated thermopile obtained from the Eppley Laboratories; it possesses a constant of  $6.98 \text{ mv} \cdot \text{cal}^{-1} \cdot \text{cm}^{-2} \cdot \text{min}^{-1}$ . The operating characteristics of any given lamp are determined by measuring its output at 25 cm. These data are then plotted on Figure 4a and a line is drawn through this point parallel to the average data curve (tedius calibration is thus avoided on a routine basis). Reference is then made to Figure 4b, which is a plot of the equivalent solar (ultraviolet) factor as a function of total radiation received (by the thermopile). Figure 4b was prepared by assuming that 30% of A-H6 radiation is in the 200- to 400-nm range and that "one" solar factor is  $13 \text{ mv/cm}^2$ . These two plots are thus sufficient to establish the lamp-to-sample distance of a given lamp required to achieve a given solar factor.

## 2. The Mercury-Xenon Source

A 5000 watt Hanovia mercury-xenon burner was employed in conjunction with all IRIF-II tests (in the gas adsorbate studies). The power supply and universal housing (which will accept 5 kw xenon arcs also and which are used in other studies) are shown in Figure 2. We prefer the mercury-xenon to the xenon lamp for two reasons: (1) Hg-Xe sources possess a greater amount of ultraviolet in the 200- to 230-nm wavelength region, and (2) xenon sources possess intense emission bands in the near infrared (850- to 1000-nm) that require filtering. The combination of filtering and low ultraviolet intensity at short wavelengths make accelerated testing with a xenon lamp difficult, if not impossible, for single arrays. The lamp output of the two sources are compared for 1000 watt sources below:

Spectral Range (nm)	Total Watts Radiated*	
	Hg-Xe	Xe
200 - 210	0.19	0.04
210 - 220	0.72	0.07
220 - 230	1.09	0.10
230 - 240	2.15	0.14
240 - 250	2.86	0.18

\*Hanovia product data.

IIT RESEARCH INSTITUTE

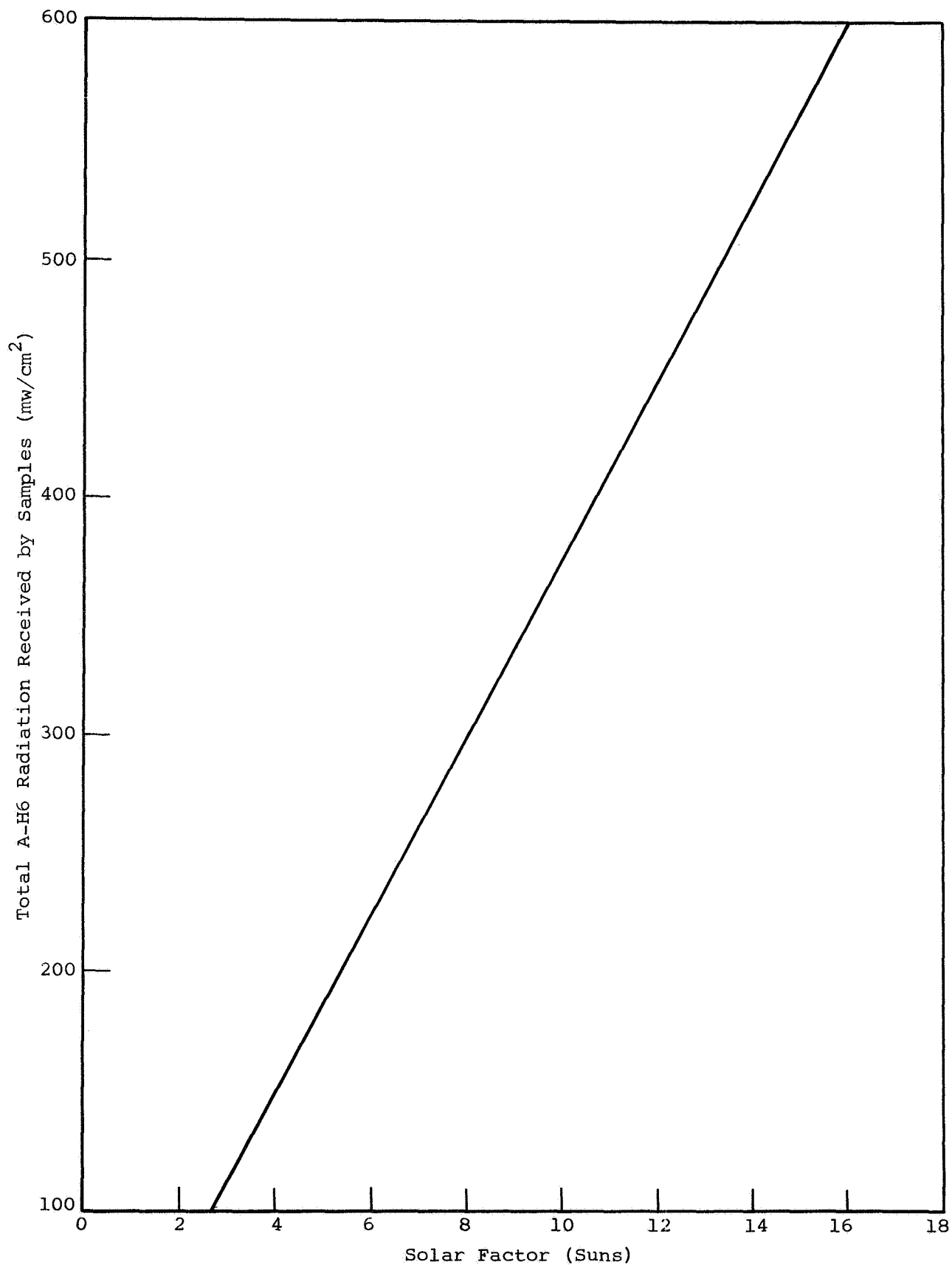


Figure 4b: SOLAR FACTOR AT SAMPLE SURFACE AS A FUNCTION OF TOTAL ENERGY RECEIVED

We therefore chose the Hg-Xe burner for the gaseous adsorbate tests. The source was operated at 80% of capacity (4000 watts input) in order to minimize instability and maximize life. No data has been collected on spectral instability and disproportionate spectral degradation; lamps are currently changed after 1000 hr of accumulated operation.

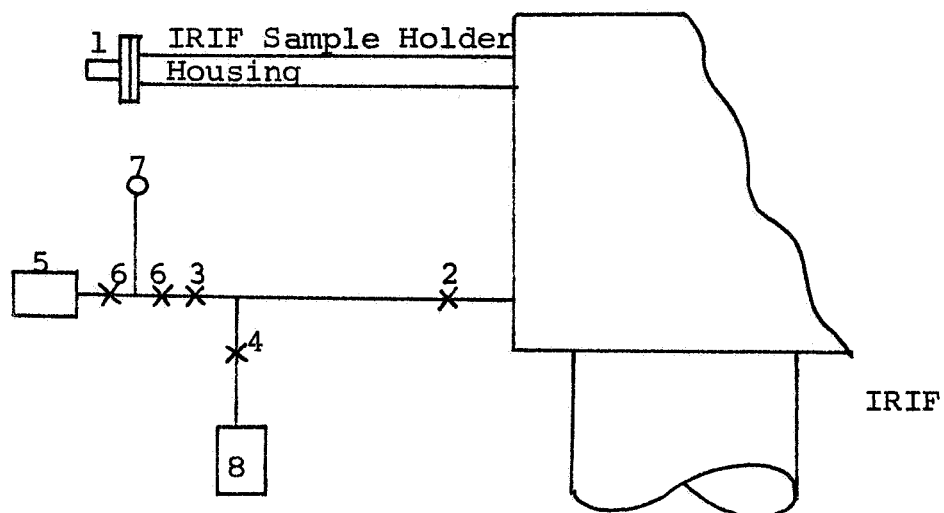
#### E. Gas Adsorbate Apparatus

The controlled and slow admission of high-purity adsorbate gases was performed as the terminating procedure in IRIF-II space-simulation tests 2, 3, 5 and 6. The admission of research gases was controlled with two Granville-Phillips Type C valves and an NRC #720 Alphatron pressure gauge. A schematic of the test setup employed in the gas adsorbate experiments is shown in Figure 5. A photograph of the IRIF-II's main valve and the two Granville-Phillips gauges is shown in Figure 6.

The entire IRIF-II facility, including the valves and gauges, was enclosed in a polyethylene "tent" and pressurized with the same gas that was admitted to the IRIF in the adsorbate experiment. The use of a highly pure (but not research grade because of the cost) gas to pressurize the polyethylene envelope ensured that the admission of gases other than the gas being investigated would be precluded (except for major leaks). Close-up photographs of the bagged valve arrangement and the Alphatron gauge are shown in Figures 7 and 8, respectively. The bottle of research gas, in this case carbon dioxide, is shown in Figure 7.

Typical operating procedures for the gas adsorbate studies are presented in Appendix A. In general, the procedure consisted of placing the specimen to be studied in the integrating sphere and setting the Beckman DK-1 spectrophotometer on the wavelength of interest. For zinc oxide, and in particular for IITRI's S-13 thermal control coating, the wavelength of interest was 2050 nm. The strip chart was operated with the slit-servo-controlled wavelength drive disconnected. In this manner the





- 1 - Pressure Gauge 0-800 torr
- 2 - Main System Valve
- 3 - 4 - Granville Phillips Type C Leak Valve
- 5 - Gas Supply Tank
- 6 - Control Valves
- 7 - Pressure Gauge
- 8 - Mechanical Pump

Figure 5: CONTROLLED LEAK ASSEMBLY

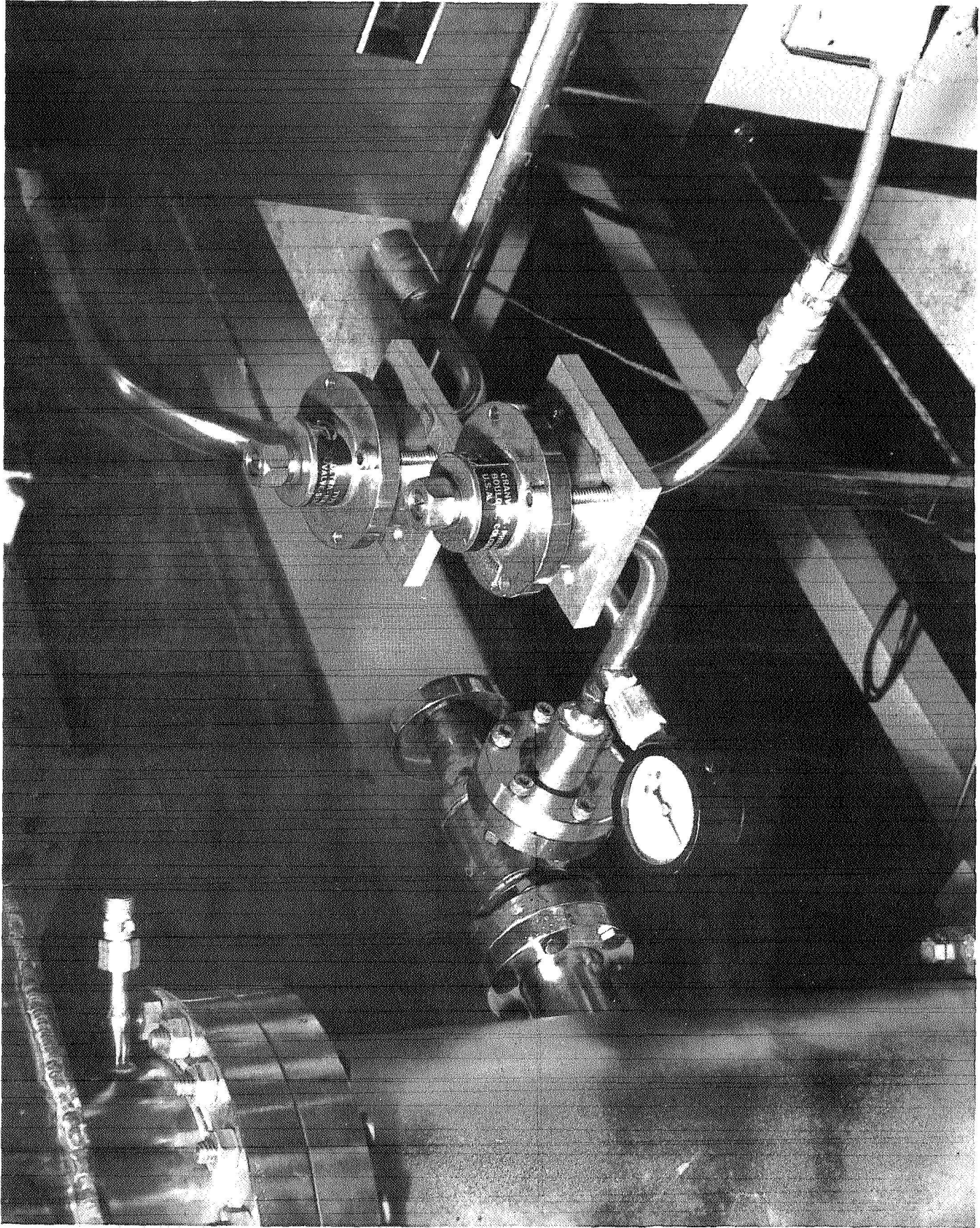


Figure 6: GRANVILLE-PHILLIPS CONTROLLED LEAK





Figure 7: BAGGED IRIF-II: PUMP ADAPTOR COLUMN AND VALVE SOURCE ASSEMBLY



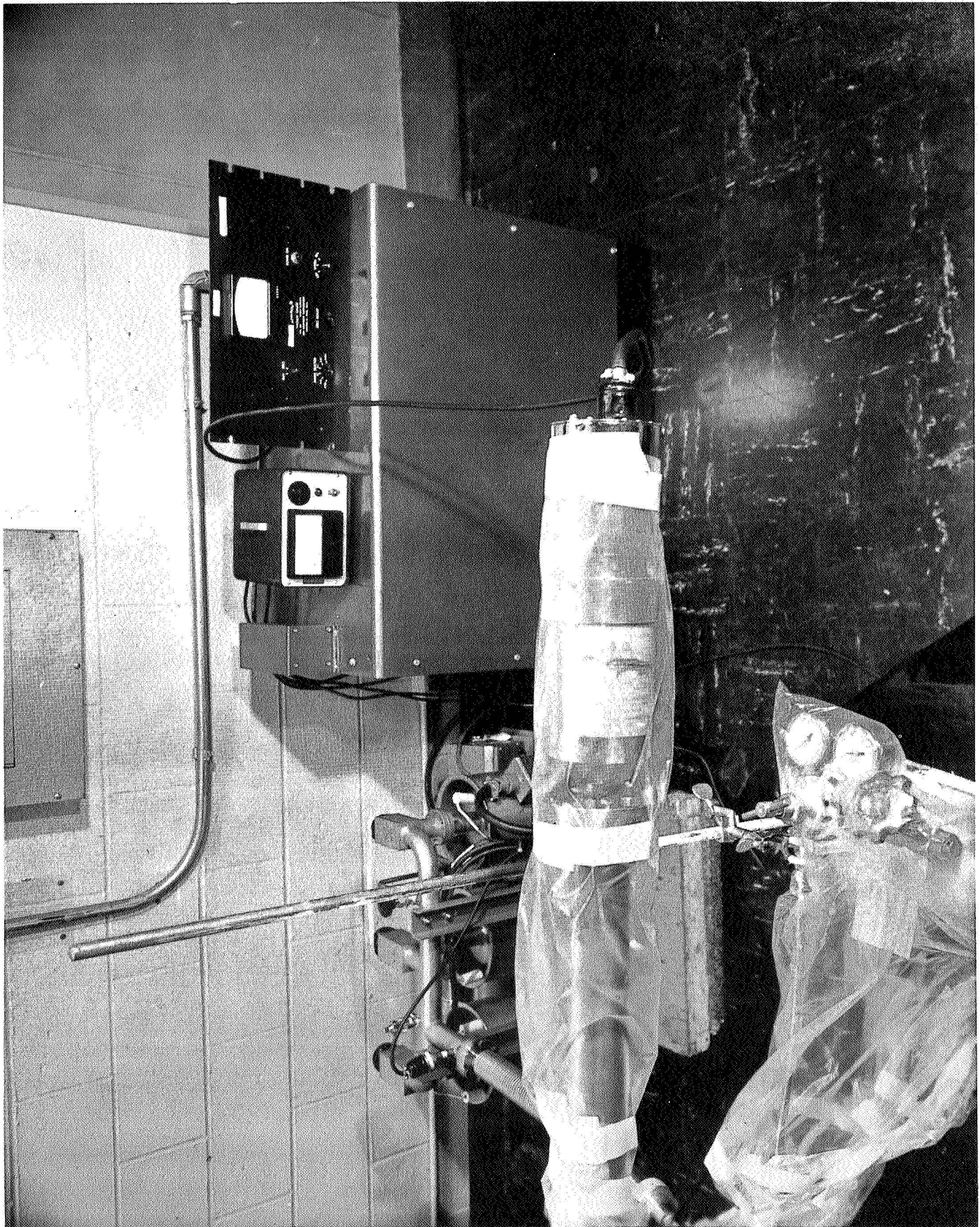


Figure 8: BAGGED IRIF-II: ALPHATRON GAUGE

reflectance at the wavelength of interest could be monitored as a function of time and the partial pressure of the adsorbate gas being studied.

The research gases employed were purchased from the Matheson Company. A compilation of the analyses of the research gases purchased, and of competitive sources, are presented in Table 4. All four gases - oxygen, nitrogen, argon, and carbon dioxide - were employed in the gaseous adsorbate studies.

#### F. Major Problems Encountered

##### 1. Detector Mode Mismatch in IRIF-I

A serious mismatch in absolute hemispherical spectral reflectance values at 700-nm wavelength occurred. The trouble was attributed quickly to the ultraviolet/visible detector mode and was manifested in visible reflectance (i.e., 1P-28 phototube) that were often as great as 10% less than the infrared reflectance (i.e., PbS cell) at 700 nm. This discrepancy was considerably greater than experienced previously and, unlike our earlier observations (ref. 3), the mismatch could not be prevented by etching the photomultiplier tube's quartz envelope.

The problem was subsequently traced to the fact that the photocathode (in certain photomultiplier tubes) was fragile and, due to the movement of IRIF-I from the irradiation station to the Beckman DK-2A, became displaced. When the displacement resulted in an increase in the distance between the photocathode and the tangential plane to the inside of the sphere, the specular sensitivity of the 1P-28 severely increased; the specular sensitivity was more pronounced for specimens that exhibited a specular component of total reflection. (Diffusely reflecting specimens, as for example IITRI's Z-93 thermal-control coating, did not exhibit the 1P-28-detector anomaly).

The problem was solved by using the more rugged 1P-28A photomultiplier tube, combined with lightly etching its surface.

Table 4

## ANALYSIS OF RESEARCH GASES

Gas	Assay	Impurities, ppm (less than)									
		Ar	CO <sub>2</sub>	He	H <sub>2</sub>	CH <sub>4</sub>	H <sub>2</sub> O	Ne	N <sub>2</sub>	O <sub>2</sub>	CO
Argon:											
JTB	99.9995	--	1.0	--	1	2.0	3	1	2	1	--
ARC	--	--	1.0	--	5	1.0	1	--	5	5	--
MC	99.995	--	0.5	--	1	0.5	--	--	5	1	--
Nitrogen:											
JTB	99.998	20	1.0	2	1	1.0	1	3	--	1	--
MC	99.999	5	0.5	1	1	0.5	--	1	--	1	--
Carbon Dioxide:											
JTB	99.995	5	---	--	1	5.0	5	--	20	5	--
MC	99.995	--	---	--	10	---	--	--	50	10	--
Oxygen:											
JTB	99.997	10	1.0	1	1	2.0	3	--	10	--	--

JTB = J.T. Baker Company  
 ARC = Air Reduction Corporation  
 MC = Matheson Company

An etched 1P-28A photomultiplier tube is now used in the integrating spheres of both IRIF-I and IRIF-II.

## 2. Glow Discharge Effects in IRIF-I

Severe glow discharge was noted during the pump-down of IRIF-I in several space simulation tests. The damage exhibited by certain specimens was immediately greater than could be accounted for by ultraviolet irradiation alone. The test was therefore aborted and data were not evaluated. (It should be noted that no effects of glow discharge were noted in the initial reflectance measurements taken in vacuum.) Glow discharge was also noted in IRIF tests 13 and 15, but was considerably less than test 11.

An ion-sputter pump creates a glow discharge during start-up. This glow discharge is composed of electrons and positively

charged ions. The ions result mostly from desorbed molecules which are sorbed by the metal on the pump surface. If the pump is "dirty," the start-up time can be prolonged while the pump outgasses - usually, and predominantly, water - prolonging glow discharge.

We therefore installed three grids in both IRIF-I and IRIF-II, just above the throat of the sputter-ion pumps. These grids are screens with 80% open area; they are electrically isolated from the pump and from one another. They are designed so that a voltage in excess of 2000 v can be impressed on each of the two top grids.

Our initial experiments have indicated that by maintaining the top grid at approximately -25 v and the middle grid (closer to the pump) at +30 v, the current to each grid can be minimized (see Figure 9). The voltage impressed on the grids must be varied slightly as the pump voltage changes.

Employment of this procedure proved to be effective in eliminating anomalous degradation.

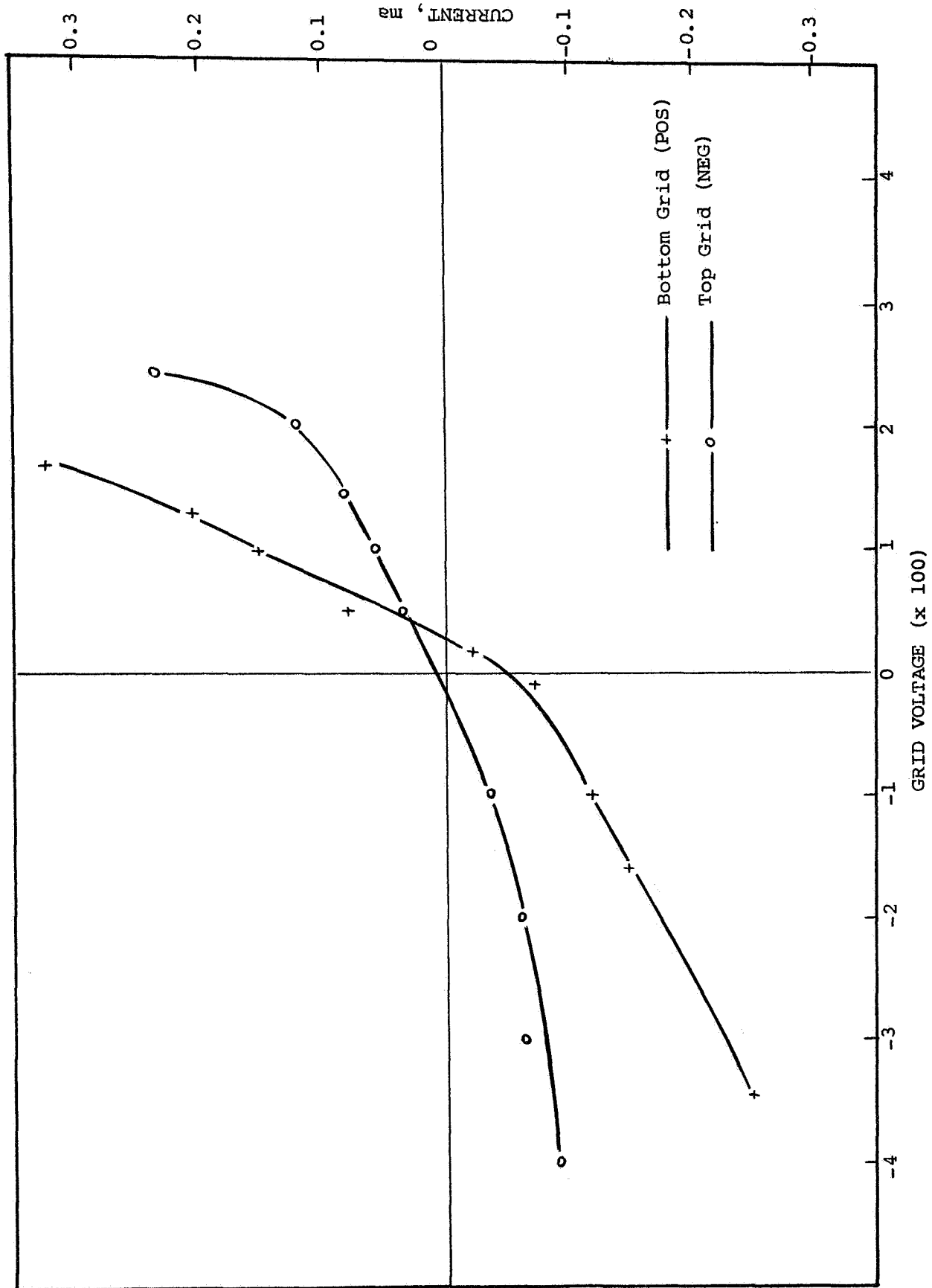


Figure 9: GRID CURRENT AS A FUNCTION OF GRID VOLTAGE



#### IV. SPACE SIMULATION SCREENING TESTS

##### A. Introduction

The principal objective of the screening tests was the elucidation of the in situ-spectral-reflectance behavior of a broad range of Pegasus III coating systems as a function of simulated-space-ultraviolet irradiation. The behavior was sought in terms of the increase in solar absorptance,  $\Delta\alpha_s$ , as a function of irradiation dose and as a function of substrate temperature during irradiation.

A secondary objective of the screening tests was the establishment of the requirement for in situ testing of each of the specimens irradiated. For example, it was originally planned that some of the post-exposure reflectance measurements would be performed in air. This plan had to be abandoned when it was apparent that all surfaces exhibit "pressure-dependent" spectral reflectance to some degree. Furthermore, the excellent precision achieved with both IRIF's would have made the determination of reflectance in air undesirable, even if some of the specimens would have been observed to be completely insensitive to the absence of gaseous adsorbates on their surfaces.

All screening tests were therefore performed in IRIF-I employing a 1000 watt mercury-argon A-H6 ultraviolet source (refer to Section III-A).

##### B. IRIF-I Test No. 10

Test 10 involved a solar-ultraviolet-acceleration factor of 5X; the irradiation times after which in situ reflectance measurements were taken were 40 and 160 hr, resulting in solar ultraviolet radiation doses of 200 and 800 equivalent sun hours (ESH), respectively. The samples were maintained at a nominal temperature of 8°C by pumping cold tap water through the IRIF sample table. The average pressure during the irradiation period was  $3 \times 10^{-7}$  Torr.

The specimens irradiated in test 10 are presented in Table 5 along with their solar absorptance data,  $\alpha_s$ , as a function of exposure (ESH). It will be noted that the solar absorptance data presented in Table 5 is divided into  $\alpha_1$  and  $\alpha_2$ , each corresponding to exactly one-half of the total solar energy. The spectral data for each of the test specimens are presented in Figures 10 through 33: two figures are presented for each specimen -- one for exposures of 0, 200, and 800 ESH and the other for exposures of 0 and 800 ESH and back-filled with ambient air.

A brief description of the in situ reflectance spectra of the irradiated specimens follows.

1. The IRIF blank (NaOH-etched aluminum) sustained a surprising amount of damage in the ultraviolet and visible wavelengths (5% at 325-nm wavelength). This damage is similar to the other specimens that possess aluminum oxide surface layers. Because of the behavior of several of these, especially the GT-1015 alumina-coated aluminized Mylar, we believe that the bulk of the loss in ultraviolet reflectance of the IRIF coupon is due to damage to the oxidized surface of the aluminum.

2. The solar absorptance of the manganese black (Tabor Coating; prepared by Dr. Henry Tabor, National Physical Institute of Israel) did not exhibit significant degradation in any wavelength region. The  $\Delta\alpha_s$  was only 0.003 in 800 ESH of ultraviolet irradiation. The spectra are presented in Figures 12 and 13.

3. Like the Tabor coating, the MTL-3 Alodine surface (Item 3) exhibited little damage. However, the MTL-3 coating exhibited interference bands and a degradation of about 3% in the 325-nm wavelength region. No degradation was observed at wavelengths greater than about 600 nm. The damage spectra of MTL-3 are presented in Figures 14 and 15.

4. The GT-1275 Alodine specimen (Item 7) exhibited mild interference effects and a loss in reflectance of 3% and 8% at 400- and 325-nm wavelength, respectively. It exhibited

Table 5

EFFECT OF 800 ESH ULTRAVIOLET IRRADIATION  
IN THE IRIF ON PEGASUS COUPONS  
(Solar Intensity, 5X; Sample Temperature 8°C)

Item No.	Surface	Exposure (ESH)	Solar Absorptance			
			$\alpha_1$	$\alpha_2$	$\alpha_s$	$\Delta\alpha_s$
	Etched aluminum blank	0	.158	.094	.252	-
		200	.161	.091	.251	.001
		800	.173	.101	.274	.022
2	Manganese black	0	.427	.212	.639	-
		200	.428	.212	.640	.001
		800	.430	.212	.642	.003
5	MTL-3	0	.359	.211	.570	-
		200	.363	.211	.574	.004
		800	.366	.211	.577	.007
7	GT-1275	0	.235	.119	.354	-
		200	.248	.119	.367	.013
		800	.254	.121	.375	.021
8	GT-1015	0	.169	.081	.250	-
		200	.242	.093	.335	.085
		800	.288	.085	.373	.123
17	Ta <sub>2</sub> O <sub>5</sub> /PS7	0	.139	.097	.236	-
		200	.222	.119	.341	.105
		800	.241	.123	.364	.128
19	LiF/PS7	0	.078	.050	.128	-
		200	.184	.058	.242	.114
		800	.238	.068	.306	.178
23	ZrO <sub>2</sub> /PS7	0	.118	.102	.220	-
		200	.159	.106	.265	.045
		800	.187	.108	.295	.075
24	Z93	0	.126	.041	.167	-
		200	.132	.040	.172	.005
		800	.140	.041	.181	.014
30	S-13 (clean) <sup>b</sup>	0	.131	.078	.209	-
		200	.142	.135	.277	.068
		800	.150	.142	.292	.083
34	S-13 (uncleaned)	0	.138	.083	.221	-
		200	.149	.138	.287	.066
		800	.161	.145	.306	.085
35	S-13G, Batch A-295	0	.132	.064	.196	-
		200	.142	.071	.213	.017
		800	.160	.070	.230	.034

a See Tables 1 to 3.

b S-13 cleaned with 5% Alconox, distilled water, and absolute ethyl alcohol.

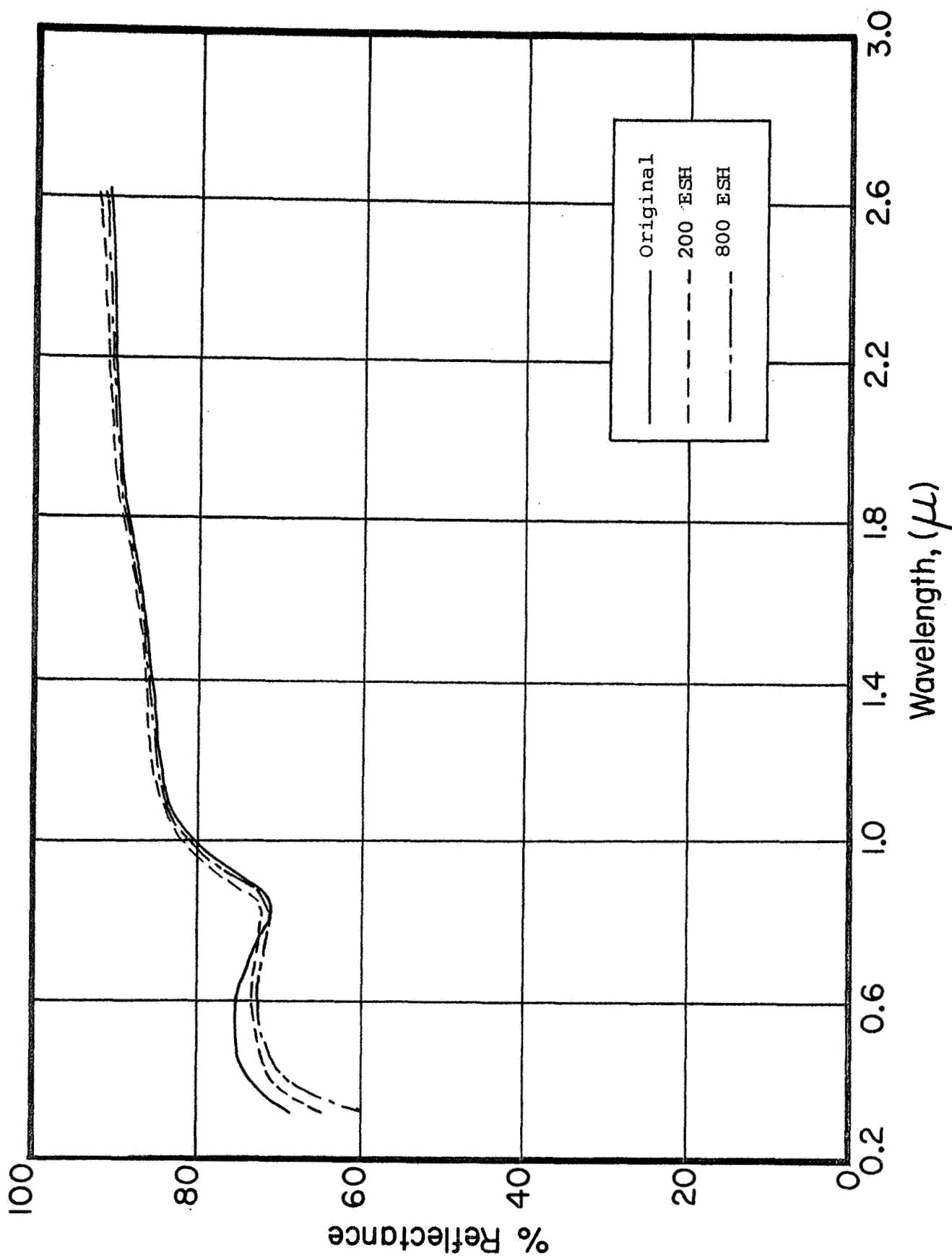


Figure 10: ABSOLUTE REFLECTANCE OF ETCHED ALUMINUM SUBSTRATE AS A FUNCTION OF UV IRRADIATION IN IRIF TEST 10 (Not shown in Table 1)

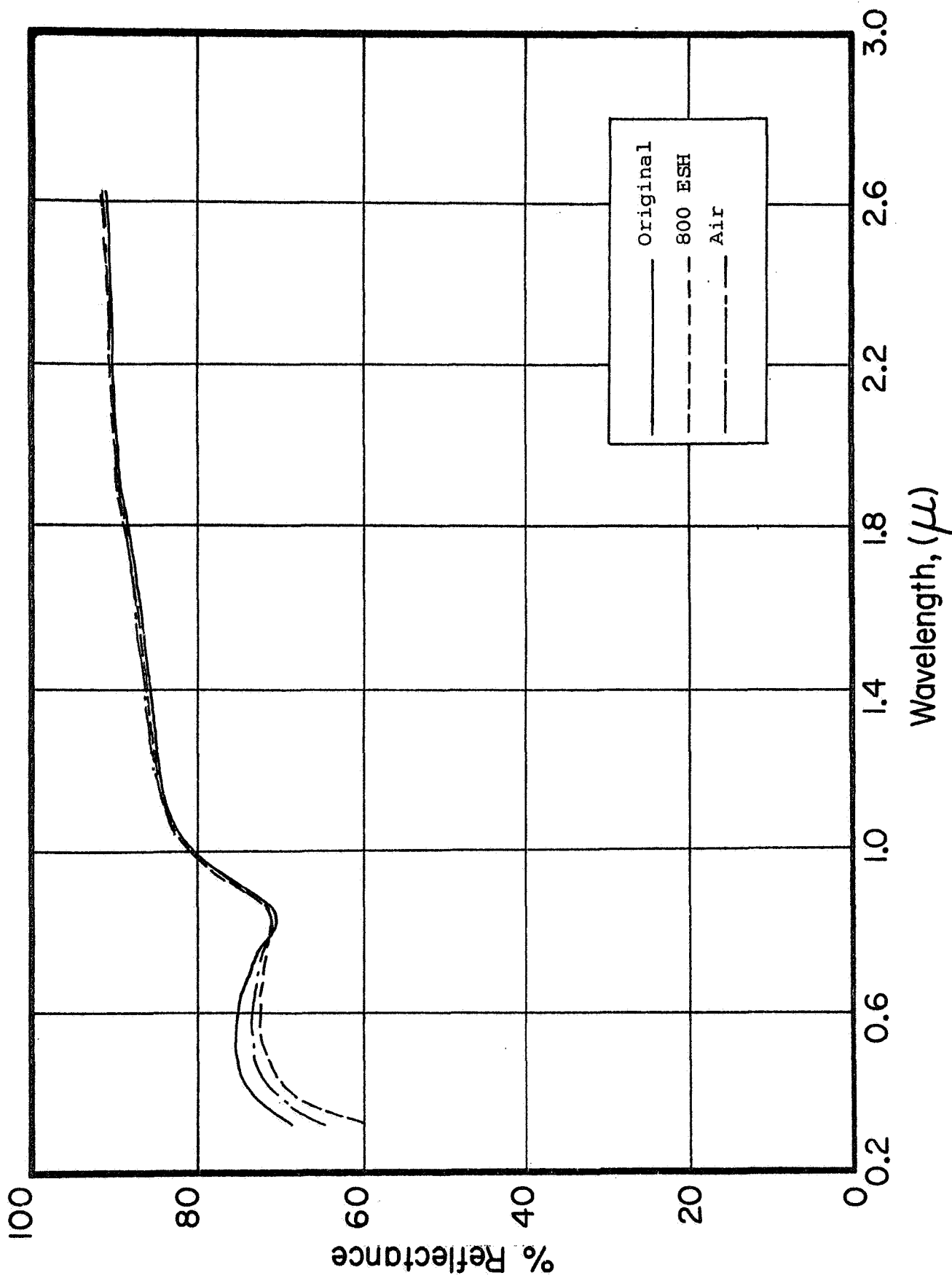


Figure 11: ABSOLUTE REFLECTANCE OF ETCHED ALUMINUM SUBSTRATE AS A FUNCTION OF UV IRRADIATION IN IRIF TEST 10 (Not shown in Table 1)

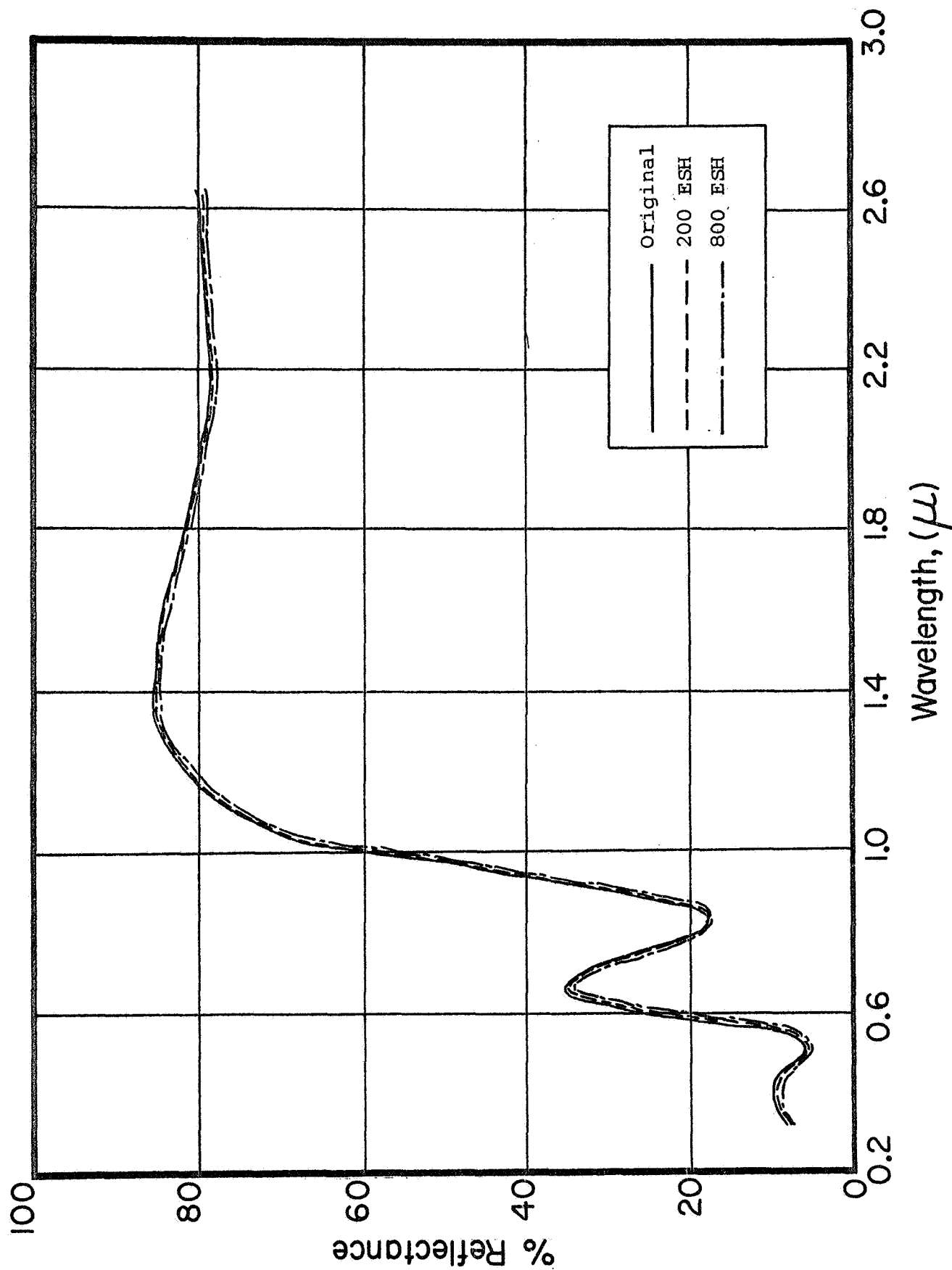


Figure 12: ABSOLUTE REFLECTANCE OF TABOR MANGANESE BLACK SPECIMEN (#2) AS A FUNCTION OF UV IRRADIATION IN IRIF TEST 10

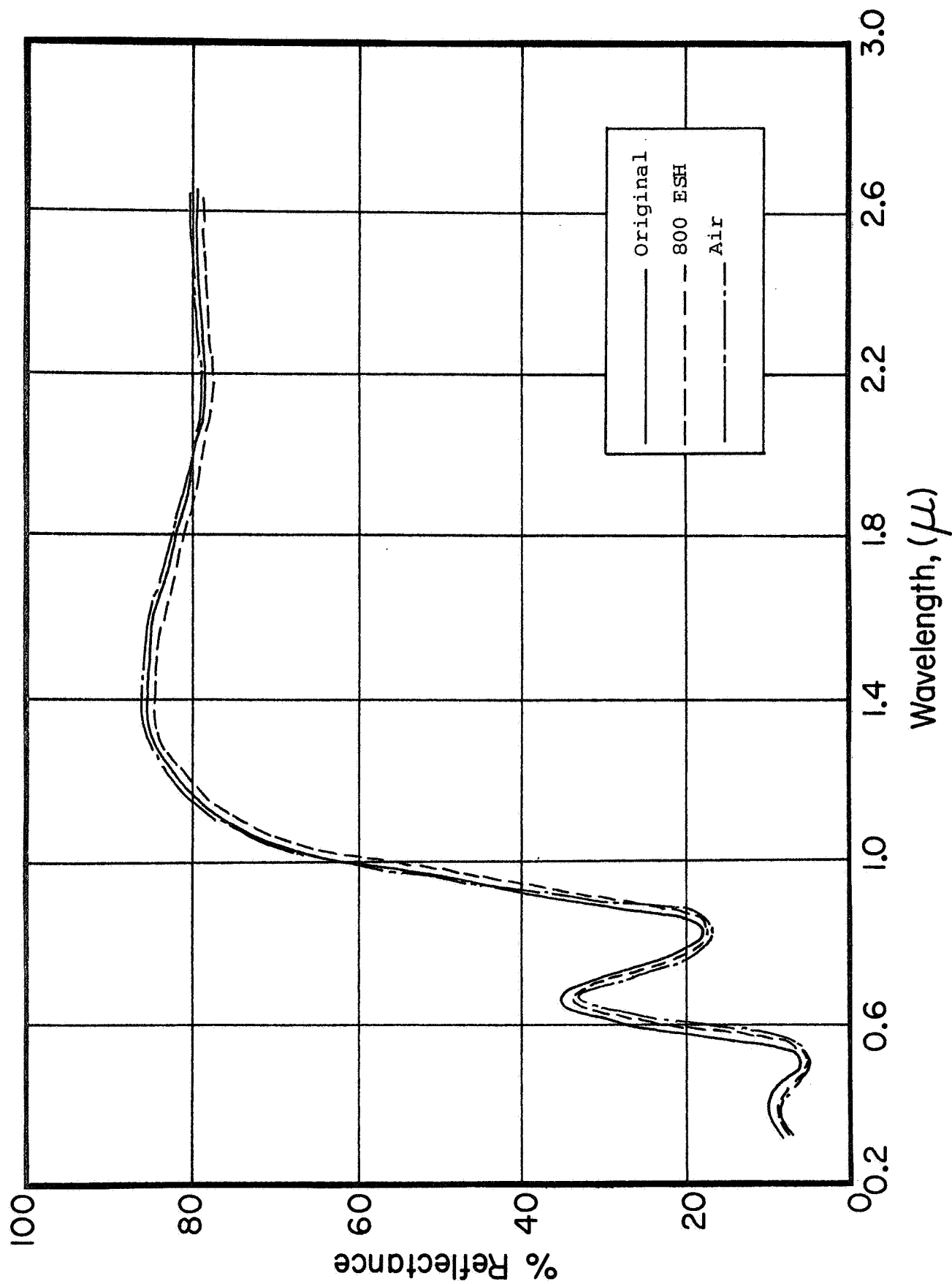


Figure 13: ABSOLUTE REFLECTANCE OF TABOR MANGANESE BLACK SPECIMEN (#2) AS A FUNCTION OF UV IRRADIATION IN IRIF TEST 10

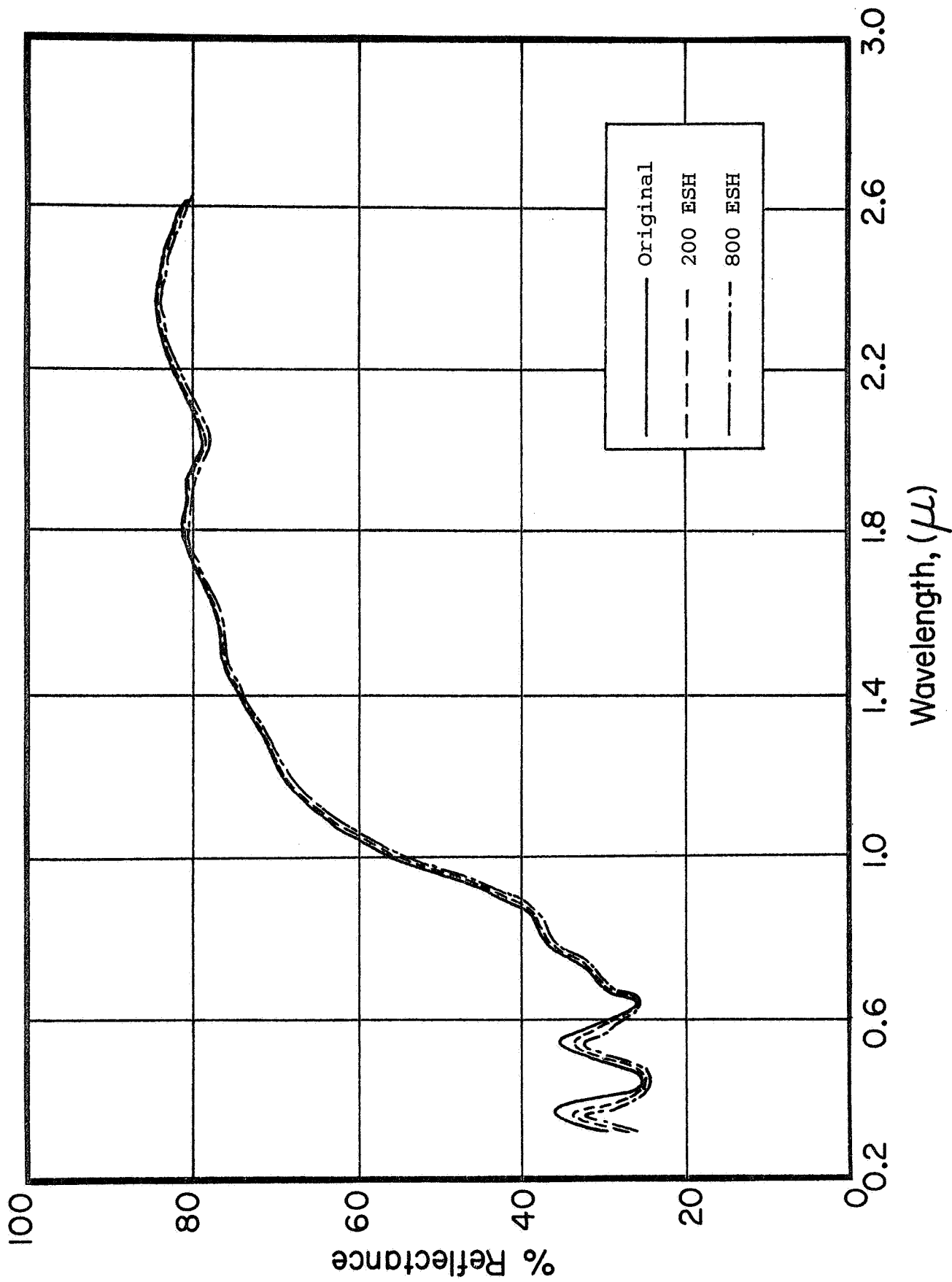


Figure 14: ABSOLUTE REFLECTANCE OF MTL-3 CONVERSION COATING (#5) AS A FUNCTION OF UV IRRADIATION IN IRIF TEST 10



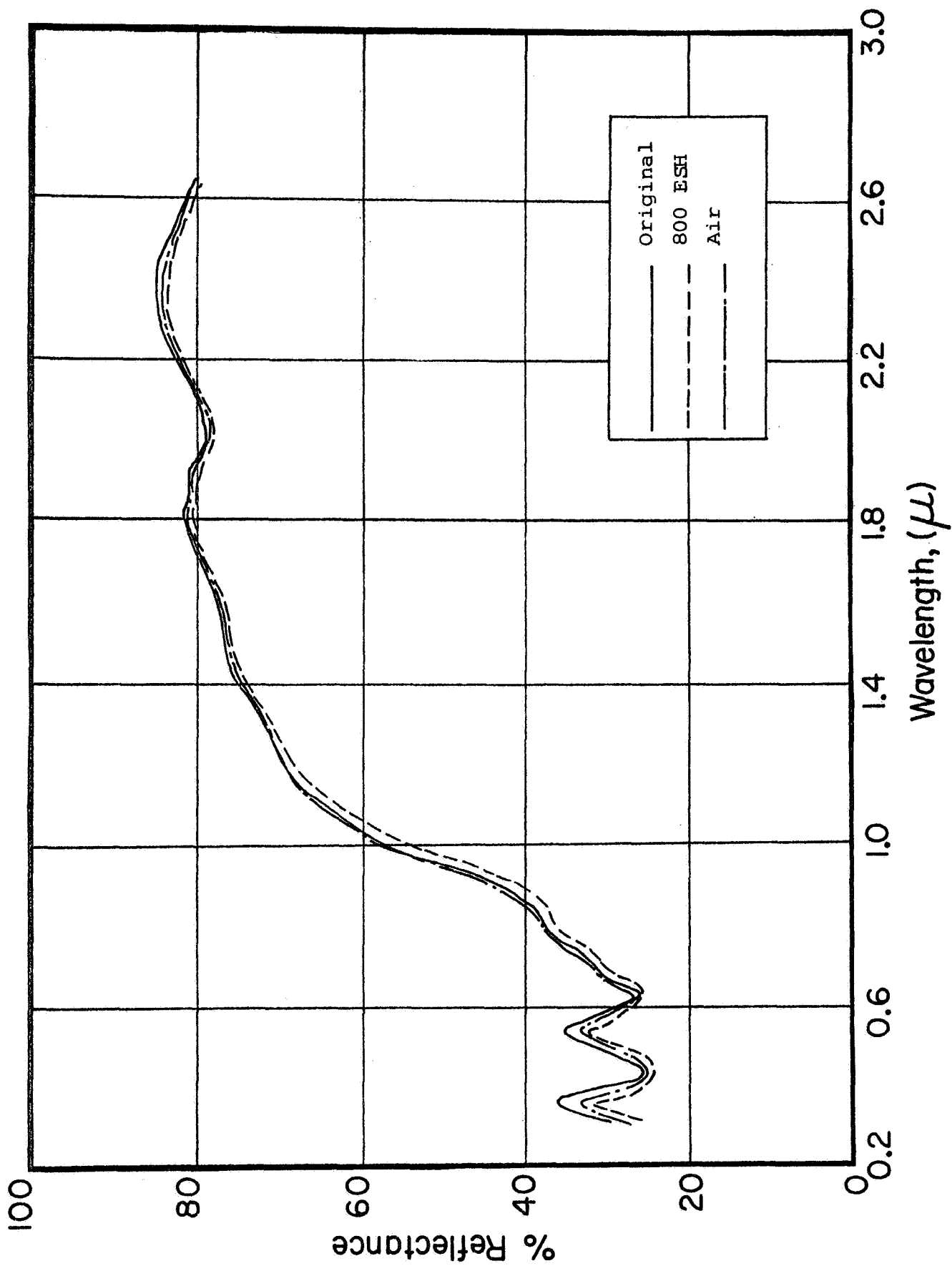


Figure 15: ABSOLUTE REFLECTANCE OF MTL-3 CONVERSION COATING (#5) AS A FUNCTION OF UV IRRADIATION IN IRIF TEST 10

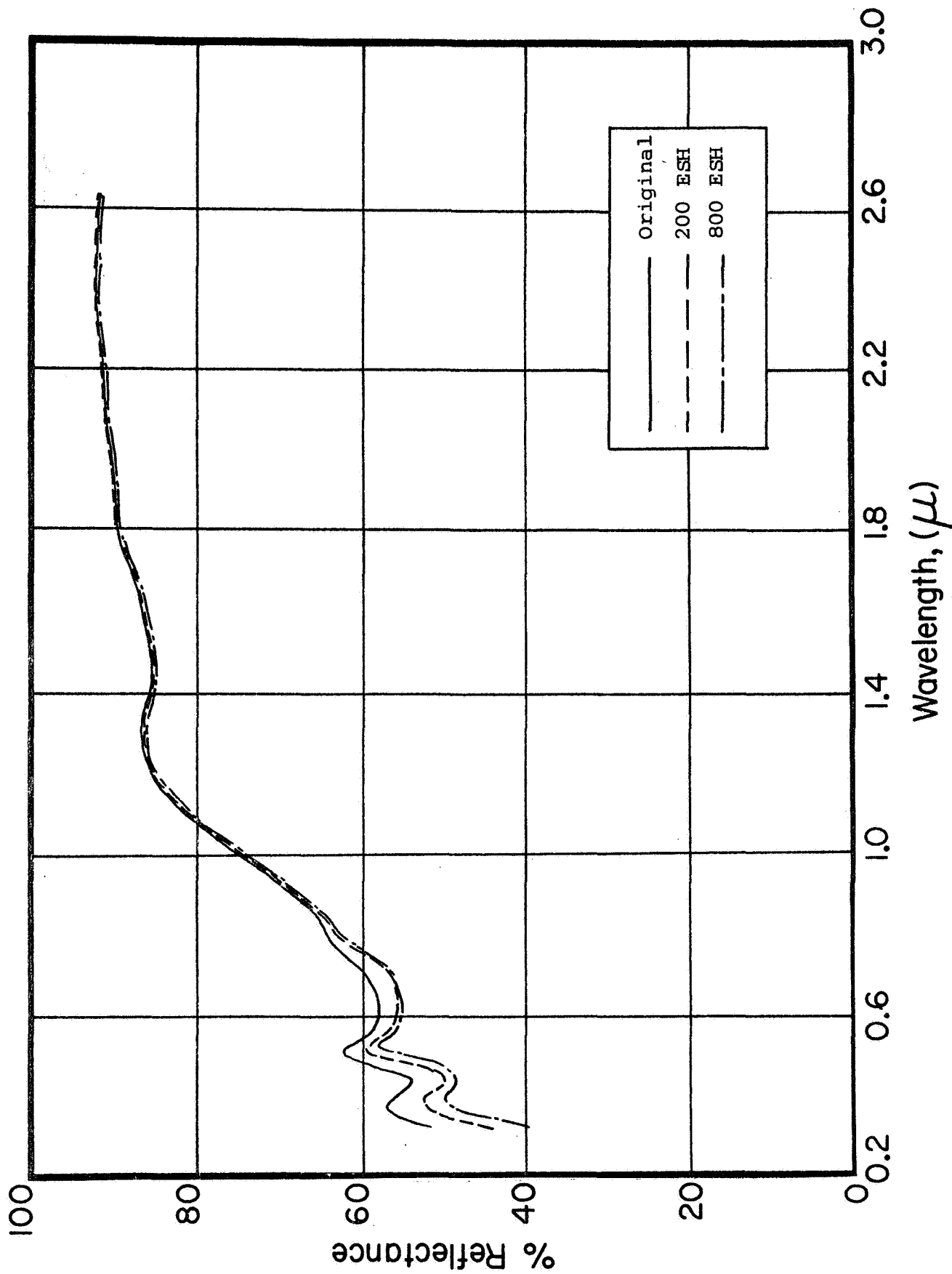


Figure 16: ABSOLUTE REFLECTANCE OF SCHEIDAH 1275 ALODINED ALUMINIZED MYLAR (#7)  
AS A FUNCTION OF UV IRRADIATION IN IRIF TEST 10

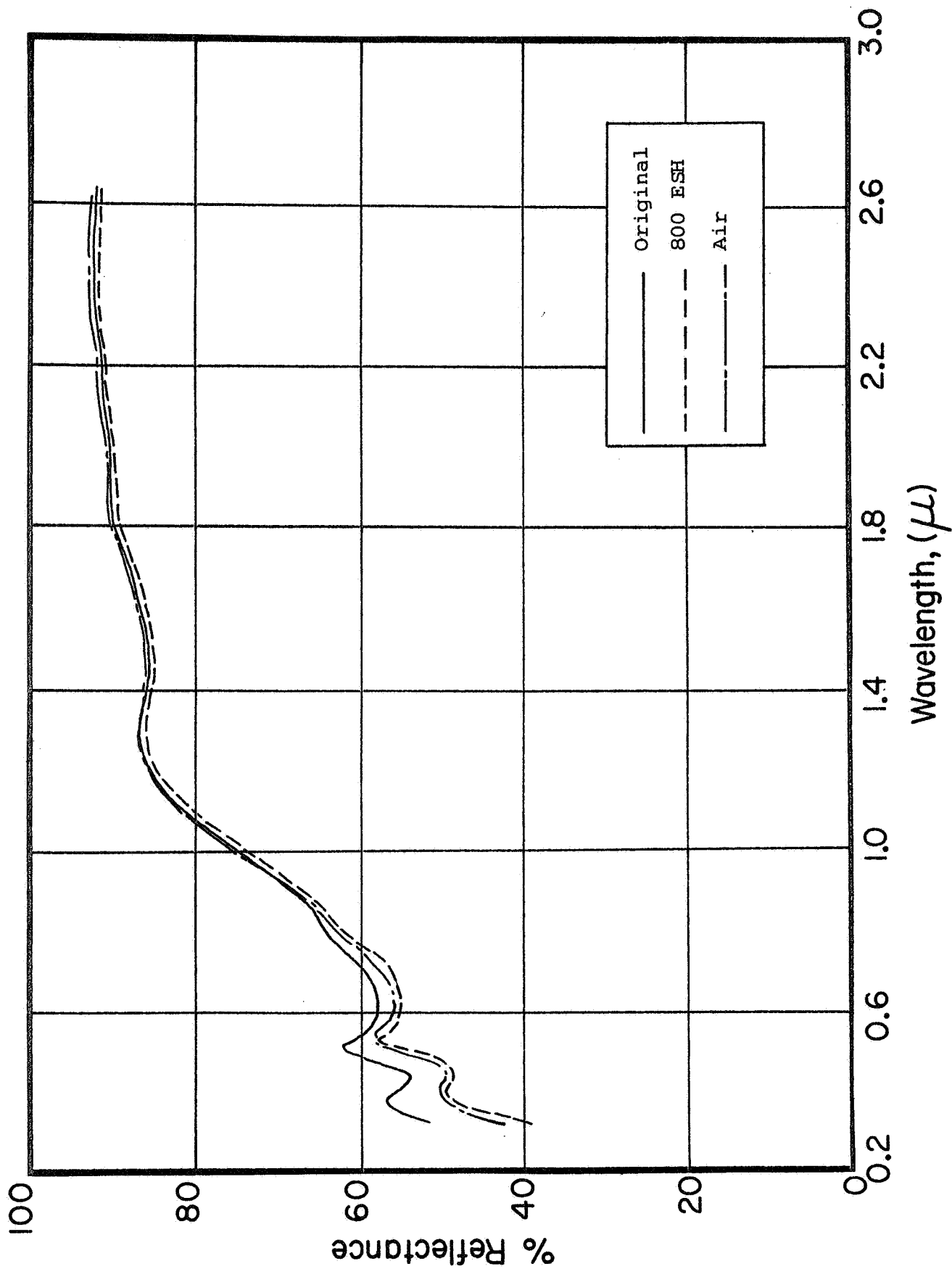


Figure 17: ABSOLUTE REFLECTANCE OF SCHEIDAH 1275 ALODINED ALUMINIZED MYLAR (#7)  
AS A FUNCTION OF UV IRRADIATION IN IRIF TEST 10

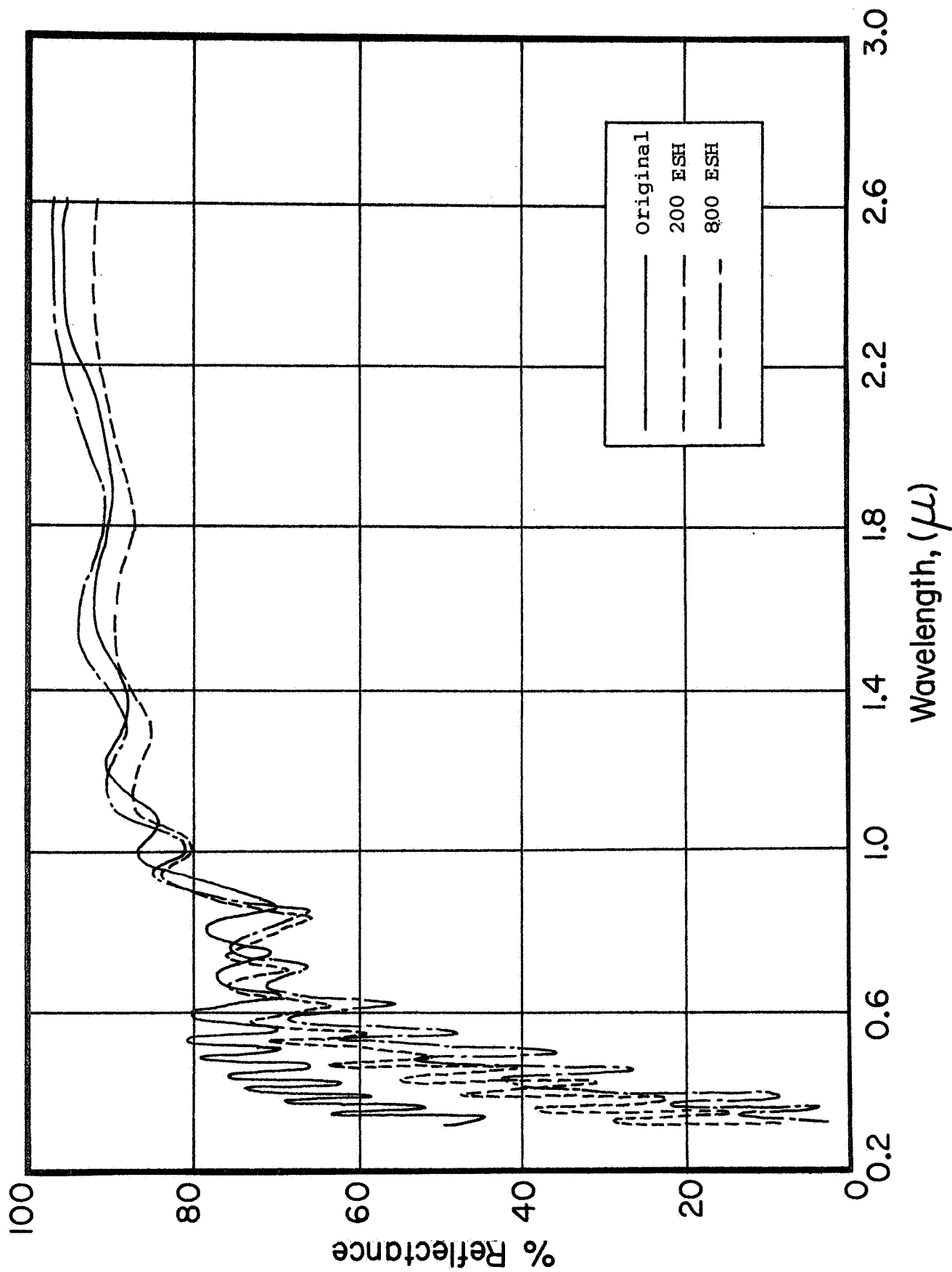


Figure 18: ABSOLUTE REFLECTANCE OF SCHEIDLAHL GT-1015 ALUMINA COATED ALUMINUM (#8)  
AS A FUNCTION OF UV IRRADIATION IN IRIF TEST 10

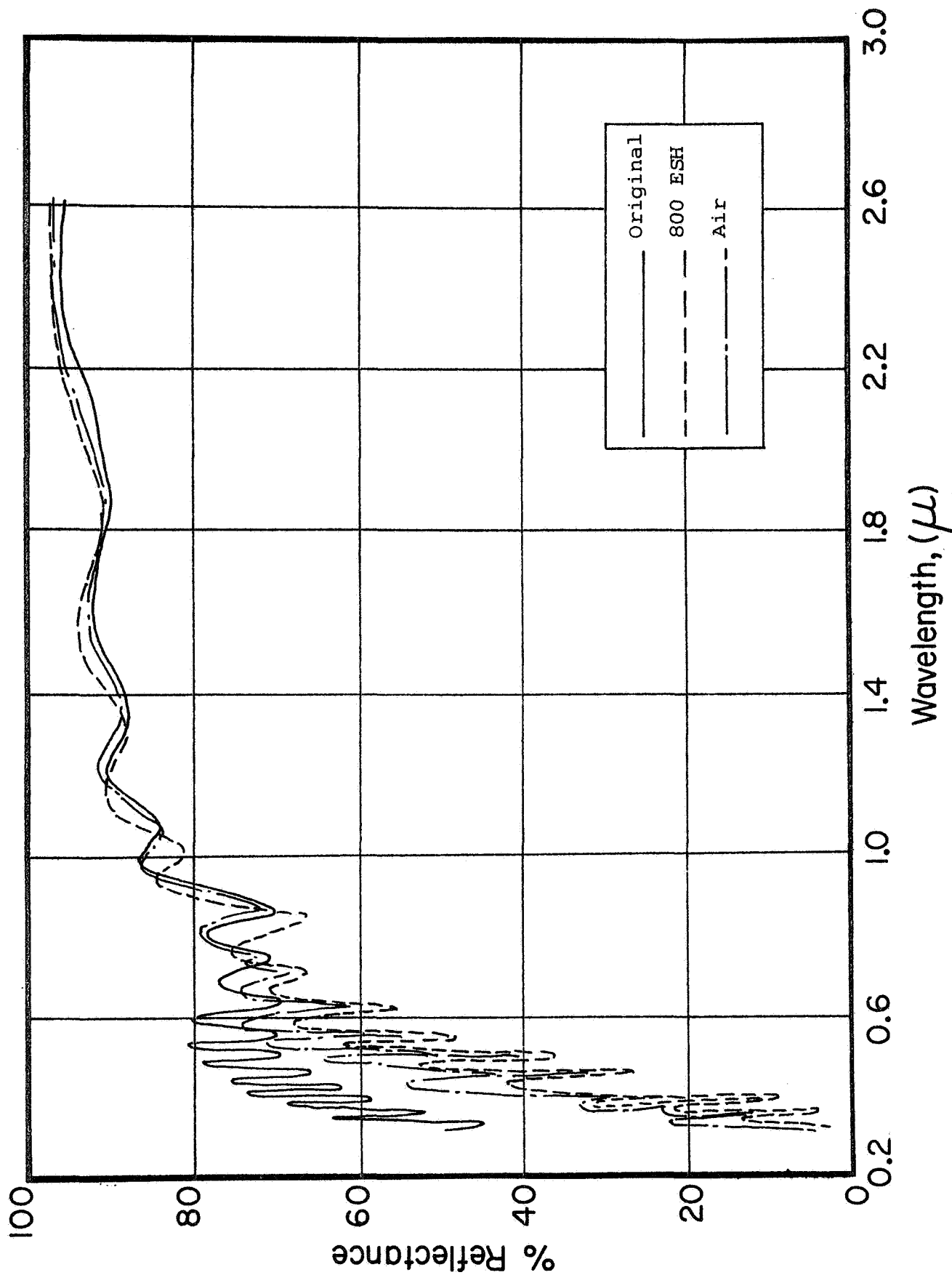


Figure 19: ABSOLUTE REFLECTANCE OF SCHEIDAH L GT-1015 ALUMINA COATED ALUMINUM (#8) AS A FUNCTION OF UV IRRADIATION IN IRIF TEST 10

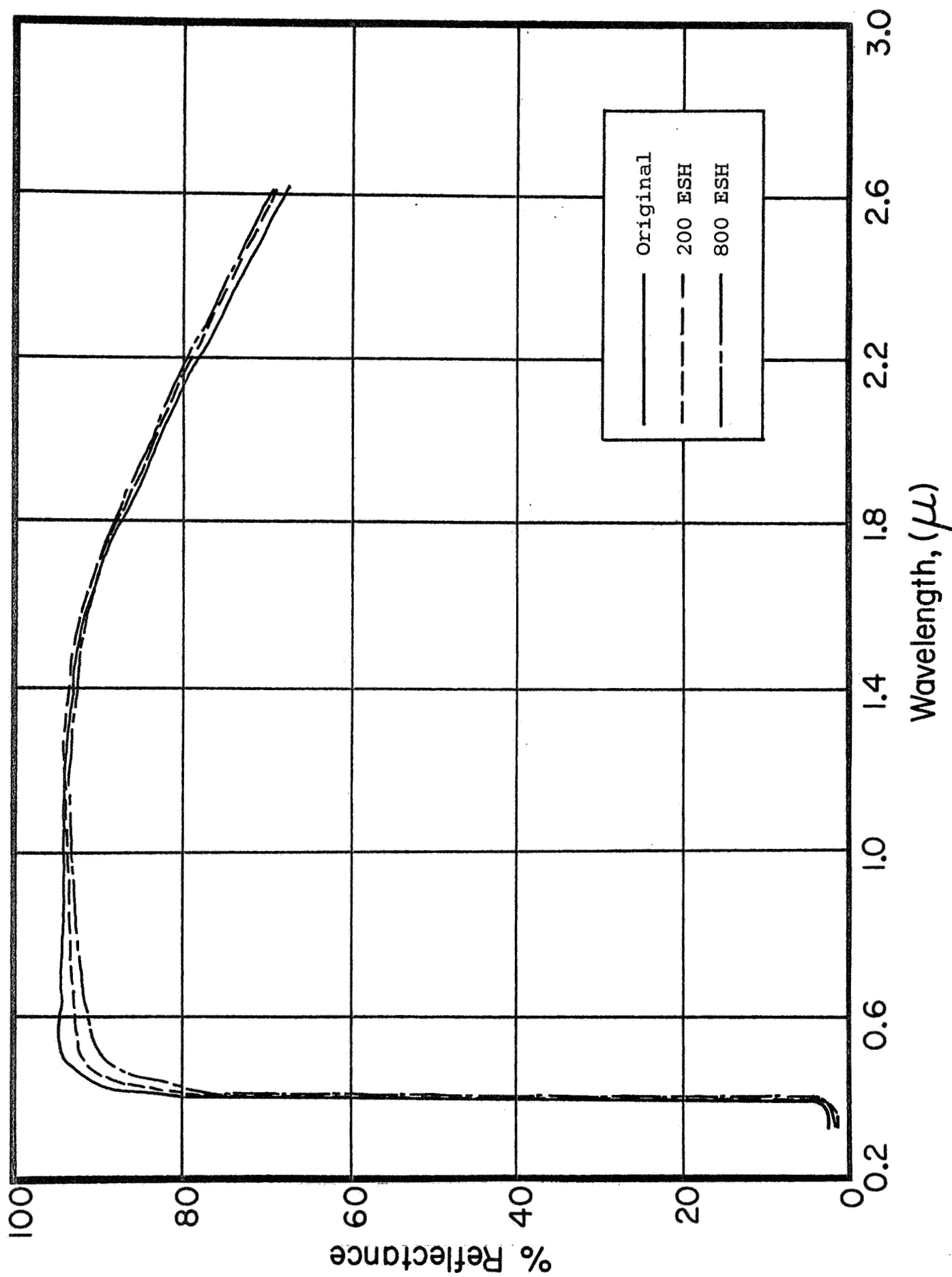


Figure 20: ABSOLUTE REFLECTANCE OF Z93 (#16) AS A FUNCTION OF UV IRRADIATION IN IRIF TEST 10

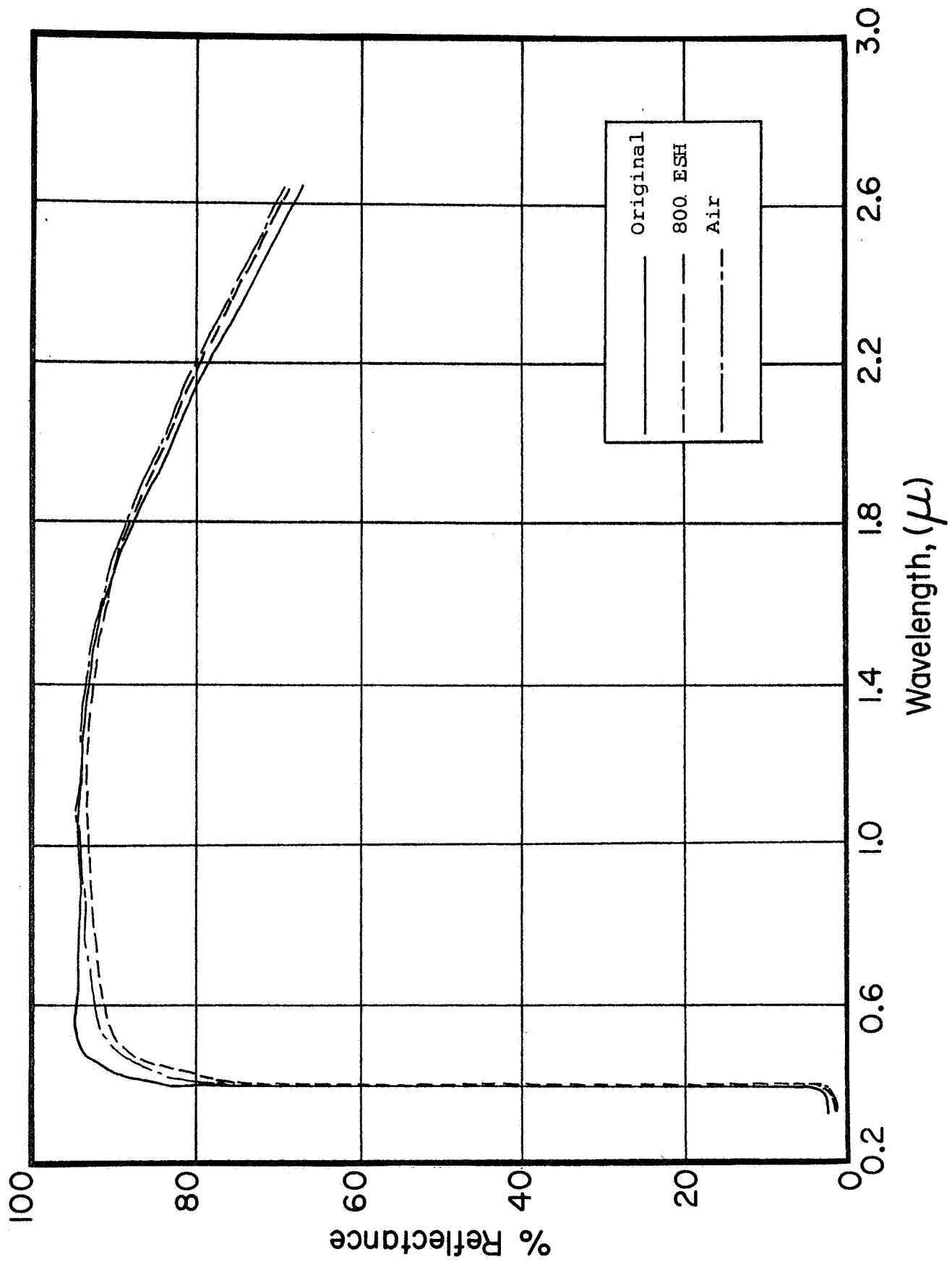


Figure 21: ABSOLUTE REFLECTANCE OF Z93 (#16) AS A FUNCTION OF UV IRRADIATION IN IRIF TEST 10

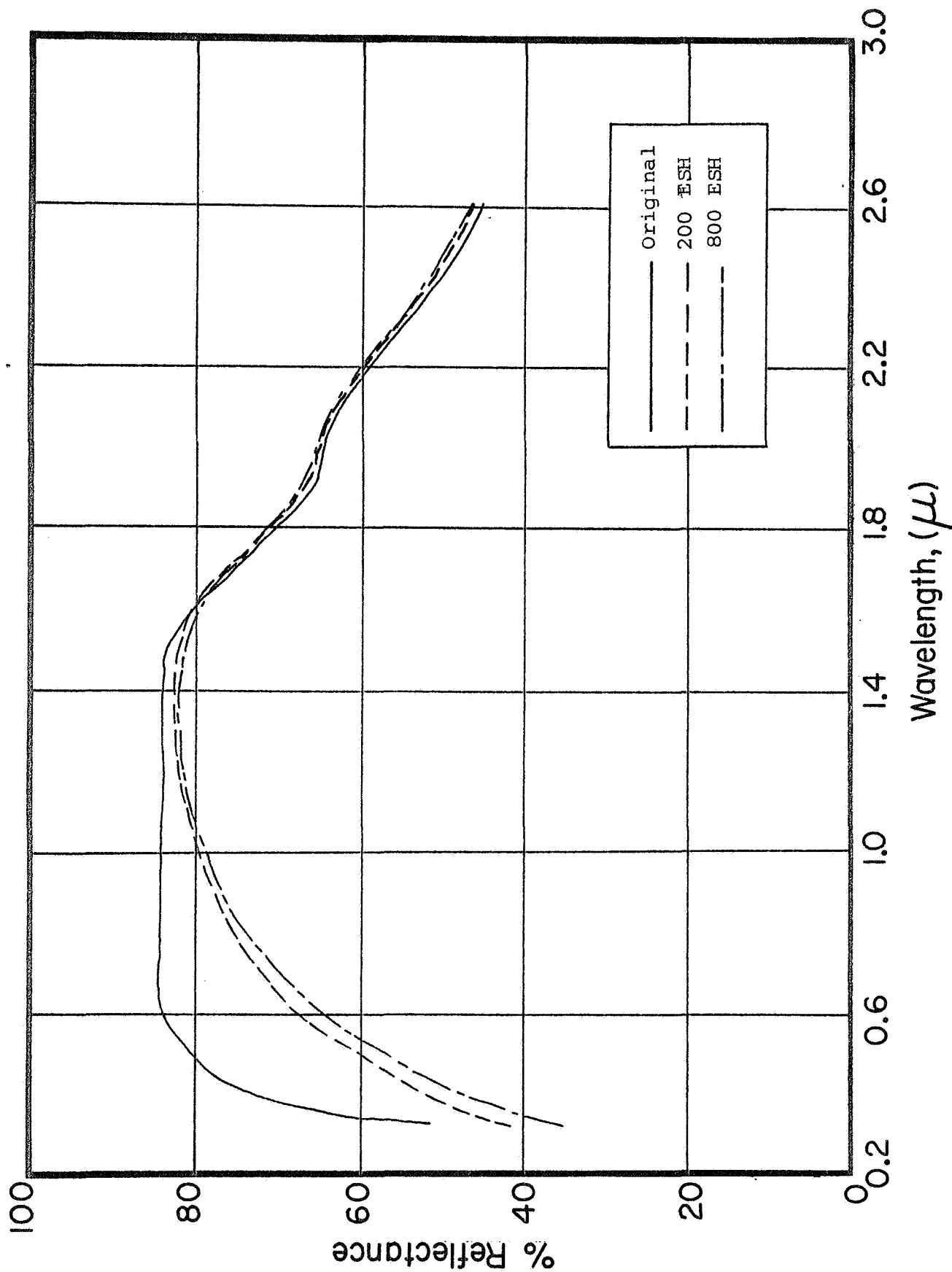


Figure 22: ABSOLUTE REFLECTANCE OF TANTALUM-PIGMENTED POTASSIUM SILICATE PAINT (#17) AS A FUNCTION OF UV IRRADIATION IN IRIF TEST 10



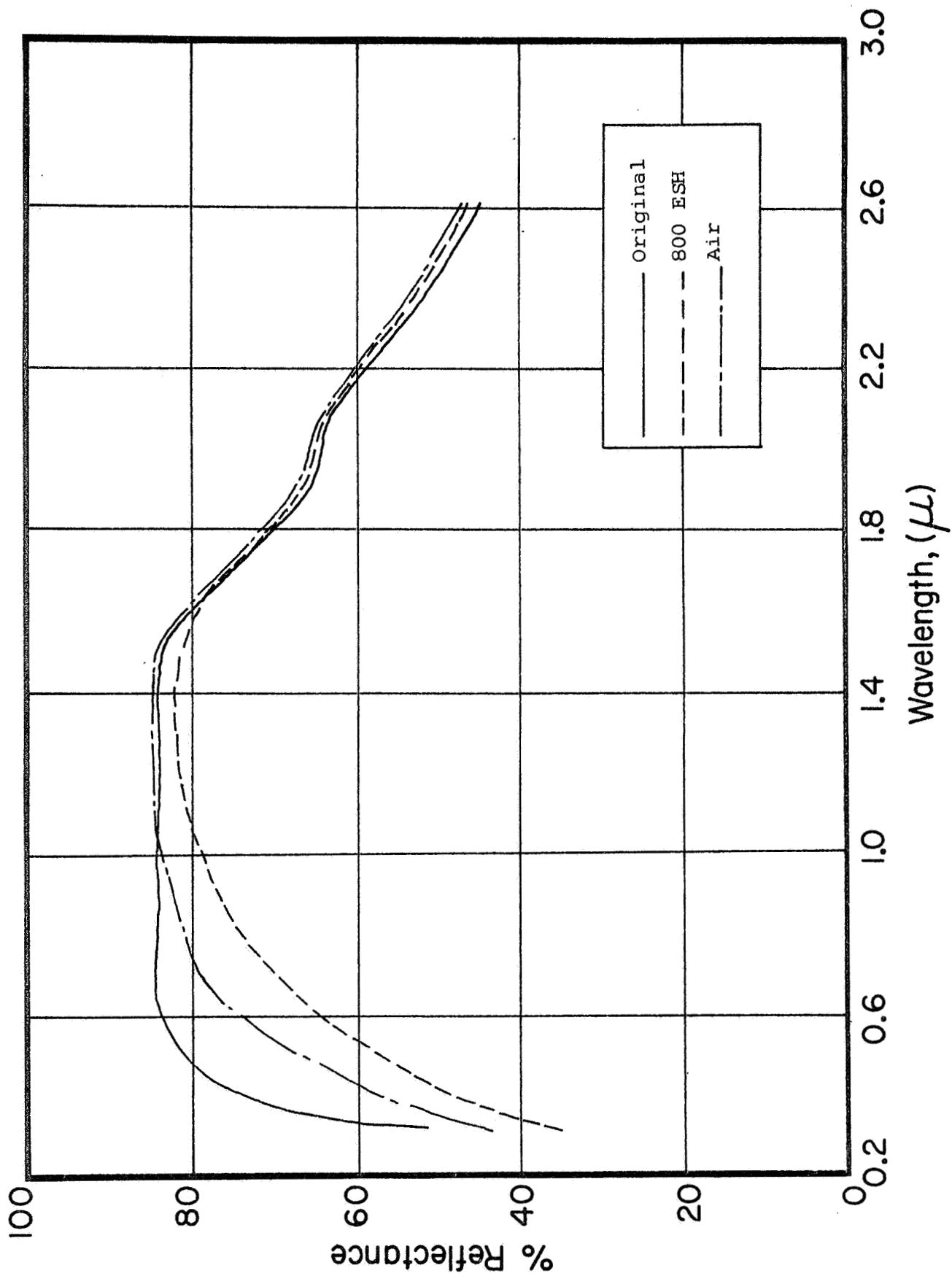


Figure 23: ABSOLUTE REFLECTANCE OF TANTALA-PIGMENTED POTASSIUM SILICATE PAINT (#17)  
AS A FUNCTION OF UV IRRADIATION IN IRIF TEST 10

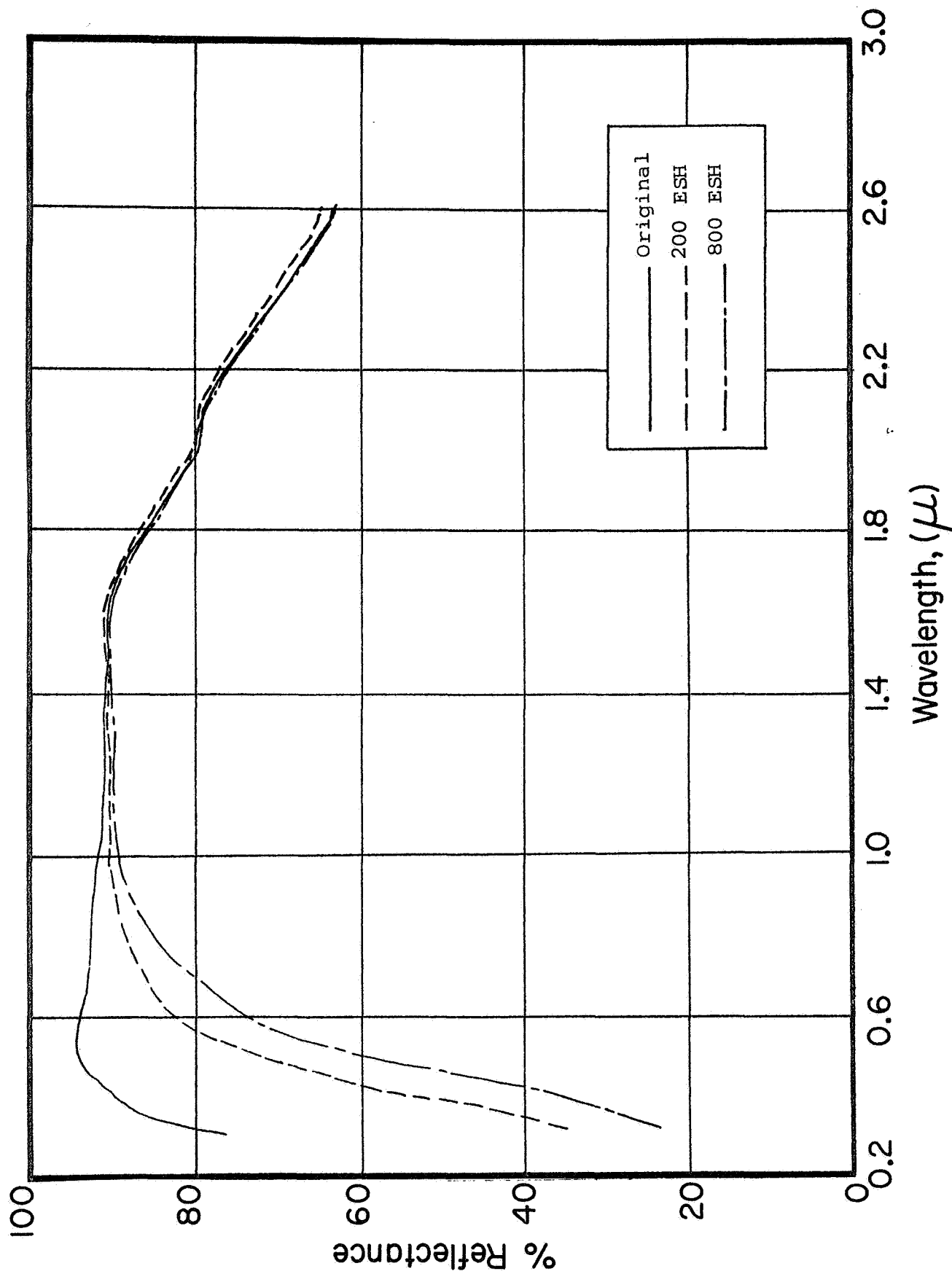


Figure 24: ABSOLUTE REFLECTANCE OF LITHIUM FLUORIDE-PIGMENTED POTASSIUM SILICATE PAINT (#19) AS A FUNCTION OF UV IRRADIATION IN IRIF TEST 10

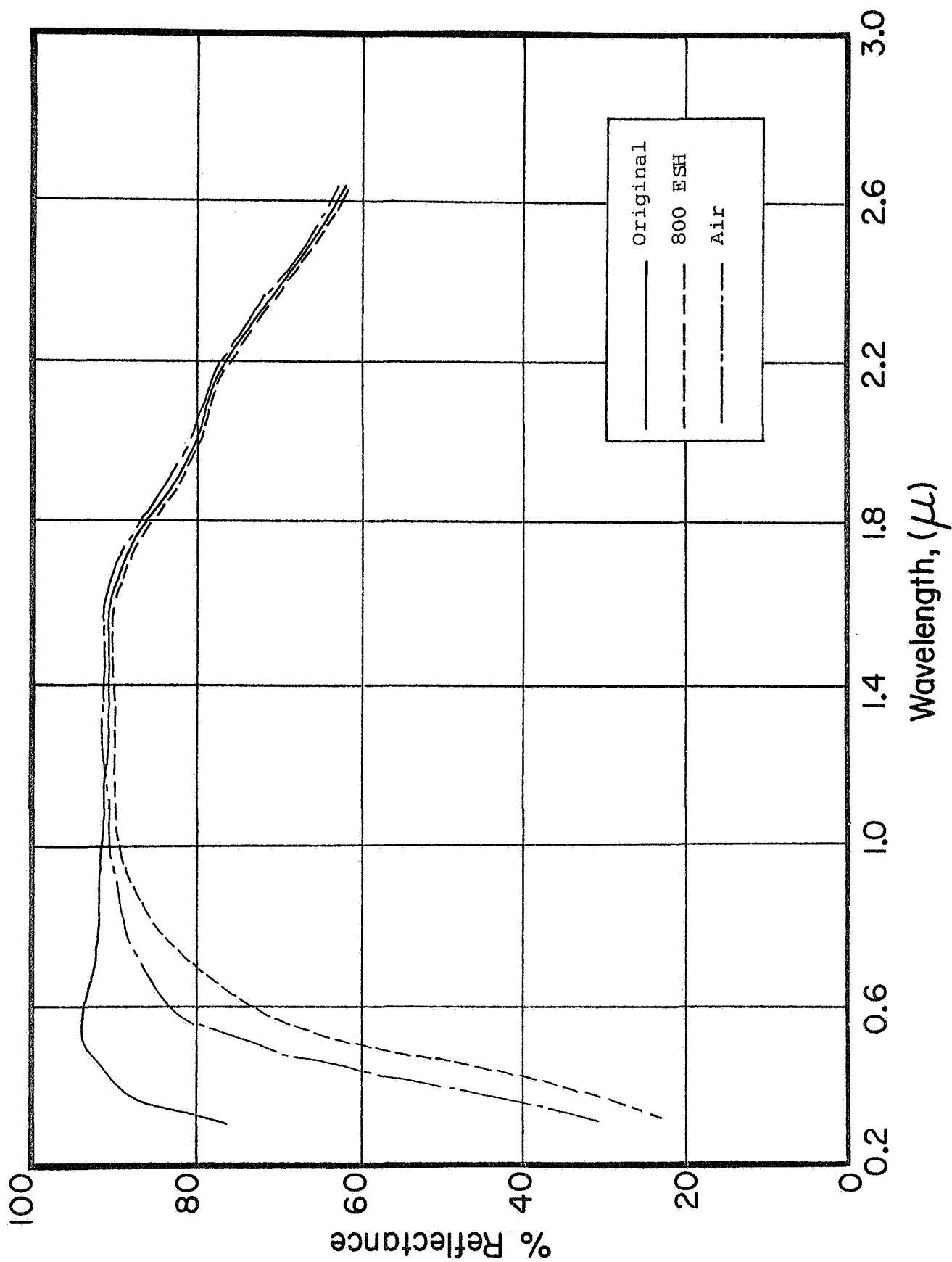


Figure 25: ABSOLUTE REFLECTANCE OF LITHIUM FLUORIDE-PIGMENTED POTASSIUM SILICATE PAINT (#19)  
AS A FUNCTION OF UV IRRADIATION IN IRIF TEST 10

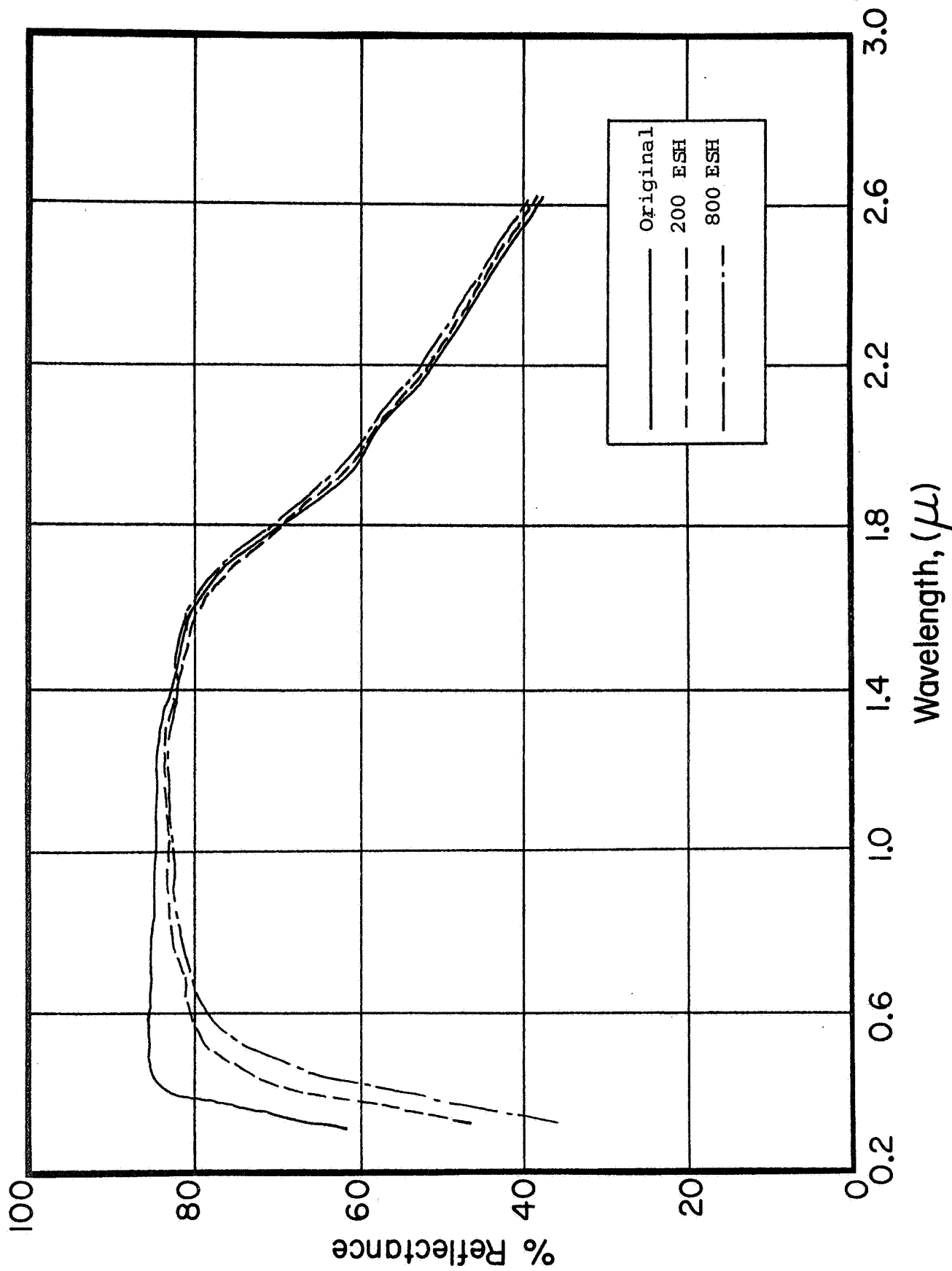


Figure 26: ABSOLUTE REFLECTANCE OF ZIRCONIA-PIGMENTED POTASSIUM SILICATE PAINT (#23)  
AS A FUNCTION OF UV IRRADIATION IN IRIF TEST 10

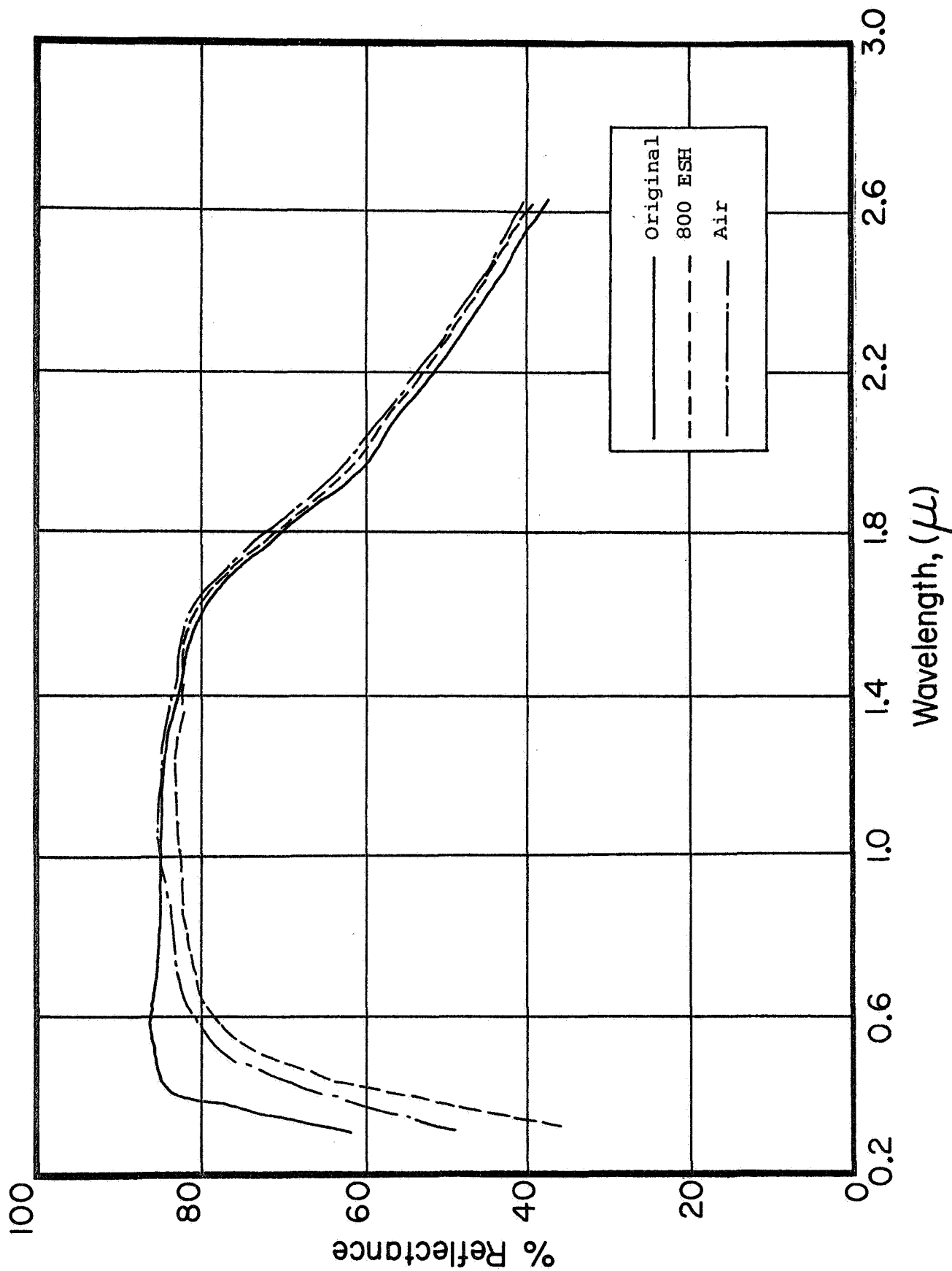


Figure 27: ABSOLUTE REFLECTANCE OF ZIRCONIA-PIGMENTED POTASSIUM SILICATE PAINT (#23) AS A FUNCTION OF UV IRRADIATION IN IRIF TEST 10

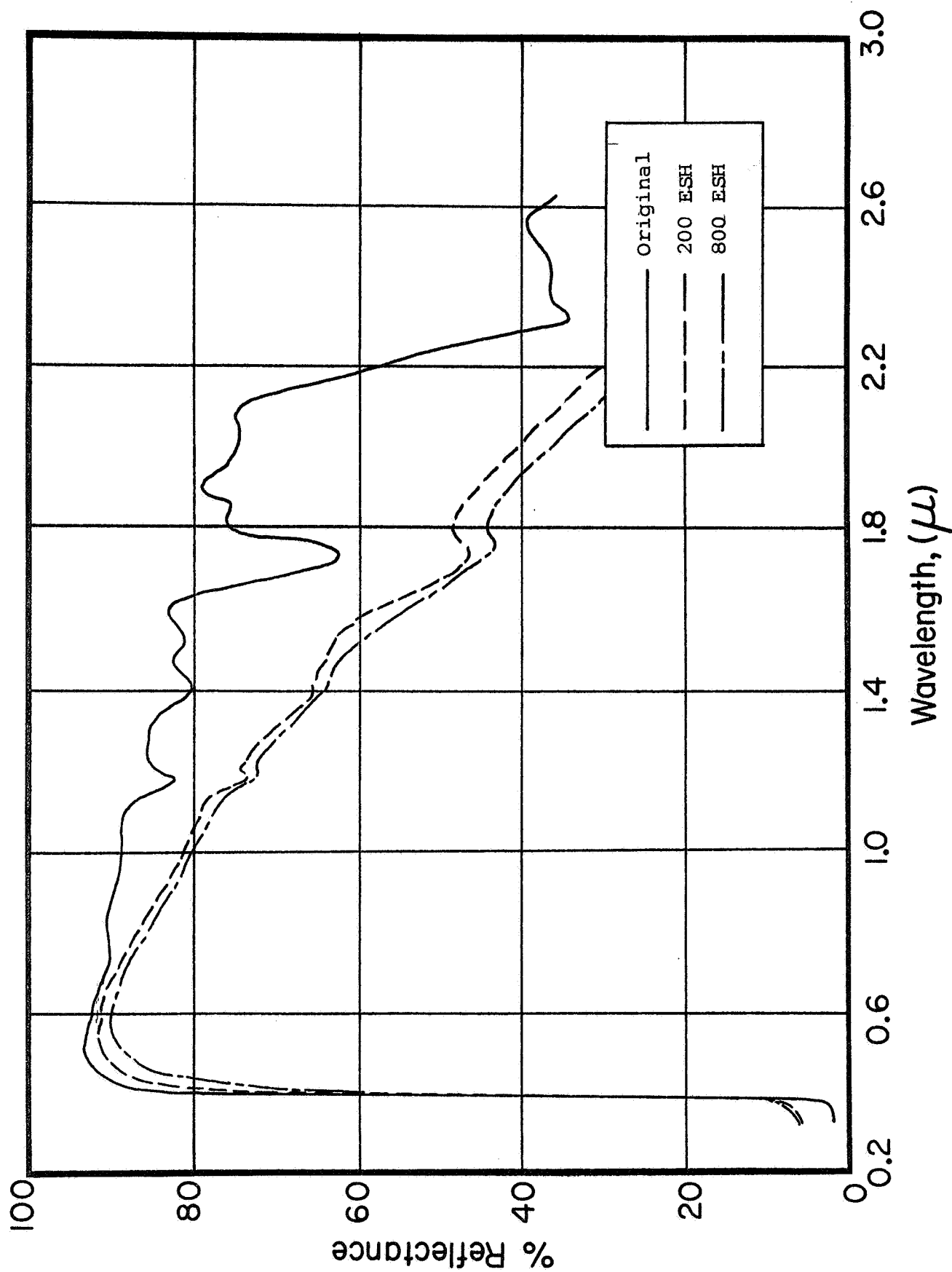


Figure 28: ABSOLUTE REFLECTANCE OF CLEANED S-13 (#30) AS A FUNCTION OF UV IRRADIATION IN IRIF TEST 10

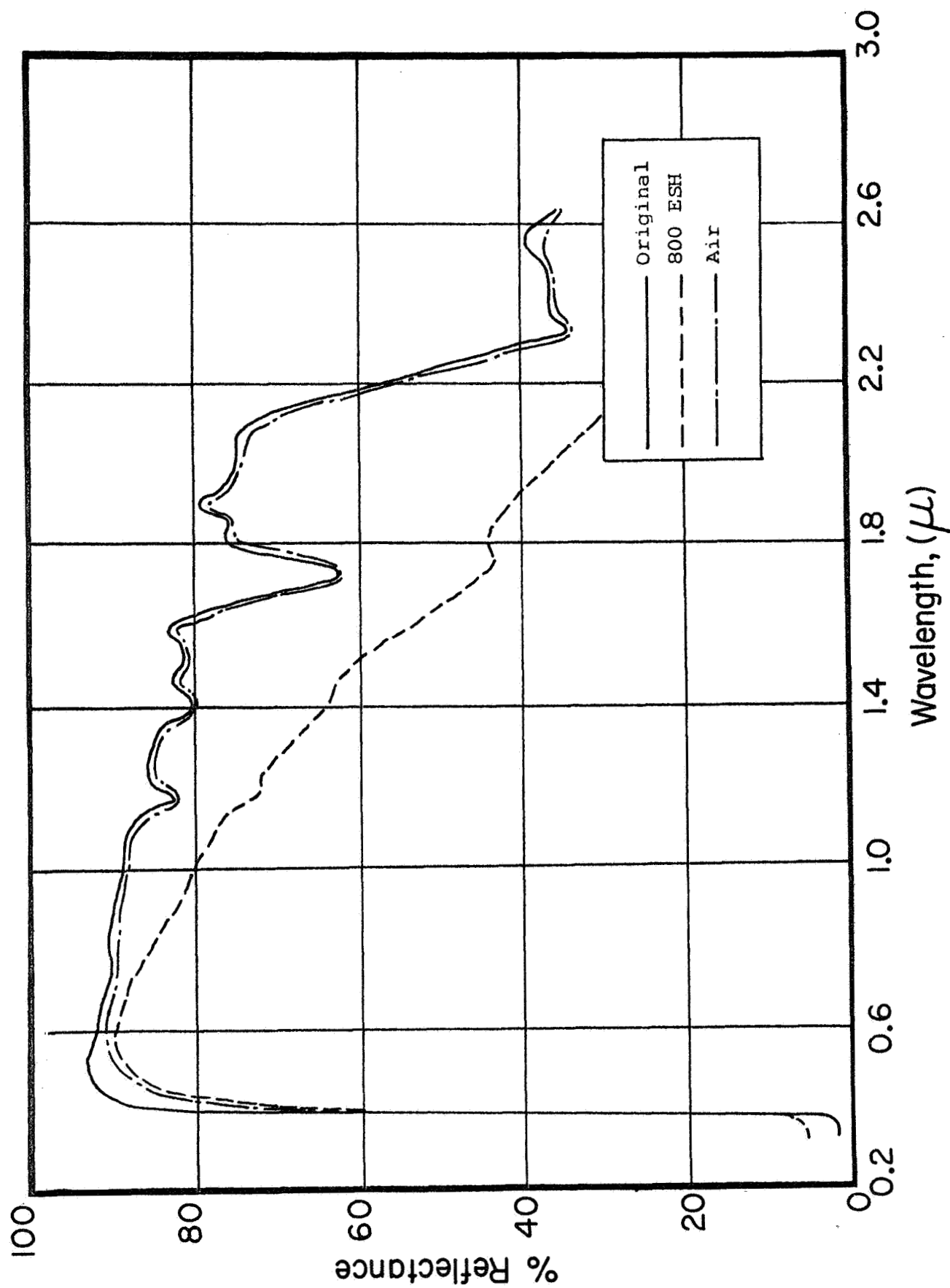


Figure 29: ABSOLUTE REFLECTANCE OF CLEANED S-13 (#30) AS A FUNCTION OF UV IRRADIATION IN IRIF TEST 10

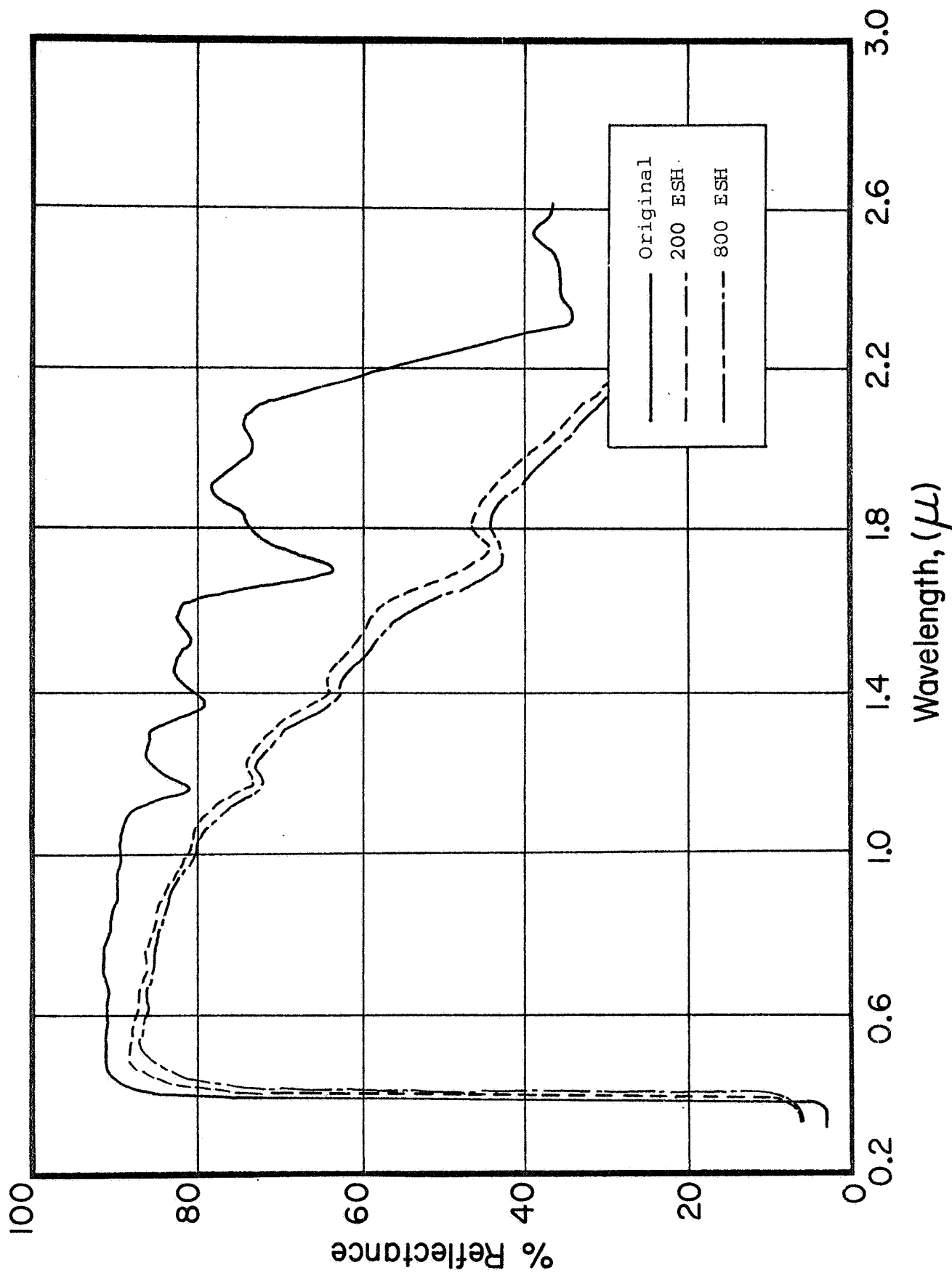


Figure 30: ABSOLUTE REFLECTANCE OF S-13 (UNCLEANED) (#34) AS A FUNCTION OF UV IRRADIATION IN IRIF TEST 10



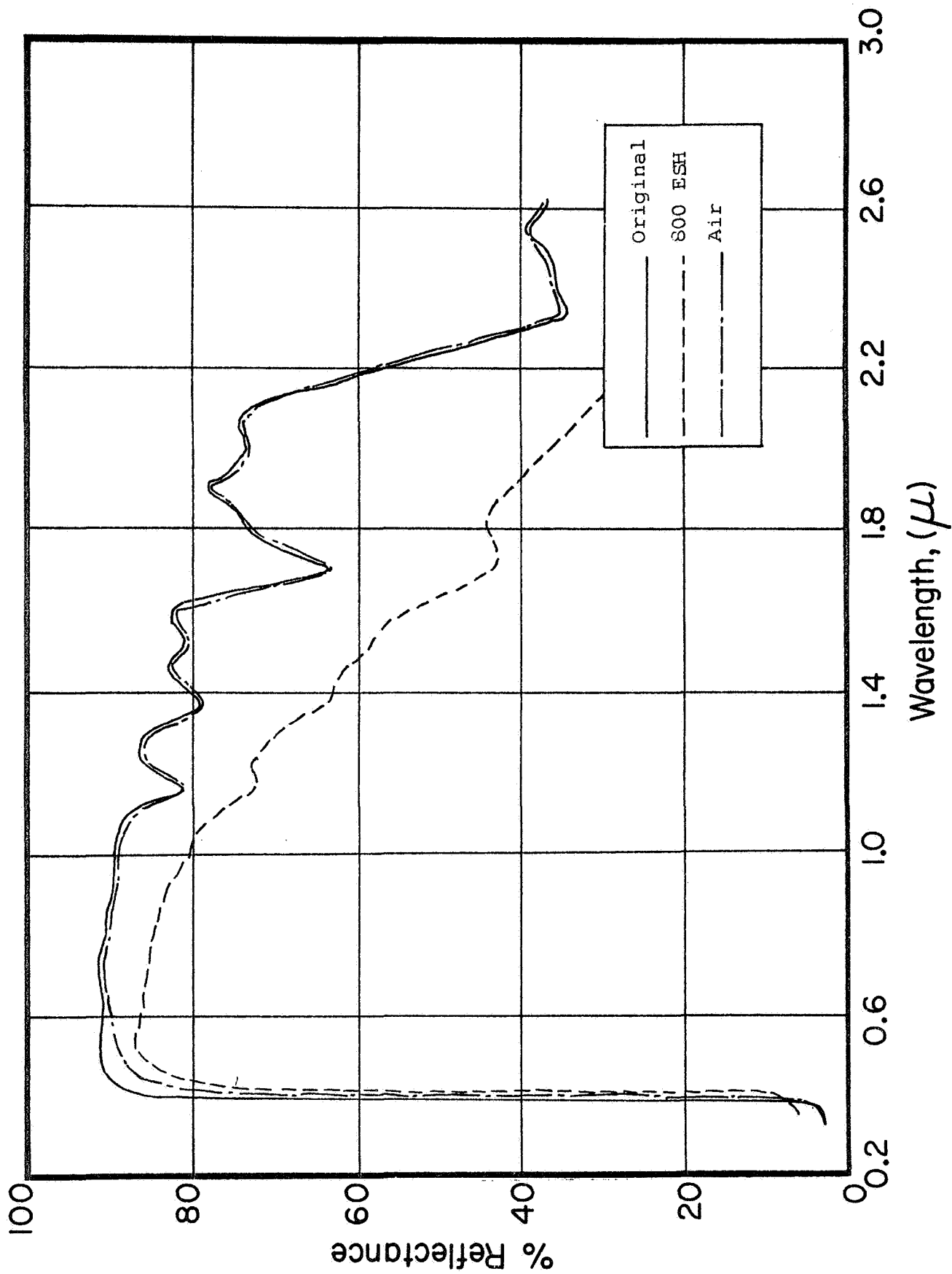


Figure 31: ABSOLUTE REFLECTANCE OF S-13 (UNCLEANED) (#34) AS A FUNCTION OF UV IRRADIATION IN IRIF TEST 10

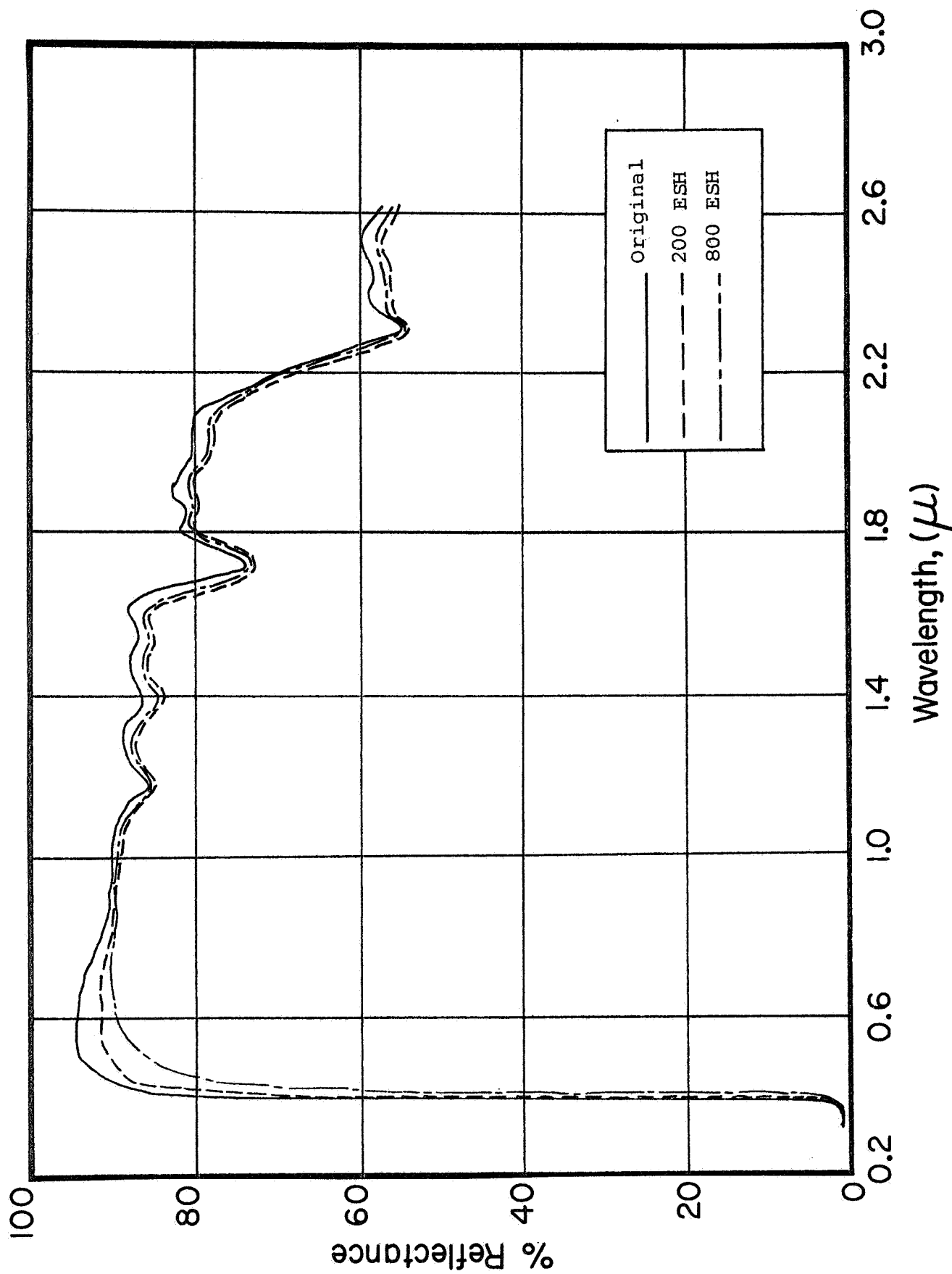


Figure 32: ABSOLUTE REFLECTANCE OF S-13G (BATCH A-295) (#35) AS A FUNCTION OF UV IRRADIATION IN IRIF TEST 10

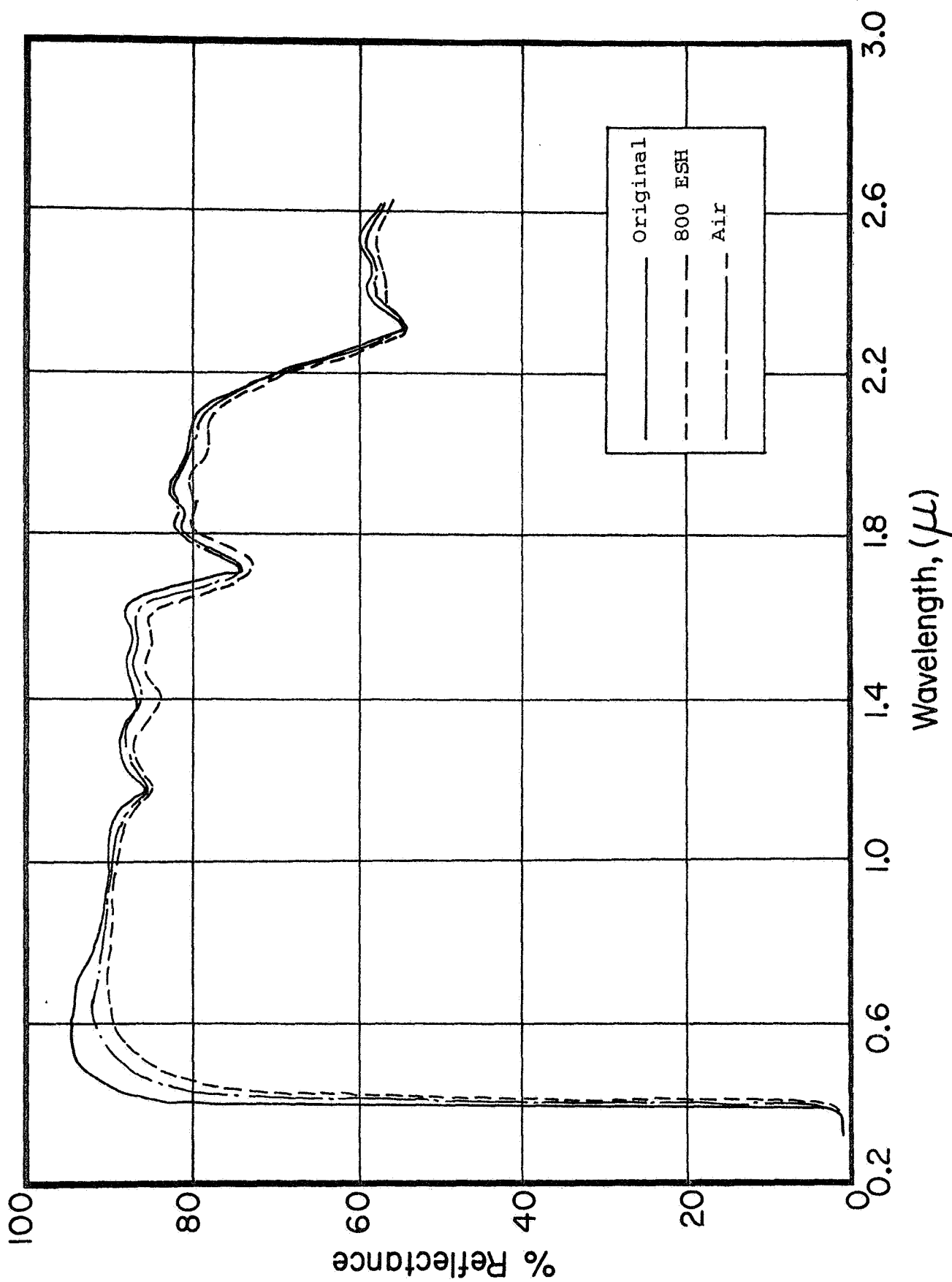


Figure 33: ABSOLUTE REFLECTANCE OF S-13G (BATCH A-295) (#35) AS A FUNCTION OF UV IRRADIATION IN IRIF TEST 10

damage to about 1000-nm wavelength (see Figures 16 and 17); its  $\Delta\alpha_s$  in 800 ESH was 0.021.

5. The behavior of GT-1015 leads us to rule out significant contamination as having been responsible for the damage exhibited by the aluminum blank (and the lesser damage sustained by the MTL-3 and GT-1295 specimens). This contention is supported by the absence of damage in the ultraviolet region to either Tabor's manganese black, MTL-3 or the Z93 specimen (Item 24). The interference peaks (Figures 18 and 19) shifted to lower wavelengths in the degraded conditions (GT-1015 exhibits 14 orders of interference in the 325 to 2700-nm wavelength region). The displacement of the interference maxima at 412-nm wavelength (4125 Å) was 13 nm (130 Å). The reflectance decrease in this region is approximately 27% measured as a peak-to-peak loss; its  $\Delta\alpha_s$  was 0.123 in 800 ESH of ultraviolet irradiation.

6. The specimen of Z93 (Item 24), which was about 2-1/2 yr old when irradiated, exhibited a reflectance decrease of less than 2% at 400-nm wavelength and a reflectance increase of 2% beyond about 1800-nm wavelength (Figures 20 and 21). The reflectance increase in the 1800-nm region is attributed to photodesorption of adsorbed water.

7. The tantalum oxide and lithium fluoride-pigmented potassium silicate paints (Items 17 and 19, respectively) both exhibited severe degradation in the entire visible spectrum. The  $Ta_2O_5$  paint exhibited a loss in reflectance of 21% at 400-nm wavelength (Figures 22 and 23); the LiF paint exhibited a loss of 38% at 400 nm (Figures 24 and 25). The tantala paint degraded out to 1600-nm wavelength whereas the LiF specimen exhibited no damage beyond 1200-nm; the  $Ta_2O_5$  and LiF paints exhibited solar absorptance increases of 0.128 and 0.178, respectively, in 800 ESH of ultraviolet irradiation. Both paints showed reflectance increases in the 1800- to 2600-nm wavelength region.

8. The zirconia-pigmented potassium silicate specimen

(Item 23) exhibited a  $\Delta\alpha_s$  of 0.075 in 800 ESH of ultraviolet irradiation. Like the Z93,  $Ta_2O_5$  and LiF specimens, the  $ZrO_2$  paint exhibited no degradation in the infrared. Also, like the other silicate paints, it exhibited a reflectance increase in the 1800-nm wavelength region, presumably due to the photo-desorption of water.

9. Little difference in  $\Delta\alpha_s$  was observed between the cleaned and the uncleaned S-13 specimens (Items 30 and 34). However, the uncleaned S-13 exhibited approximately 25% greater damage at 412-nm wavelength than the specimen cleaned with Alconox, distilled water and ethyl alcohol. No such differences were observed in other wavelength regions and the cleaned specimen exhibited only a slightly lower value for  $\Delta\alpha_s$  than the uncleaned S-13 (0.083 compared to 0.085). As expected from our earlier studies (ref. 4), the bulk of the infrared damage sustained by the S-13 specimens occurred in the first 200 ESH of ultraviolet exposure. The infrared damage was almost completely bleached on admission of air to the IRIF-I space chamber (Figures 28 to 31).

10. The S-13G specimen (Item 35) exhibited a  $\Delta\alpha_s$  of 0.034 in 800 ESH of ultraviolet irradiation. This is considerably greater damage than exhibited by specimens prepared from current batches of S-13G (ref. 5). However, Batch A-295 contained petroleum ether as one of the solvents; petroleum ether subsequently has been observed to cause severe degradation in S-13G specimens (ref. 4, 5).

#### C. IRIF-I Test No. 13

Test No. 13 involved a solar-ultraviolet-acceleration factor of 6X. The total exposure in Test 13 was 2800 ESH of ultraviolet irradiation; in situ hemispherical spectral reflectance measurements were performed after 0, 75, 150, 650, 1000, 1700 and 2800 ESH and after admission of air to the IRIF as the terminal operation of Test 13. The samples were maintained at a nominal temperature of 8°C; the average pressure during the irradiation period was  $2 \times 10^{-7}$  Torr.

IIT RESEARCH INSTITUTE

The specimens irradiated in Test 13 are presented along with the calculated results of the incremental ultraviolet exposures in Table 6. Examination of the data presented in Table 6 shows that S-13 (Item 30),  $\text{ZrO}_2/\text{PS7}$  (Item 23), GT-1275 (Item 7), GT-1015 (Item 8), Lithafrax (Item 10) and S-13G all exhibited significant bleaching on admission of air, although all specimens bleached to some extent. It should be noted that admission of 150 Torr of nitrogen (held for one hr) did not cause a measurable increase in the infrared reflectance of S-13 specimen (Item 30) at 2050-nm wavelength. (Bleaching studies are the subject of a later section of this report.)

The data presented in Table 6 are plotted in Figures 34 through 36. Comparison of the data contained in Table 6 and Figures 34 through 36 with the data in Table 5 shows that Test 13 was somewhat more severe than Test 10 for the Pegasus S-13 (Item 30) and GT-1015 (Item 8) specimens. The reverse was true for the zirconia paint (Item 23) and both Z93 specimens (Items 16 and 24). However, the damage sustained by both MTL-3 and GT-1275 (Items 5 and 7, respectively) was approximately equal in both tests.

The scatter in the data plotted for GT-1015 (Figure 34) is attributed to the errors propagated in calculating the solar absorptance of a surface that exhibits the degree in interference peaks that characterize this surface.

The increasing slope of the Lithafrax (Item 10), Plasmoclay (Item 20) and zirconia (Item 23) paints may be due to the fact that these pigments are ultraviolet scatterers and the ultraviolet is attenuated less readily at the coating's surface. Severe initial damage, as observed in the Lithafrax paint, quickly increases the ultraviolet extinction, which in turn militates against the tendency for a linear relationship between damage and exposure. Unstable pigments that are ultraviolet absorbers, such as rutile and anatase, can be expected to possess decreasing slopes at moderately long exposures when plotted against the log of exposure.

Table 6

EFFECT OF UV IRRADIATION IN THE IRIF ON  
SELECTED THERMAL-CONTROL SURFACE COATINGS  
(IRIF Test 13; Solar Intensity = 6X)

Item No.	Surface	Exposure (ESH)	Solar Absorptance			
			$\alpha_1$	$\alpha_2$	$\alpha_s$	$\Delta\alpha_s$
30	S-13 Cleaned	0	.130	.101	.231	-
		75	.157	.138	.295	.064
		150	.161	.139	.300	.069
		650	.196	.154	.350	.119
		1000	.204	.162	.366	.135
		1700	.220	.167	.387	.156
		2800	.244	.172	.416	.185
		Air	.221	.101	.322	.091
23	ZrO <sub>2</sub> /PS7	0	.121	.152	.273	-
		75	.138	.153	.291	.018
		150	.144	.153	.297	.024
		650	.164	.156	.320	.047
		1000	.165	.159	.324	.051
		1700	.191	.161	.354	.079
		2800	.230	.168	.398	.125
		Air	.219	.158	.377	.104
16	Z93 (Fresh)	0	.138	.084	.222	-
		75	.141	.082	.223	.001
		150	.142	.084	.226	.004
		650	.146	.084	.230	.008
		1000	.146	.084	.230	.008
		1700	.152	.083	.235	.013
		2800	.158	.082	.240	.018
		Air	.156	.081	.237	.015
5	MTL-3	0	.348	.219	.567	-
		75	.347	.214	.561	-.008
		150	.350	.214	.564	-.003
		650	.354	.219	.573	+.006
		1000	.351	.222	.573	.006
		1700	.364	.222	.586	.019
		2800	.369	.227	.596	.029
		Air	.368	.223	.591	.024
7	GT-1275	0	.203	.120	.323	-
		75	.206	.117	.333	.010
		150	.210	.129	.339	.016
		650	.216	.132	.348	.025
		1000	.215	.133	.348	.025
		1700	.220	.135	.352	.032
		2800	.221	.138	.359	.036
		Air	.215	.123	.338	.015
20	Plasmoclay/K <sub>2</sub> O·SiO <sub>2</sub>	0	.129	.123	.252	-
		75	.148	.125	.273	.021
		150	.155	.125	.280	.028
		650	.186	.129	.315	.063
		1000	.195	.132	.327	.075
		1700	.211	.130	.341	.089
		2800	.225	.138	.363	.111
		Air	.221	.132	.353	.101

Table 6 (cont'd)

Item No.	Surface	Exposure (ESH)	Solar Absorptance			
			$\alpha_1$	$\alpha_2$	$\alpha_s$	$\Delta\alpha_s$
10	Lithafrax	0	.051	.081	.132	-
		75	.113	.087	.200	.068
		150	.125	.089	.214	.082
		650	.175	.093	.268	.136
		1000	.189	.094	.283	.151
		1700	.222	.100	.322	.190
		2800	.247	.106	.353	.221
		Air	.230	.097	.327	.195
24	Z93 (old)	0	.125	.074	.199	-
		75	.128	.069	.197	-.002
		150	.132	.070	.202	+.003
		650	.138	.070	.208	.009
		1000	.140	.069	.209	.010
		1700	.142	.069	.211	.012
		2800	.147	.073	.220	.021
		Air	.148	.066	.214	.015
9	FEP Teflon second-surface mirror	0	.097	.075	.172	-
		75	.109	.081	.190	.018
		150	.108	.080	.188	.016
		650	.114	.078	.192	.020
		1000	.114	.07	.193	.021
		1700	.117	.077	.194	.022
		2800	.118	.077	.195	.023
		Air	.115	.074	.189	.017
25	Rutile-opacified-Porcelain Enamel	0	.148	.144	.292	-
		75	.152	.144	.296	.004
		150	.152	.145	.297	.005
		650	.160	.145	.305	.013
		1000	.160	.143	.303	.011
		1700	.162	.145	.307	.015
		2800	.164	.145	.309	.017
		Air	.162	.142	.304	.012
8	GT-1015	0	.148	.098	.246	-
		75	.198	.095	.293	.047
		150	.217	.096	.313	.067
		650	.287	.100	.387	.141
		1000	.306	.118	.424	.178
		1700	.312	.119	.431	.185
		2800	.327	.125	.452	.206
		Air	.309	.114	.423	.177
	S-13G (Hand-mulled pigment)	0	.132	.104	.236	-
		75	.150	.110	.260	.024
		150	.160	.111	.271	.035
		650	.186	.114	.300	.064
		1000	.198	.110	.308	.072
		1700	.209	.109	.318	.082
		2800	.224	.113	.337	.101
		Air	.212	.105	.317	.081



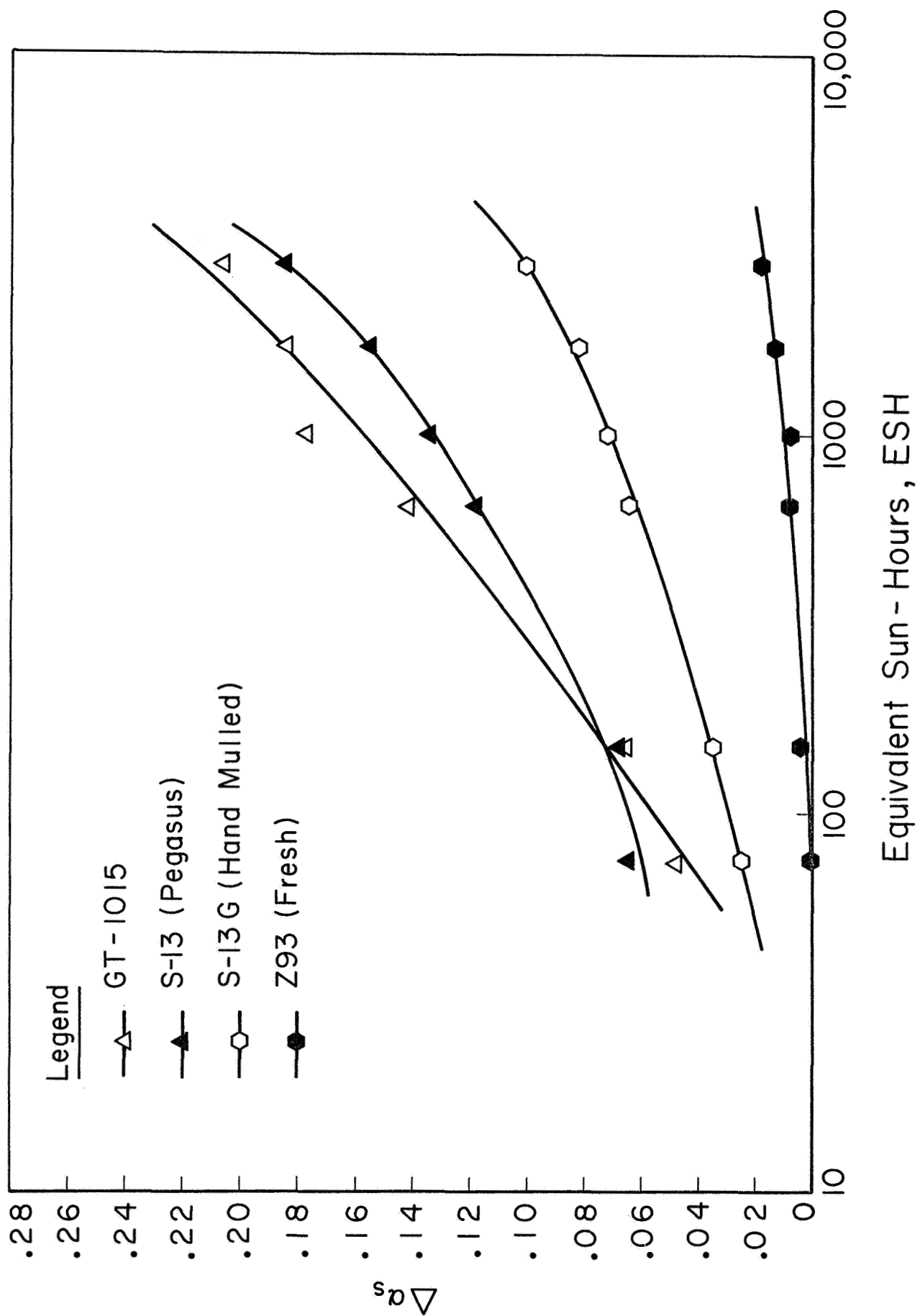


Figure 34: DEGRADATION RATES OF SEVERAL SURFACES EVALUATED IN IRIF-I TEST 13

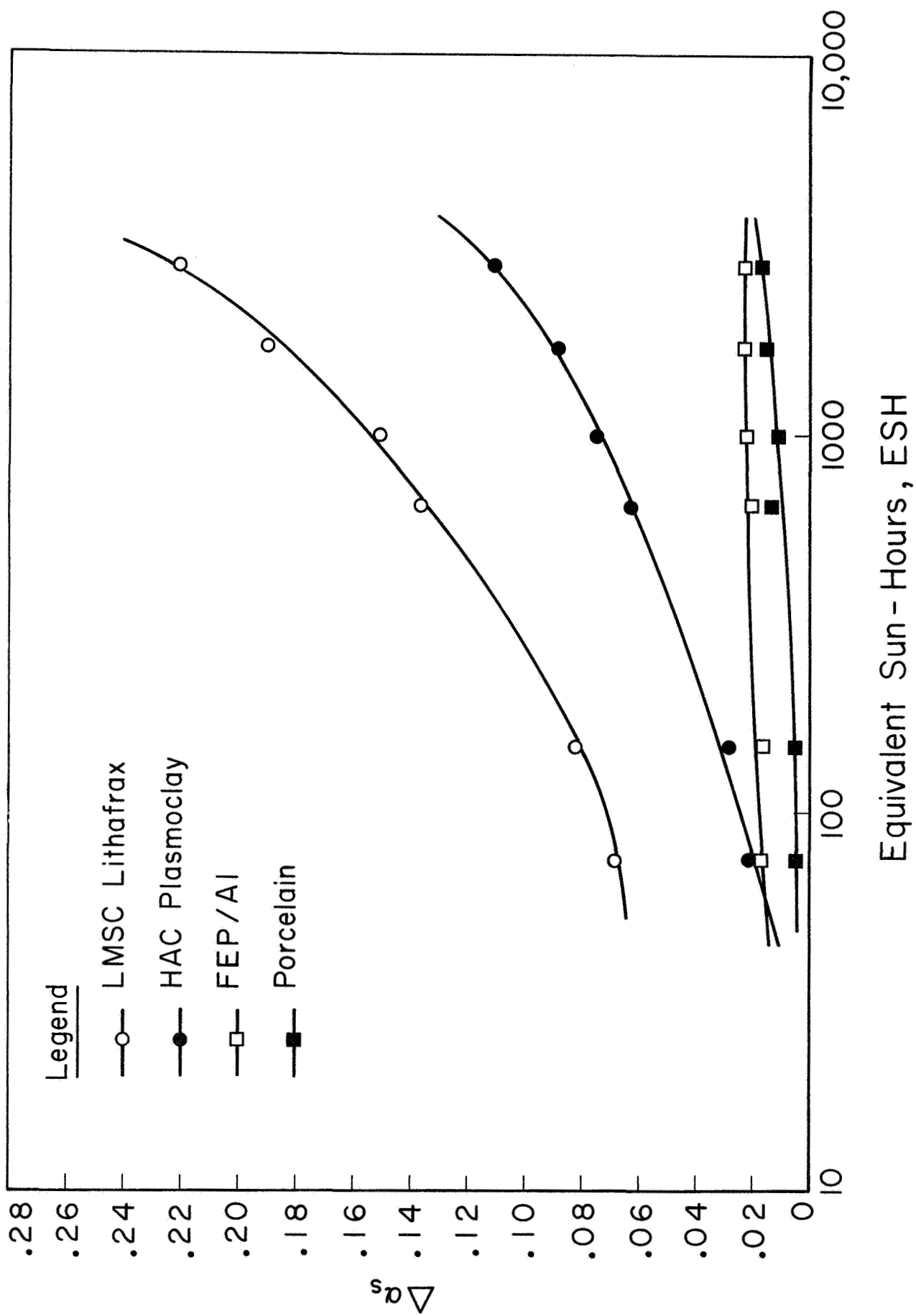


Figure 35: DEGRADATION RATES OF SEVERAL SURFACES EVALUATED IN IRIF-I TEST 13

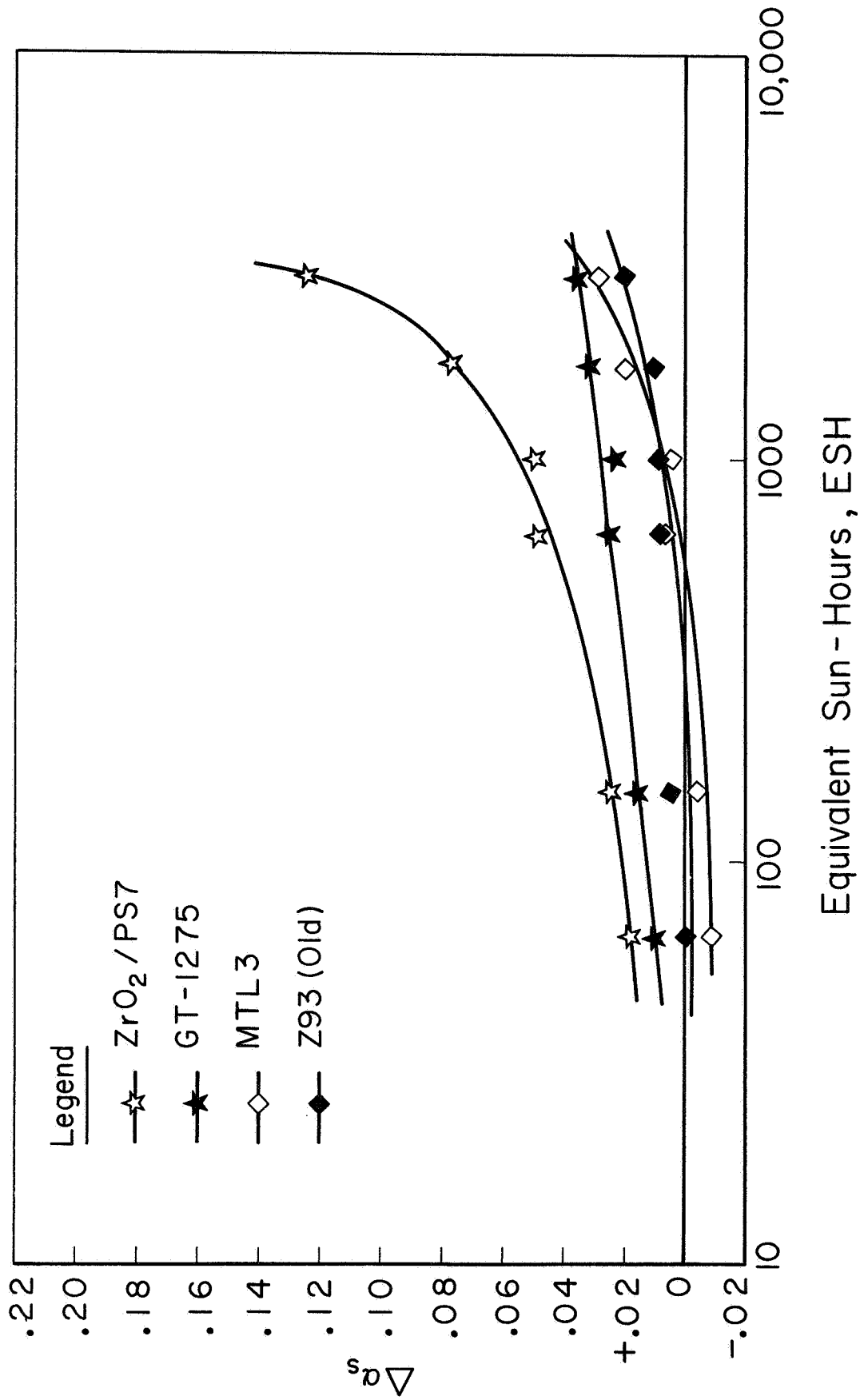


Figure 36: DEGRADATION RATES OF SEVERAL SURFACES EVALUATED IN IRIF-I TEST 13

The initial severe damage to S-13 is consistent with previous observations that have contributed to the concept that rapid photodesorption of zinc oxide in vacuum is involved with the damage mechanism. Since the photosensitivity of zinc oxide is known to extend beyond the edge to about 5000 Å, the untreated pigment is expected to slowly undergo damage in the infrared as a result of the deep scattering penetration of light of slightly longer wavelength than the edge. This may account for the increasing slope observed for S-13 in Figure 34.

The S-13G specimen employed was known to be "damaged" by the hand-mulling procedure employed and we believe that this explains the initially high damage as well as the increasing slope observed as a function of exposure.

The Plasmoclay specimen (Item 20) was observed to undergo a  $\Delta\alpha_s$  of 0.06 in 600 ESH of ultraviolet exposure. This compares very favorably with the flight values reported by Hagemeyer (ref. 1) for the Surveyor paint (also HAC's Plasmoclay). He reported a  $\Delta\alpha_s$  of 0.06 in 600 ESH for flight measurements.

The damage spectra of the Surveyor paint (Item 20), the Lithafrax paint (Item 10), the FEP-Teflon second-surface mirror (Item 9) and the rutile-opacified porcelain enamel (Item 25) are presented in Figures 37 through 40. The spectra of the other specimens irradiated in Test 13 are not presented here since the damage that they exhibited was in no cases qualitatively different from what they exhibited after irradiation in Test 10 (Figures 10 through 33). The Plasmoclay and Lithafrax paints were severely damaged in Test 13, exhibiting  $\Delta\alpha_s$  values of 0.11 and 0.20 respectively, after 2800 ESH of ultraviolet irradiation. However, neither the FEP Teflon mirror nor the porcelain enamel were seriously damaged; both surfaces exhibited a  $\Delta\alpha_s$  of only 0.02 in 2800 ESH of irradiation.

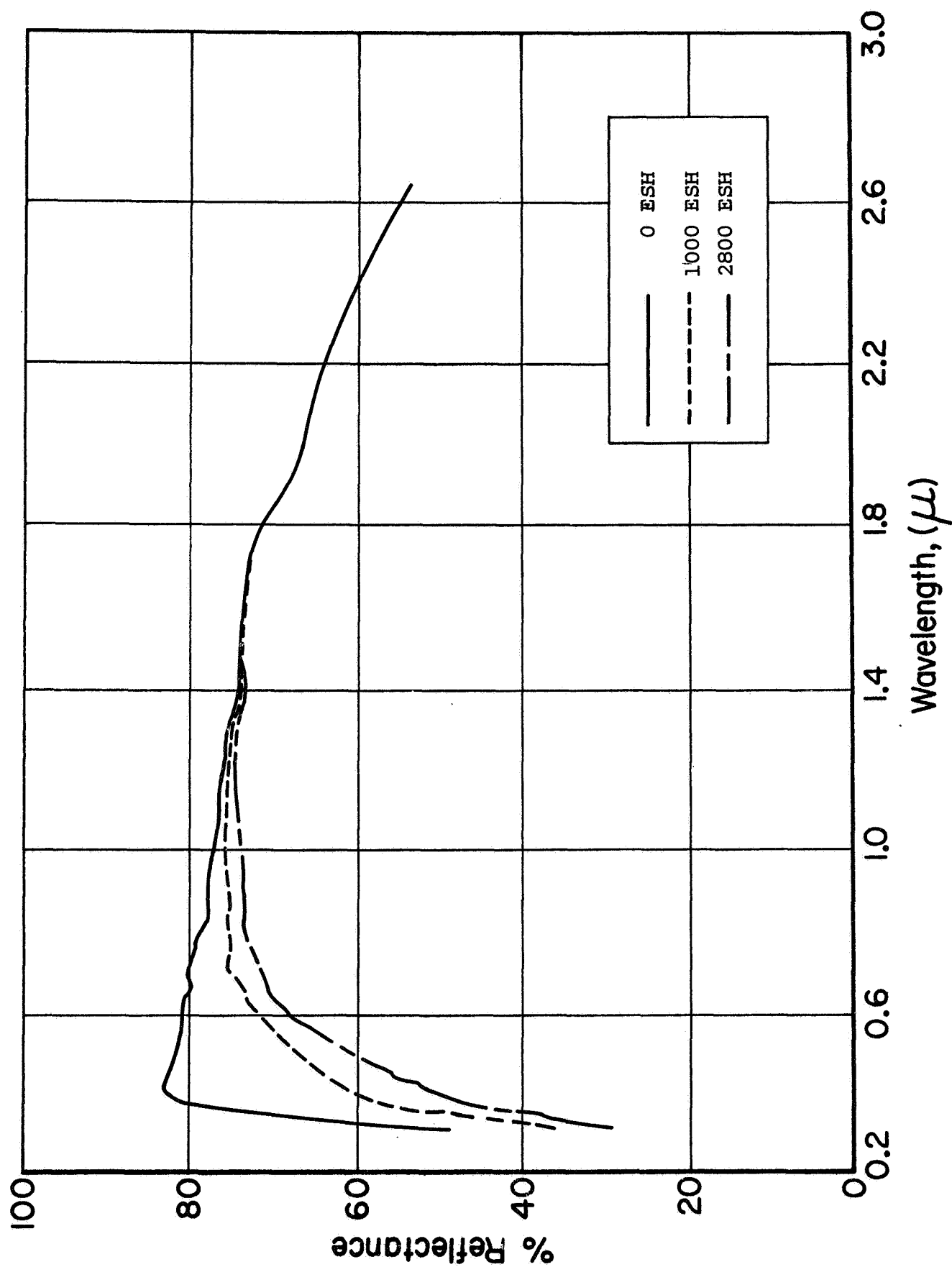


Figure 37: ABSOLUTE REFLECTANCE OF PLASMOCLAY/K<sub>2</sub>O·SiO<sub>2</sub> (#20) AS A FUNCTION OF UV IRRADIATION IN IRIF TEST 13

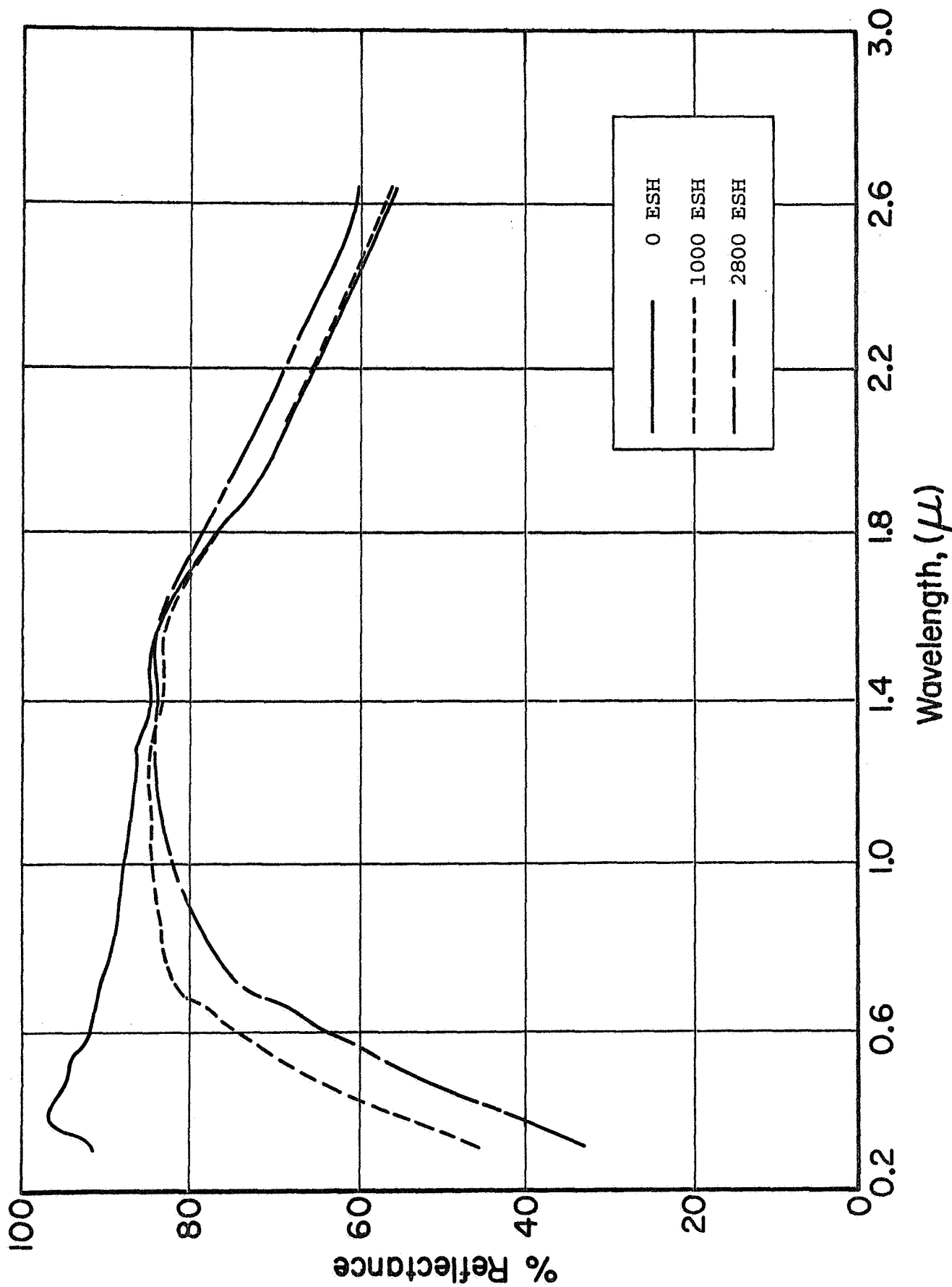


Figure 38: ABSOLUTE REFLECTANCE OF LITHAFRAX (#10) AS A FUNCTION OF UV IRRADIATION IN IRIF TEST 13

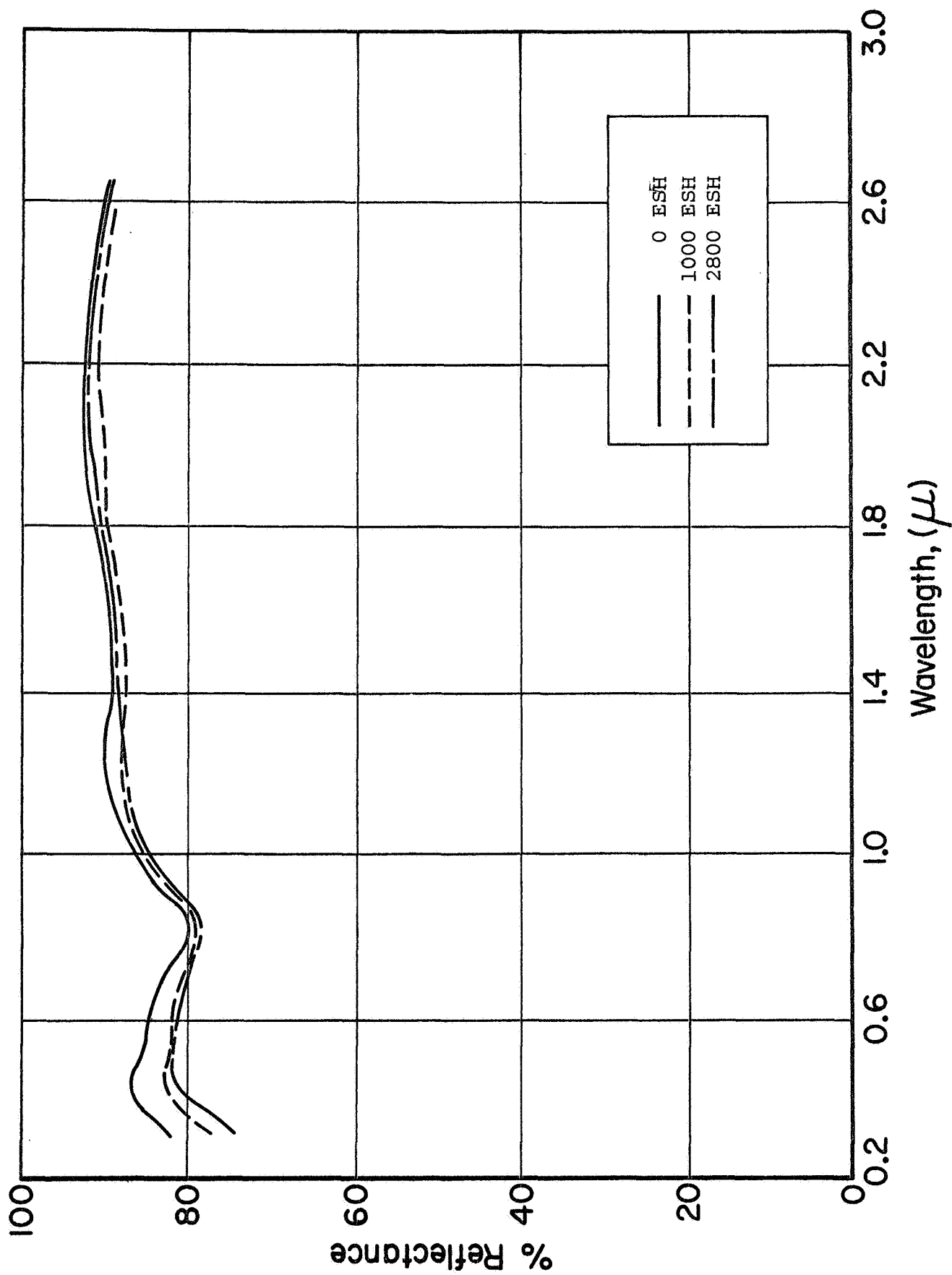


Figure 39: ABSOLUTE REFLECTANCE OF FEP TEFLON MIRROR AS A FUNCTION OF UV IRRADIATION IN IRIF TEST 13

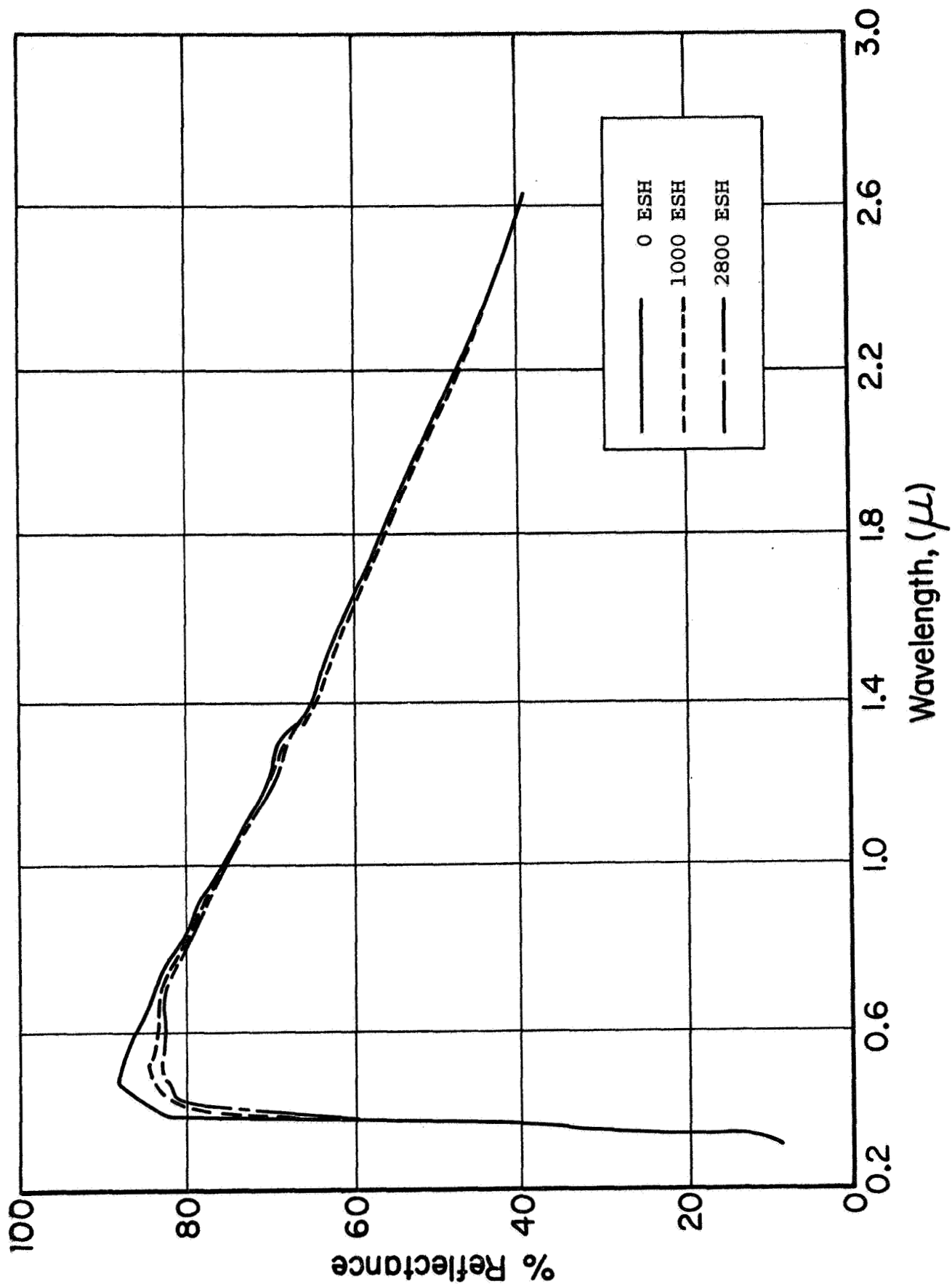


Figure 40: ABSOLUTE REFLECTANCE OF RUTILE-OPACIFIED-PORCELAIN ENAMEL (#25)  
AS A FUNCTION OF UV IRRADIATION IN IRIF TEST 13



#### D. IRIF-I Test No. 15

Test No. 15 involved a solar-ultraviolet-acceleration factor of 6X and a nominal substrate temperature of approximately 85°C (185°F). This temperature was achieved by running hot water through the IRIF-I sample table. The total exposure was for 800 ESH of ultraviolet irradiation; in situ spectral reflectance measurements were performed after 0, 110 and 800 ESH and after admission of air to the IRIF. The average pressure during the irradiation was  $1 \times 10^{-7}$  Torr.

The specimens irradiated in IRIF Test 15 and their respective solar absorptance increases are presented in Table 7. Because of the severity of the damage, the spectra are presented for exposures of 0 and 800 ESH and after admission of air. The reflectance spectra are shown in Figures 41 through 49. A summary of the spectral damage,  $R_{\lambda}$ , after 800 ESH of irradiation is presented in Table 8. Massive damage occurred to all specimens

Table 8

CHANGE IN SPECTRAL ABSORPTANCE (%) OF SEVERAL PEGASUS  
COUPONS ON IRRADIATION FOR 800 ESH (Test 15)

<u>Specimen</u>	<u>Wavelength, nm</u>				
	<u>350</u>	<u>400</u>	<u>700</u>	<u>1500</u>	<u>2000</u>
LMSC OSR	2	2	1	0	0
LMSC Lithafrax	53	58	36	3	+6*
LMSC r-TiO <sub>2</sub>	0	6	15	6	2
ZnS (O-I 650)	3	12	1	0	+2
$\alpha$ -Al <sub>2</sub> O <sub>3</sub> (PS-7)	54	61	36	5	+6
White Kemacryl	0	32	25	11	6
Pegasus S-13	0	44	14	41	60
ZrO <sub>2</sub> (PS-7)	17	38	18	2	+6

\*Positive sign denotes bleaching

Table 7

EFFECT OF ULTRAVIOLET IRRADIATION IN THE IRIF  
ON SELECTED THERMAL-CONTROL SURFACE COATINGS

(IRIF Test 15; Solar Intensity, 6X; Substrate Temperature 85°C)

Item No.	Surface	Exposure (ESH)	Solar Absorptance			
			$\alpha_1$	$\alpha_2$	$\alpha_s$	$\Delta\alpha_s$
1	Optical solar re- flector (LMSC-1)	0	.043	.026	.069	-
		110	.048	.025	.073	.004
		800	.049	.027	.076	.007
		Air	.053	.026	.079	.010
10	Lithafrax (LMSC-2)	0	.080	.069	.149	-
		110	.234	.089	.323	.174
		800	.416	.142	.558	.409
		Air	.294	.108	.402	.253
27	LMSC-3	0	.130	.065	.195	-
		110	.171	.104	.275	.080
		800	.188	.116	.304	.109
		Air	.149	.071	.220	.025
36	ZnS/O-I 650	0	.110	.113	.223	-
		110	.125	.114	.239	.016
		800	.148	.114	.262	.039
		Air	.138	.112	.250	.027
26	Al <sub>2</sub> O <sub>3</sub> /PS7	0	.061	.054	.115	-
		110	.199	.073	.272	.157
		800	.296	.124	.420	.305
		Air	.272	.097	.369	.254
37	Kemacryl (white)	0	.160	.122	.282	-
		110	.235	.168	.403	.121
		800	.342	.196	.538	.856
		Air	.314	.149	.463	.181
38	Cat-a-lac black	0	.478	.484	.962	-
		110	.430	.355	.785	.177
30	S-13 (cleaned)	0	.121	.079	.200	-
		110	.160	.150	.310	.110
		800	.243	.212	.455	.255
		Air	.217	.103	.320	.120
23	ZrO <sub>2</sub> /PS7	0	.093	.082	.175	-
		110	.159	.084	.243	.068
		800	.231	.110	.341	.166
		Air	.211	.095	.306	.131

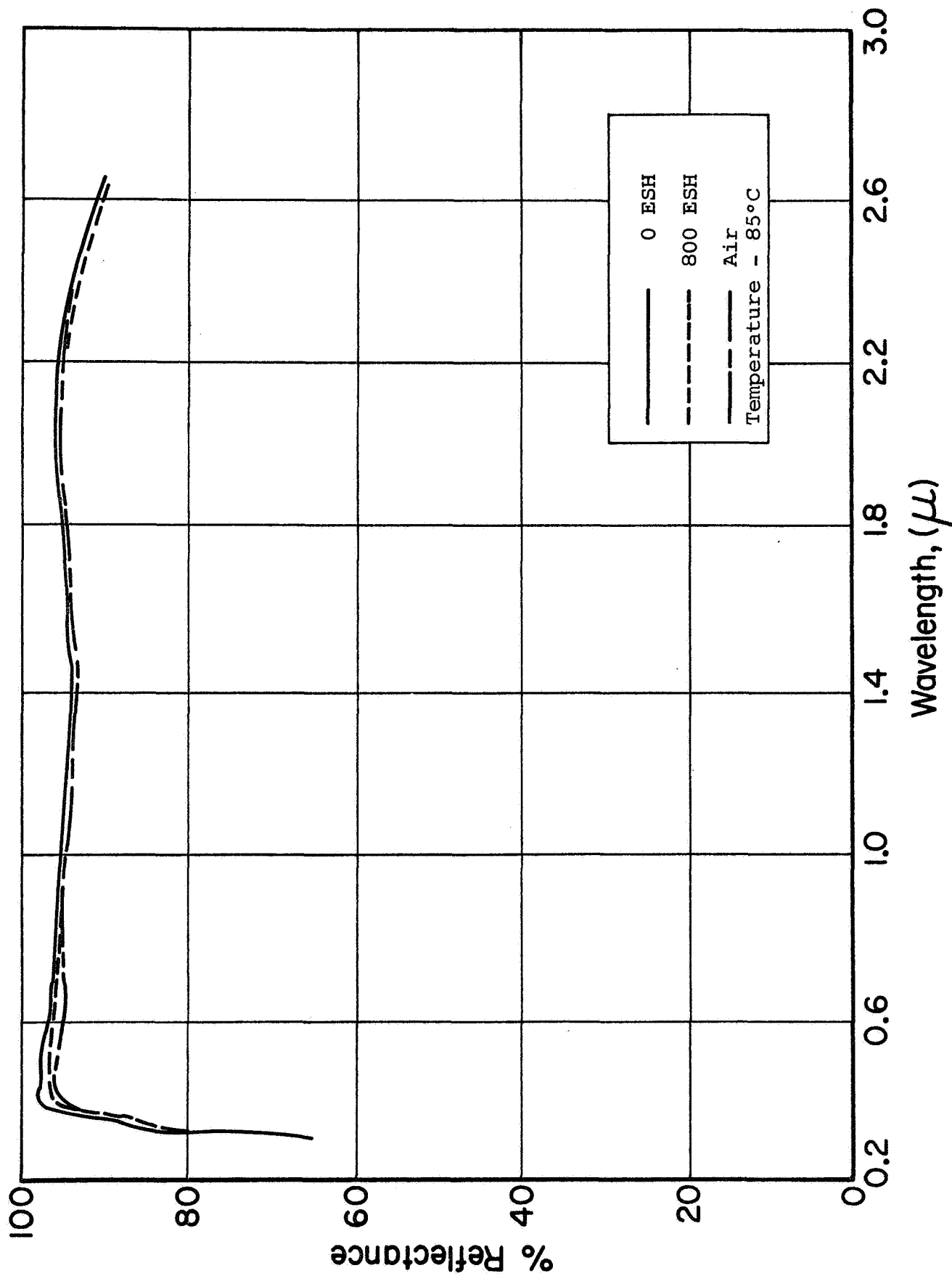


Figure 41: ABSOLUTE REFLECTANCE OF AN OPTICAL SOLAR REFLECTOR (#2) AS A FUNCTION OF UV IRRADIATION IN IRIF TEST 15

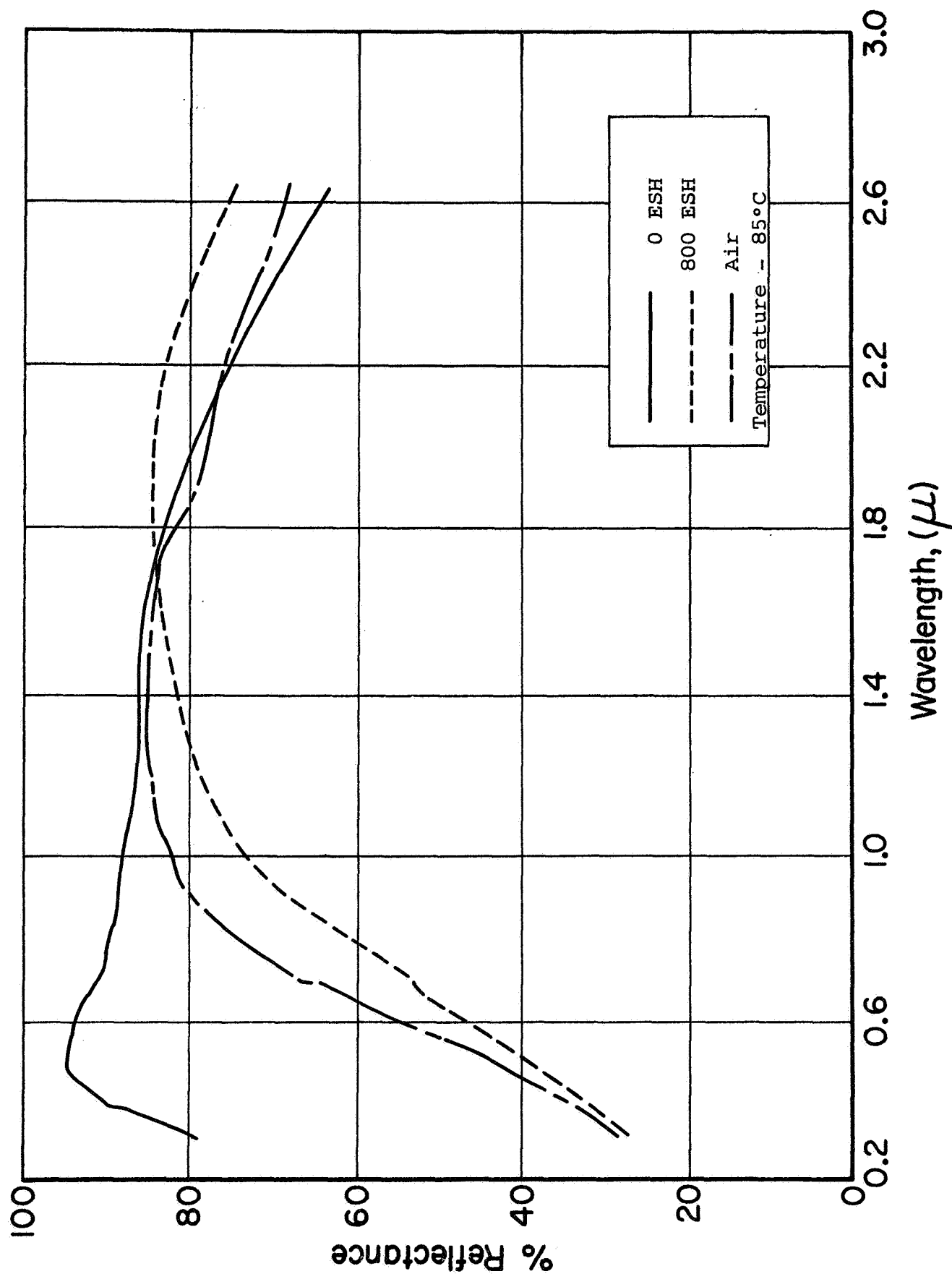


Figure 42: ABSOLUTE REFLECTANCE OF LITHAFRAX (#11) AS A FUNCTION OF UV IRRADIATION IN IRIF TEST 15

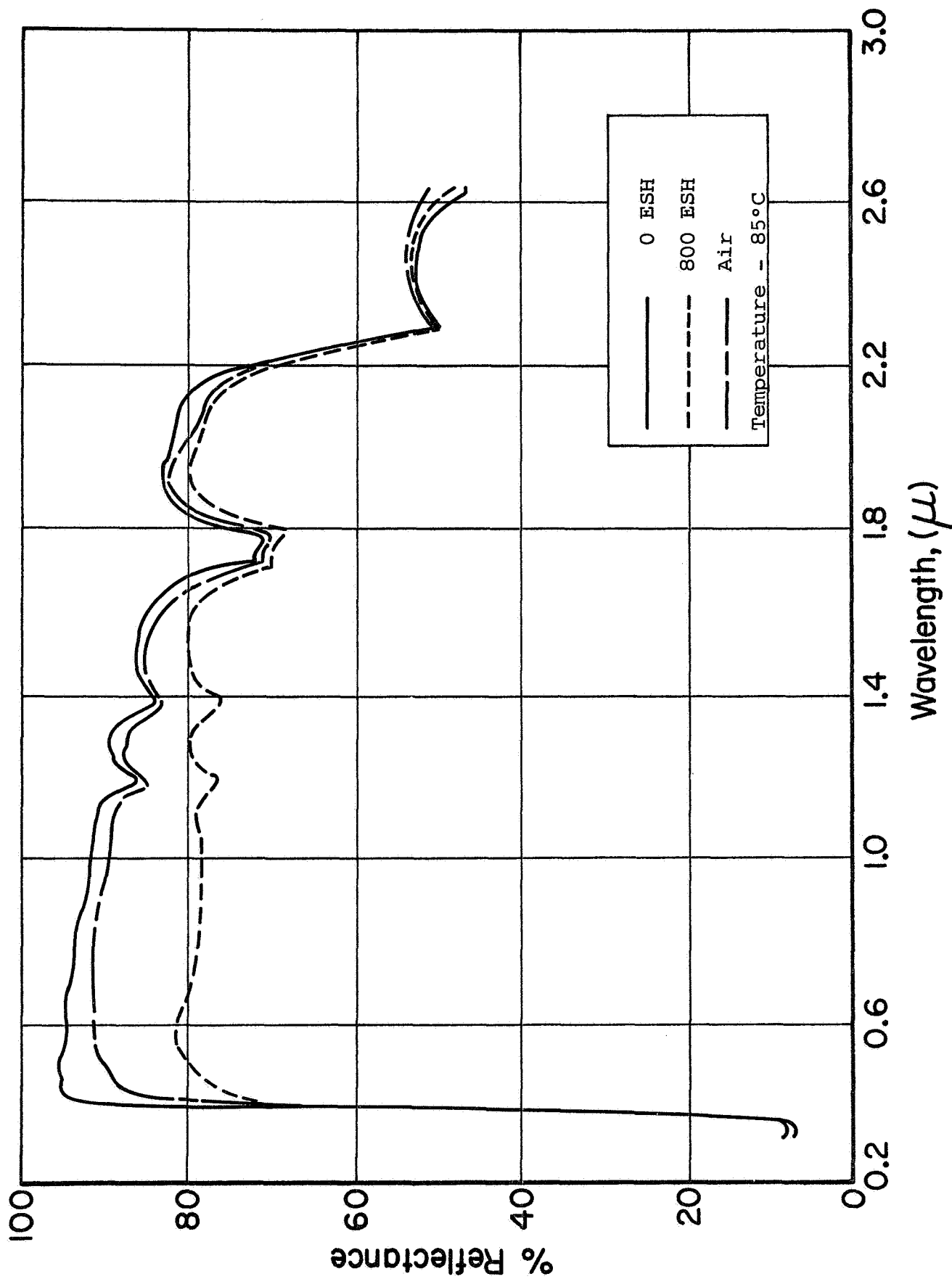


Figure 43: ABSOLUTE REFLECTANCE OF RUTILE-PIGMENTED IMSC-3 (#27) AS A FUNCTION OF UV IRRADIATION IN IRIF TEST 15

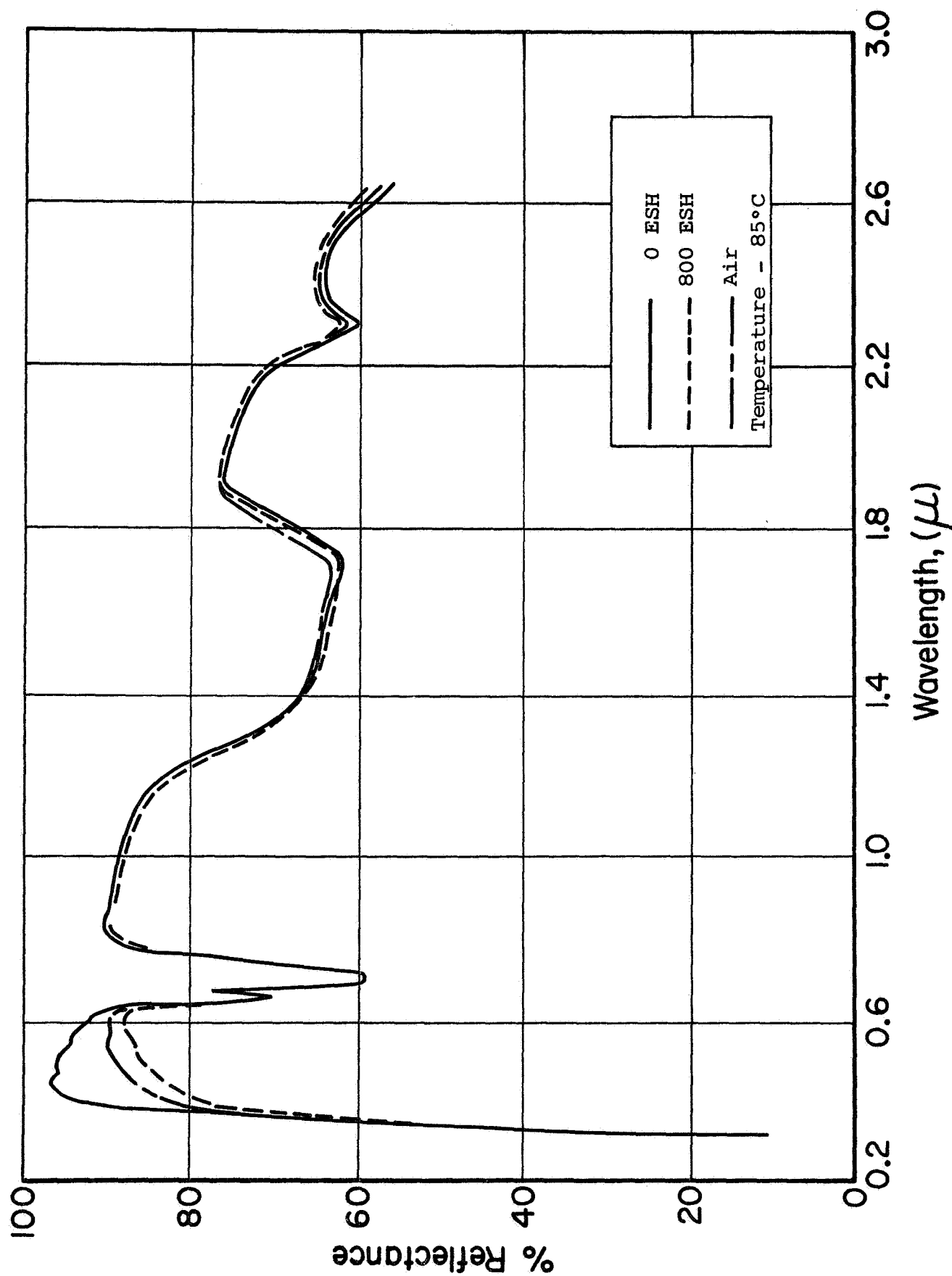


Figure 44: ABSOLUTE REFLECTANCE OF ZINC SULFIDE/O-I 650 (#36) AS A FUNCTION OF UV IRRADIATION IN IRIF TEST 15

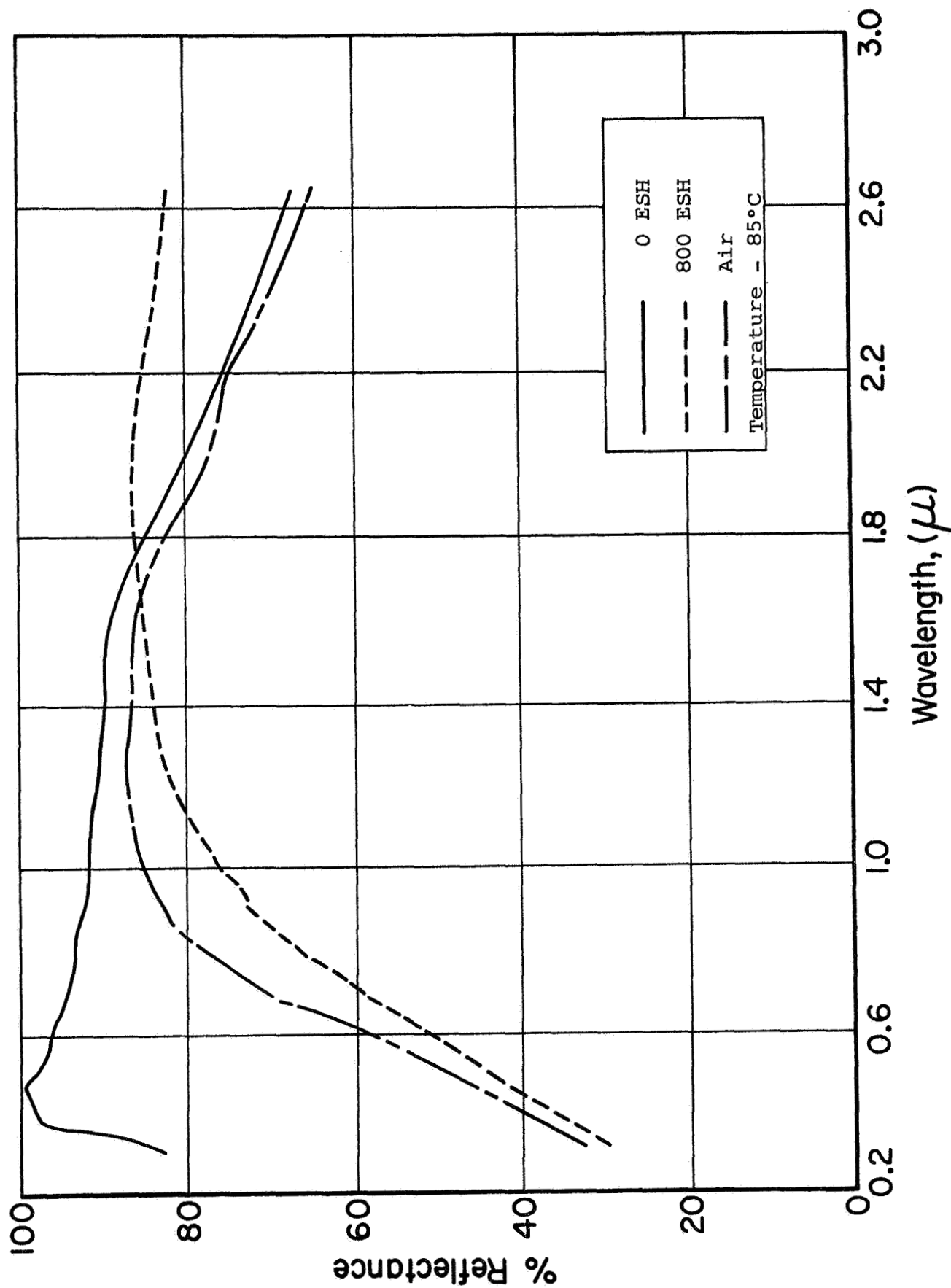


Figure 45: ABSOLUTE REFLECTANCE OF ALUMINA/K-Sil (#26) AS A FUNCTION OF UV IRRADIATION IN IRIF TEST 15

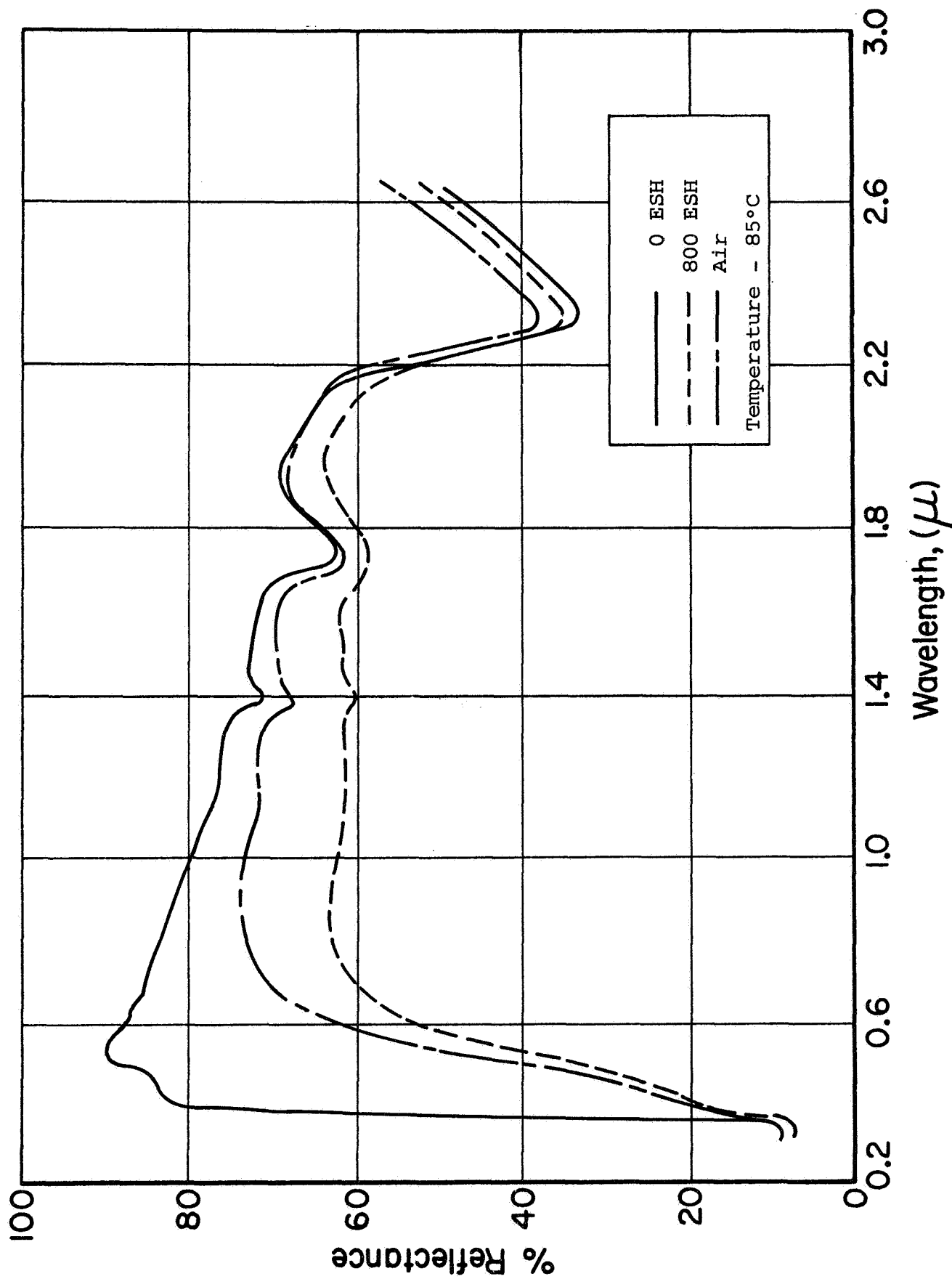


Figure 46: ABSOLUTE REFLECTANCE OF WHITE KEMACRYL (#37) AS A FUNCTION OF UV IRRADIATION IN IRIF TEST 15



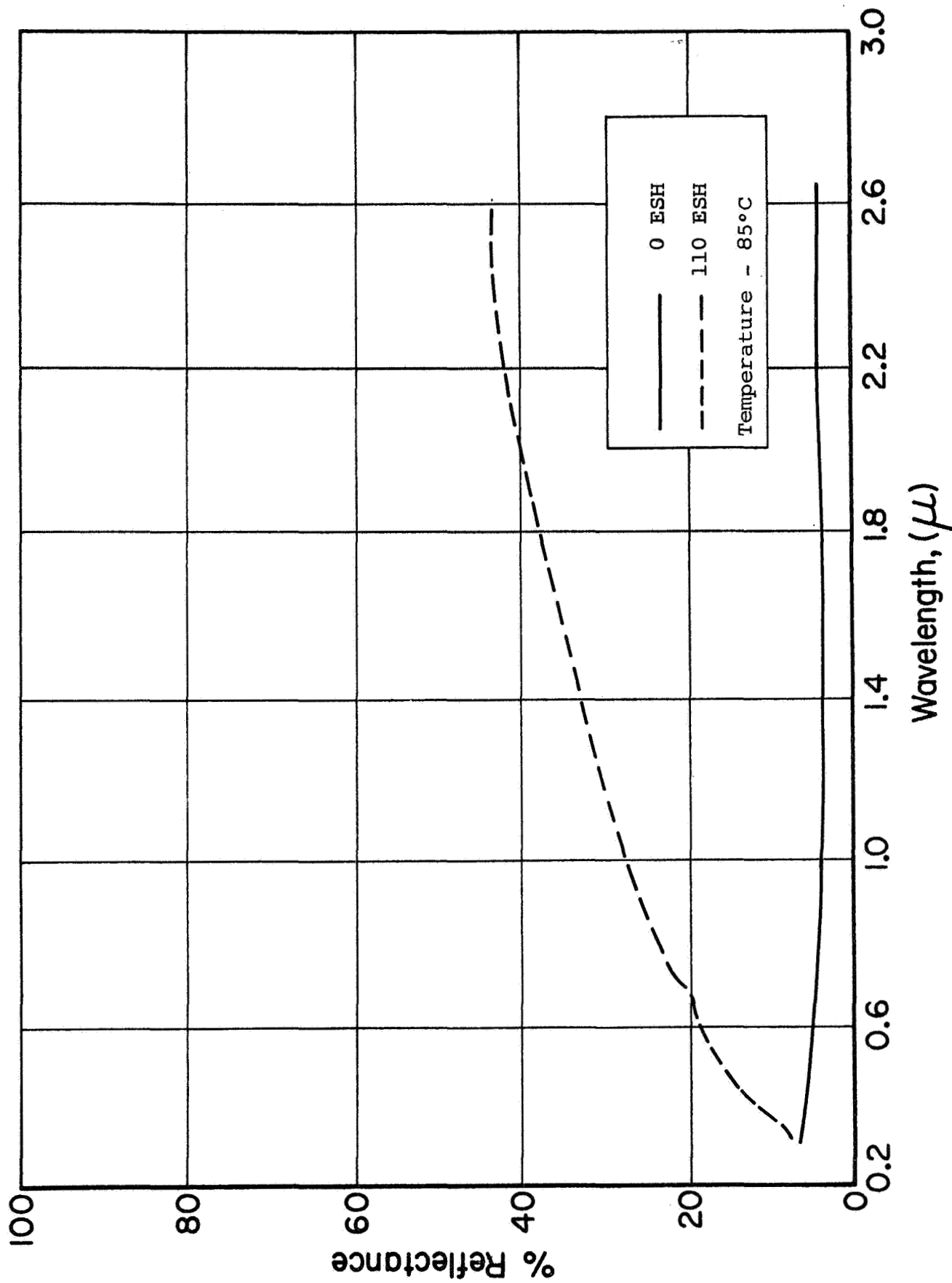


Figure 47: ABSOLUTE REFLECTANCE OF CAT-A-LAC BLACK (#38) AS A FUNCTION OF UV IRRADIATION IN IRIF TEST 15

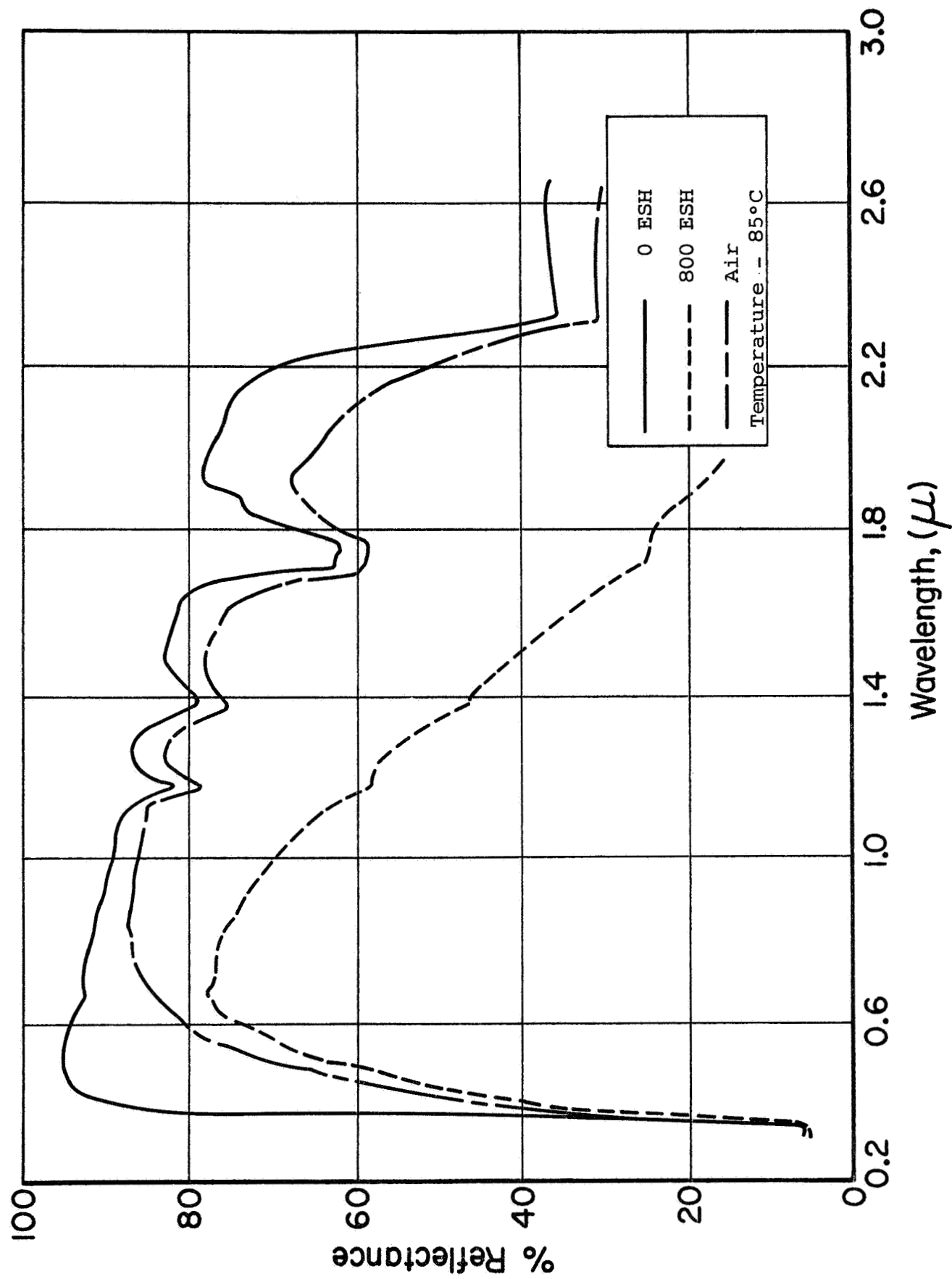


Figure 48: ABSOLUTE REFLECTANCE OF CLEANED PEGASUS S-13 (#30) AS A FUNCTION OF UV IRRADIATION IN IRIF TEST 15

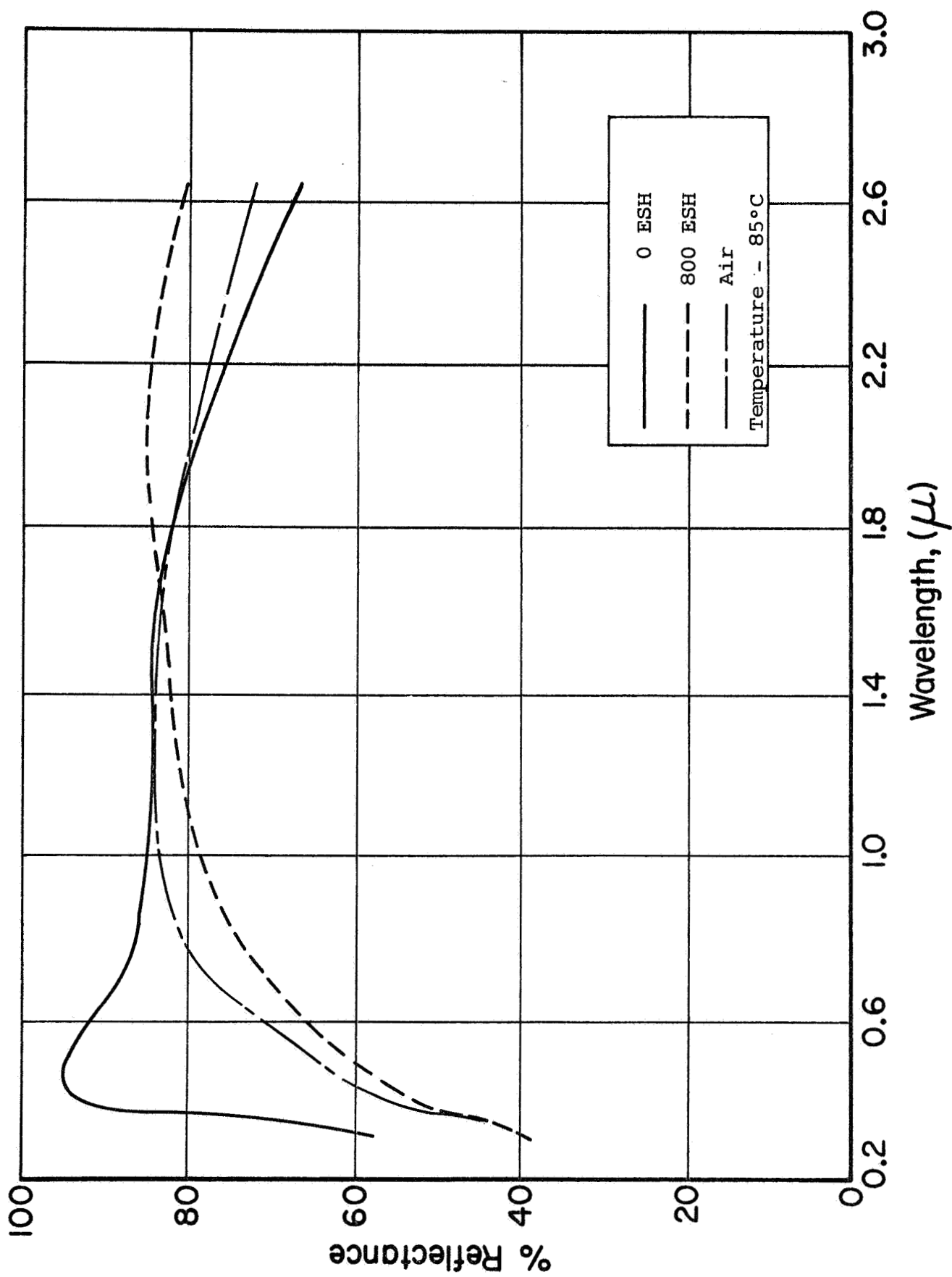


Figure 49: ABSOLUTE REFLECTANCE OF ZIRCONIA/K-SIL (#23) AS A FUNCTION OF UV IRRADIATION IN IRIF TEST 15

except the Optical Solar Reflector (Item 1) and the r-TiO<sub>2</sub>/silicone elastomer (Item 27) and ZnS/O-I 650 (Item 36) paints; especially damaged were the Lithafrax (Item 11) and  $\alpha$ -Al<sub>2</sub>O<sub>3</sub>/PS7 (Item 26) paints. Surprising stability was exhibited by the zinc sulfide specimen. Indeed, the two worst coatings were based on alkali silicate binders and the two best systems were based on silicone binders! The high temperature of irradiation, (i.e., 85°C) caused significant infrared bleaching (loss of chemically-bound water) of all three coatings based on alkali silicates. The increase in reflectance of the zinc sulfide coating at 2000-nm wavelength is attributed to a loss of functionality, especially residual -OH groups, as a result of thermal- and photo-initiated cross linking.

Admission of air to the IRIF resulted in significant bleaching to the following specimens (also see the spectra, Figures 41 through 49):

LMSC Lithafrax	1000-nm region only (10%)
LMSC r-TiO <sub>2</sub>	entire 400 to 2000-nm region
ZnS (O-I 650)	400 to 600-nm region (slight; 4%)
$\alpha$ -Al <sub>2</sub> O <sub>3</sub> (PS-7)	1000-nm region only (10%)
White Kemacryl	500 to 2000-nm region (10%)
Pegasus S-13	400 to 1000-nm region (8%)
	1000 to 2700-nm region (complete)
ZrO <sub>2</sub> (PS-7)	500 to 1000-nm (slight; 5%)

The Cat-a-lac Black specimen was lost during sample manipulation in IRIF Test 15 and was not measured after the 800-ESH incremental exposure. The Cat-a-lac Black specimen was remeasured after admission of air, however, and the "bleached" Cat-a-lac Black specimen was observed to return to its original reflectance.

#### E. IRIF-I Test No. 16

IRIF screening Test 16 represented the longest exposure performed during the course of the program; it was completed after a total exposure of 3600 ESH of ultraviolet irradiation in vacuum. In situ reflectance measurements were performed after exposures of 0, 100, 450, 1050, 2000, 2900 and 3600 ESH and after 18 hr at atmospheric pressure. Test 16 involved a solar-ultraviolet-irradiation factor of 6X and a nominal substrate temperature of 8°C. The average pressure during irradiation was  $1 \times 10^{-7}$  Torr. Because of a leak that developed in a bellows during the terminal in situ measurements (after 3600 ESH of irradiation), only two specimens were measured in vacuum; however, all specimens were measured in air. Furthermore, all specimens were measured in vacuum after 2900 ESH of ultraviolet irradiation. The results of Test 16 are presented in Table 9 for each of the specimens irradiated. These data are plotted in Figures 50 through 52. Because qualitative damage spectra have been presented for the other specimens, the spectra of the ZnS and SnO<sub>2</sub> paints are the only specimens irradiated in Test 16 that are presented here. They are presented in Figures 53 and 54 respectively.

The surprising stability of the zinc sulfide paint (Item 36) that was observed in Test 15 was repeated in Test 16. Unfortunately, zinc sulfide paints have a high initial solar absorptance and they therefore have little value at this time. Furthermore, a plot of the solar absorptance increase,  $\Delta\alpha_s$ , of the ZnS specimen against the logarithm of exposure indicates that a serious escalation of damage begins at about 3000 ESH of ultraviolet irradiation (see Figure 52). The damage spectra of the ZnS paint are presented in Figure 53.

The Cat-a-lac Black specimen (Item 38) did not exhibit the excessive photo-induced bleaching at 8°C (Test 16) that it sustained in the 85°C test (Test 15). The  $-\Delta\alpha_s$  of the Cat-a-lac Black

Table 9

EFFECT OF UV IRRADIATION IN THE IRIF ON  
SELECTED THERMAL-CONTROL SURFACE COATINGS  
(IRIF Test 16; Solar Intensity 6X)

Item No.	Surface	Exposure (ESH)	Solar Absorptance			
			$\alpha_1$	$\alpha_2$	$\alpha_s$	$\Delta\alpha_s$
27	IMSC r-TiO <sub>2</sub>	0	.124	.062	.186	-
		100	.158	.097	.255	.069
		450	.168	.106	.274	.088
		1050	.183	.119	.302	.116
		2000	.206	.126	.332	.146
		2900	.210	.140	.350	.164
		3600	.216	.140	.356	.170
		Air	.181	.086	.267	.081
36	ZnS (O-I 650 Resin)	0	.112	.153	.265	-
		100	.118	.152	.270	.005
		450	.126	.151	.277	.012
		1050	.140	.146	.286	.021
		2000	.160	.146	.306	.041
		2900	.163	.147	.310	.045
		3600	.191	.169	.360	.095
		Air	.181	.156	.337	.072
26	$\alpha$ -Al <sub>2</sub> O <sub>3</sub> (PS-7)	0	.055	.058	.113	-
		100	.094	.057	.151	.038
		450	.153	.061	.214	.101
		1050	.200	.074	.274	.161
		2000	.233	.081	.314	.201
		2900	.244	.092	.336	.223
		Air*	.250	.110	.360	.247
37	White Kemacryl	0	.165	.148	.313	-
		100	.214	.186	.400	.087
		450	.268	.184	.452	.139
		1050	.314	.190	.504	.191
		2000	.359	.197	.556	.243
		2900	.369	.217	.586	.273
		Air*	.373	.192	.565	.252
30	S-13 (Pegasus)	0	.116	.083	.199	-
		100	.127	.128	.255	.056
		450	.156	.161	.317	.118
		1050	.179	.180	.359	.160
		2000	.208	.180	.388	.189
		2900	.224	.203	.427	.228
		Air*	.223	.112	.335	.136
23	ZrO <sub>2</sub> (PS-7)	0	.094	.080	.174	-
		100	.148	.089	.237	.063
		450	.236	.104	.340	.166
		1050	.260	.097	.357	.183
		2000	.272	.120	.392	.218
		2900	.288	.155	.443	.269
		Air*	.280	.134	.414	.240
38	Cat-a-lac Black	0	.478	.487	.965	-
		100	.476	.487	.963	-.002
		450	.472	.486	.958	-.007
		1050	.470	.477	.947	-.018
		2000	.470	.478	.948	-.017
		2900	.468	.467	.935	-.030
		Air*	.468	.486	.954	-.011
22	SnO <sub>2</sub> (PS-7)	0	.092	.061	.153	-
		100	.111	.064	.175	.022
		450	.143	.065	.208	.055
		1050	.190	.077	.267	.114
		2000	.209	.079	.288	.135
		2900	.232	.083	.315	.162
		Air*	.209	.085	.294	.141
	S-13G (Batch A-466)	0	.119	.097	.216	-
		100	.126	.104	.230	.014
		450	.143	.101	.244	.028
		1050	.148	.109	.257	.041
		2000	.174	.103	.277	.061
		2900	.189	.109	.298	.082
		Air*	.190	.109	.299	.083

\*Air measurement taken after 3600 ESH.

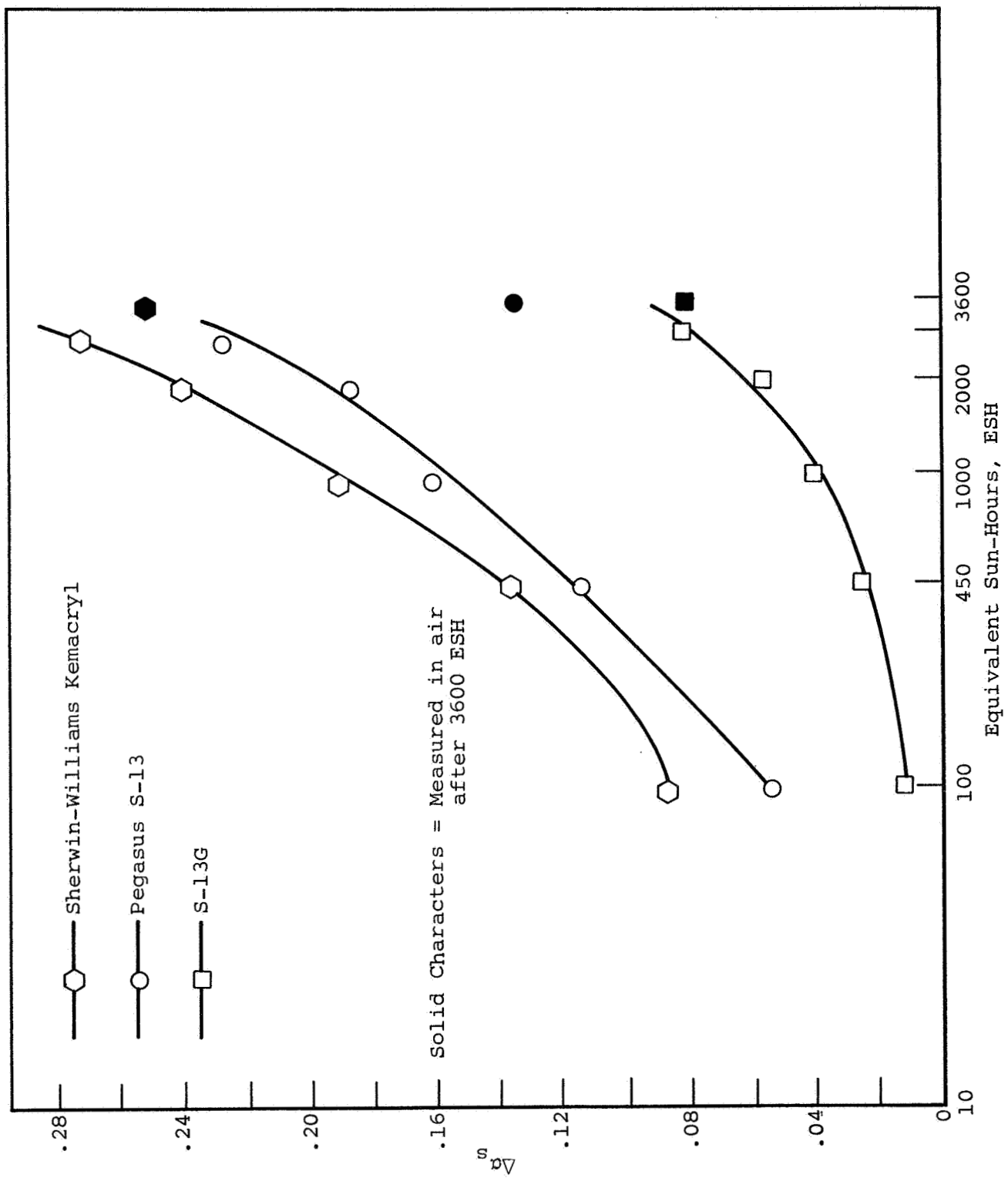


Figure 50: DEGRADATION RATES OF SEVERAL SURFACES EVALUATED IN IRIF TEST 16

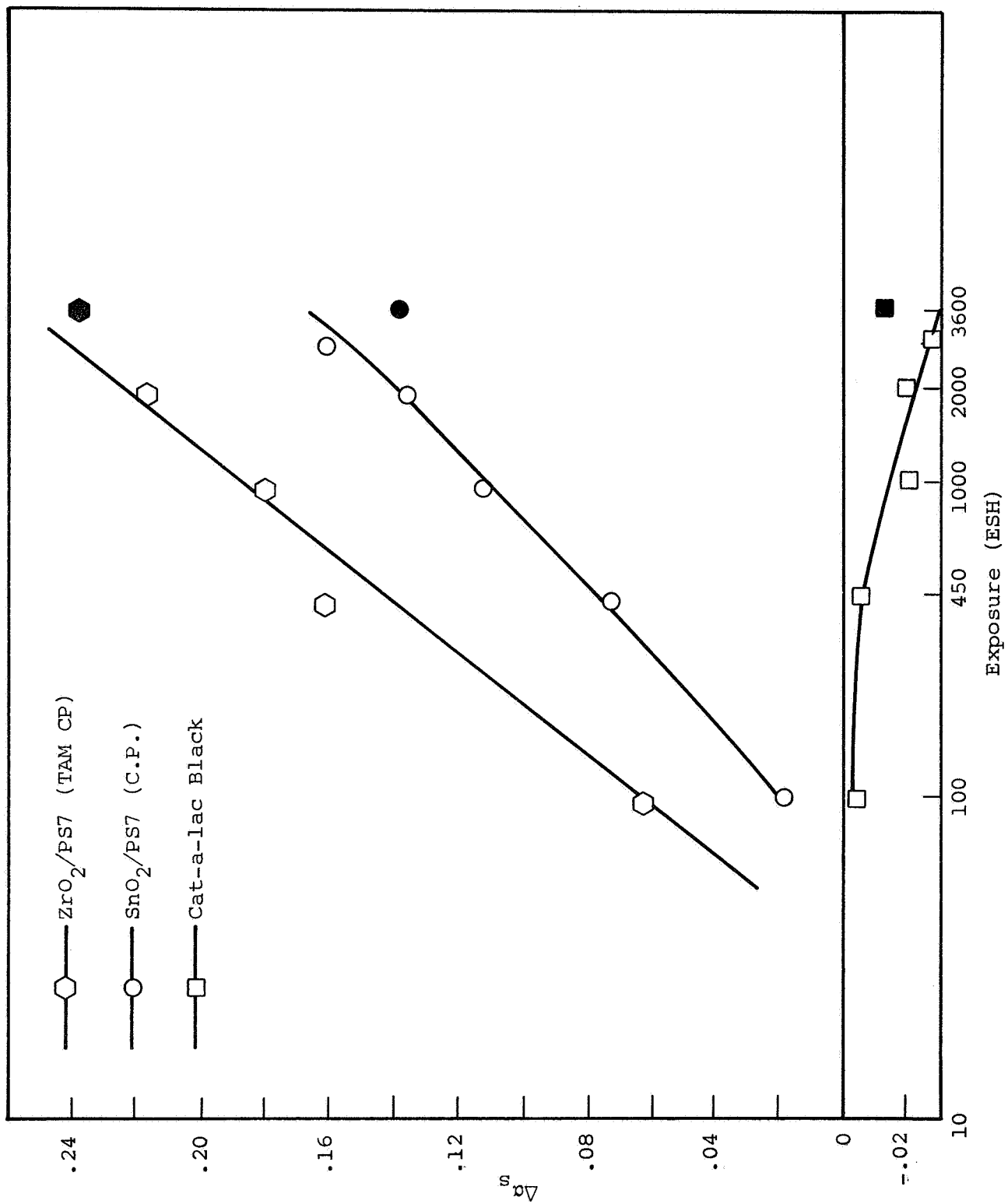


Figure 51: DEGRADATION RATES OF SEVERAL SURFACES EVALUATED IN IRIF TEST 16



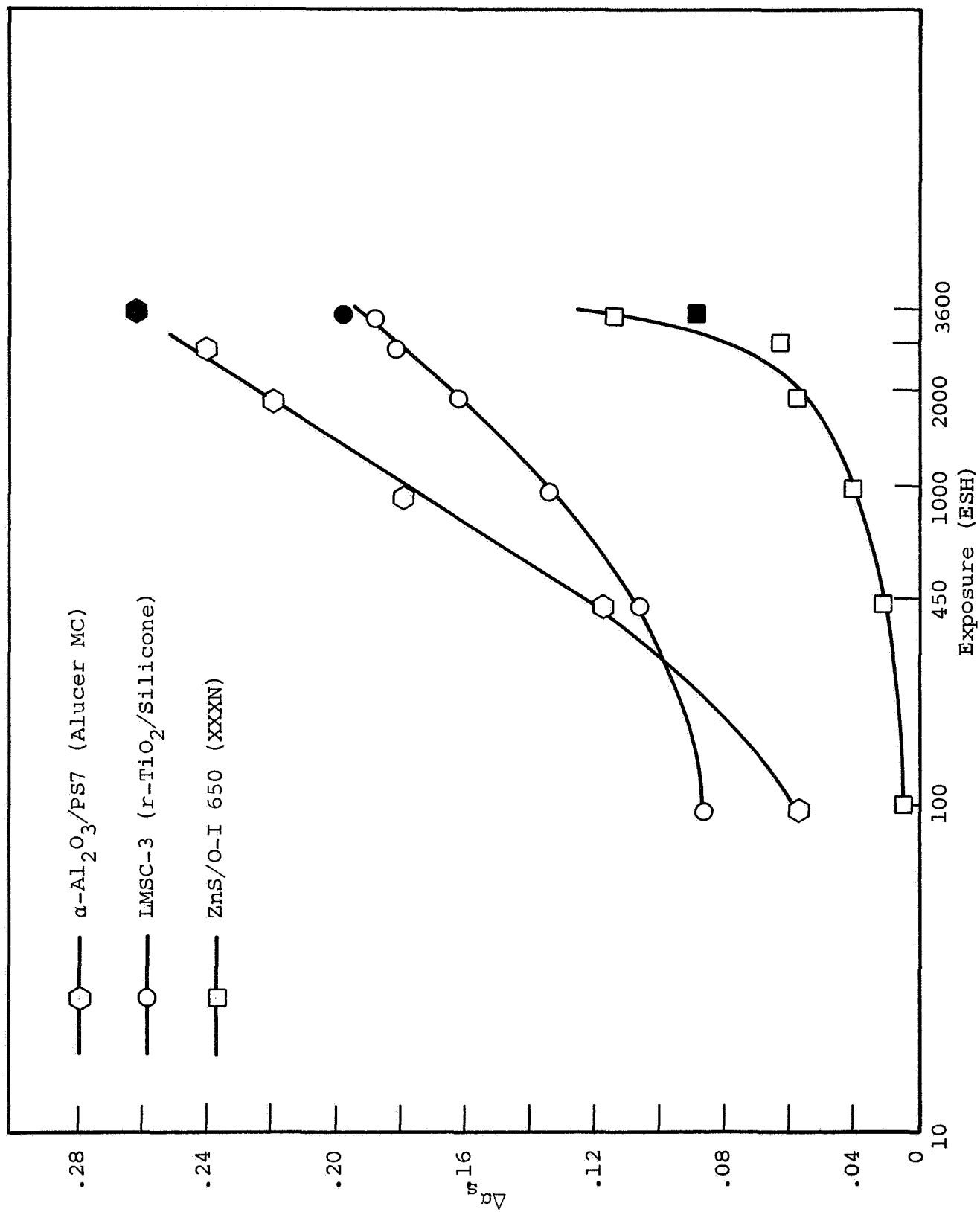


Figure 52: DEGRADATION OF SEVERAL SURFACES EVALUATED IN IRIF TEST 16

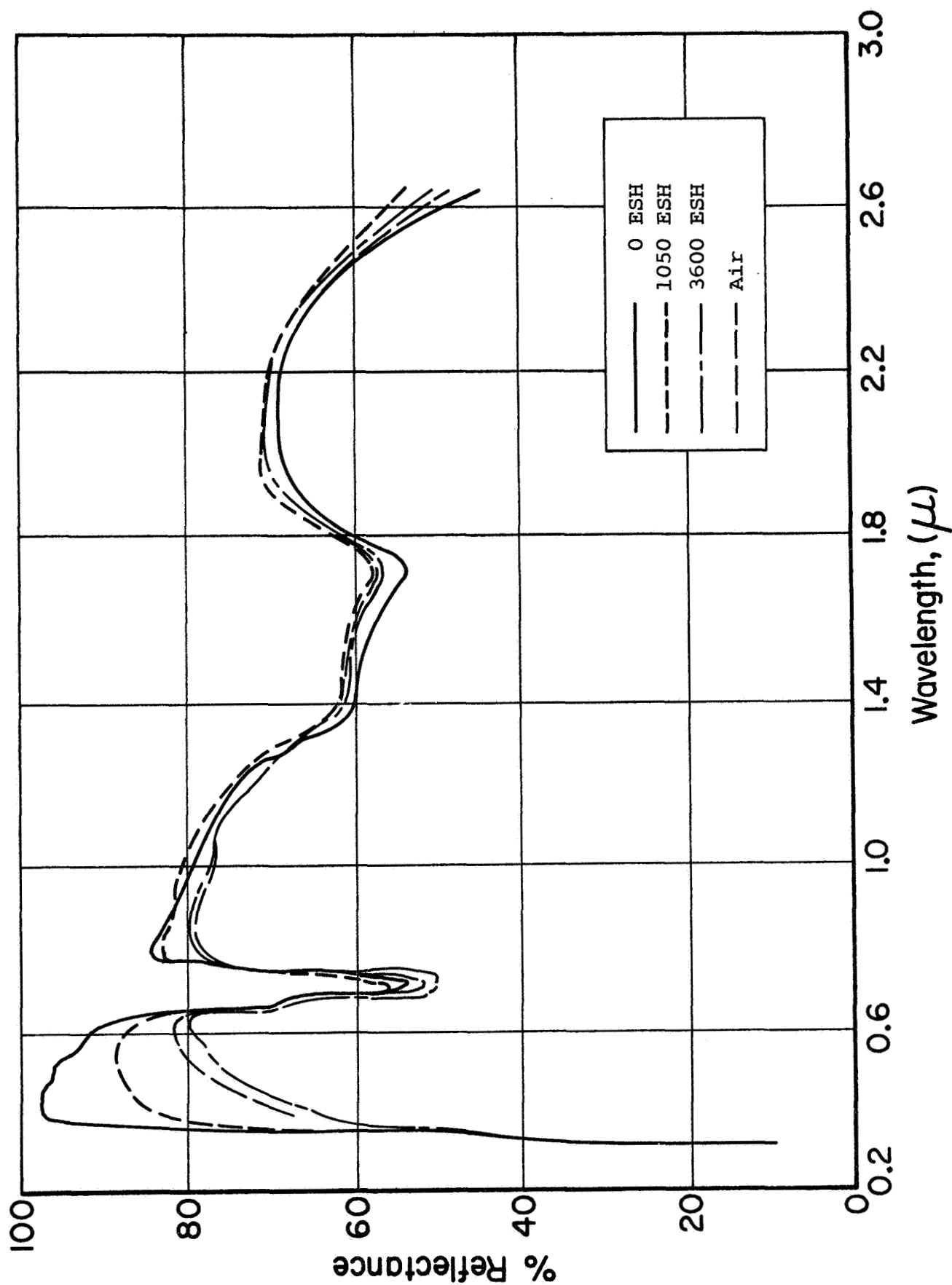


Figure 53: ABSOLUTE REFLECTANCE OF ZINC SULFIDE/O-I 650 (#36) AS A FUNCTION OF UV IRRADIATION IN IRIF TEST 16

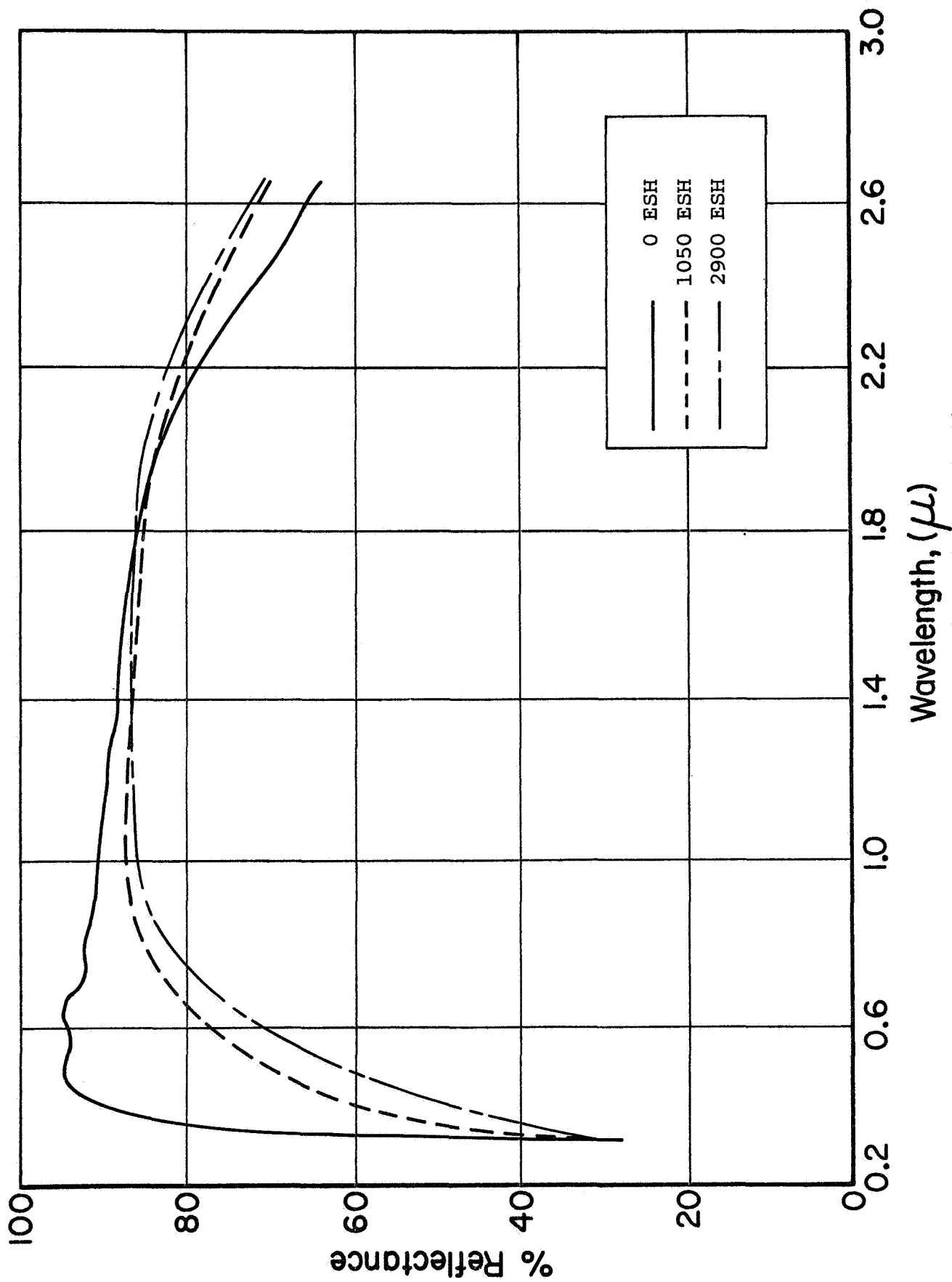


Figure 54: ABSOLUTE REFLECTANCE OF TIN OXIDE/K-Sil (#22) AS A FUNCTION OF UV IRRADIATION IN IRIF TEST 16

specimen was 0.03 after 2900 ESH. The damage rate data for Cat-a-lac Black are presented in Figure 51.

The tin oxide coating (Item 22) exhibited severe damage at all exposures. Its damage spectra are presented in Figure 54; the solar absorptance data are plotted in Figure 51.

The  $\Delta\alpha_s$  of S-13 (Pegasus) was 0.19 in ca. 2000 ESH in Test 16; the  $\Delta\alpha_s$  of an identical specimen was about 0.16 in ca. 2000 ESH in the previous screening test performed at the same temperature (IRIF Test 13). On the basis of this data it is believed that Tests 13 and 16 are similar in their ultraviolet irradiation rates.

The zirconium dioxide specimen (Item 23) behaved much different in this test (IRIF Test 16) than in IRIF Test 13. The  $\Delta\alpha_s$  was 0.27 and 0.12 in about 2800 ESH in the two tests, respectively.

The S-13G specimen degraded much less in Test 16 than in Test 13. This is attributed primarily to the improvement in the pigment (and coating) preparation that was achieved after the specimens for Test 13 were prepared. Still much greater improvements have been realized (ref. 5).

#### F. Discussion

The ultraviolet and short-wavelength visible damage exhibited by the two aluminum conversion coatings (MTL-3 and GT-1275) and the  $\text{Al}_2\text{O}_3$ -sputtered coating (GT-1015) is believed to be due primarily to ultraviolet-induced bound-state defects in the  $\text{Al}_2\text{O}_3$ . The  $\text{Al}_2\text{O}_3$  films are transparent and the defects increase the extinction for ultraviolet and visible light within the films, especially in the GT-1015 which exhibits strong interference effects.

The effect of ultraviolet irradiation in vacuum on the GT-1015 is of special interest. Because the interference patterns could not be reproduced faithfully in the "reduced" reflectance plots presented earlier, they are presented in much greater detail

in Figures 55 and 56. Examination of these data show that increased irradiation produces an ever increasing displacement of the interference-peak heights to shorter and shorter wavelengths, but with the greatest displacement occurring after initial exposure to ultraviolet radiation. The surprising observation was that admission of air to the IRIF-I space chamber not only bleached the damage in terms of increasing the average reflectance, a phenomenon that lends further credence to the theory that the damage is due principally to bound-state defects, but resulted in a displacement of the peak heights back toward longer wavelengths.

The displacement of interference patterns to shorter wavelengths is normally associated with losses in thickness and/or refractive index of the dielectric layer. (A complete absence of contamination is therefore suggested.) Since it is highly inconceivable that ultraviolet radiation could have caused a decrease in the thickness of the  $\text{Al}_2\text{O}_3$  layer, the displacements are believed to be due to refractive index changes. We do not believe that the simple adsorption and desorption of gaseous matter can provide sufficient mass to effect the real part of the refractive index. Refractive index is written as a complex number; the real part corresponds to the refractive index as it is usually written, and the imaginary part to the adsorbing properties of the medium. The complex refractive index,  $n^*$ , is defined by:

$$n^* = n(1 - ik) \qquad K = \mu/4$$

As the adsorption coefficient,  $\mu$ , diminishes to zero in the limit the medium becomes transparent and  $n^*$  becomes equal to  $n$  and Snell's law applies. Snell's law is not obeyed for transmitting media with adsorption. Therefore, since the creation of bound-state defects increases the adsorption coefficient, the net effect is the same as decreasing the term  $n^*d$  which defines interference.

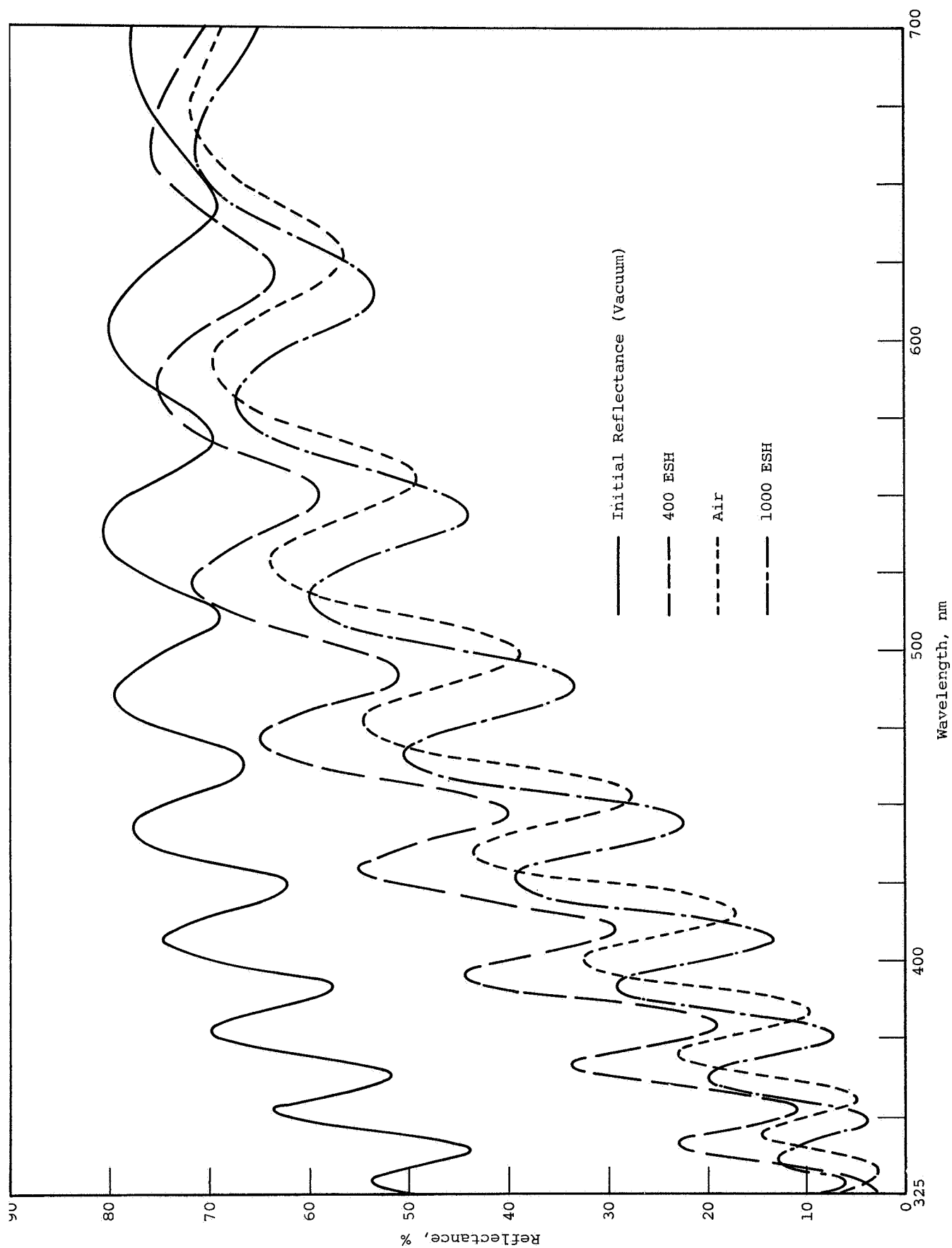


Figure 55: DETAILED SPECTRA OF SCHJELDAHL GT-1015 (UV AND VISIBLE)

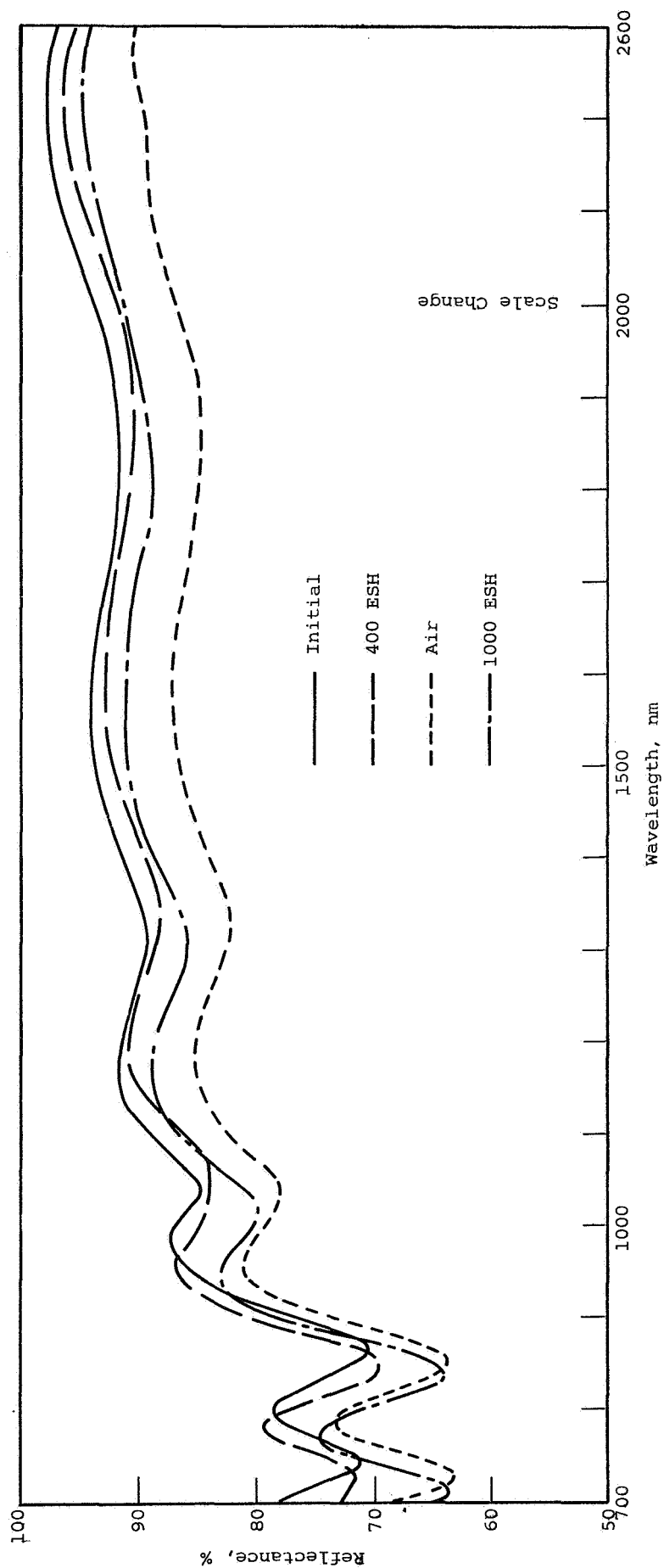


Figure 56: DETAILED SPECTRA OF SCHJELDAHL GT-1015 (INFRARED)

Admission of air (oxygen) bleaches out some of the defects and the term  $n \cdot d$  is increased.

\* \* \* \* \*

Although space-simulation tests 10, 13 and 16 compare favorably for many of the specimens irradiated, they do not compare in severity for either the Pegasus-I S-13 or the zirconia-pigmented potassium silicate paint. The damage to these coatings is plotted as a function of  $\Delta\alpha_s$  versus the logarithm of exposure (ESH) for all four tests in Figures 57 and 58. Figure 58 shows that no correlation is possible for the zirconia paint. Indeed, the zirconia specimen was more severely degraded by Test 16, which involved a nominal substrate temperature of 8°C, than by Test 15, which was performed at a nominal sample temperature of 85°C. On the other hand, Tests 13 and 16 gave fairly comparable results for the S-13 specimen (Figure 58); the zirconia paint was least degraded by Test 13 and most severely degraded by Test 16.

These data tend to confirm the fact that greater variations in behavior are exhibited by the least stable materials. For example, Z93, the FEP Teflon mirror, MTL-3, and the zinc sulfide paint, all of which showed better than average stability, exhibited the least test-to-test variance in ultraviolet-irradiation effects.

Since the zirconia specimens irradiated in all four experiments were prepared from the same batch at the same time, subtleties in the test conditions are suggested as being responsible for the variations in damage that it sustained in the four tests. Since gross test parameters were controlled (they had less of an effect on other materials), it is concluded that zirconia and zinc oxide (in S-13) may be more spectrally sensitive than the other materials (but for different reasons, mechanistically). The variations observed could therefore be explained by assuming that the



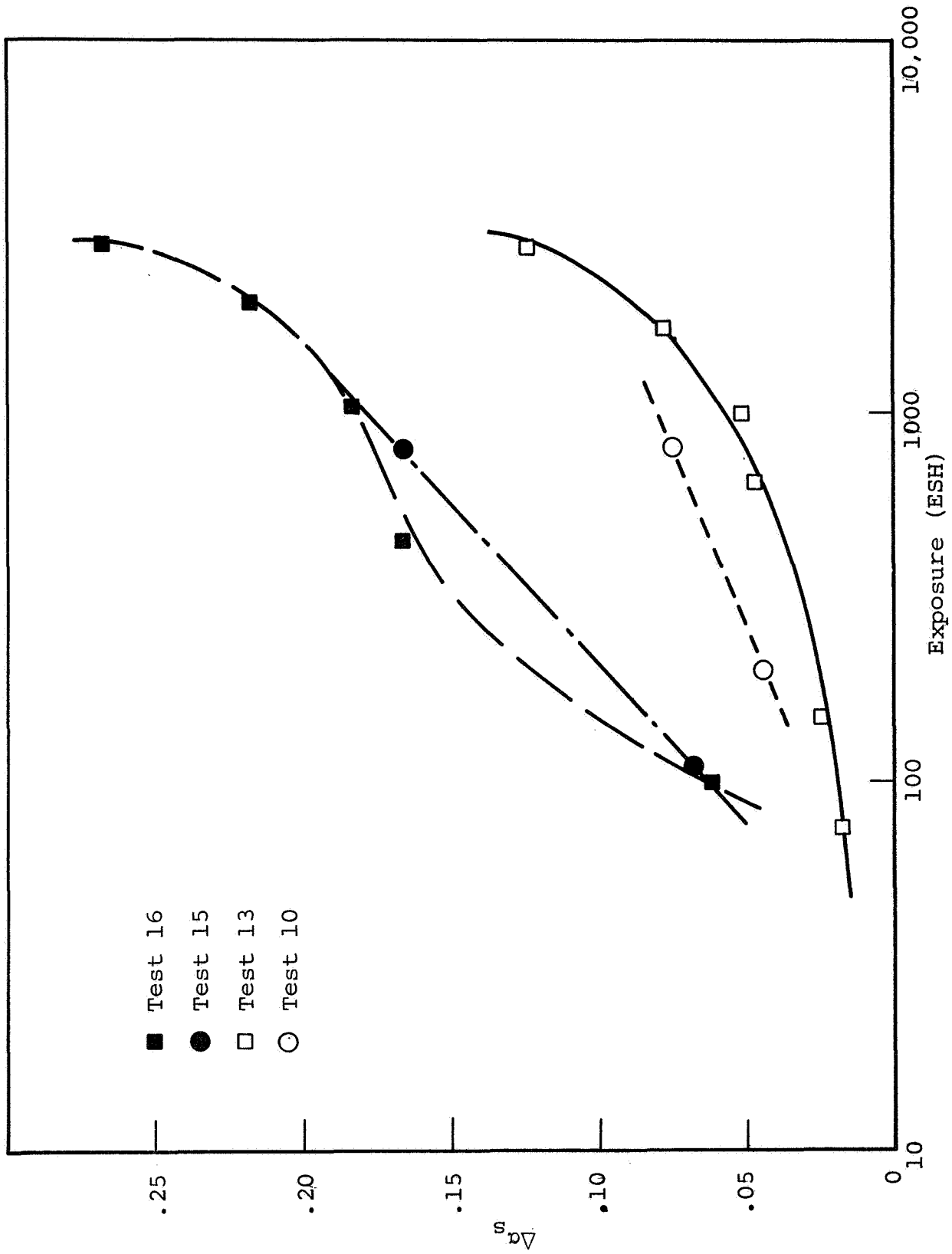


Figure 57: COMPARISON OF RATE DATA FROM IRIF-I TESTS FOR THE PEGASUS S-13 SPECIMENS (#30)

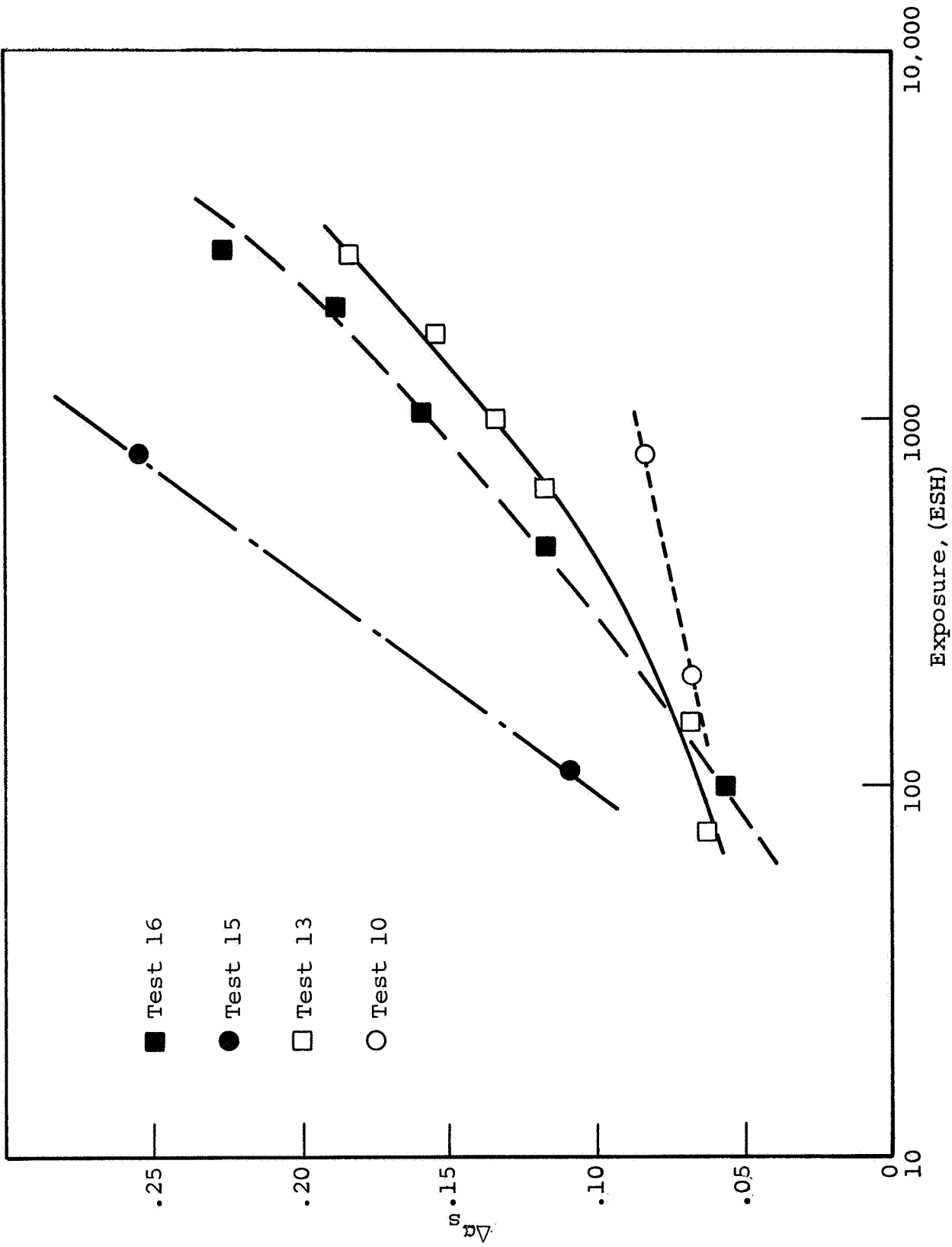


Figure 58: COMPARISON OF RATE DATA FROM IRIF-I TESTS FOR THE ZIRCONIA/K-Si1 SPECIMENS (#23)

spectral character of the A-H6 lamps were different for the four tests - or that they spectrally degraded at different rates (i.e., spectrally disproportionate).

## V. GAS ADSORBATE TESTS

### A. Introduction

The gas adsorbate experiments were planned as a result of the numerous observations that most, if not all, ultraviolet-damaged surfaces undergo optical bleaching of the damage spectra when air is admitted to the vacuum/irradiation chamber. We have long advocated that this phenomenon is related to the photolysis mechanisms that are responsible for the bleachable damage in the first place (ref. 4, 6) and that a study of the processes related to optical bleaching by gaseous adsorbates will aid in the eventual and more thorough understanding of the mechanisms associated with ultraviolet-radiation damage. The specimens chosen for the gaseous adsorbate experiments were chosen therefore on the basis of their known or anticipated damage (all were found to be severely damaged in at least one region of the solar spectrum).

The IRIF-II space-simulation facility and a 5-kW Hanovia mercury-xenon ultraviolet source were employed in all gas adsorbate tests. This facility, as well as the procedure employed, are discussed in Section III of this report.

### B. IRIF-II Test 2-2 (Oxygen Bleaching)

Test 2-2 was performed at a solar-ultraviolet-acceleration factor of 4X. The nominal sample temperature was maintained at 10°C and the average pressure during irradiation was  $4 \times 10^{-7}$  Torr. Absolute spectral reflectance data were obtained after 0, 200 and 700 ESH of ultraviolet radiation and after admission of oxygen to partial pressures of  $8 \times 10^{-8}$  Torr.

The specimens irradiated in Test 2-2 are listed in Table 10, along with the spectral damage at several wavelengths. The spectral behavior of the six most interesting coatings are presented in Figures 59 through 64.

Table 10  
BEHAVIOR OF A NUMBER OF SPECIMENS IN THE GASEOUS  
ADSORBATE TEST (OXYGEN)

Item No.	Surface	Exposure (ESH) and Pressure (Torr)	$-(\Delta R_{\lambda})^*$ , $\lambda = \text{nm}$				
			354	444	788	1900	2400
39	RF-1 $\text{TiO}_2/650$	700 ESH	0	7.0	10.5	3.0	2.0
		$8 \times 10^{-3}$ Torr	0	5.0	6.8	1.3	1.5
		8 Torr	0	3.0	2.3	0	0
22	$\text{SnO}_2/\text{PS7}$	700 ESH	7.0	9.0	2.3	3.2	2.6
		$8 \times 10^{-3}$ Torr	7.0	9.2	2.1	3.0	2.0
		8 Torr	4.0	7.8	1.7	2.0	1.2
26	$\alpha\text{-Al}_2\text{O}_3/\text{PS7}$	700 ESH	33.6	24.8	2.8	-3.5	-4.6
		$8 \times 10^{-3}$ Torr	31.4	23.0	1.7	-3.2	-4.8
		8 Torr	32.4	23.0	2.8	-2.0	-3.8
23	$\text{ZrO}_2/\text{PS7}$	700 ESH	11.5	10.0	-0.5	-0.8	-1.0
		$8 \times 10^{-3}$ Torr	10.9	9.2	+0.5	-0.8	-1.0
		8 Torr	11.7	10.0	+1.0	-0.8	-1.0
20	HAC Plasmoclay	700 ESH	11.6	9.0	--	--	--
		$8 \times 10^{-3}$ Torr	11.6	9.2	--	--	--
		8 Torr	9.5	8.8	--	--	--
30	S-13 (#7) Pegasus	700 ESH	-3.0	8.3	5.1	38.3	19.7
		$8 \times 10^{-3}$ Torr	+0.8	7.2	1.2	22.3	10.0
		8 Torr	+2.4	7.8	0	2.0	0.5
27	LMSC-3 ( $\text{TiO}_2/\text{Silicone}$ )	700 ESH	0	12.5	13.7	5.0	1.0
		$8 \times 10^{-3}$ Torr	0.4	10.0	8.0	2.0	-0.5
		8 Torr	1.0	5.8	2.3	1.3	0
11	LMSC-2 (Lithafrax)	700 ESH	58.1	49.0	15.7	-1.5	-3.1
		$8 \times 10^{-3}$ Torr	57.5	48.4	15.0	-1.1	-2.3
		8 Torr	58.0	49.7	15.0	-0.8	-1.4
30	S-13 (#4) Pegasus	700 ESH	-3.6	5.5	3.0	29.2	14.1
		$8 \times 10^{-3}$ Torr	+0.8	4.5	1.5	16.8	7.0
		8 Torr	+2.4	4.2	0	0	0
36	$\text{ZnS}/650$	700 ESH	9.0	4.5	1.0	1.0	1.0
		$8 \times 10^{-3}$ Torr	9.0	2.2	-1.0	-0.5	-0.5
		8 Torr	9.0	2.3	0	+1.0	+1.0

\* In reality,  $-(\Delta R_{\lambda})$  is an increase in absorption and positive numbers thus represent reflectance decreases.

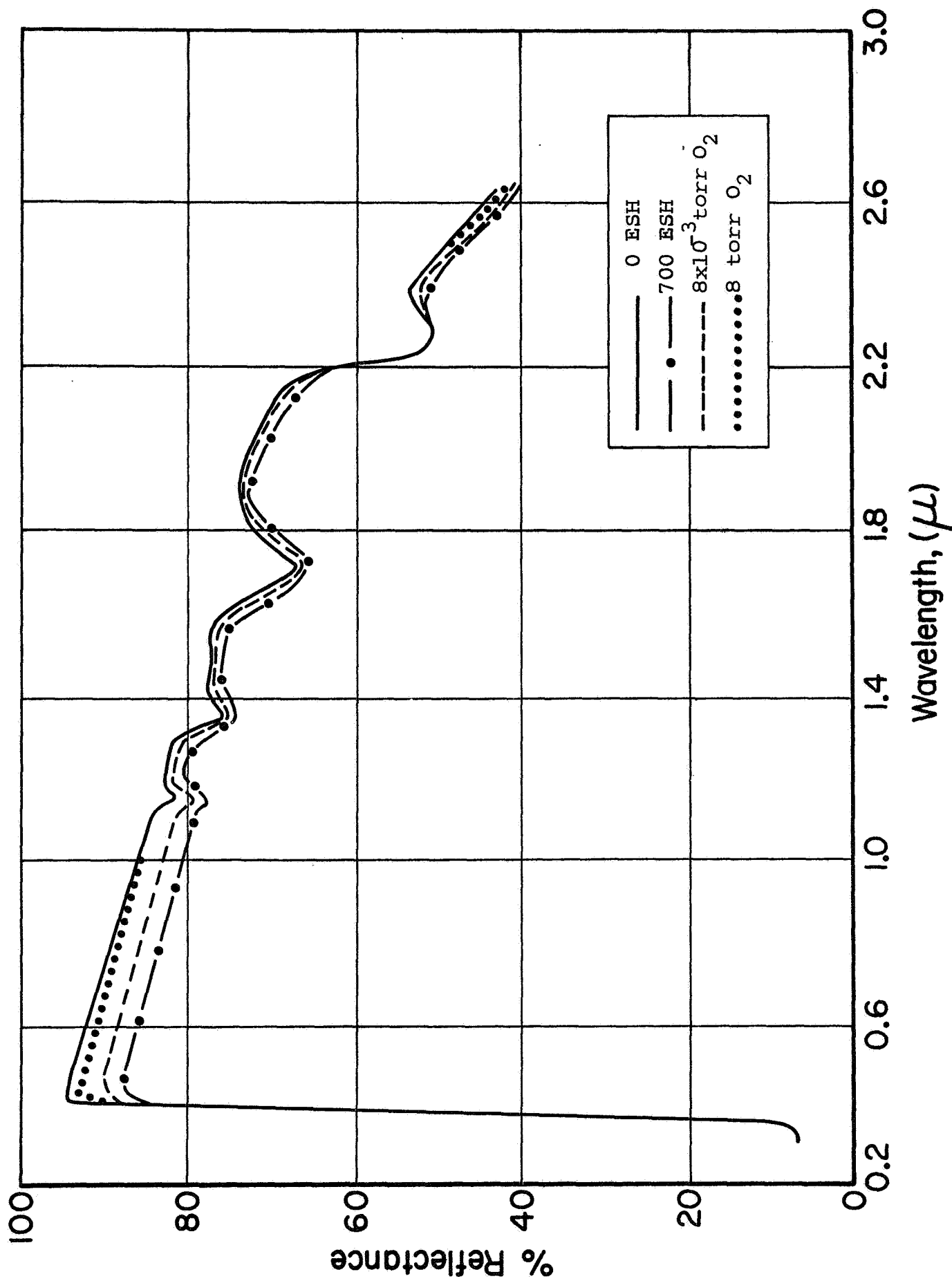


Figure 59: EFFECT OF PARTIAL PRESSURES OF  $O_2$  ON IRRADIATED RF-1  $TiO_2/O-I$  650 (#39) TEST 2-2

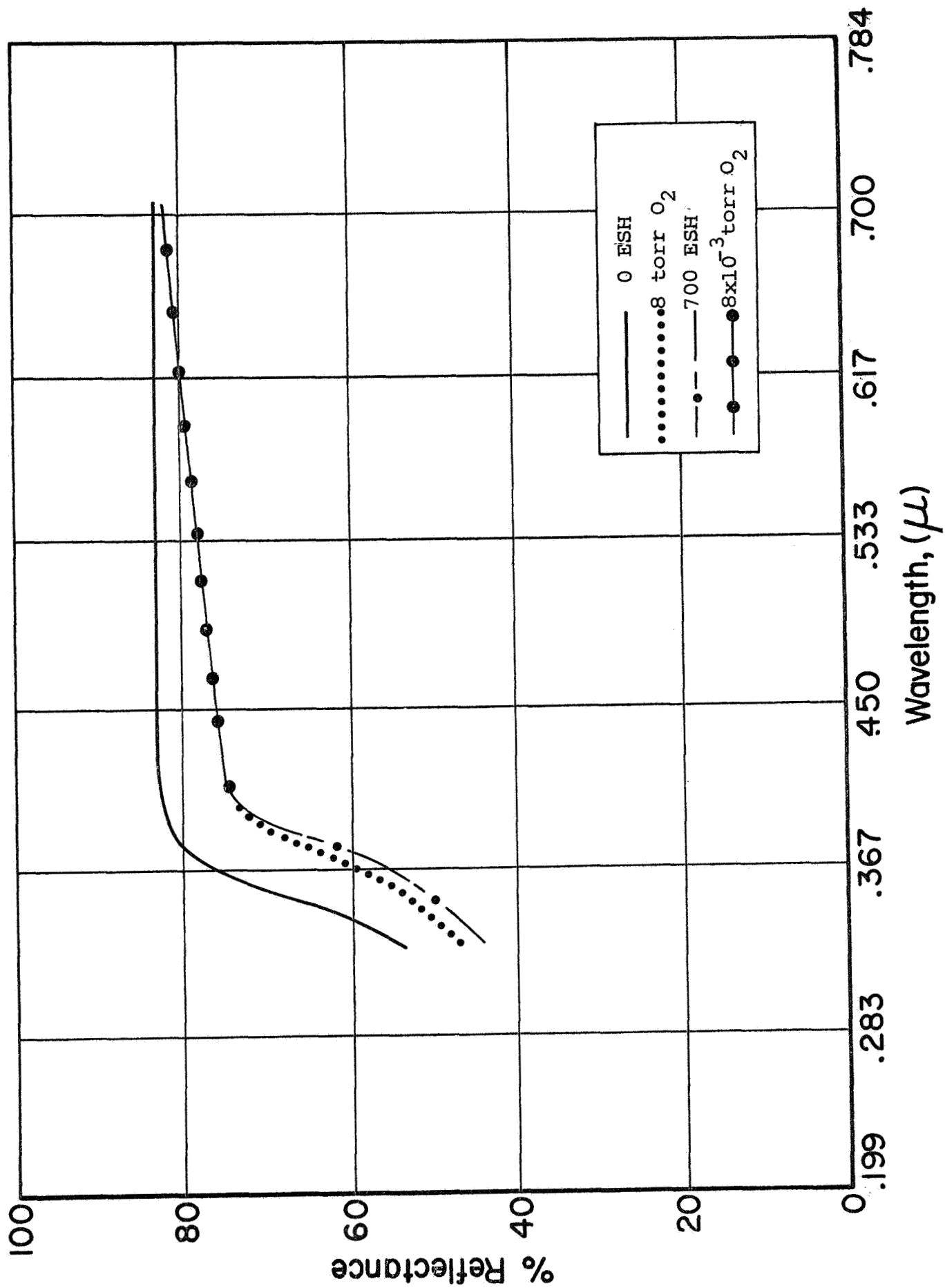


Figure 60: EFFECT OF PARTIAL PRESSURES OF  $O_2$  ON IRRADIATED PLASMOCLAY/ $K_2O \cdot SiO_2$  (#20) TEST 2-2

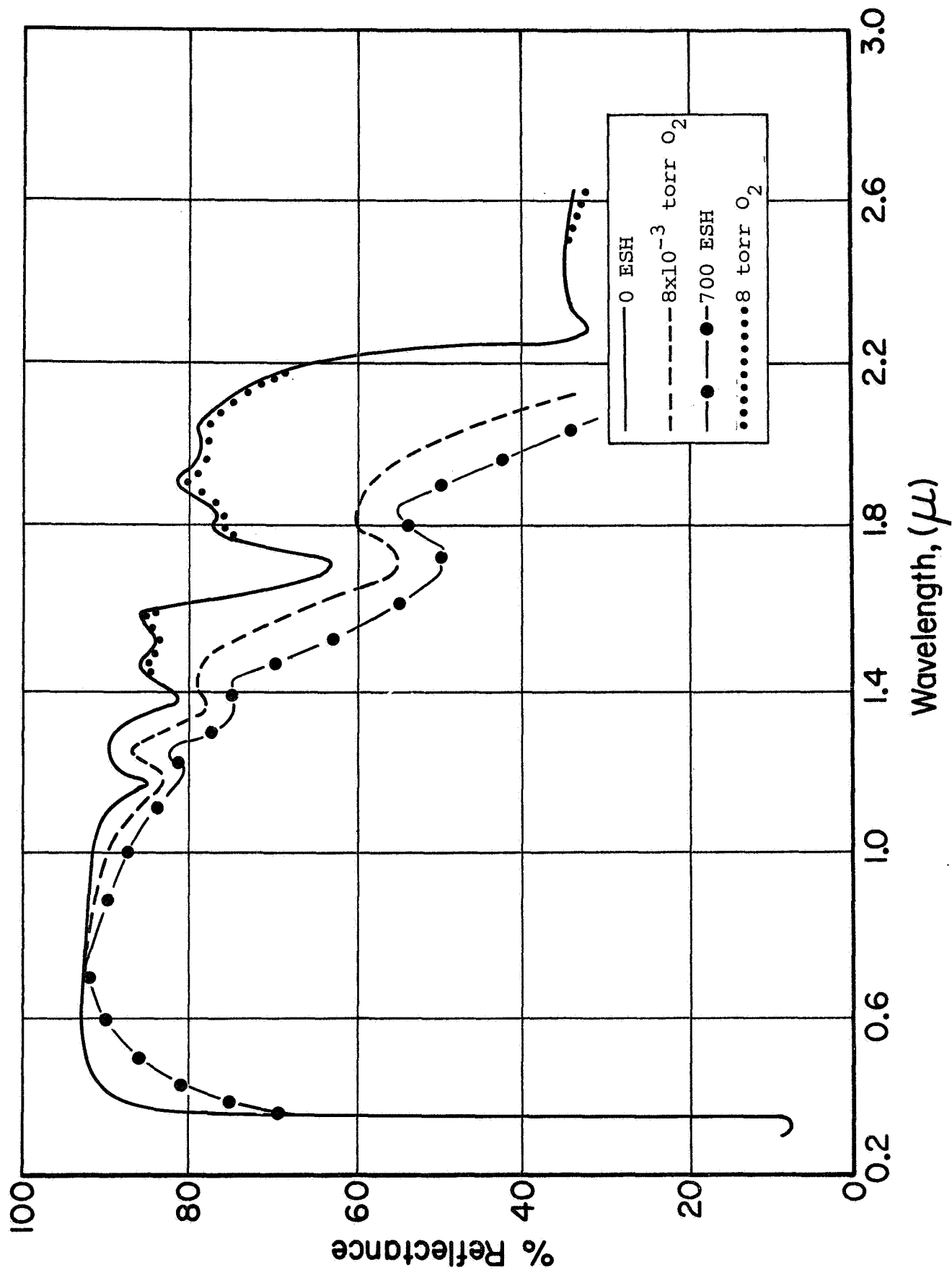


Figure 61: EFFECT OF PARTIAL PRESSURES OF  $O_2$  ON IRRADIATED PEGASUS S-13 (#30) TEST 2-2



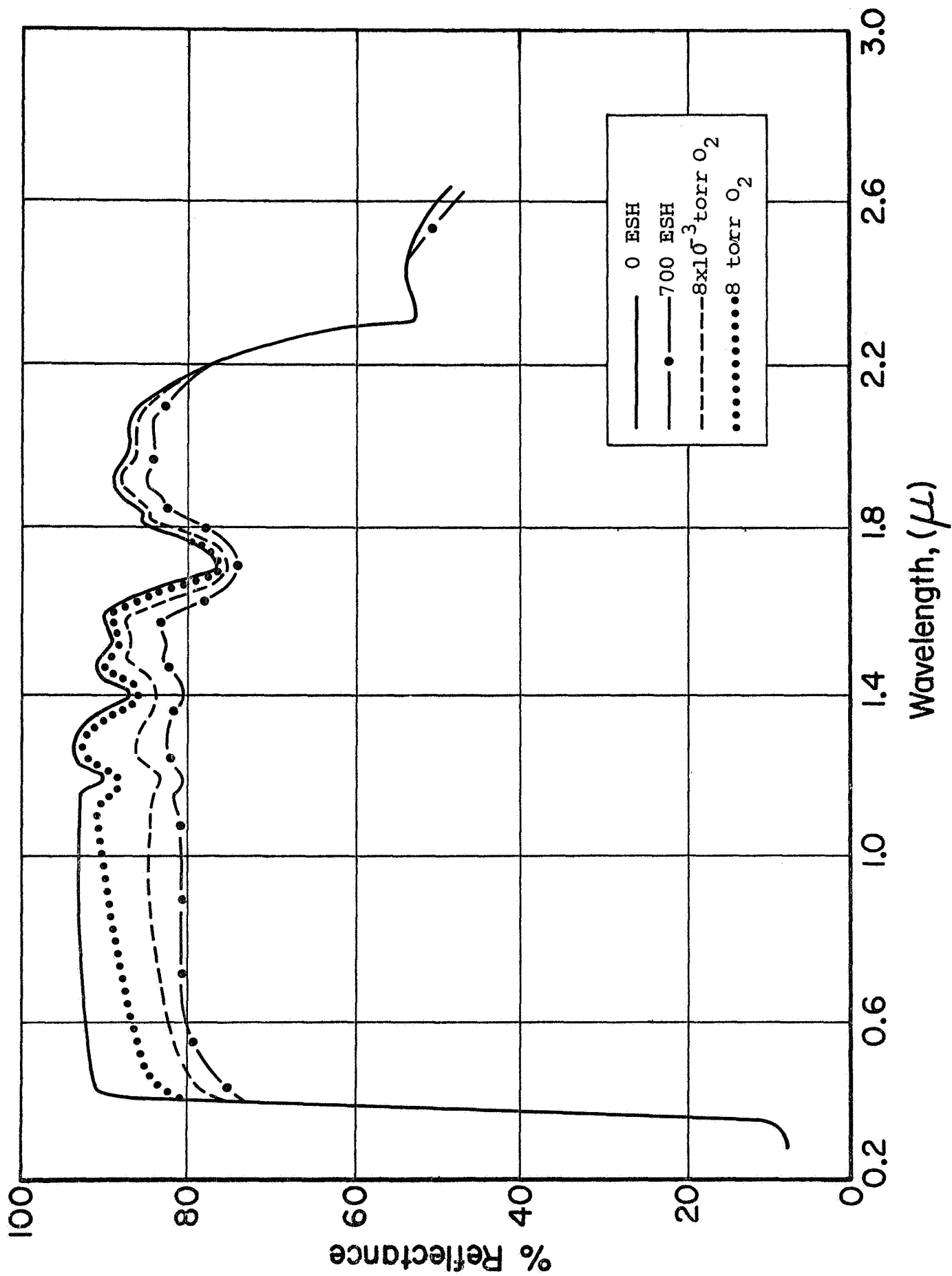


Figure 62: EFFECT OF PARTIAL PRESSURES OF  $O_2$  ON IRRADIATED RUTILE-PIGMENTED LMSC-3 (#27) TEST 2-2

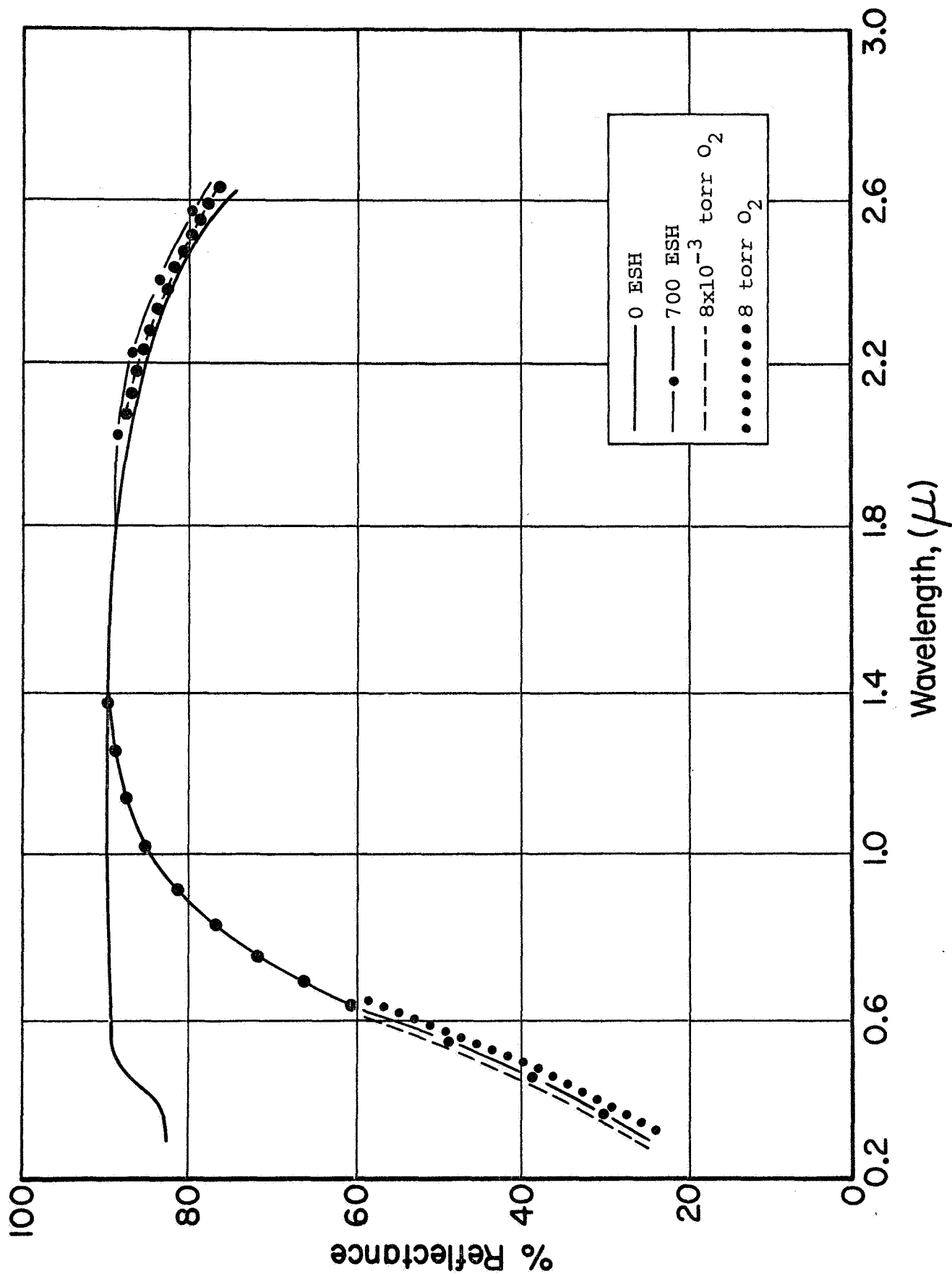


Figure 63: EFFECT OF PARTIAL PRESSURES OF  $O_2$  ON IRRADIATED LITHAFRAX (#11) TEST 2-2

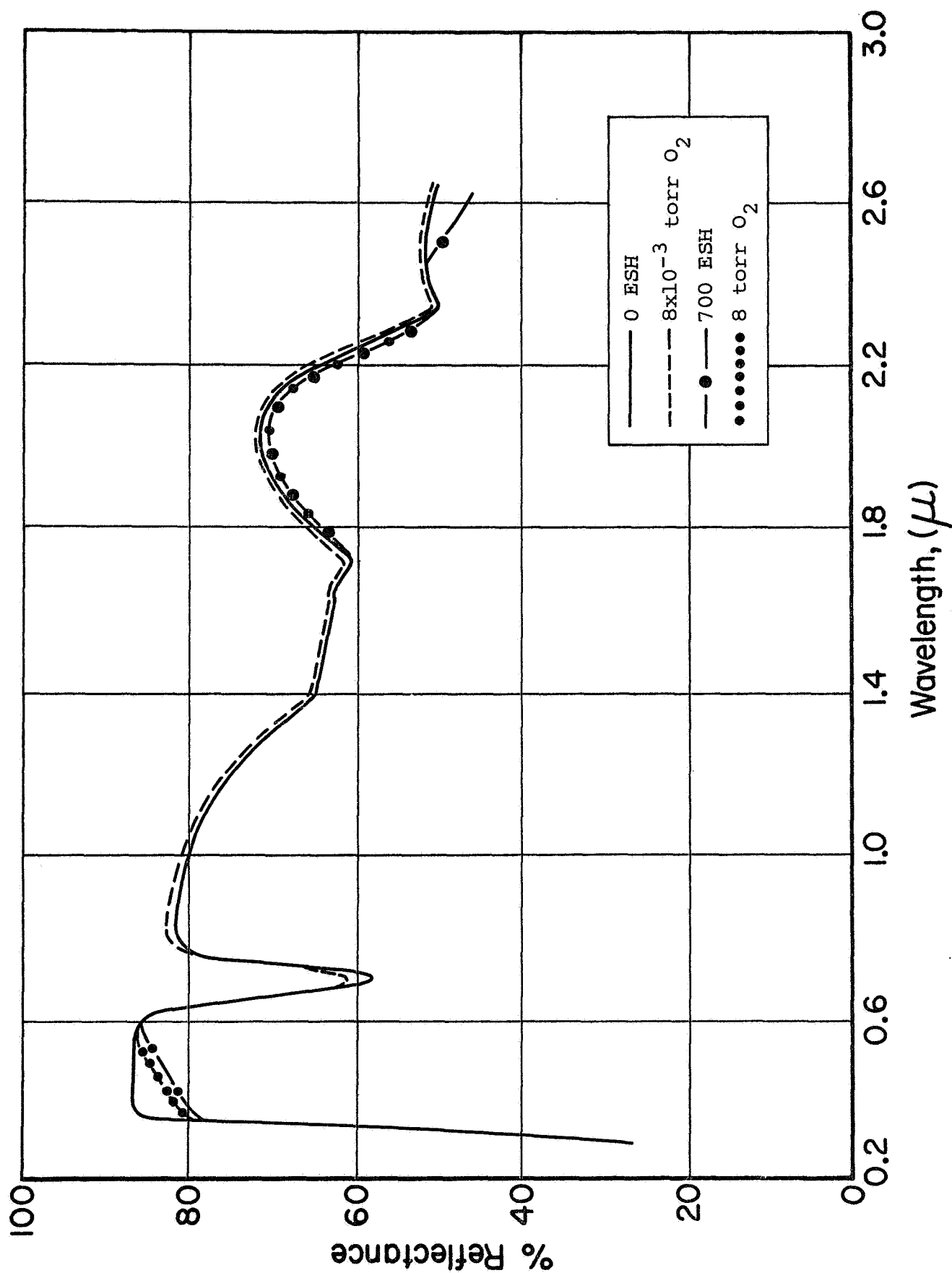


Figure 64: EFFECT OF PARTIAL PRESSURES OF O<sub>2</sub> ON IRRADIATED ZINC SULFIDE/O-I 650 (#36) TEST 2-2

The careful, and slow, admission of high purity (99.99+ %) oxygen was performed after the measurement of reflectance following the completion of 700 ESH of ultraviolet irradiation. The admission was accomplished with a Pegasus S-13 specimen in the integrating sphere and the Beckman DK-1 locked onto a wavelength of 2050 nm. The admission of oxygen was performed by controlling the pressure with two Granville-Phillips valves and an Alpatron gauge (NRC #720) as discussed in Section III and the Appendix. The major decades of oxygen pressure employed are given in Table 11, along with a general qualitative description of the results. Complete spectra were determined at an oxygen partial pressure of  $8 \times 10^{-3}$  Torr. (These data are included in Figures 59 through 64.)

Table 11  
EFFECT OF OXYGEN PRESSURE ON S-13

<u>Pressure, Torr</u>	<u>Observation of <math>R_{2.05 \text{ nm}}</math></u>
$1.0 \times 10^{-7}$	initial pressure
$1.0 \times 10^{-6}$	no change in 13 min
$2.0 \times 10^{-6}$	no change in 53 min
$1.5 \times 10^{-5}$	1/4-1/2% increase in R in 60 min
$1.0 \times 10^{-4}$	ion pump shut itself off and IRIF valve closed
$2.0 \times 10^{-3}$	1-1/4% increase in R in 50 min
$5.0 \times 10^{-3}$	5% increase in R in 80 min and continued rise for 700 min; total increase was 13%
8.0	23% increase in R in 1200 min

The reflectance of the S-13 specimen at 2.05-nm wavelength is plotted as a function of time after admission of oxygen in Figure 65. Also shown on the abscissa are the various oxygen pressures as recorded with the ion current and the Alpatron gauge. Overnight periods are from 500 to 1350 minutes and from 1850 to 3150 minutes.

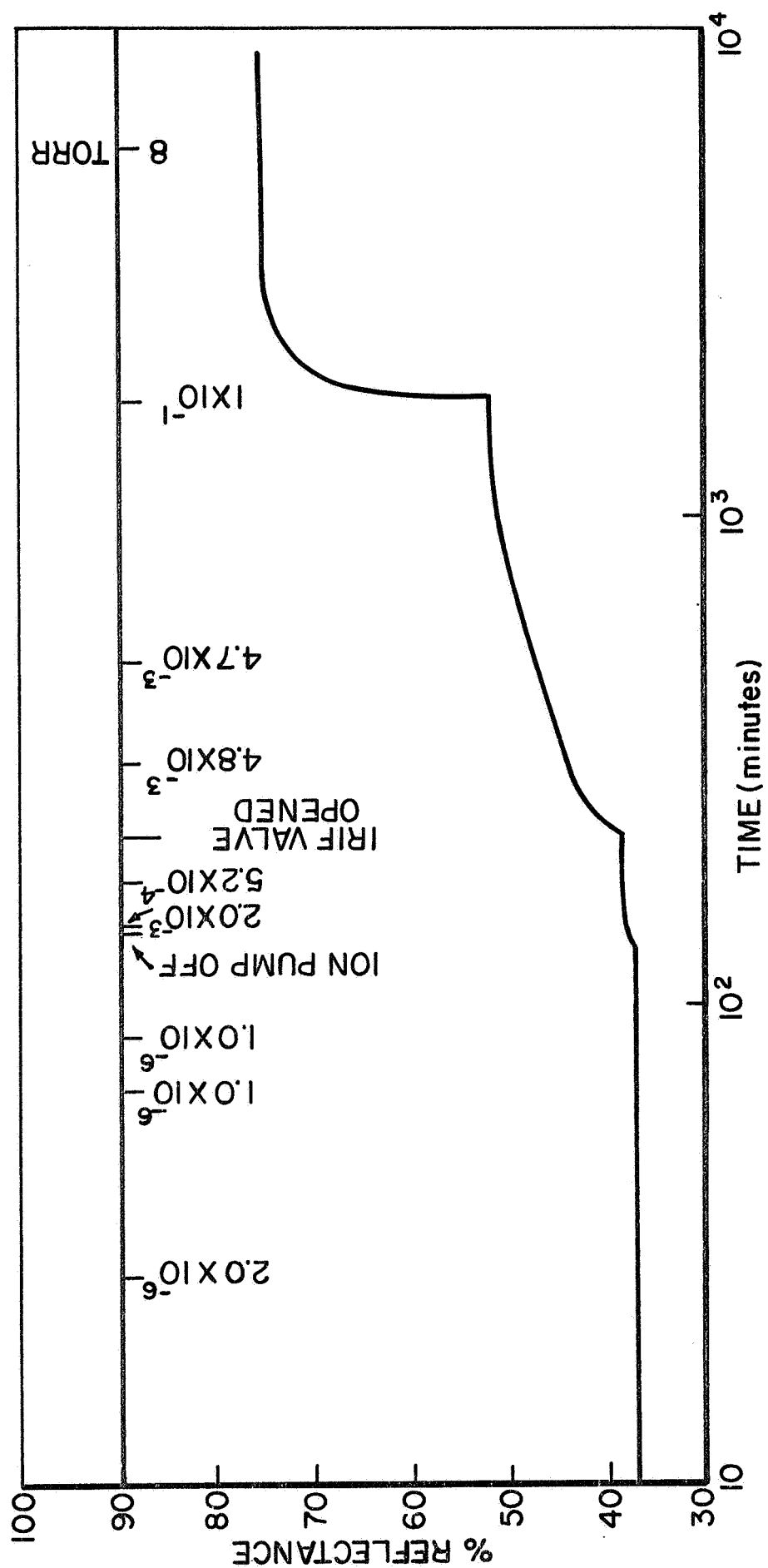


Figure 65: OXYGEN BLEACHING  
S-13 at 2.05  $\mu$

Examination of the original data and the data in Table 9 shows that: (1) a partial oxygen pressure of  $8 \times 10^{-3}$  Torr causes approximately 50% bleaching in the infrared spectrum of IITRI's S-13 thermal-control coating (Figure 61) and in the 400- to 1700-nm region of the two rutile coatings (Figures 59 and 62); (2) the RF-1 rutile-pigmented Owens Illinois 650-resin paint degraded in a qualitatively identical manner to the Lockheed (LMSC-2) coating, but only by about 40% of LMSC-2 quantitatively; (3) both S-13 specimens exhibited an increase in measured reflectance (attributed to fluorescence) in the region below the absorption edge - an effect that was quenched on admission of oxygen (even at  $8 \times 10^{-3}$  Torr) to the extent that finally degradation was observed to have occurred; (4) the potassium silicate paints generally exhibited bleaching in the infrared on irradiation (as a result of photodesorption of water) followed by slight decreases on admission of oxygen (Figures 60 and 63); (5) zinc sulfide exhibited a slight bleaching on admission of oxygen that was independent of the pressure, although its total bleaching was nonexistent in the ultraviolet and only slight in the visible spectrum (Figure 64); (6) neither the alumina nor the Lithafrax coatings exhibited significant bleaching on admission of oxygen - however, both exhibited less bleaching at 8 than at  $8 \times 10^{-3}$  Torr of oxygen pressure (this was also true to a slight extent for the S-13 and zirconia coatings); (7) the HAC Plasmoclay and tin oxide coatings did not exhibit bleaching at  $8 \times 10^{-3}$  Torr, but did bleach slightly at 8 Torr of oxygen pressure.

#### C. IRIF-II Test 2-3 (Oxygen Bleaching)

The second gas adsorbate (oxygen) test involved a nominal 500-ESH ultraviolet irradiation experiment of twelve specimens; the samples irradiated are presented in Table 12. Except for the average pressure during irradiation ( $1 \times 10^{-6}$  Torr) and an initial reflectance measurement performed in air, the test parameters employed in Test 2-3 were identical to those in Test 2-2.

Table 12

## BEHAVIOR OF A NUMBER OF SPECIMENS IN THE GASEOUS ADSORBATE TEST (OXYGEN)

Item No.	Surface	Exposure (ESH) and Pressure (Torr)	$R_{\lambda}$ , $\lambda = \text{nm}$				
			354	444	788	1900	2400
40	A605 $\text{Zn}_2\text{TiO}_4/650$	ATM**	59.5	86.0	84.6	81.6	65.0
		$5 \times 10^{-6}$ Torr	59.5	85.6	84.6	82.2	65.0
		500 ESH	55.6	73.5	66.0	79.8	64.8
		ATM**	58.3	83.8	81.2	81.6	64.8
41	$\text{CaWO}_4/650$	ATM**	80.0	89.6	89.0	87.6	65.0
		$5 \times 10^{-6}$ Torr	81.0	89.6	88.6	89.0*	66.4
	SL3G (A524)	ATM**	3.8	83.6	80.0	72.0	52.5
		$5 \times 10^{-6}$ Torr	3.8	84.0	80.6	75.0*	55.0*
39	RF-1 $\text{TiO}_2/650$	500 ESH	2.5	81.2	80.9	72.0	51.5
		ATM**	3.8	81.4	80.2	73.6*	53.0
		ATM**	4.2	91.0	88.3	69.6	49.5
		$5 \times 10^{-6}$ Torr	4.9	90.6	88.3	72.2*	50.5
22	$\text{SnO}_2/\text{PS7}$	500 ESH	4.9	86.5	82.6	70.8	49.7
		ATM**	5.1	89.5	87.0	71.2	49.5
		ATM**	49.0	87.2	93.5	80.0	67.0
		$5 \times 10^{-6}$ Torr	50.0	86.0	92.5	84.6*	71.0
26	$\alpha\text{-Al}_2\text{O}_3/\text{PS7}$	500 ESH	47.0	81.0	91.5	82.5	68.5
		ATM**	46.0	82.8	92.0	80.8*	67.0
		ATM**	77.0	91.8	96.0	78.5	65.0
		$5 \times 10^{-6}$ Torr	77.0	90.8	96.0	83.3*	68.5*
23	$\text{ZrO}_2/\text{PS7}$	500 ESH	47.0	64.5	92.5	84.2*	70.2*
		ATM**	48.2	66.4	93.5	81.0*	67.0*
		ATM**	65.5	86.0	86.0	64.0	43.0
		$5 \times 10^{-6}$ Torr	65.5	86.0	86.8	68.5*	47.0*
20	HAC Plasmoclay	500 ESH	52.6	77.0	86.0	68.5	47.0
		ATM**	53.0	78.0	86.0	68.5	46.5*
		ATM**	55.5	79.5	82.0	69.0	59.0
		$5 \times 10^{-6}$ Torr	55.5	79.5	82.0	74.5*	63.8*
36	$\text{ZnS}/650$	500 ESH	49.0	73.2	81.5	74.5	63.8
		ATM**	49.0	73.7	81.3	72.5*	61.8*
		ATM**	4.5	87.6	84.5	68.2	44.0
		$5 \times 10^{-6}$ Torr	5.9	86.1	84.5	71.0*	46.0*
30	Pegasus S-13	500 ESH	4.3	84.8	84.5	70.5	45.2
		ATM**	4.1	85.6	83.0	69.5	43.8*
		ATM**	2.5	88.2	93.8	79.5	38.0
		$5 \times 10^{-6}$ Torr	5.0	88.2	93.2	78.5	38.0
27	LMSC-3 (r- $\text{TiO}_2/\text{Silicone}$ )	500 ESH	6.0	85.2	90.6	56.0	25.0
		ATM**	3.8	86.0	93.2	79.0	38.0
		ATM**	4.2	88.5	94.0	83.3	53.0
		$5 \times 10^{-6}$ Torr	5.8	89.3	94.0	84.7*	55.0*
		500 ESH	5.0	77.5	83.5	81.5	53.8
		ATM**	4.5	84.0	92.4	83.0	53.0*

\* Changes ascribed to sorption of water.

\*\* Atmospheric pressure, air.

Only one S-13 was tested since the previous test showed them to be identical; an S-13G specimen was tested instead. Because we only possessed one remaining specimen of LMSC's Lithafrax, we replaced this specimen with a specimen of  $\text{Zn}_2\text{TiO}_4$ . Zinc orthotitanate had previously been shown to develop a broad adsorption band centered at about 850-nm wavelength.

It was decided that oxygen again would be bled into the IRIF in order to obtain more definite information concerning bleaching reactions. A different bleaching curve was obtained and the significance of these data is discussed in a later paragraph.

The spectral data were examined; the data were abstracted for wavelengths of 354, 444, 788, 1900 and 2400 nm and are presented in Table 11. This data is presented as  $R_\lambda$  rather than  $\Delta R_\lambda$ . The spectra of seven of the most interesting specimens are presented in Figures 66 through 72. Complete spectra on all specimens were determined first in air, then in vacuum at  $5 \times 10^{-6}$  Torr, after an exposure of 500 ESH in vacuum and finally in air at atmospheric pressure.

(1) Many of the specimens exhibited an increase in reflectance in the near infrared (peaking at about 1950-nm wavelength) solely as a result of evacuation - presumably due to the desorption of water from the pigment and/or alkali silicate surfaces. Most of these specimens readsorbed water (see the  $R_{1900\text{-nm}}$  column in Table 11) on opening from 8 Torr oxygen pressure to air. Although several Owens-Illinois Type "650" silicone resin paints exhibited desorption of water at 1900-nm wavelength, desorption was more prevalent for the potassium silicate paints. See Figures 67 through 72.

(2) S-13G exhibited a decrease and S-13 an increase in reflectance at 354-nm wavelength on irradiation - both of which were quenched on admission of 8 Torr of oxygen (Figure 67).

(3) The zinc sulfide specimen exhibited an increase in ultraviolet reflectance on evacuation only; in addition, this



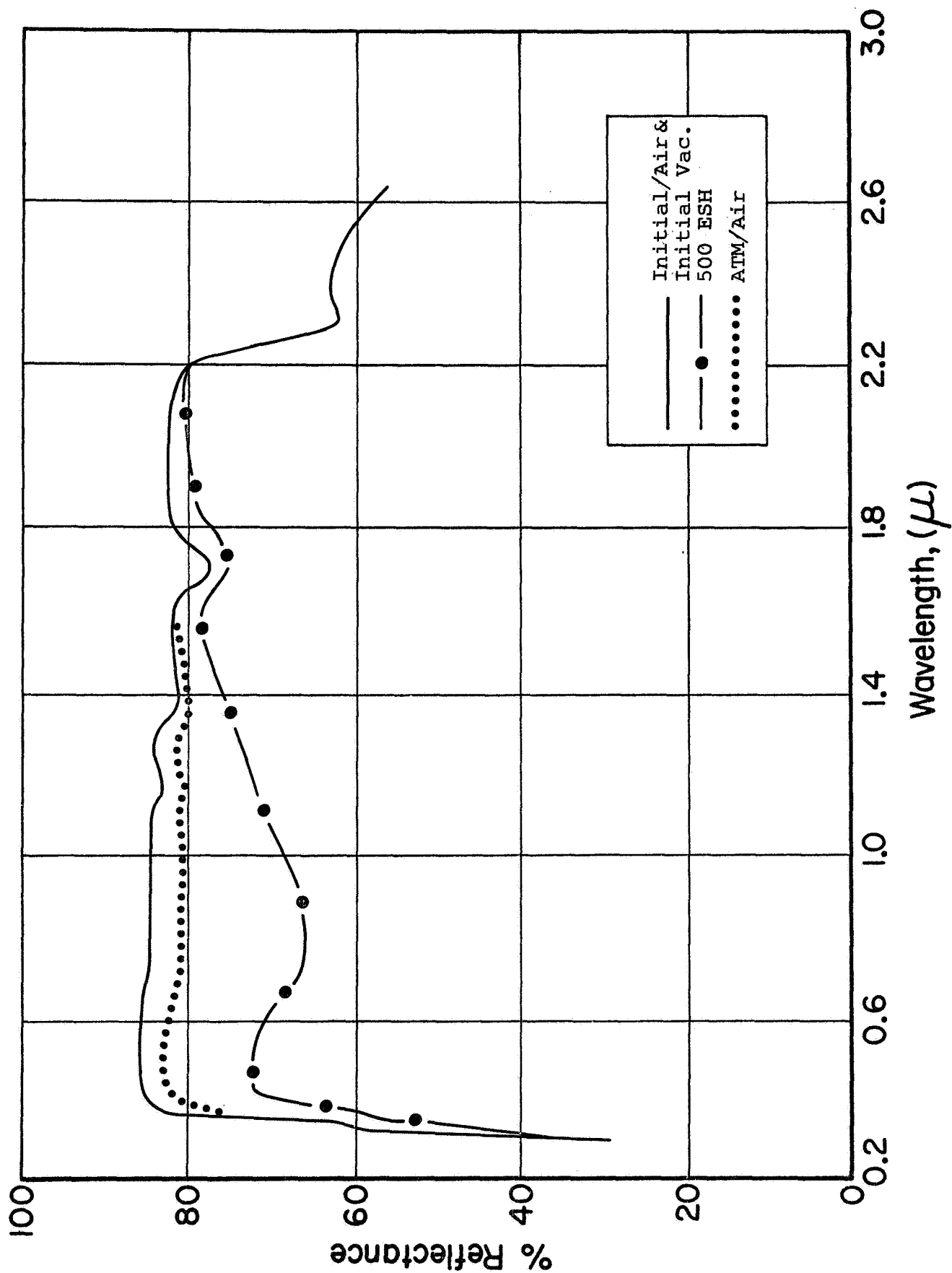


Figure 66: EFFECT OF 500 ESH Hg-Xe IRRADIATION AND BLEACHING WITH 760 TORR AMBIENT AIR ON A ZINC ORTHOTITANATE/O-I 650 PAINT - TEST 2-3

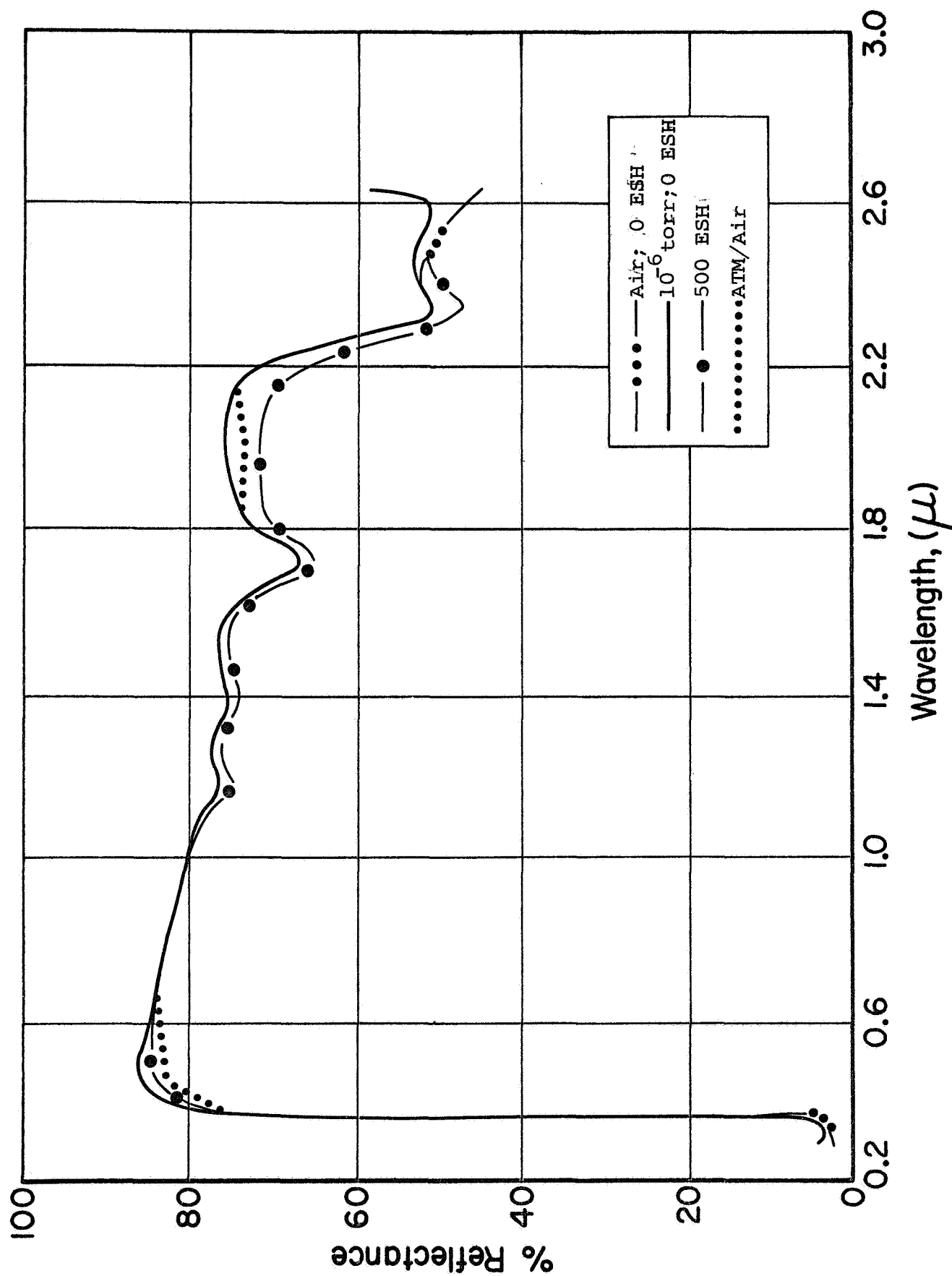
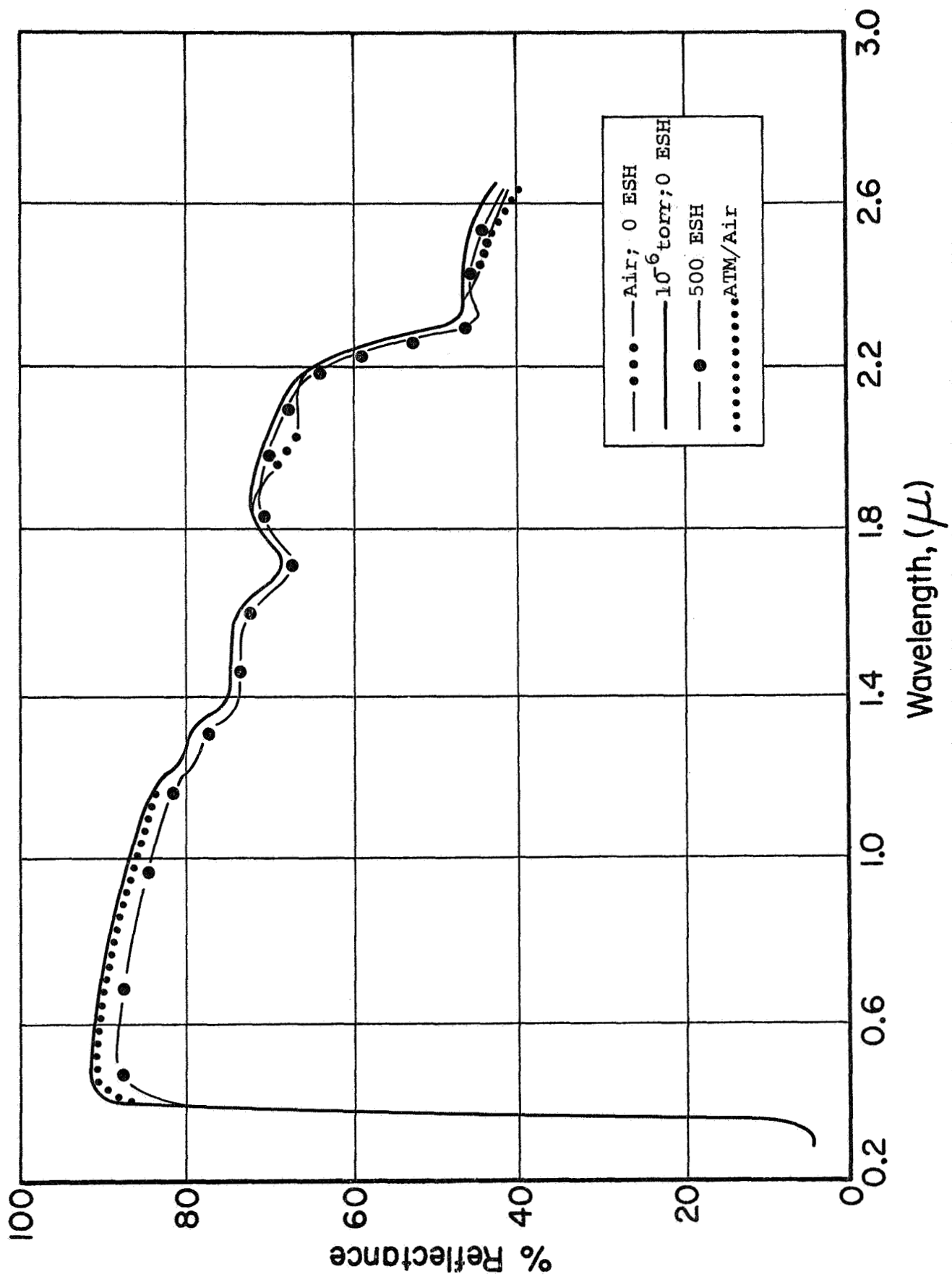


Figure 67: EFFECT OF 500 ESH Hg-Xe IRRADIATION AND BLEACHING WITH 760 TORR AMBIENT AIR ON IITRI'S BATCH A-574 S-13G - TEST 2-3



Wavelength, ( $\mu$ )

Figure 68: EFFECT OF 500 ESH Hg-Xe IRRADIATION AND BLEACHING WITH 760 TORR AMBIENT AIR ON RF-1  $\text{TiO}_2/\text{O-I 650}$  (#39) - TEST 2-3

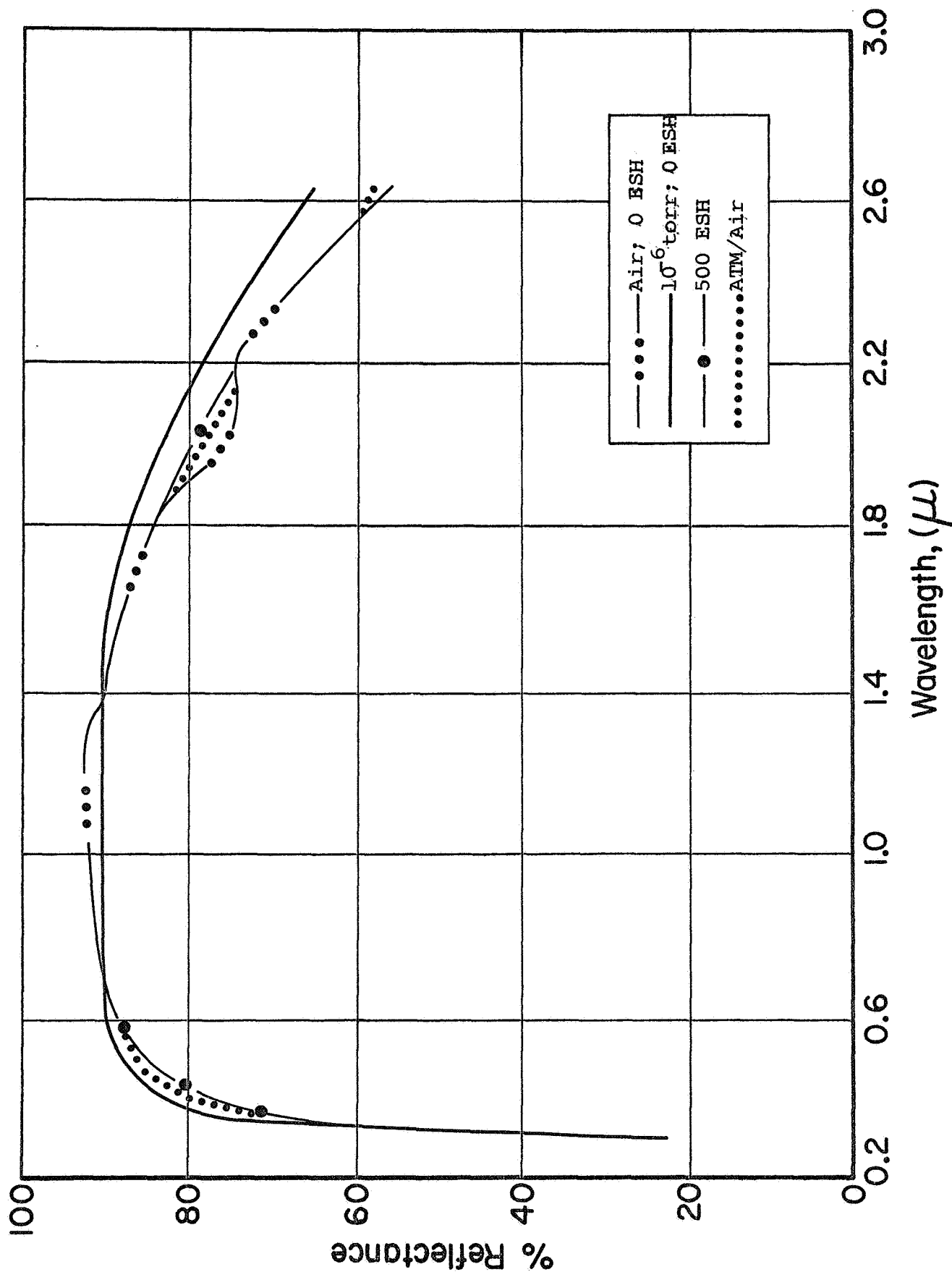


Figure 69: EFFECT OF 500 ESH Hg-Xe IRRADIATION AND BLEACHING WITH 760 TORR AMBIENT AIR ON TIN OXIDE/K-Sil (#22) - TEST 2-3

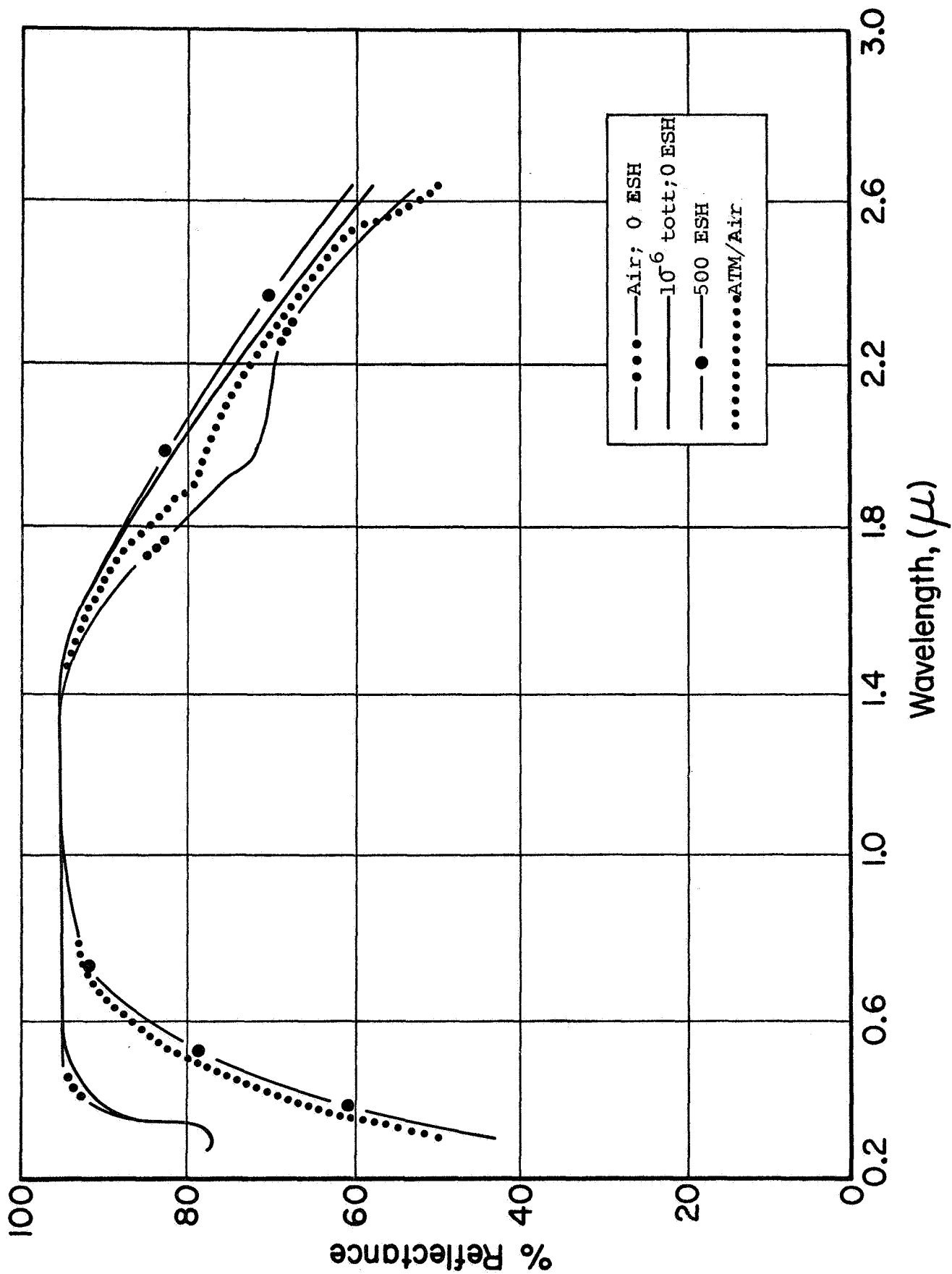


Figure 70: EFFECT OF 500 ESH Hg-Xe IRRADIATION AND BLEACHING WITH 760 TORR AMBIENT AIR ON ALUMINA/K-Sil (#26) - TEST 2-3

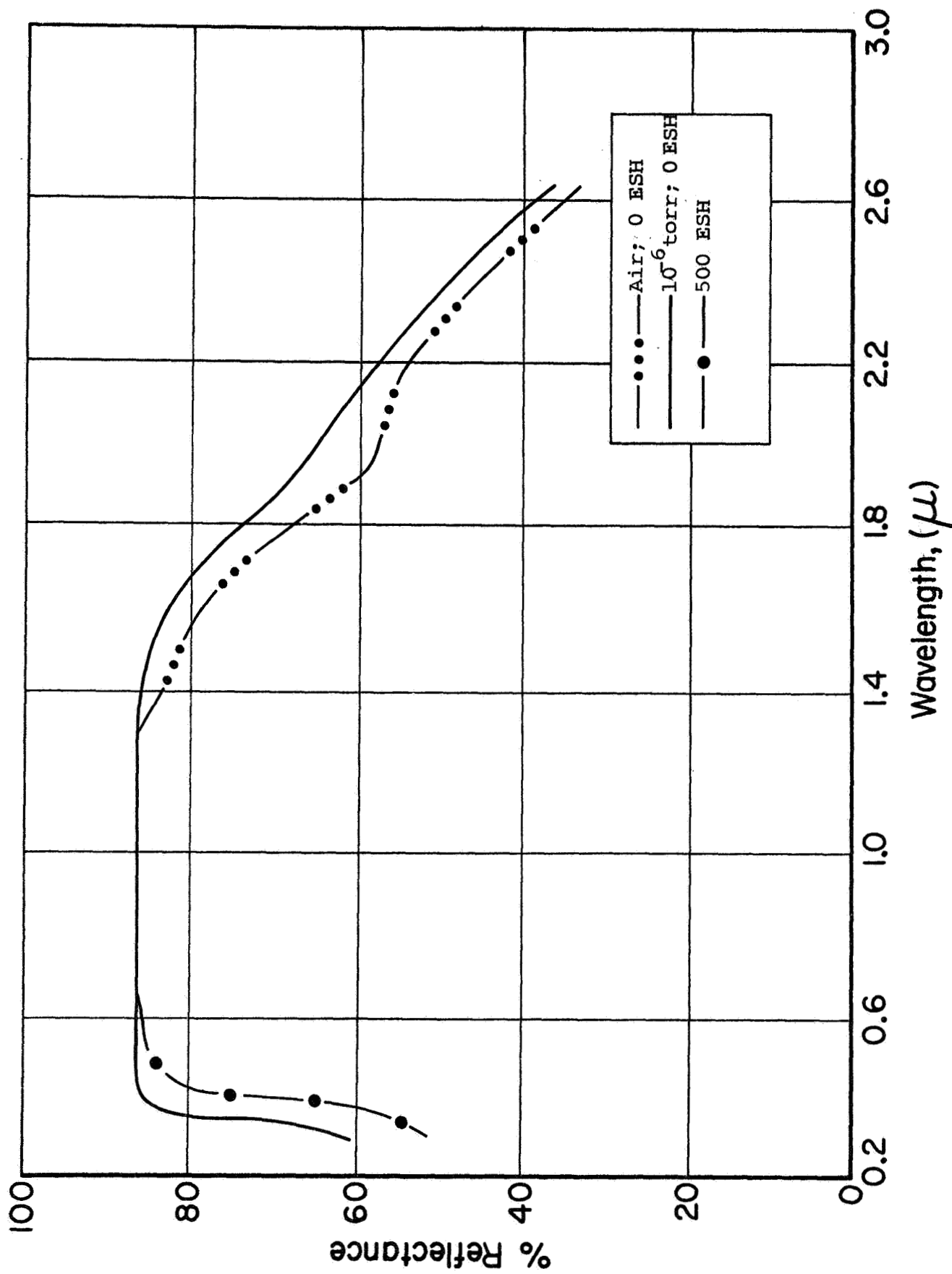


Figure 71: EFFECT OF 500 ESH Hg-Xe IRRADIATION AND BLEACHING WITH 760 TORR AMBIENT AIR ON ZIRCONIA/K-Sil (#23) - TEST 2-3

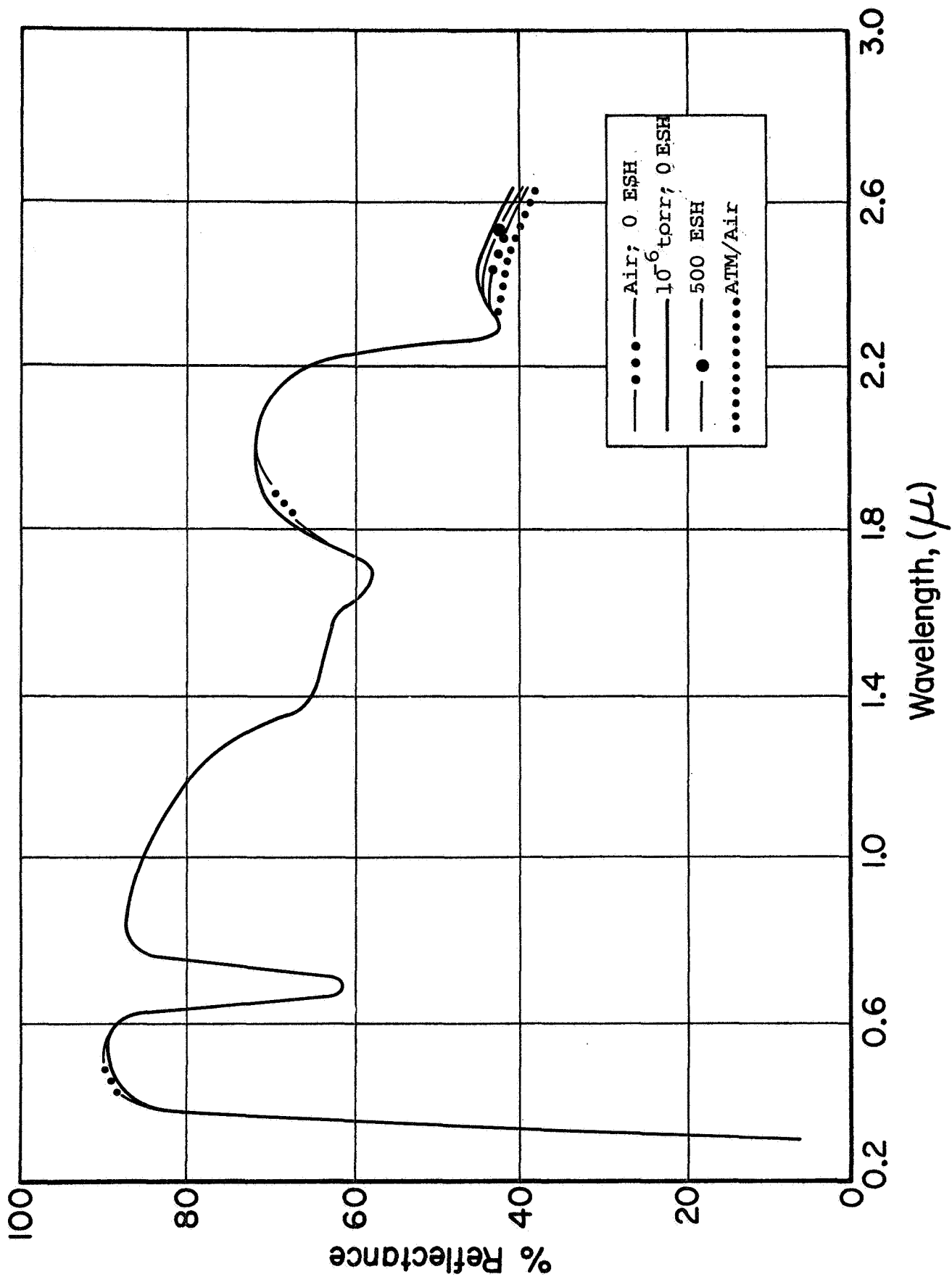


Figure 72: EFFECT OF 500 ESH Hg-Xe IRRADIATION AND BLEACHING WITH 760 TORR AMBIENT AIR ON ZINC SULFIDE/O-I 650 (#36) - TEST 2-3

specimen was considerably more stable in this test than in the previous test (Figure 72).

(4) The behavior of the 2050-nm absorption of S-13 was much different in Test 2-3 than in the previous test. While no change in  $R_{\lambda}$  at 2050-nm was observed after 18 hr at  $1 \times 10^{-5}$  Torr, like the previous test, unlike the previous test (See Figure 65), no change in  $R_{\lambda}$  occurred after 1 hr at  $1 \times 10^{-2}$  Torr. We therefore immediately admitted oxygen to a pressure of 5 Torr. The reflectance at 2050-nm wavelength immediately began to rise; the reflectance at 2050 nm is plotted (in Figure 73) as a function of time after admittance of oxygen.

The interesting fact, one that we have begun to understand, is that the S-13 specimen in Test 2-3 exhibited no bleaching until the pressure reached 5 Torr, the approximate pressure required to raise the reflectance above 52% in Test 2-2 (see Figure 65).

The bleaching-rate data from the second oxygen adsorbate tests were plotted with that of the first in order to make the rate curves coincide relative to the admission of oxygen at approximately  $10^{-1}$  Torr. These data, which are plotted in Figure 74, were taken from Figures 65 and 73. Figure 75 also contains data from the oxygen bleaching of an S-13 sample inserted into a space simulation test on another program: the S-13 was degraded to a  $\Delta R_{2050}$  of only 14% in this test. Since the curves are somewhat nonresponsive to the actual data for the range 1000 to 5000 minutes, we replotted that portion by beginning the 1000-minute data at 1 min; these replotted data are presented in Figure 75.

Examination of Figure 75 shows that the kinetics of bleaching the last decade ( $\sim 10^{-1}$  to  $\sim 8$  Torr) are essentially identical even though no bleaching occurred prior to the 8-Torr plateau for one of the two specimens. Examination of the data in Figures 74 and 75 show the following:



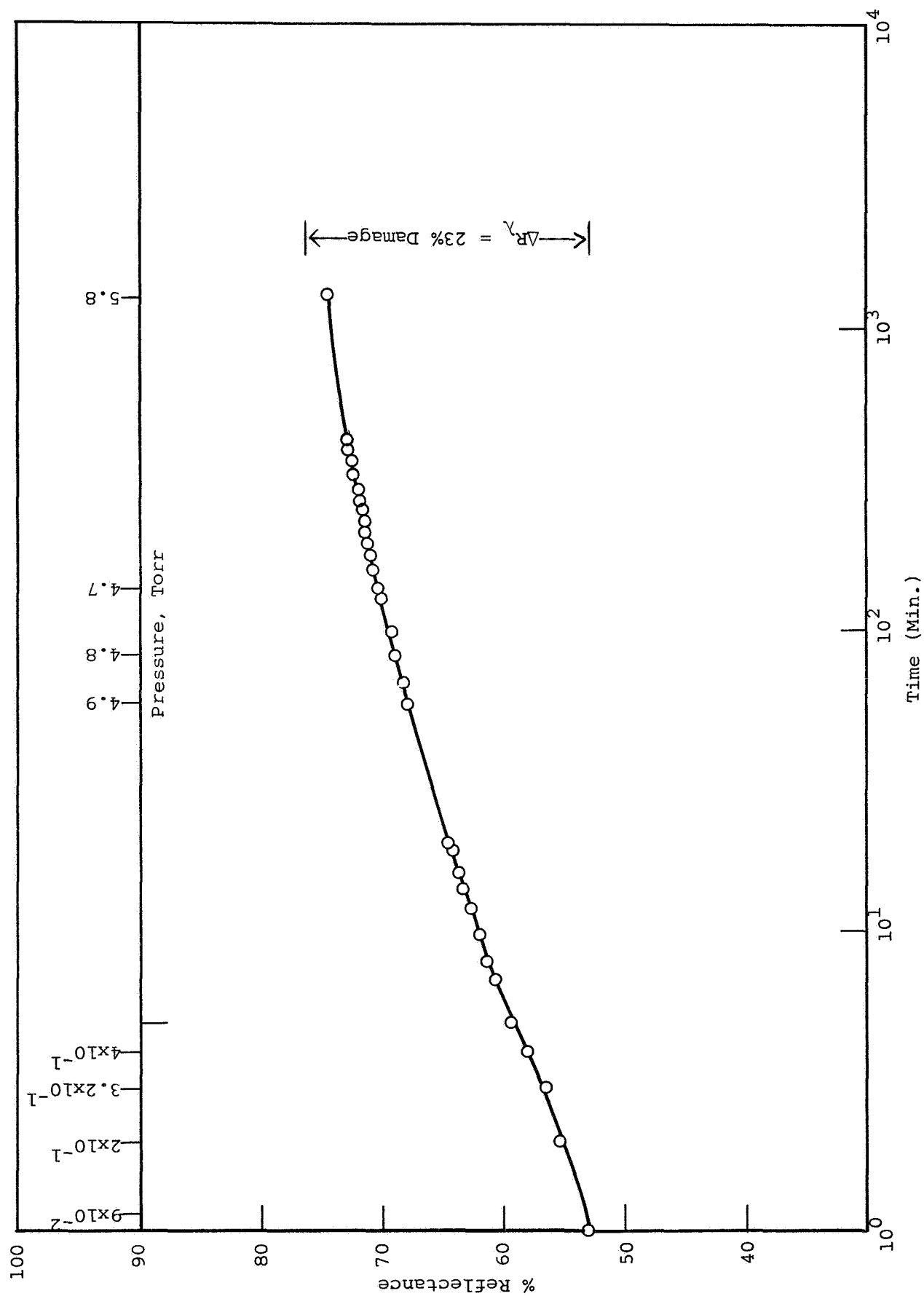


Figure 73: BLEACHING BEHAVIOR TO OXYGEN OF S-13 AT 2050-nm WAVELENGTH (TEST 2-3)

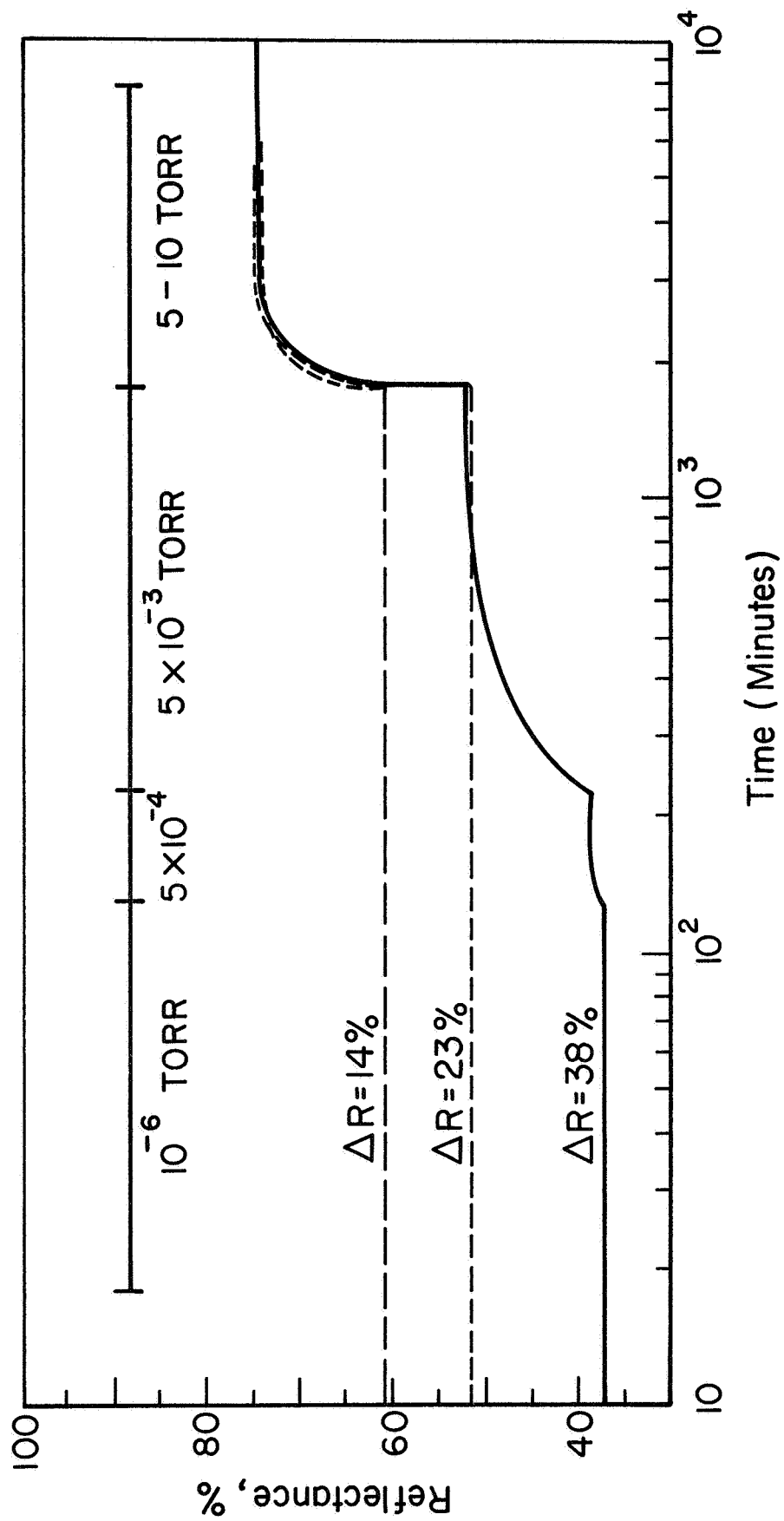


Figure 74: OXYGEN BLEACHING OF S-13 THERMAL COATING AT 2.05 MICRONS

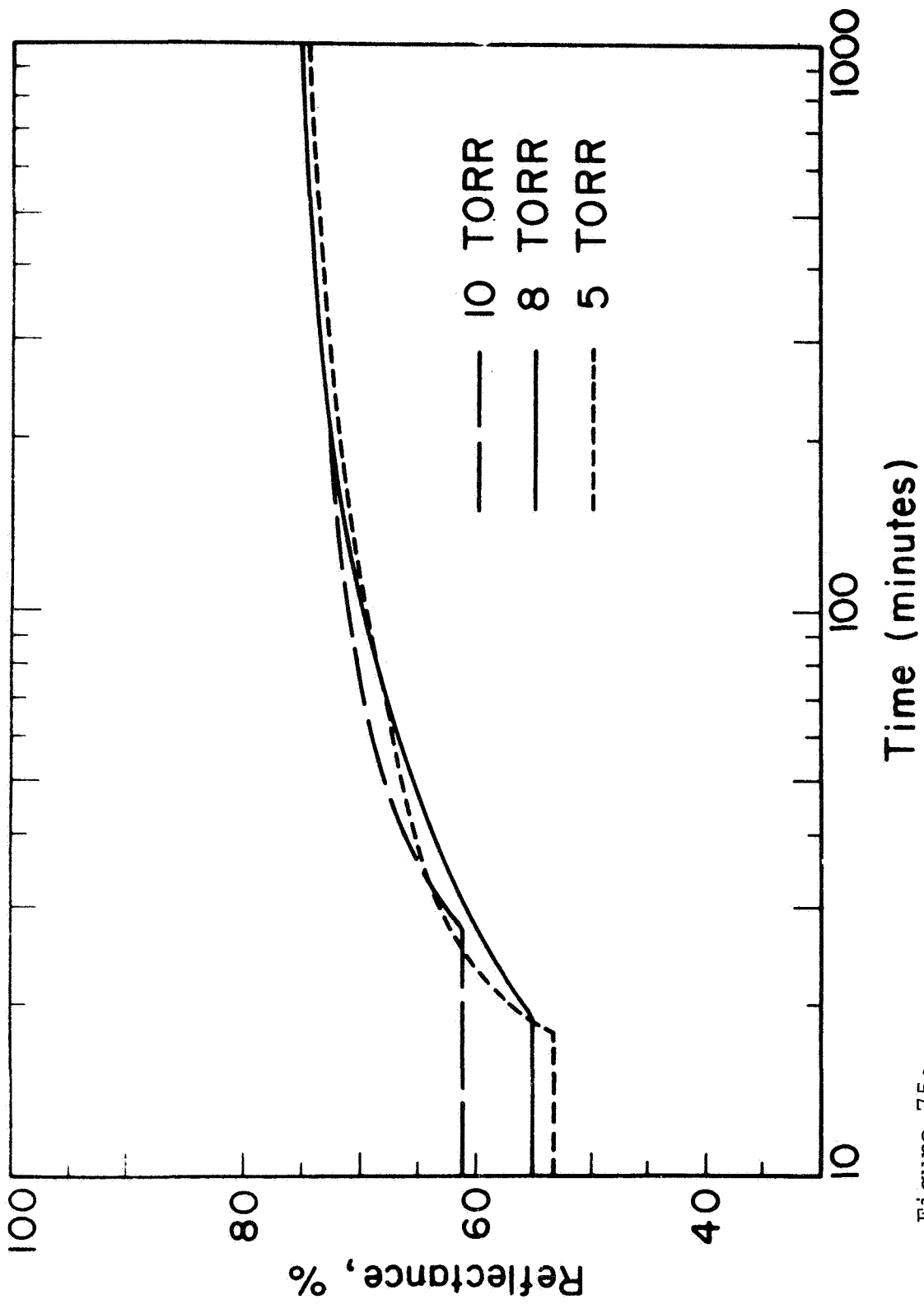


Figure 75:

**OXYGEN BLEACHING RATES OF S-13 AT 2.05 MICRONS**

1. The specimens were irradiated to three different degrees of damage ( $\Delta R_{2.05}$ ) - 38% in Test 2-2, 23% in Test 2-3, and 14% in the third test.
2. Admission of oxygen had no effect on the induced damage until a pressure of  $10^{-3}$  Torr was reached in Test 2-2, and until a pressure of  $\sim 5$  Torr was reached in Tests 2-3 and the third oxygen bleaching test on S-13.
3. The reflectance at which the Test 2-2 pressure corresponded to the "incipient" pressure observed in Test 2-3 was 52% - the actual reflectance of the induced absorption band in the Test 2-3 specimen.

This data suggests that there is a relationship between induced damage and the incipient pressure required to begin interacting with that band, such that a gas pressure that is sufficient to interact at a high concentration of defects per unit surface is insufficient to interact at a lower concentration of defects.

It is important to note that this same phenomena was observed with other semiconductor pigments (rutile and zinc orthotitanate), but with less surety since we have "locked-on" the  $2.05\text{-}\mu$  band of the S-13 specimen only.

#### D. IRIF-II Test 2-4 (Nitrogen Bleaching)

Bleaching Test 2-4 involved 740 ESH of mercury-xenon radiation in IRIF-II and admission of nitrogen (99.999%) during the gas adsorbate/bleaching experiment. The average pressure during irradiation was  $2 \times 10^{-7}$  Torr; the nominal sample temperature was  $10^\circ\text{C}$ . The samples irradiated in Test 2-4 and a quantitative description of their behavior are provided in Table 13.

Argon was first admitted to the IRIF-II chamber and had no effect on the optical properties of the irradiated specimens. It was subsequently pumped out, "saving" the damage for the nitrogen bleaching studies.

Examination of the data presented in Table 13, as well as the spectra themselves (Figures 76 through 79), shows that specimens that were bleached with oxygen are also bleached by

Table 13

BEHAVIOR OF A NUMBER OF SPECIMENS IN THE GASEOUS  
ADSORBATE TEST (NITROGEN)

Item No.	Surface	Exposure (ESH) and Pressure (Torr)	$R_{\lambda}$ , nm		
			444	788	2400
--	$Gd_2O_3/650$	0 ESH	72.5	89.0	63.5
		740 ESH	53.5	86.0	64.5
		650 Torr	54.0	85.0	63.5
26	$\alpha-Al_2O_3/PS7$	0 ESH	80.2	95.6	69.6
		740 ESH	57.5	94.0	71.5
		650 Torr	57.5	93.0	68.5
23	$ZrO_2/PS7$	0 ESH	72.5	87.5	43.5
		740 ESH	67.5	88.3	45.0
		650 Torr	67.0*	86.0*	44.4
22	$SnO_2/PS7$	0 ESH	67.5	94.0	74.0
		740 ESH	66.5	92.0	71.5
		650 Torr	65.0*	91.0*	70.0*
39	RF-1 $TiO_2/650$	0 ESH	82.0	89.0	49.0
		740 ESH	81.0	84.0	49.0
		650 Torr	81.0	86.0	50.0
	$Zn_2TiO_4/650$	0 ESH	67.0	84.5	66.0
		740 ESH	66.5	77.5	66.0
		650 Torr	66.5	82.5	66.0
36	$ZnS/650$	0 ESH	60.0	84.0	54.5
		740 ESH	60.0	84.0	55.0
		650 Torr	60.0	83.0*	55.0
	$CaWO_4/650$	0 ESH	66.5	82.0	61.0
		740 ESH	64.0	81.5	61.0
		650 Torr	64.0	80.8*	61.0
30	S-13 (Pegasus)	0 ESH	82.8	93.0	37.5
		740 ESH	79.5	90.0	23.5
		650 Torr	79.0*	92.8	34.0
27	LMSC-3 $r-TiO_2/Silicone$	0 ESH	83.5	95.0	54.0
		740 ESH	74.0	83.0	53.2
		650 Torr	77.5	91.5	54.5
20	HAC Plasmoclay	0 ESH	70.0	82.0	62.0
		740 ESH	62.0	81.5	64.0
		650 Torr	61.0*	80.8*	62.0

\* Represents decreases due to nitrogen adsorption.

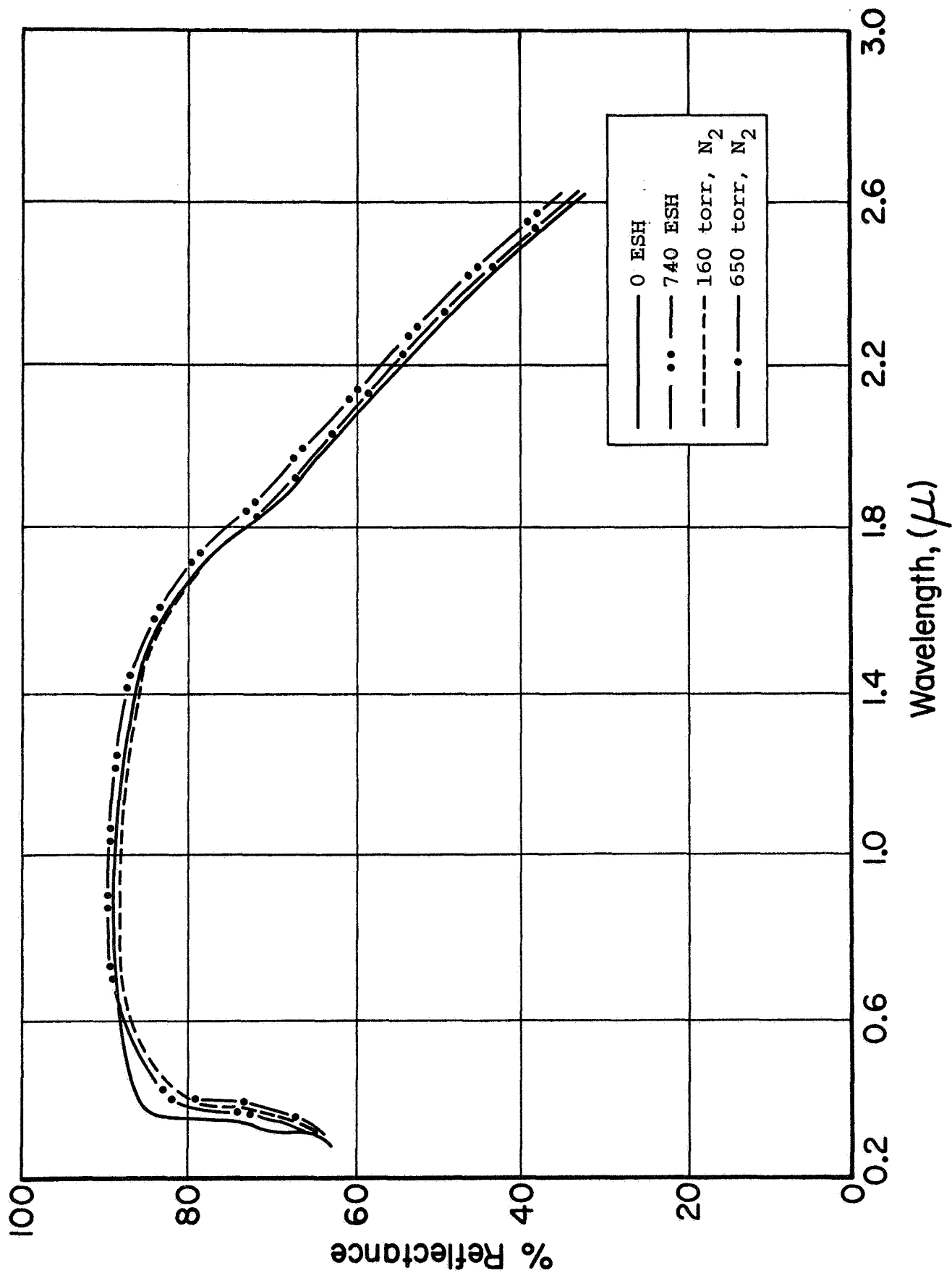


Figure 76: EFFECT OF 740 ESH Hg-Xe IRRADIATION AND BLEACHING WITH N<sub>2</sub> OF ZIRCONIA/K-Sil (#23) - TEST 2-4

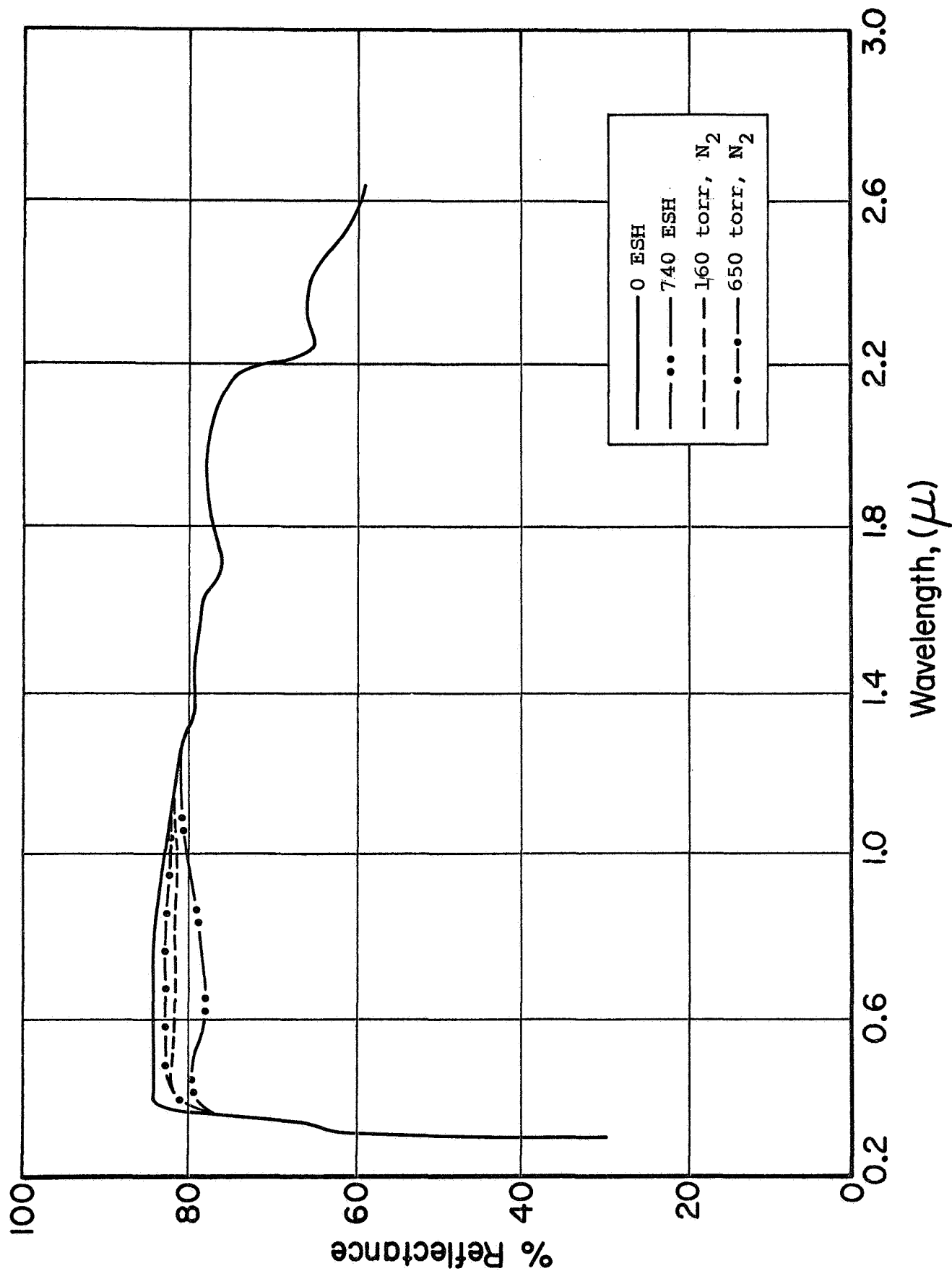


Figure 77: EFFECT OF 740 ESH Hg-Xe IRRADIATION AND BLEACHING WITH N<sub>2</sub> OF A ZINC ORTHOTITANATE/O-I 650 PAINT - TEST 2-4

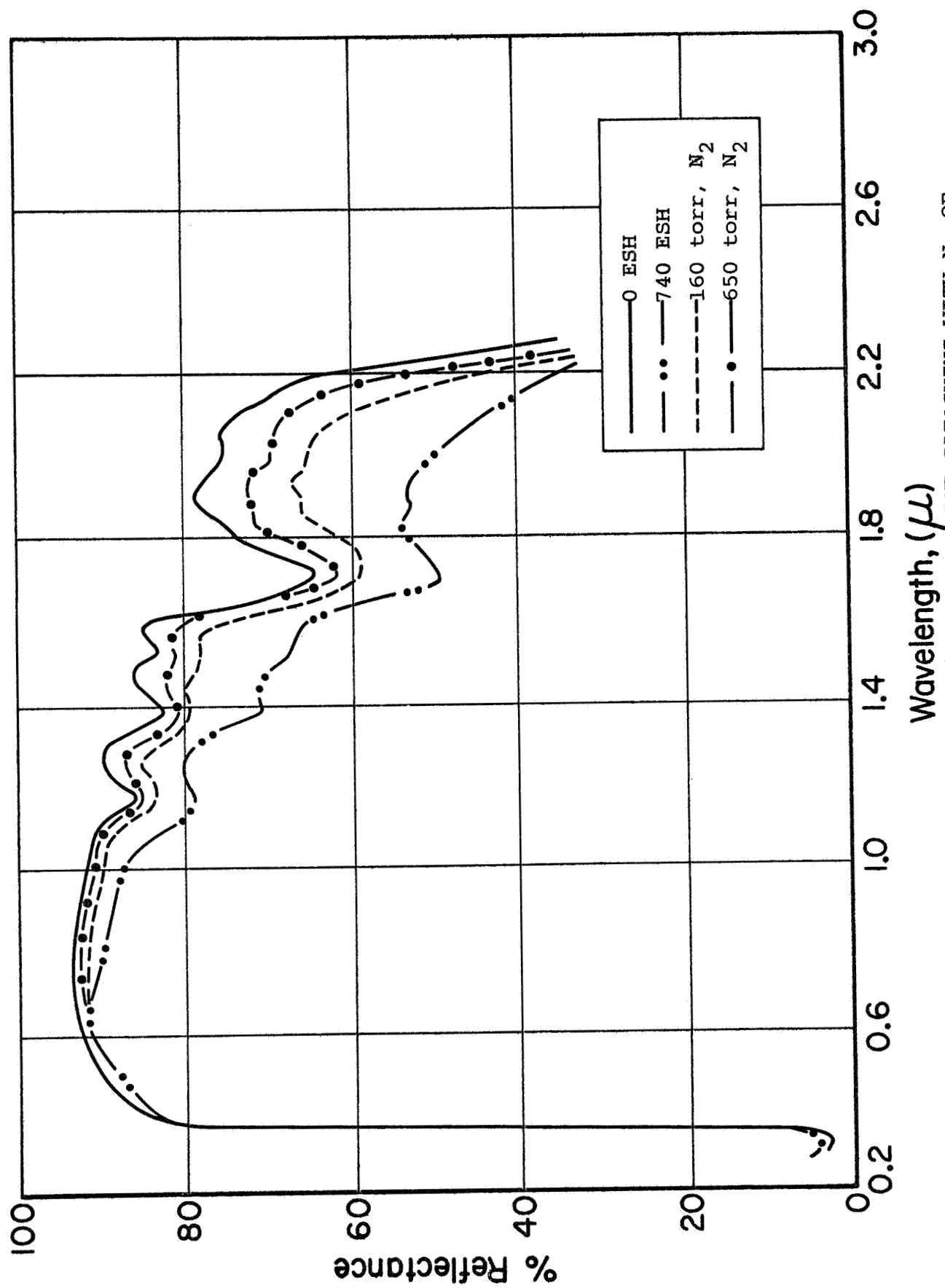


Figure 78: EFFECT OF 740 ESH Hg-Xe IRRADIATION AND BLEACHING WITH  $N_2$  OF PEGASUS S-13 (#30) - TEST 2-4



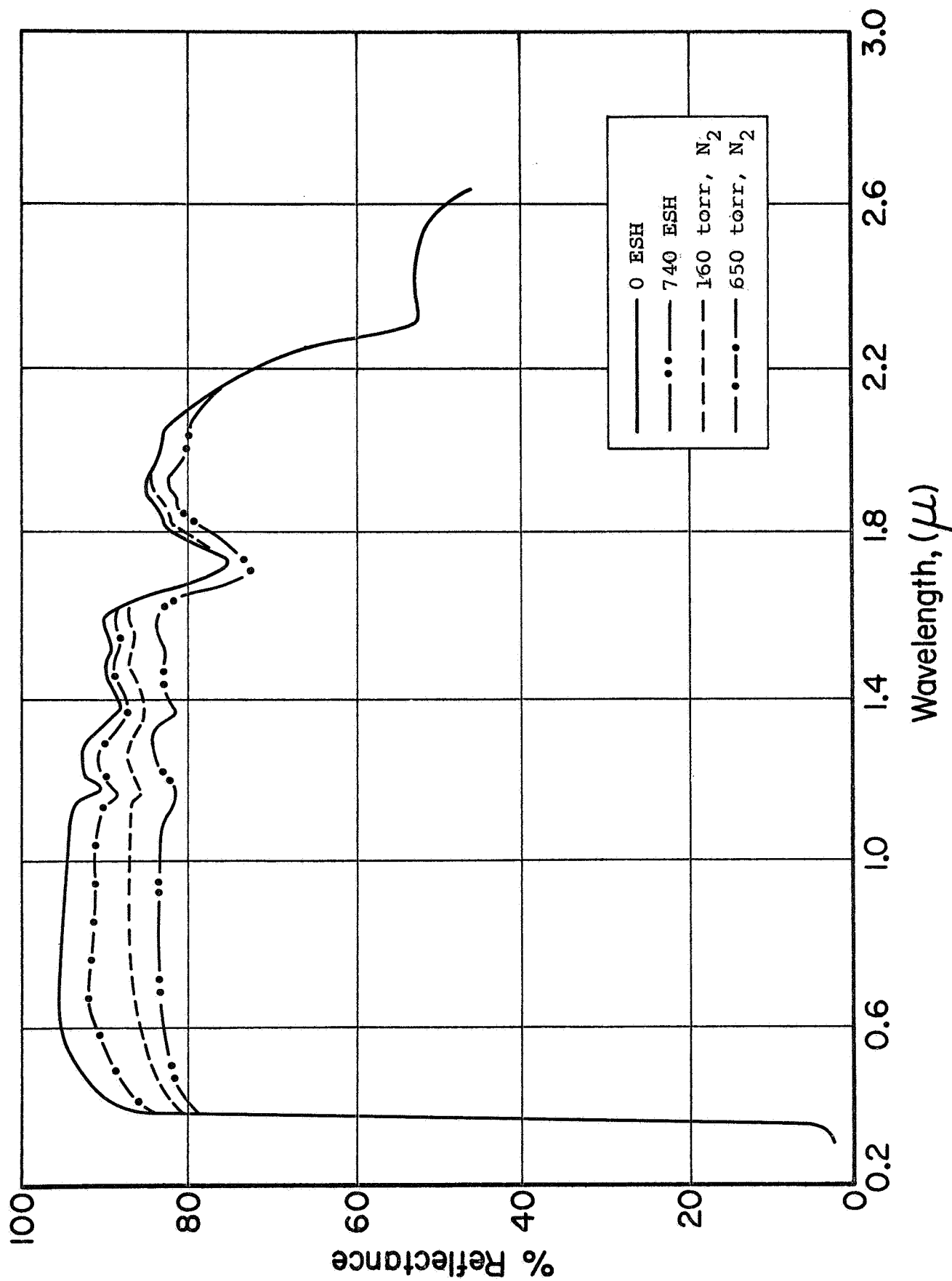


Figure 79: EFFECT OF 740 ESH Hg-Xe IRRADIATION AND BLEACHING WITH  $N_2$  OF  
RUTILE-PIGMENTED LMSC-3 (#27) - TEST 2-4

nitrogen, but considerably greater gas pressures are required for a like increase in reflectance of any given damage band. See in particular Figures 77 through 79.

The nitrogen-bleaching-rate data for S-13 at 2050-nm wavelength are presented in Figure 80. The bleaching spectra are shown in Figure 78. These data show that pressure/reflectance plateaus are also exhibited by specimens bleached by nitrogen, but at an order of magnitude greater pressure. The solid line in Figure 80 is the data as taken. The broken line is the original data replotted with 1000 min becoming 1 min.

Monsanto Chemical Company asserts that the total oxygen impurities in the "research grade" nitrogen is less than 1 ppm. If this is the case, the partial pressure of oxygen at 40 Torr (a pressure that caused 2% bleach) would be

$$40 \times 10^{-6} \text{ Torr} = 4 \times 10^{-5} \text{ Torr}$$

which is far below the threshold exhibited by oxygen. At 160 Torr, the oxygen partial pressure would be  $1.6 \times 10^{-4}$  for an oxygen impurity of 1 ppm and  $1.6 \times 10^{-3}$  Torr for 10 ppm (which would be sufficient to cause oxygen bleaching).

Several irradiated specimens exhibited reflectance decreases on admission of nitrogen: the spectra of the  $\text{ZnO}_2$ , shown in Figure 76, is an example. No explanation can be given for such behavior at this time.

#### E. IRIF-II Test 2-8 (Carbon Dioxide Bleaching)

Test 2-8 involved 660 ESH of mercury-xenon radiation in IRIF-II and the controlled admission of 99.995% carbon dioxide at the completion of the test. The average pressure during irradiation was  $1 \times 10^{-7}$  Torr and the nominal sample temperature was 8°C. Bleaching data were determined for the following specimens: Pegasus S-13; du Pont R900 rutile  $\text{TiO}_2$  powder; ZnO:Zn-pigmented Owens-Illinois (O-I) 650 resin; ZnS-pigmented O-I 650

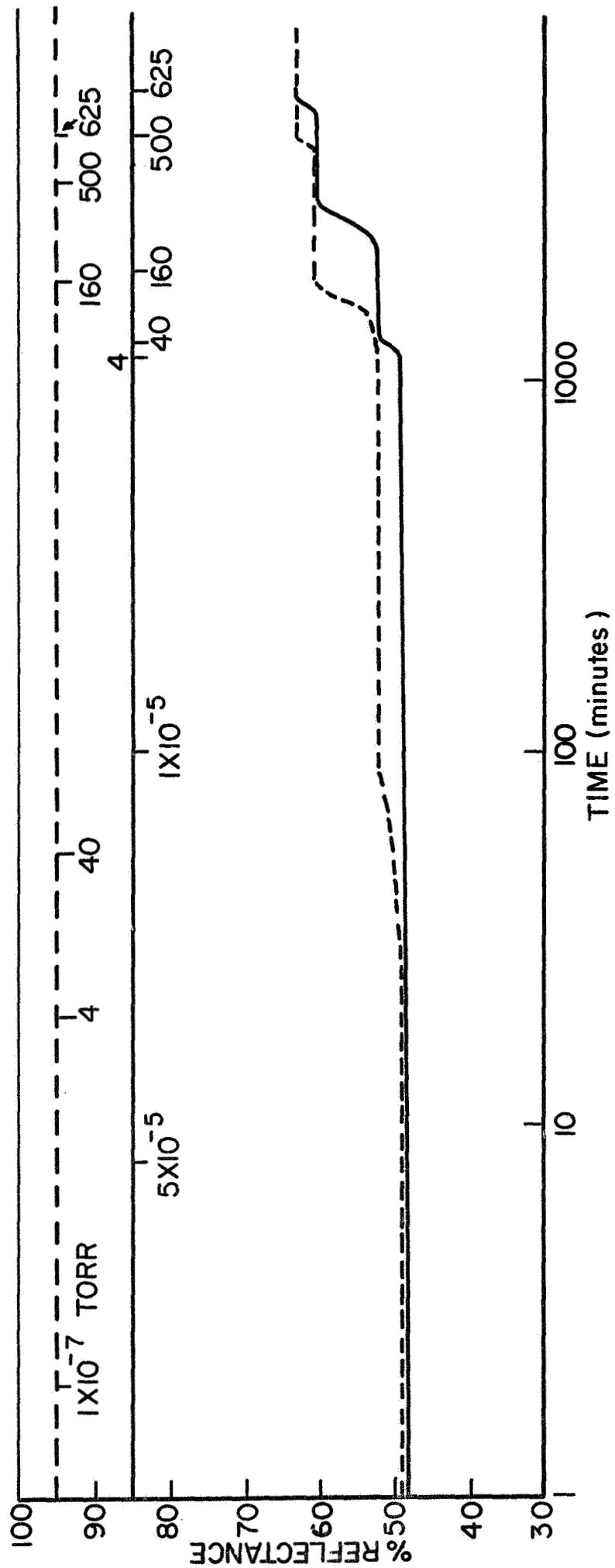


Figure 80: NITROGEN BLEACHING  
S-13 at 2.05 μ

resin; and a  $\text{Zn}_2\text{TiO}_4$ -pigmented O-I 650 resin. Tracings of the original IRIF-II data are presented in Figures 81 through 85.

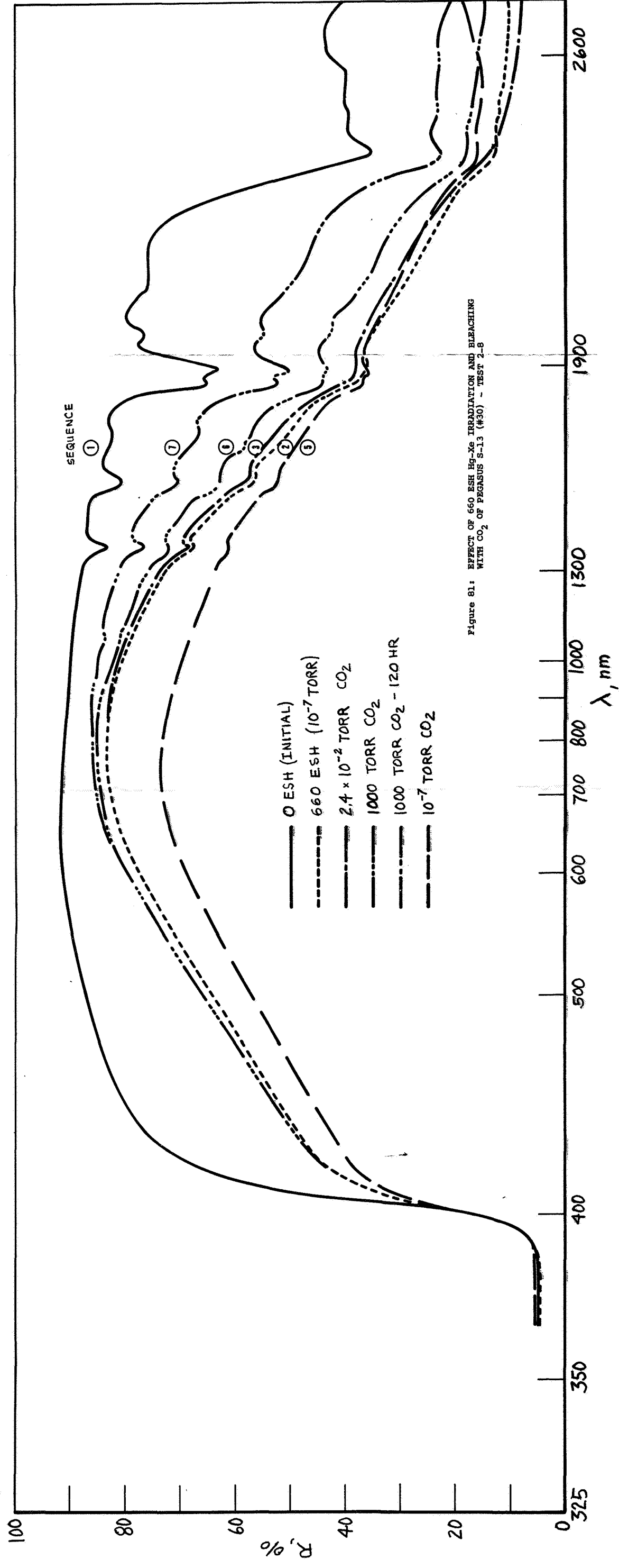
Figure 86 is the reflectance of the S-13 specimen (Figure 81) at 2050-nm wavelength plotted as a function of the pressure of carbon dioxide in the IRIF-II chamber. The reflectances represent values recorded 30 min after pressure equilibrium was observed. These data show that carbon dioxide causes bleaching at much lower adsorbate pressures than nitrogen, but at greater pressures than are required when back-filling with oxygen.

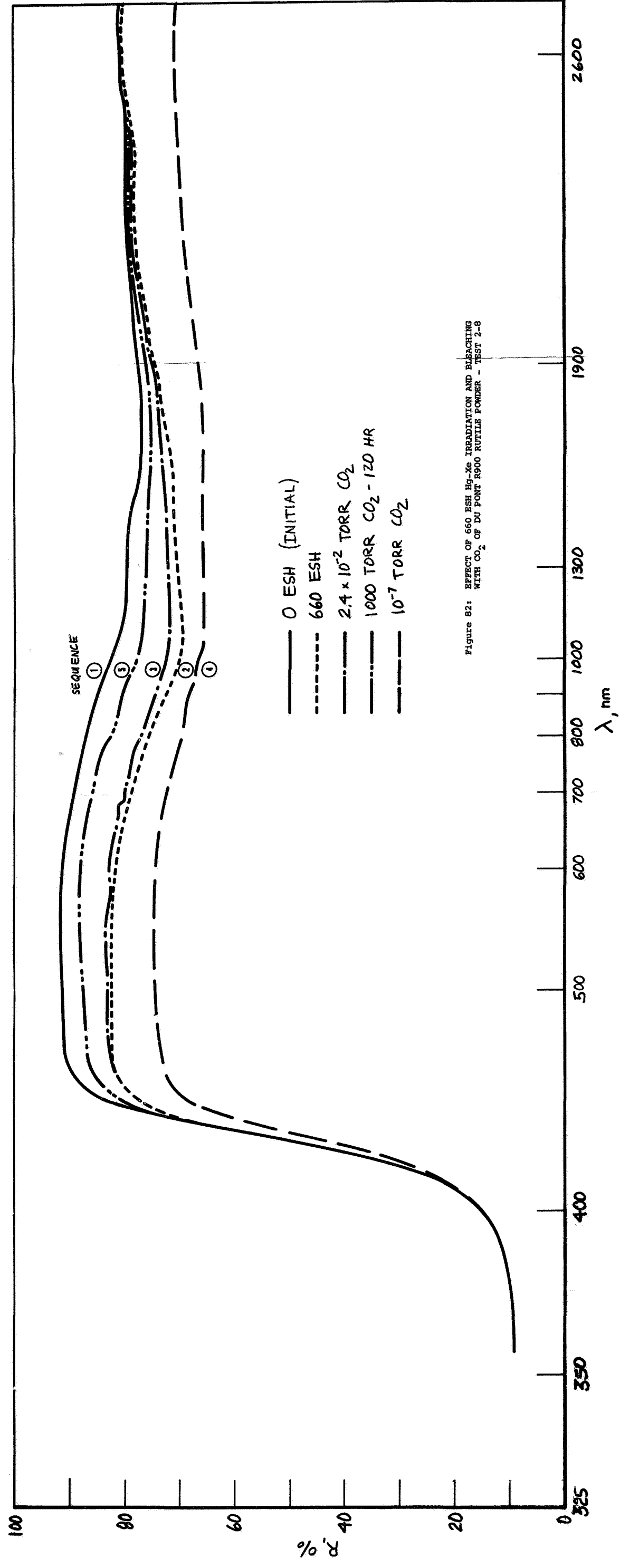
The Matheson Company guarantees that the partial pressure of oxygen in the research-grade  $\text{CO}_2$  employed is less than 10 ppm. Thus, at  $2.4 \times 10^{-2}$  Torr, the pressure at which bleaching first occurred (Figure 81), the partial pressure of oxygen would not have exceeded  $2.4 \times 10^{-7}$  Torr. At a  $\text{CO}_2$  pressure of 10 Torr, the partial pressure of  $\text{O}_2$  could have been  $10^{-4}$  Torr at 10 ppm concentration, which is sufficient to cause bleaching. Since no sharp increase in reflectance occurred through the next decade and one-half, it is almost certain that the oxygen concentration did not exceed 10 ppm.

Since a sharp increase in reflectance was noted at a  $\text{CO}_2$  pressure of above 700 Torr, and since a pressure of  $5 \times 10^{-32}$  Torr of  $\text{O}_2$  caused such an increase in the reflectance of S-13 at 2050 nm, an approximate oxygen concentration can be calculated as follows:

$$\begin{aligned} 0.7 \times 10^3(x) &\leq 5 \times 10^{-3} \\ x &\leq 7 \times 10^{-6} \\ x &\leq 7 \text{ ppm} \end{aligned}$$

where x is the concentration of oxygen. The data therefore shows conclusively that carbon dioxide causes bleaching, but at a considerably reduced rate compared to oxygen. Indeed, the maintenance of 1000 Torr of  $\text{CO}_2$  for 120 hr did not result in complete bleaching of the "totally" oxygen-bleachable damage in any of the specimens (Figures 81 through 85).





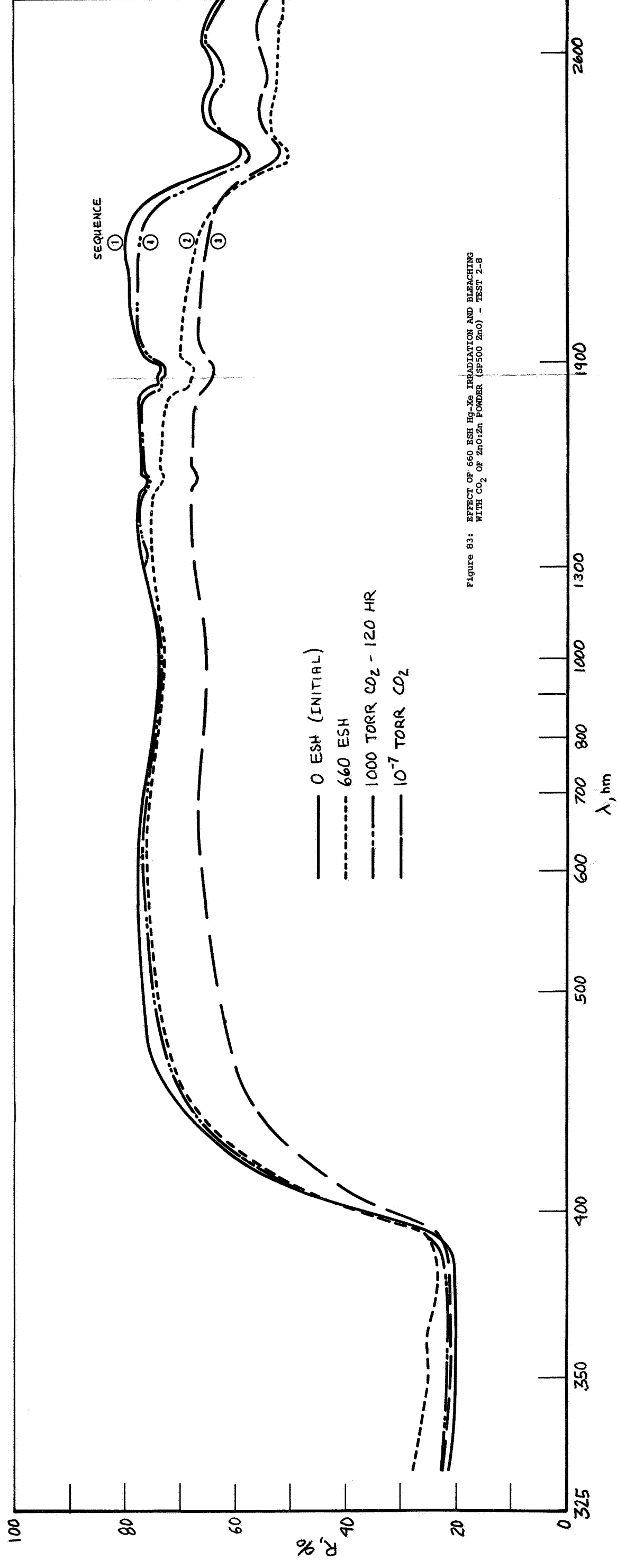


Figure 83: EFFECT OF 660 ESH Hg-Xe IRRADIATION AND BLEACHING WITH  $\text{CO}_2$  OF ZnO:Zn POWDER (SP500 ZnO) - TEST 2-8

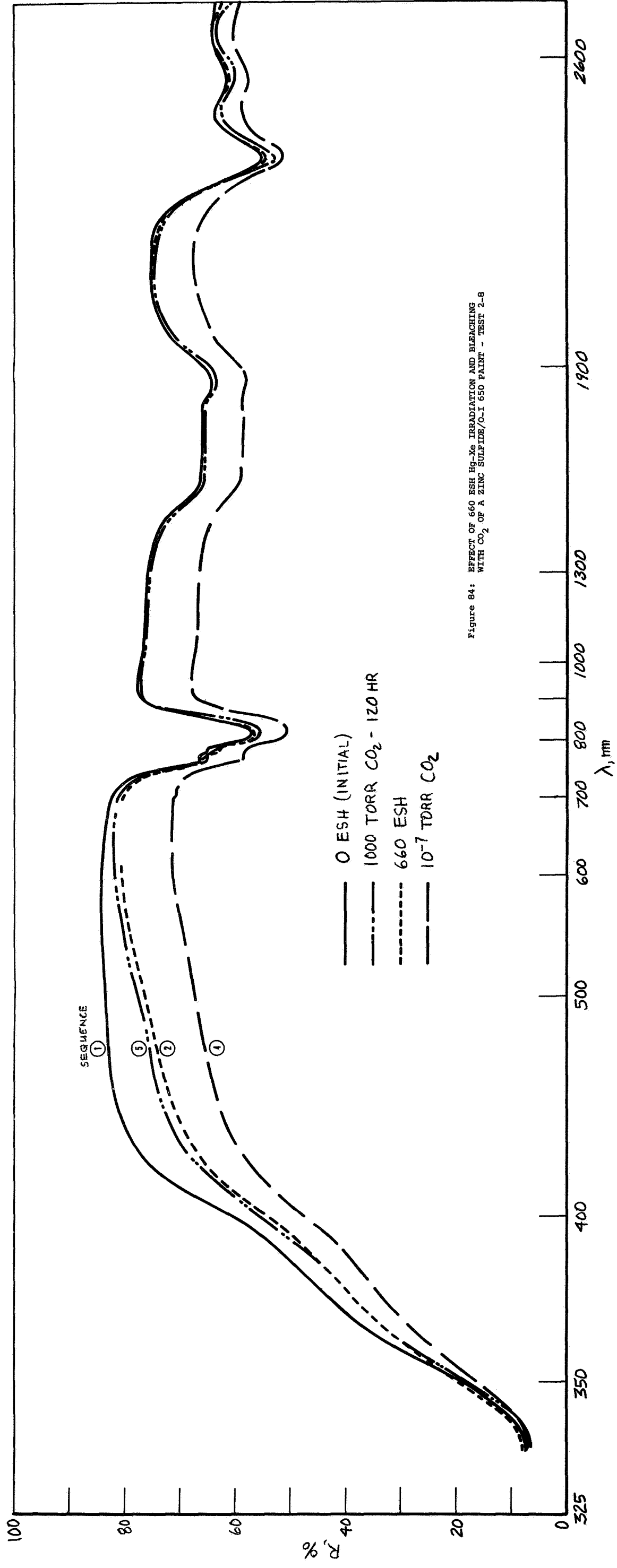
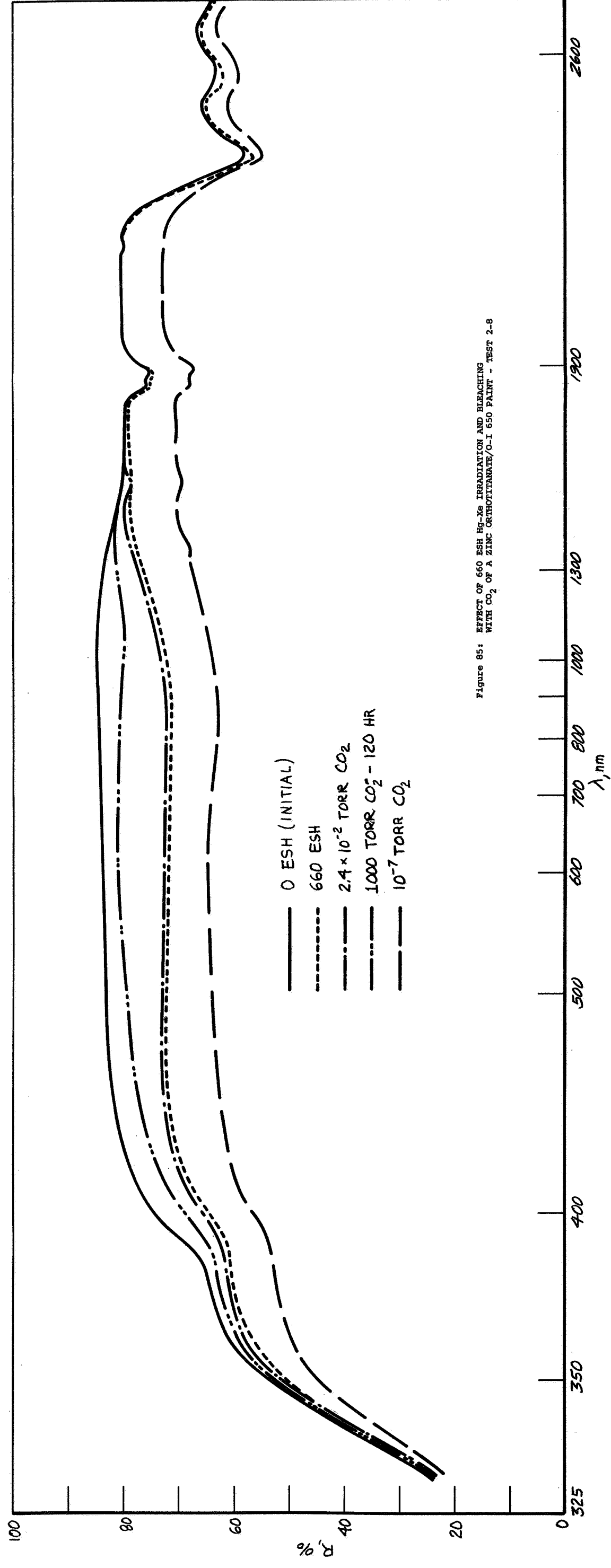


Figure 84: EFFECT OF 660 ESH Hg-Xe IRRADIATION AND BLEACHING WITH CO<sub>2</sub> OF A ZINC SULFIDE/O-I 650 PAINT - TEST 2-8





The sequence of the operations performed, operations that coincided with the various spectra recorded for each of Figures 81 through 86, were as follows:

<u>Operation</u>	<u>Description</u>
1	Record spectra of evacuated "virgin" samples
2	Record spectra of irradiated samples (660 ESH)
3	Record spectra of "bleached samples at $2.4 \times 10^{-2}$ Torr
4	Continue to add $\text{CO}_2$ to $10^3$ Torr (no spectra taken)
5	Evacuate samples to $10^{-7}$ Torr and record spectra
6	Back fill with $\text{CO}_2$ to $10^3$ Torr and record spectra
7	Record spectra after 120 hr at $10^3$ Torr $\text{CO}_2$ .

All specimens exhibited slight bleaching at  $2.4 \times 10^{-2}$  Torr  $\text{CO}_2$ . However, a defective control on the Alphatron gauge at about 1000 Torr prompted us to re-evacuate in order to preserve the damage for subsequent bleaching experiments once the defect could be repaired. The spectra were taken again at  $10^{-7}$  Torr to determine if the damage "pumped" back in. A surprising result of the pump down was the generation of reflectance spectra for all specimens that was from 5 to 15% below the spectra recorded for the damaged condition (prior to admission of carbon dioxide). (These spectra are shown as the bottom curve in Figures 81 through 85.)

These puzzling spectra were "bleached" on admission of air to the chamber and were immediately determined to not be due to relaxation or misalignment of optics. They have subsequently been attributed to the formation of solid carbon dioxide "snow" on the surface of the samples due to the rapid evacuation of the chamber.

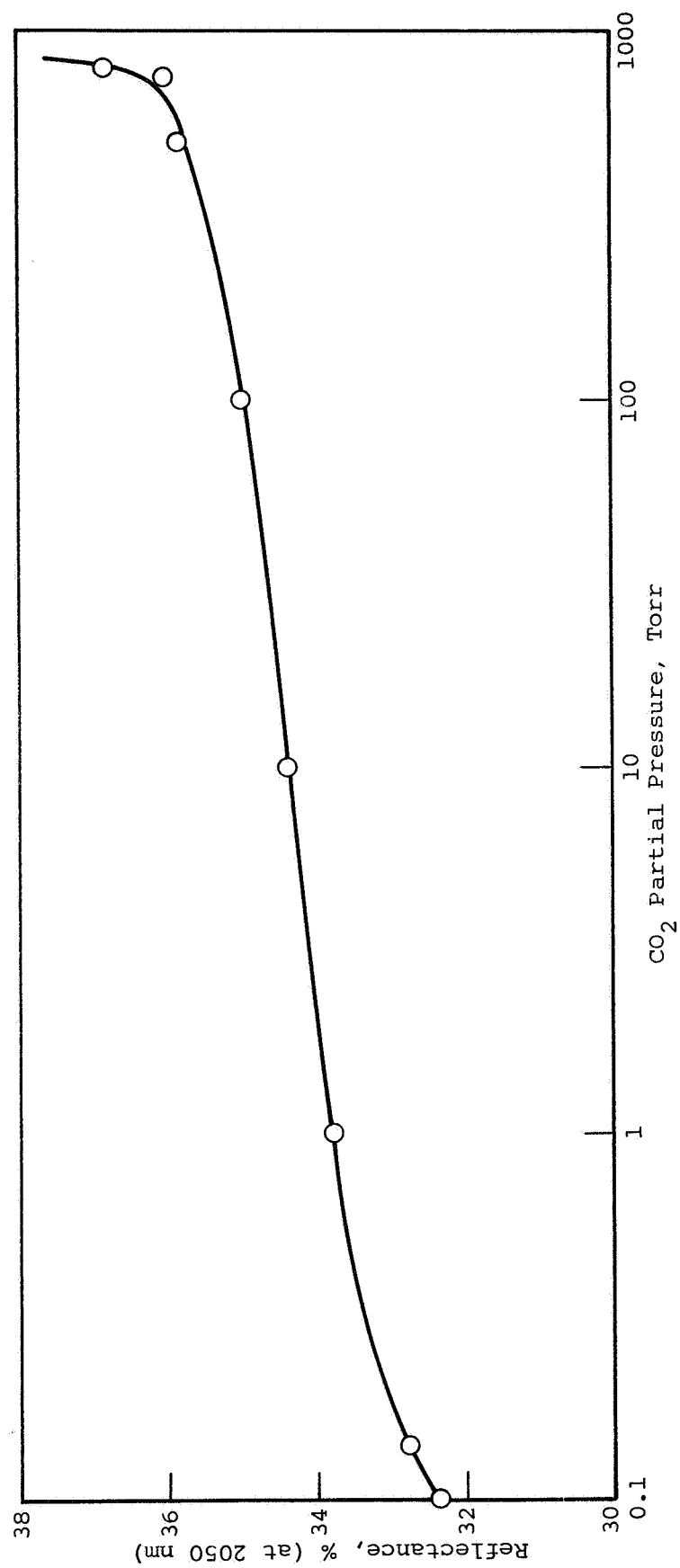


Figure 86: REFLECTANCE OF S-13 AT 2050 nm AS A FUNCTION OF CARBON DIOXIDE PRESSURE

Examination of the data shows that all specimens exhibited substantial bleaching after 120 hr at a  $\text{CO}_2$  pressure of  $10^3$  Torr. The S-13 specimen was only 50% bleached in the 2050-nm wavelength region (Figure 81). The rutile specimen (Figure 82) was also only partially bleached in the 1000-nm wavelength region - compared to nearly 100% bleaching of rutile by oxygen.

Figure 83 presents the spectra of a zinc-rich SP500 zinc oxide obtained from New Jersey Zinc. Several features distinguish its behavior from that of the host SP500: (1) it's overall reflectance is somewhat lower (although the film shown in Figure 83 was only 3.5 mil thick); (2) the ultraviolet reflectance was much higher (20% compared to 50% for SP500 ZnO); (3) the coating exhibited little damage in the visible region of the spectrum (due probably to O-I 650's greater stability compared to RTV 602); (4) it suffered only about 30% of the infrared damage (at ~2050-nm); and, (5) its infrared damage at about 2000-nm wavelength was almost totally bleached by  $10^3$  Torr of  $\text{CO}_2$ .

The behavior of zinc sulfide is shown in Figure 84. The ZnS irradiated in the studies reported herein consistently exhibited greater stability than anticipated, especially in the high-temperature test described earlier (Figure 44). It should be noted that all ZnS specimens irradiated in this study employed Owens-Illinois 650 "Glass Resin" as the binder.

The zinc orthotitanate exhibited the damage and bleaching spectra typical of this material (see Figure 85). However, carbon dioxide did not completely bleach out the fat  $\text{Ti}^{+3}$  peak at ~850-nm that is completely eliminated by oxygen.

#### F. Discussion

The instantaneous bleaching effect makes it evident that the defects responsible for the increased optical absorption (and decreased reflectance) are located in the surfaces of the pigment. This conclusion is readily supported by the fact that the materials exhibiting the bleaching effects described here all have very

strong absorption in the ultraviolet region and that very little radiative penetration would be expected. In effect then, they are "surface" defects.

The number density of defects created is obviously in some proportion to the absorbed ultraviolet dose; unfortunately, however, the quantitative relationships are unknown. In any case, the defect is created by the ultraviolet and is bleachable by oxygen, partly so by nitrogen, and presumably, unaffected by the noble gases. Many explanations are possible, including those proposed by Collins and Thomas (ref. 6), Gilligan (ref. 7) and Greenberg et al (ref. 8). The explanation that follows is substantially that proposed by Collins and Thomas for zinc oxide: ultraviolet absorption causes hole-electron pairs near the pigment surfaces. The holes, in the presence of a small electronic field established by the adsorbed gases at the surface, migrate to the surface and discharge these gases and in so doing reduce the field as well; the binding energy of the adsorbed gases depends, of course, on the nature of the gas and the type of bonding. The net result is a reduction of the concentration of surface adsorbates until the electronic field they produce is no longer influential in attracting holes. At this point continued irradiation would only occasionally produce more defects, by providing an opportunity for the regular lattice oxygens to be desorbed.

This model is consistent with the experimental results in this way. Oxygen is obviously a major lattice element in the oxide semiconductors. Accordingly, it is permitted several states of bonding in these materials, ranging from the doubly charged oxygen lattice ion, and the chemisorbed  $O^-$  ion, to the physically adsorbed oxygen (hydrogen bonded) to even the oxygens which are mechanically trapped. When placed under vacuum, the latter ones are removed according to the above model. Lattice oxygens are removed at a very much lesser rate. After most or all of the adsorbates are removed, the "active" surface can accommodate oxygen in all the states mentioned; however, nitrogen can be accommodated

in only the physically adsorbed state. Though the experimental results are not conclusive enough to rule out oxygen impurities, measurement inaccuracies, etc., they do support our earlier views.

Therefore, the reflectance/pressure plateaus, or levels, may result from the equilibrium between adsorption and desorption rates at the partial pressure of the adsorbate gas at the surface. It should be noted that the energies involved are small and are of thermal magnitudes. In fact we can point to a memory effect that says that the physically readsorbed oxygen can be removed (ref. 7) from previously irradiated zinc oxide to regenerate the damage, but only so long and to the extent that the oxygen has not chemisorbed back onto the surface. Therefore, if our view of the mechanism is correct, the reflectance/pressure plateaus should exhibit temperature dependence.

The behavior of carbon dioxide is almost impossible to interpret in terms of mechanism from the data obtained. Carbon dioxide is known to chemisorb to metal oxides to form simple carbonates ( $\text{CO}_3^{=}$ ), unidentate carbonates ( $\text{M}-\text{O}-\text{C}\begin{smallmatrix} \text{O} \\ \swarrow \end{smallmatrix}$ ), bidentate carbonate ( $\text{M}\begin{smallmatrix} \text{O} \\ \swarrow \end{smallmatrix}\text{C}=\text{O}$ ) and organic carbonates ( $\begin{smallmatrix} \text{O} \\ \swarrow \end{smallmatrix}\text{C}=\text{O}$ ). Very often, all three carbonates form on the surface of metal oxides. Indeed, simple carbonate and unidentate carbonates have been observed employing infrared spectroscopy on the surface of zinc oxide (ref. 9, 10); a unidentate carbonate on the surface of rutile  $\text{TiO}_2$  has been reported (ref. 11). Determinations of the structures of chemisorbed  $\text{CO}_2$  on the surface of evacuated zinc oxide that has been activated by irradiation must await further study. (A special cell is being constructed for this purpose.) However, the puzzling aspect of the carbon dioxide data is the failure to ever totally bleach out the damage (in  $\text{ZnO}$  and  $\text{TiO}_2$ ), even at partial pressures of  $\text{CO}_2$  in excess of one atmosphere. In the absence of confirming data, we can only assume that the equilibrium between adsorption and desorption is largely a result not only of the chemistry involved but the steric effects of  $\text{CO}_2$ . That is,  $\text{CO}_2$ 's failure to bleach out the  $\text{ZnO}$  and  $\text{r-TiO}_2$  damage at  $10^3$  Torr

might be attributable to the bulkiness of the unidentate carbonate, which may preclude interaction with a sufficiently large number of free carrier electrons (in ZnO) or, in the case of  $\text{TiO}_2$ , bound state defects, to spectroscopically eliminate their contribution to adsorption.

## VI. SUMMARY AND CONCLUSIONS

The spectral reflectance data obtained with IRIF's I and II, much of which has been presented herein, is judged to be very accurate and is representative of the type of "absolute" data that can be obtained with an Edwards-type integrating sphere. A typical 100% line for the IRIF-II is presented in Figure 87.

Gross contamination due to sample outgassing during the tests was monitored by employing an OSR second-surface mirror control. Except in Test 15, which was performed at 85°C (see Figure 41), no changes in the absolute reflectance attributable to contamination were observed for the OSR controls. A typical spectra for the OSR are presented in Figure 88. The slight structure in the 2400- to 2600-nm wavelength region is attributed to adsorbed OH<sup>-</sup> as a result first of photodesorption and then admission of moist air. Obviously, gross contamination was absent in this test.

\* \* \* \*

The lack of test-to-test correlation that manifested itself during the course of the program, in spite of the care taken to ensure quantitatively equal energy deposition rates, strongly suggests that a serious problem exists relative to our knowledge and control of the spectral character of the sources employed - regardless of whether the 1000-watt A-H6 mercury-argon or the 5000-watt mercury-xenon or xenon lamps are employed. That is, we believe that no two xenon or mercury-xenon sources are spectrally alike in the 200- to 250-nm wavelength region and, if they should fortuitously agree spectrally, that they most assuredly will not agree in the manner in which they spectrally degrade with age! Thus, for coatings and materials that are peculiarly sensitive to wavelengths in the 200- to 250-nm region only, such as, for example, most dielectric pigments, PS-7 potassium silicate,

IIT RESEARCH INSTITUTE



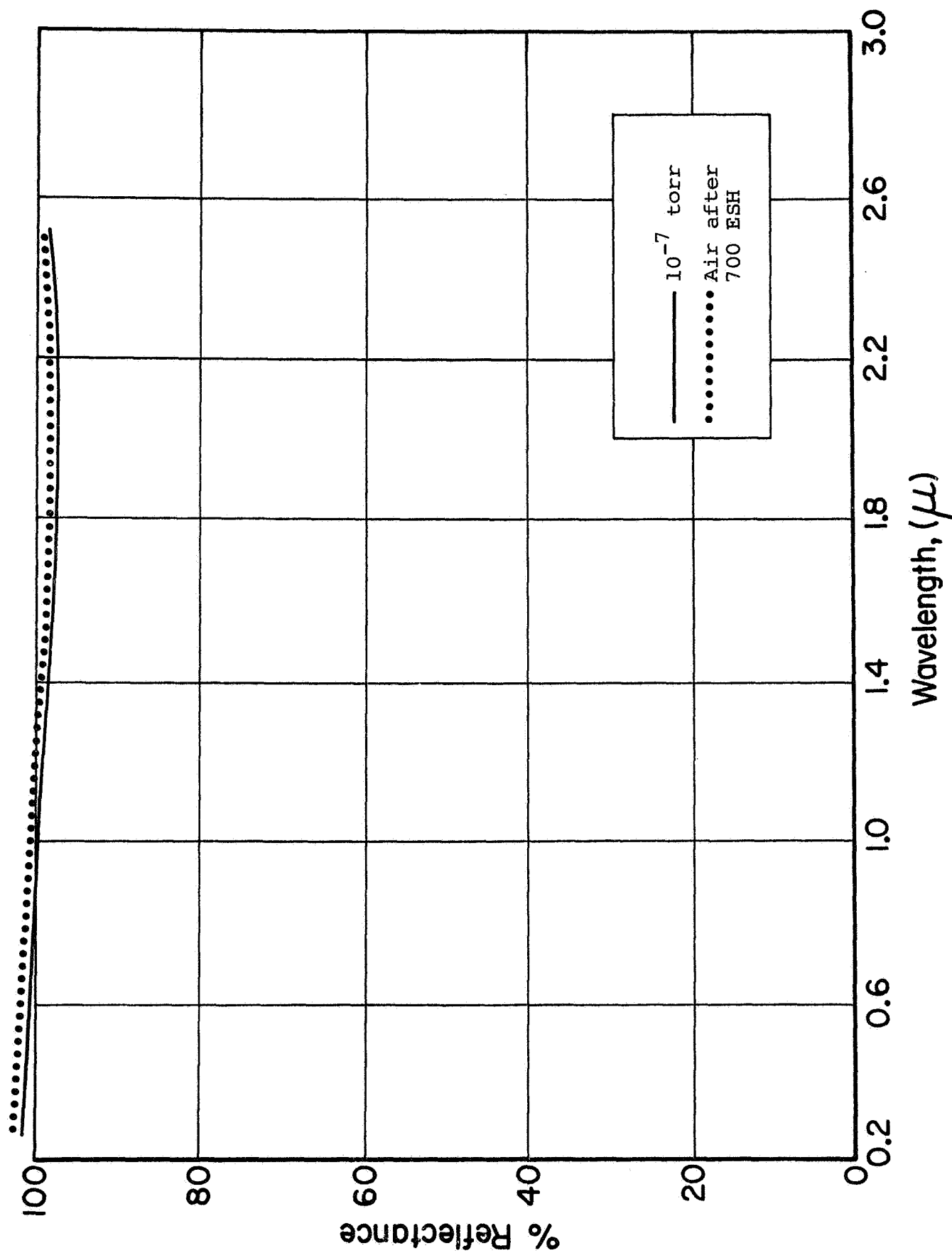


Figure 87: A TYPICAL 100% LINE FOR THE IRIF-II FACILITY

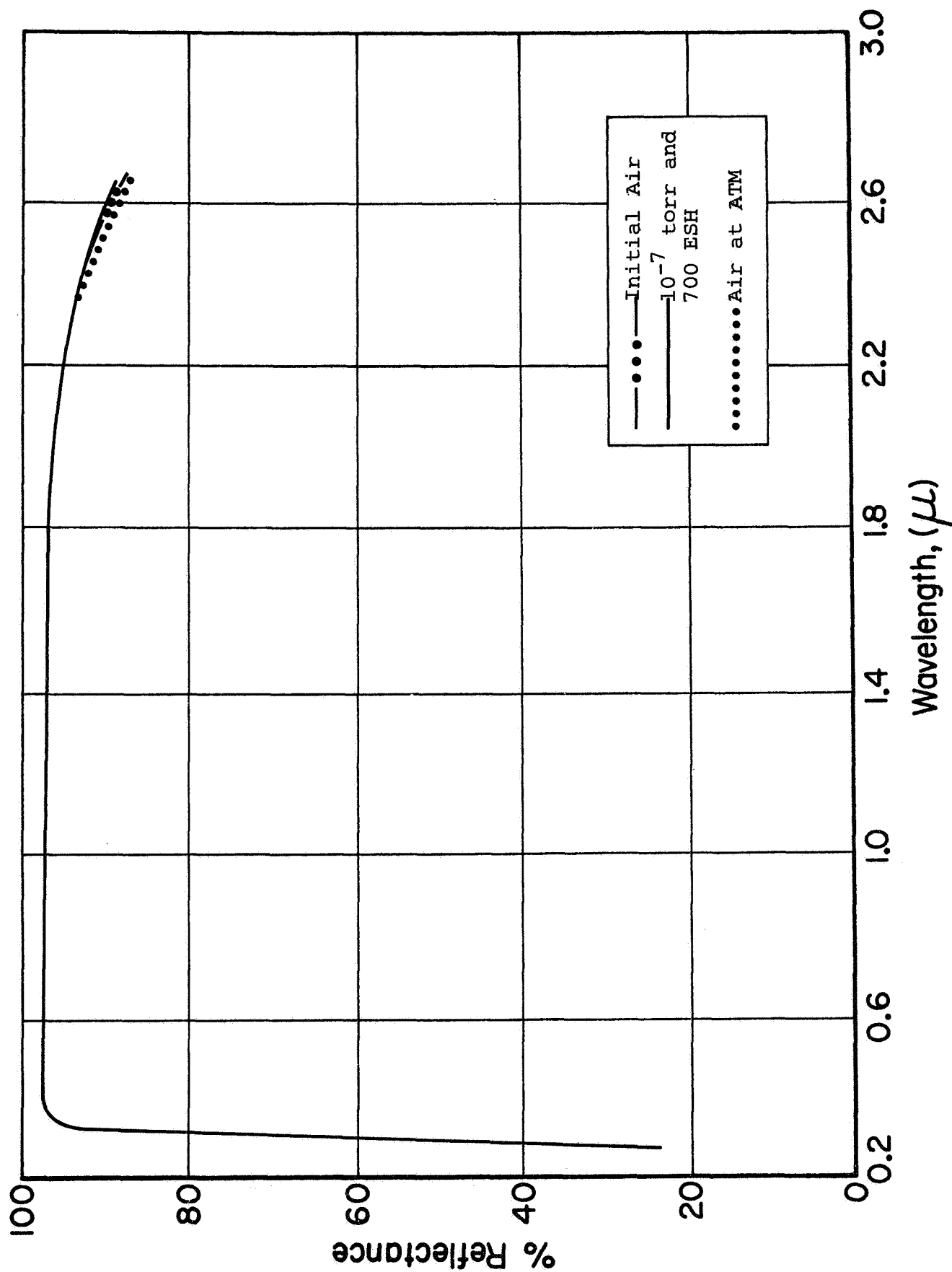


Figure 88: SPECTRA OF UV IRRADIATED OSR (LMSC-1)

RTV-602 silicone elastomer, etc., lamp-to-lamp disparities in spectral output and stability at these wavelengths will be critically important. To cite an example, IRIF-I Tests 13 and 16 (A-H6 lamps) agree for the zirconia/PS-7 paint but not for S-13: Furthermore, Test 10 was much more severe than Test 13 for the Pegasus S-13 paint but the converse was true for the zirconia coating (the specimens of each were identical and were cut from the same sample in the case of the S-13 coupons). In general, the less stable the candidate, the greater the variations in response to irradiation from test-to-test.

\* \* \* \*

Aside from the changes in spectral reflectances of certain ultraviolet-irradiated materials by gaseous adsorbates, it is of interest to ask what else can be learned from the adsorbate tests. There are several points that can be made in this regard. It is apparent that gaseous bleaching generally affects only the infrared reflectance. Secondly, potassium silicate has a bleachable band; the spectrum of LiF/PS-7, for example, does not show an F-center spike where it should and hence, the damage at the LiF F-center wavelength must be due to the silicate binder. If this is true, then one can attribute the bleachable damage in tantalum ( $\text{Ta}_2\text{O}_3$ ) and zirconia ( $\text{ZrO}_2$ ) to the silicate vehicle. In fact, the lack of any substantial change in the infrared reflectance compared to that in the visible strongly suggests that alpha-alumina ( $\alpha\text{-Al}_2\text{O}_3$ ) as well does not oxygen bleach. When bleachable binders are used, the "damage" spectra will be more complicated, and care must be taken to distinguish pigment and vehicle behavior.

The significant point to adsorbate testing is that one can immediately distinguish materials whose reflectance degradation is surface related from those which are not. This distinction,

it turns out, separates the semiconductor materials in which surface effects are accentuated from dielectric materials in which bulk properties predominate. In large band gap semiconductor materials such as  $\text{SnO}_2$ ,  $\text{ZnO}$ ,  $\text{TiO}_2$ , etc., surface structure becomes important for two reasons: First, ultraviolet adsorption is concentrated in a depth very small compared to particle dimensions. Second, the very nature of a semiconductor implies a concentration of free electrons or free holes quite large compared to dielectric materials. Because of the regular crystalline structure and the periodic lattice, the free electrons or holes tend to localize on the surface where they are more readily accommodated; that is, at a natural discontinuity of the periodic structure.

The free electron (or free hole) excess, however, is not stable, because many gases have an affinity for them. (None of the materials discussed in this report are p-type, i.e. have free holes.) Consequently, any material with an affinity for free electrons will be adsorbed readily, particularly in materials in which the anion is a gas with a high electron affinity. Zinc oxide and titania are notable examples. In the case of zinc oxide the electrons are free; not associated with a specific atom; in titania the electrons are bound in a shallow trap at or near the surface. These conclusions are based on observations of the nature of the "damage" spectra.

The theory of gas adsorbate interactions is highly complex; the fact that some gases are adsorbed weakly and others strongly and that there may be several possible bonding levels in adsorption should in some way be correlated to reflectance changes. Unfortunately, time and funding have not permitted anything more than a cursory look at this aspect of the work.

Let us now examine the reflectance versus pressure curves (Figures 65, 73 through 75, 80 and 86); attempt to explain them on a qualitative basis. Ultraviolet irradiation quite effectively removes all weakly bound adsorbates, including water. The reflectance spectra of paints which utilize PS-7 as the binder

almost inevitably show a rapid improvement in the near infrared region due to water desorption. This generally occurs before degradation due to the induced defects. Hence the apparent damage to a silicate coating does not make manifest the history of the degradation. In any case, the spectral reflectance upon admission of a test gas generally recovers to a value somewhat higher than its initial or pre-ultraviolet exposure value. The adsorbate data thus show the extent of "contamination," in this case defined by the amount of adsorbed material which causes adsorption; the difference between the initial value of the spectral reflectance at a given wavelength and that to which it recovers, when the adsorbate is the anion of the pigment, is related to the amount of contaminant.

Another aspect of the reflectance versus pressure data has to do with the response times of the reflectance. The test gas is almost always admitted in a time much less than that required for the spectral reflectance to equilibrate to the new pressure. We believe that this time response will be indicative of the mechanism of adsorption and that, if the kinetics are quantitatively described, the mechanisms will be much better understood. It should be possible, for example, to study the bleaching rates of the individual color centers and from such studies to deduce the energetics and kinetics of these reactions. Obviously, too, the defects which are not bleachable will also be identifiable. This latter point we suggest should lead to important insights into the development of a pigment stabilization scheme.

Finally, we would like to examine the nature of the reflectance response and the equilibria reached when stepwise pressure increases are made, as for example, in Figure 74. Upon admission of the adsorbate, the spectral reflectance (at a specific wavelength) increases and reaches an equilibrium value, one which is dependent upon the partial pressure of the adsorbate.

This behavior implies that the adsorbed gas concentration and hence the number of defects that are bleached depends upon a balance between the two phases of the adsorbate - the adsorbed phase and the gas phase. We have not studied the data to discover such a relationship, but we strongly believe that such a relationship when known will provide even deeper insight into the degradation mechanisms of thermal control materials.

In conclusion, we would like to point out the importance adsorbate testing potentially may have in thermal control R&D. First, we are able to determine immediately if environmentally induced damage involves loss of the anion. Second, the spectral regions in which bleaching occurs is highly significant; it indicates the formation or binding energies of the defects involved.

The main purpose of these discussions has been to identify various types of information which may be obtained from adsorbate testing and to emphasize their importance in the further understanding of mechanisms and kinetics of degradation of thermal control materials. For example, non-stoichiometric zinc orthotitanate ( $\text{Zn}_2\text{TiO}_4$ ) has been found to bleach with different kinetics in three distinct bands which are attributable to  $\text{ZnO}$ ,  $\text{TiO}_2$  and  $\text{ZnTiO}_3$  (meta) (ref. 12 and 13). Furthermore, adsorbates such as amines (curing agents), alcohols and ketones (solvents) are known to adsorb to metal oxide surfaces to form strongly bonded entities with uniquely different ultraviolet and infrared adsorption spectra. Furthermore, substances such as n-hexane, acetone, benzene, etc., react with the surface hydroxyls of metal oxides and form chemisorbed species with strong coordination bonds: Amines not only react with the surface hydroxyls of  $\text{TiO}_2$ , forming a hydrogen bond, but also with the electron-acceptor (aprotonic) centers of the surface (ref. 14).\* The preparation

---

\*RTV-602 requires an amine catalyst and has been observed by us to be much less stable than Owens-Illinois 650 resin which, except that it does not require catalysis for cure, is structurally similar.

of a paint from pigment that has had its surface hydroxyls removed and which is protected from readsorption of contaminant adsorbates is therefore suggested. An understanding of this phenomenon should serve to help explain the reason for the great stability that is always observed with fused vitreous enamels (porcelain) even when opacified with zirconia and antimony oxide, i.e., their recrystallization from solid solution may serve to maintain a relatively adsorbate-free surface.

\* \* \* \*

The behavior of irradiated zinc oxide, rutile titanium dioxide and zinc orthotitanate when bleached with oxygen and carbon dioxide tends to confirm our contention that the photodesorption of oxygen plays the major role in the creation of damage in such materials. Oxygen instantaneously annihilates the damage spectra of these oxides - spectra that can be instantaneously reinduced simply by immediate re-evacuation (pumping alone is insufficient to reinstate the damage if the pigment is not re-evacuated within minutes after bleaching has occurred). On the other hand, carbon dioxide annihilates the defect centers at a higher partial pressure and at much slower rates than oxygen - in fact, carbon dioxide never does bleach more than 50% of the induced infrared damage in S-13, even at a pressure of 1000 Torr of CO<sub>2</sub>.

Although adsorbed carbon dioxide and its photodesorption on irradiation may very likely play an important role in the damage of these semiconductor pigments, its role does not exclude the role of oxygen photodesorption. The quantum yield of oxygen required to produce the number density of defects that are necessary to be spectroscopically observable is probably far too small for detection by gas chromatographic/mass spectrometry, a technique that has been reported by a number of authors during the

past two years. In addition, the monatomic oxygen that is desorbed would very likely be retained by getter-ion pumps. Also, its accommodation coefficient for vacuum-cleaned metal and glass walls is probably so high that the combination of low yield and adsorption on the walls of apparatus accounts for the fact that oxygen is seldom, if ever, detected as an irradiation product by GC-MS techniques.

\* \* \* \*

We have, as a result of these and other studies, reached certain conclusions pertaining to the philosophy of space-simulation testing of thermal-control surface coatings. First, the results and our interpretations of them suggest that testing of thermal-control materials and coatings in a simulated space environment should be confined mainly to the most stable systems available. Secondly, testing per se, unless it represents a "first look" at a new series of coatings (where, for example, little or no information is available) can easily be a gross waste of a facility's capabilities. Third, while it is obviously necessary to always strive for accurate space simulation, we believe that the real and completely accurate simulation of the total environment is possible only with the expenditure of funds of such magnitude that it begs the question of "to which approach to the solution of the thermal-control coatings problem should priority be given?" The exhaustion of funds in the creation of sophisticated simulation facilities will most likely still leave the real problem unsolved - namely, the development of stable thermal-control surface coatings. The important questions are therefore "what are the mechanisms of interaction of high energy photons (UV) and charged particles with candidate coatings and space materials?" and "how can we, using such information,

IIT RESEARCH INSTITUTE



synthesize, treat or otherwise produce materials that are stable to the space environment for long periods of time?"

Obviously, the irradiation of a stable coating with an inexactly simulated combined space environment will produce results that differ little, if at all, from real-orbit behavior! Although well characterized combined-radiation environmental facilities that are capable of equally accelerating all environments, at small nominal acceleration factors, are required as diagnostic tools, the real problem is and has always been one of determining the mechanism of damage and the alleviation of damage in thermal-control coating constituents, and finally in the effect of one constituent upon the behavior of another.

## REFERENCES

1. Miller, E.R., "Pegasus III Retrievable Thermal Control Surfaces Flight Experiment," NASA-Geo. C. Marshall Space Flight Center Internal Note R-RP-INT-66-1, Mar. 15, 1966.
2. Edwards, D.K., Gier, J.T., Nelson, R., and Roddick, R.D., J. Optical Soc. Amer. 51, 1279, 1961.
3. Zerlaut, G.A. and Courtney, W.J., "Space-Simulation Facility for In Situ Reflectance Measurements," in Thermophysics of Spacecraft and Planetary Bodies, Vol. 20, Progress in Astronautics and Aeronautics, G. Heller, ed., Academic Press, N.Y., pp. 349-368, 1967.
4. Zerlaut, G.A., Rogers, F.O., and Noble, G., "The Development of S-13G-Type Thermal-Control Coatings Based on Silicate-Treated Zinc Oxide," AIAA Paper 68-790, Los Angeles, Cal., June 1968, in press.
5. Rogers, F.O. and Zerlaut, G.A., "Development of S-13G-Type Coatings as Engineering Materials," IIT Research Institute Report No. IITRI-U6053-11 (Final Report), JPL Contract 951746, Mar. 5, 1969.
6. Collins, R.J., and Thomas, D.G., Phys. Rev. 112 (2) 388-395 (1958).
7. Gilligan, J.E., "The Optical Properties Inducible in Zinc Oxide," in Thermophysics of Spacecraft and Planetary Bodies, Vol. 20, Progress in Astronautics and Aeronautics, G. Heller, ed., Academic Press, New York, 1967.
8. Greenberg, S.A., et al, "Solar Radiation-Induced Damage to Optical Properties of ZnO-Type Pigments," Lockheed Report L-92-67-1, NASA Contract NAS8-18114, June 1967.
9. Taylor, J.H., and Amberg, C.H., Con. J. Chem., 39, 535, 1961.
10. Matsushita, S and Nakata, T., J. Chem. Phys., 36, 665, 1962.
11. O'Neill, C.E., and Yates, D.J.C., Spectrochim. Acta., 17, 953, 1961.
12. Incremental funding to this contract (NAS8-21074).
13. Contract NAS8-5379, IITRI Project U6002, NASA-Marshall Space Flight Center.
14. Kieslev, A.V., and Uvarov, A.V., Surface Science, 6, 399-421 (1967).

IIT RESEARCH INSTITUTE

APPENDIX A

GAS ADSORBATE PROCEDURE

IIT RESEARCH INSTITUTE

## APPENDIX A

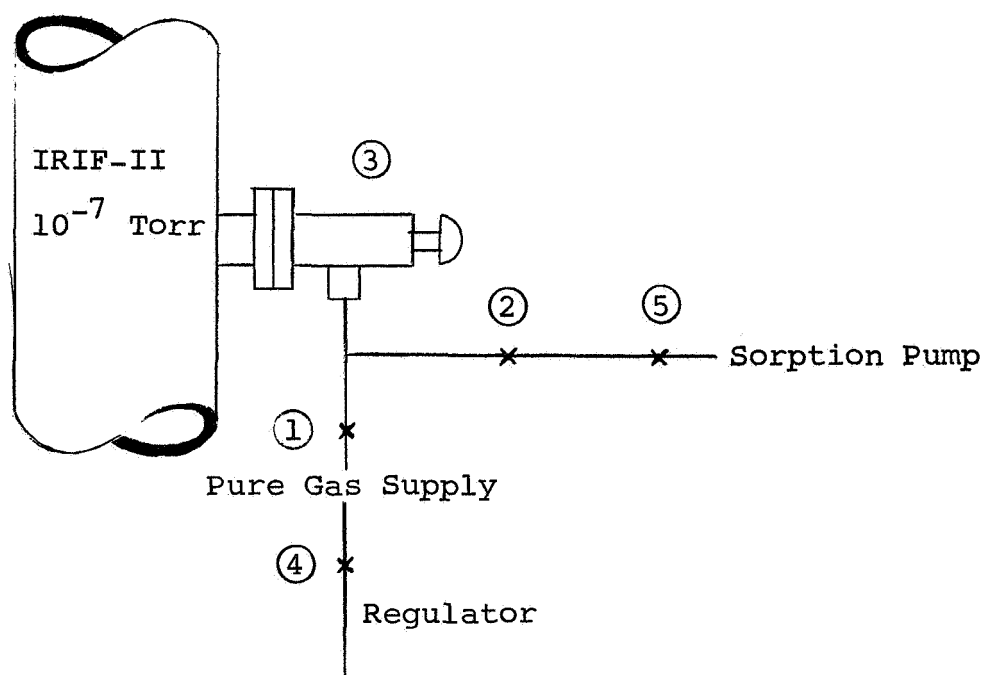
### GAS ADSORBATE PROCEDURE

#### I. GAS ADSORBATE OPERATING PROCEDURE FOR IRIF-II

1. Operate strip chart at  $2.05\mu$  to determine the noise level as a function of time.
2. Measure  $R_{\lambda}$  for all 12 specimens.
3. Place Pegasus S-13 in Integrating Sphere.
4. Set Beckman DK-1 at  $2.05\mu$ .
5. Go through Gas Admission Procedure up to item 15.
6. Item 15 of Gas Admission Procedure: Bleed in gas to  $10^{-6}$  Torr with recorder on (at  $2.05\mu$ ) - HOLD 30 min. If no change, go to Item 8. If change, see Item 7.
7. Hold until no change for 1 hr (DECISION).
8. Bleed gas to  $10^{-5}$  Torr, HOLD 30 min. If no change, go to Item 10, If change, go to Item 9.
9. Hold until no change for 1 hr (DECISION).
10. Turn off ion pump.
11. Bleed gas to  $10^{-4}$  Torr; HOLD 30 min (monitor pressure). If no change, go to Item 13. If change, go to Item 12.
12. Hold until no change for 1 hr (DECISION).
13. Bleed gas to  $3\mu$  pressure ( $3 \times 10^{-3}$  Torr); HOLD minimum 1 hr (DECISION).
14. Bleed gas to  $140\mu$  ( $1.4 \times 10^{-1}$  Torr); HOLD minimum 1 hr (DECISION).
15. Et cetera.

IIT RESEARCH INSTITUTE

## II. GAS ADMISSION PROCEDURE TO IRIF-II



1. Pressure  $10^{-7}$  Torr chamber; 760 Torr with all valves closed
2. Open valves (1) & (2) & (5)
3. Evacuate with sorption pump down to  $25\mu$
4. Close (1)
5. Set (4) at 5 psi
6. Open (1) raise pressure to 15 in. of water
7. Close (1) and open (5) until  $p \approx 25\mu$
8. Close (5)
9. Open (1) raise pressure to 15 in.
10. Close (1)
11. Open (5) reduce pressure to  $25\mu \approx 1$  part  $O_2$  in  $10^{14}$  parts test gas
12. Close (5)
13. Close (2)
14. Open (3)  $\approx 3^+$  turns
15. Adjust (1) to maintain pressure at 1 Torr.

IIT RESEARCH INSTITUTE